University of Bath

UNIVERSITY OF
BATH

PHD

Developmental changes in kainate receptors in cortical network function and oscillogenesis

Robson, Emma

Award date:
2018

Awarding institution:
University of Bath

Link to publication

Developmental changes in kainate receptors in cortical network function and oscillogenesis

Emma Robson

A thesis submitted for the degree of Doctor of Philosophy

University of Bath

Department of Pharmacy and Pharmacology

November 2017

Contents

Acknowledgements

Abstract

Kainate receptors (KAR) mediate synaptic transmission at pre- and post- synaptic locations at excitatory and inhibitory synapses. KARs also have powerful roles in the synchronisation of neuronal networks at a physiological and pathological level. The medial entorhinal cortex (MEC) has been strongly linked to pathological synchrony, particularly in neurodevelopmental disorders such as epilepsy and schizophrenia. This thesis aims to determine the physiological functions of KARs in the MEC during development.

My initial work focused on the developmental changes in the baseline background synaptic transmission in LII and LV MEC, followed by the developmental changes in the ability of KAR to modulate spontaneous transmitter release. I have provided evidence for the involvement of two types of KAR in excitatory glutamatergic neurotransmission in the juvenile rat MEC: 1) A tonically active GluK1-containing KAR located at presynaptic terminals, and 2) a postsynaptic non GluK1-containing KAR at recurrent excitatory synapses with roles in synchronised network activity. KAR modulation was largely the same in both age groups. For inhibitory neurotransmission, I have provided evidence for a presynaptic facilitatory GluK1-containing KAR at interneurone terminals, acting to tonically increase GABA release onto principal neurones, and a KAR which may be located on the soma/dendrites of interneurones, driving GABA release via direct excitation. However, in the immature MEC, activation of the GluK1-containing KAR caused a substantial increase in GABA release, which was not evident in juvenile rats, showing this receptor may be developmentally downregulated or have different levels of tonic activation.

Next, I determined a developmental profile of oscillatory activity induced by KAR activation in the MEC. Synchronised activity was a slow beta frequency in the neonate MEC, compared to a gamma frequency in juvenile slices. Activity in LII showed a large age-dependent increase in amplitude which was not present in LV. Moreover, the increase in amplitude (LII) and frequency (LII & LV) coincided with the onset of eye-opening, and may bare consequences for the synaptic organisation of the MEC.

Taken together, the results from this study show KARs have many roles in mediating synaptic transmission and synchronised neuronal activity in the MEC, and may have transient developmentally regulated roles in the immature MEC. This work has implications for understanding neuronal synchrony and normal development of cognitive function, and for neurodevelopmental disorders such as schizophrenia and epilepsy, which involve EC dysfunction.

Abbreviations

ACSF	Artificial cerebrospinal fluid
AD	Alzheimer's disease
AMPA	α-amino-3-hydroxy-5-methyl-4-isoxazolepropionate
ATP	Adenosine triphosphate
ATPA	(RS)-2-Amino-3-(3-hydroxy-5-tert-butylisoxazol-4-yl) propanoic acid
Bicuculline	([R-(*R**,*S**)]-6-(5,6,7,8-Tetrahydro-6-methyl-1,3-dioxolo[4,5-*g*]isoquinolin-5-yl)furo[3,4-*e*]-1,3-benzodioxol-8(6*H*)-one
CCK	Cholecystokinin
CNQX	6-cyano-7-nitroquinoxaline-2,3-dione
CNS	Central nervous system
DGC	Dentate granule cells
DHPG	Dihydroxyphenylglycine
DL-AP5	DL-2-Amino-5-phosphonopentanoic acid
EC	Entorhinal cortex
EEG	Electroencephalogram
EPSC	Excitatory postsynaptic potential
EPSP	Excitatory postsynaptic current
GABA	γ-aminobutyric acid
GFO	Gamma-frequency oscillations
GYKI 52466	4-(8-Methyl-9H-1,3-dioxolo[4,5-h][2,3]benzodiazepin-5-yl)-benzenamine dihydrochloride
HC	Hippocampus
Hz	Frequency
IEI	Interevent interval
iGluRs	Ionotropic glutamate receptors
I$_h$	Hyperpolarising current
IMPC	Intermediate pyramidal cell
IMSC	Intermediate stellate cell
ING	Interneurone network gamma
IPSC	inhibitory postsynaptic current
IPSP	Inhibitory postsynaptic potential
JUV	Juvenile
KA	Kainic acid
KA-O	Kainic acid oscillations
KAR	Kainate receptors
L	Layer
LEC	Lateral entorhinal cortex
MEC	Medial entorhinal cortex
mEPSCs	Miniature excitatory postsynaptic current

MF	Mossy fibre
mGluR	Metabotropic glutamate receptor
mIPSCs	Miniature inhibitory postsynaptic current
MTL	Medial temporal lobe
NEO	Neonate
NMDA	N-methyl-d-aspartate
O-LM	Oriens lacunosum moleculare
P	Postnatal day
PC	Pyramidal cell
PG	Persistent gamma
PING	Pyramidal-interneurone network gamma
PV	Parvalbumin
R	Receptor
SC	Stellate cell
SOM	somatostatin
STDP	Spike timing dependent plasticity
SWO	Slow wave oscillations
SYM 2206	(±)-4-(4-Aminophenyl)-1,2-dihydro-1-methyl-2-propylcarbamoyl-6,7-methylenedioxyphthalazine
SYM2081	2S,4R)-4-methylglutamate
Tg	Transgenic
TLE	Temporal lobe epilepsy
TM	Transmembrane domain
TTX	Tetrodotoxin
UBP-310	(S)-1-(2-Amino-2-carboxyethyl)-3-(2-carboxy-thiophene-3-yl-methyl)-5-methylpyrimidine-2,4-dione
VFO	Very fast oscillations
VG	Voltage-gated
VIP	Vasoactive intestinal peptide
α	Alpha
β	Beta
γ	Gamma
Θ	Theta

Chapter 1

General Introduction

The overarching aim of this project has been to investigate role and functions of the kainic acid receptor (KAR) in the entorhinal cortex (EC). KARs are increasingly being shown to be important in neuronal communication, particularly in physiological (e.g. cognitive processing) and pathological (e.g. epilepsy) synchronization of brain activity.

The EC plays a vital role in learning, memory and cognition, but is also a site where epileptic activity frequently arises. Previously, this laboratory has shown that KARs have multiple roles in layer III (LIII) of the EC (Chamberlain et al, 2010). In this project, I have used patch clamp and local field potential recordings in rat brain slices to further understand the roles of KARs in synaptic networks in the layer II (LII) of the EC, which processes incoming cortical activity and relays information to the hippocampus. This has been compared to layer V (LV), which receives hippocampal output and links back to neocortical areas.

Activating KARs leads to strong synchronisation of activity in neuronal networks, causing them to generate gamma-frequency oscillations (GFO) and this activity is known to be involved in processes of learning, memory and cognition. On the other hand, excessive activation of KAR can lead to pathological synchronisation in the form of epileptic-like activity. The original hypothesis to be tested in this thesis was that epileptogenesis in the EC involve changes in KAR function that reflected a recapitulation of the developmental profile in KAR expression seen during early postnatal development. This was based on two sets of data from collaborating laboratories. (1) Electrophysiological studies conducted at the University of Aston with Professor Gavin Woodhall used KA-induced GFO to monitor functional network changes in the EC in a pilocarpine model of epilepsy (Modebadze et al 2016). As yet unpublished results showed that during the early latent period (1 week) following an acute status epilepticus, GFO induced by KA are undetectable in EC slices compared to control tissue. Recovery of KAR function is detectable at 2 weeks, particularly in LV, and by 10 weeks when spontaneous seizures are becoming manifest, sensitivity is dramatically increased with the superficial layers most susceptible. (2) Immunohistochemical studies (unpublished) in the laboratory of Professor Elek Molnar at the University of Bristol established a differential developmental profile of KAR subtype expression in hippocampal areas of the rat brain, which, to a degree, reflected the change in functional effects seen in the epilepsy model (Fig. 1.6).

Thus, the aims of my project have been:

1. To compare the characteristics of excitatory transmission and its developmental profile in deep (LV) and superficial (LII) layers of the MEC, in comparison to previous work on the mid-layer (LIII) of the same structure.

2. To compare the characteristics and developmental profile of inhibitory transmission in LII and LV of the MEC, in comparison to previous work on LIII.

3. To determine the role of KARs in modulation of both excitatory and inhibitory transmission in deep and superficial layers of the EC, and the developmental profile of these effects.

4. To determine the developmental profile of KAR function in the EC in relationship to the development of epileptic activity in this region using KA-induced GFO as a functional reporter. At this point my work diverged somewhat from its original aims and concentrated more on the functional development of GFO *per se*, which proved to be interesting and instructive in relationship to how this oscillatory activity arises in networks of the EC, and how this could contribute developing processes of learning/cognition.

1.1 Synaptic Transmission

Synaptic transmission is the biological process that allows neurones to communicate with each other across synapses. In the late 19th century, dramatic advances in our understanding of the complex organisation of the nervous system were made after the Spanish neuroanatomist, Ramon y Cajal, used a silver staining technique, or the 'Golgi' method, to visualise whole neurones under light microscopy (Van der Loos, 1988). All neurones, despite differing classifications and structural complexity, shared a common general morphology consisting of a cell body (soma) containing the nucleus, an axon and dendrites. At a similar time, Charles Sherrington pushed our understanding of functional neuronal physiology, showing how reflexes are part of a complicated interplay in which the spinal cord and brain process neuronal impulses, turning them into new impulses in muscles and organs (Sherrington, 1906, Phillips, 1972).

Later, the neurophysiologist John Eccles, along with Charles Sherrington, discovered how nerve impulses are conveyed from one cell to another. They showed that different types of neurones can have a stimulating or inhibitory effect, and the output of a particular neurone is determined by the net input from these cell types (Eccles, 1945). This ground breaking work was further complimented by physiologists Alan Hodgkin and Andrew Huxley in 1952, who showed that electrical discharges transferred from cell to cell were the result of the opposite passage of sodium and potassium ions across the neuronal cell wall (Hodgkin and Huxley, 1952). Together, Eccles, Hodgkin and Huxley were jointly awarded the Nobel Prize in physiology in 1963.

More major advances in understanding the physiological functioning of neurones occurred in the late 1970's when Erwin Neher and Bert Sakmann developed the patch clamp technique for use in small mammalian neurones (Neher and Sakmann, 1976). This technique made it possible to record the electrical properties of single ion channels and therefore help understand fundamental cell processes.

The neuronal membrane has diverse ion pumps, channels and exchangers embedded in it, across which concentration gradients for principal ions are maintained between the intracellular and extracellular environments. Activation and subsequent opening of voltage-gated (VG) ion channels allows ions to flow into or out of the neurone according to their electrochemical gradients. Sufficient net influx of positive ions, or depolarisation of the neuronal membrane, can lead to the generation of an action potential. If the threshold is met, an action potential will propagate down the axon and throughout the neurone due to consecutive depolarisation of the membrane mediated by VG-sodium channels.

The action potential can be transmitted to neighbouring neurones in two distinct ways. It can be transmitted directly, as an electrical signal, through specialised channels called gap junctions. More commonly, communication is achieved via chemical synapses. When action potentials invade the presynaptic terminals, VG-calcium channels are activated. This leads to an influx of calcium ions that triggers exocytosis of vesicles containing a neurotransmitter, which is released and diffuses across the synaptic cleft. Neurotransmitters then bind to receptors on the postsynaptic membrane to elicit either

excitation (depolarisation) or inhibition (hyperpolarisation). Feedback mechanisms are also in place to maintain a dynamic equilibrium within the network. For example, neurotransmitters can bind to receptors on the same presynaptic terminal from which they were released, triggering positive or negative feedback systems.

In the central nervous system, excitatory neurones, or 'principal cells', use the amino acid glutamate as the neurotransmitter, and they exhibit long range and diverse connectivity within neuronal networks. Inhibitory neurones, or interneurones, exhibit local connectivity enabling feedforward and feedback inhibition, and the neurotransmitter is another amino acid, γ-aminobutyric acid (GABA).

Two studies in the early 1950's revolutionised our understanding of the basic principles of synaptic transmission using intracellular recordings from muscle fibres of the frog neuromuscular junction. In the first study, the presence of small, spontaneous depolarisations or miniature potentials' at the postsynaptic membrane was documented in the absence of neuronal stimulation (Fatt and Katz, 1952). These potentials had numerous properties resembling the events evoked by direct presynaptic stimulation, suggesting they were the result of *spontaneous* presynaptic transmitter release. The second study undertook a retrospective quantitative analysis of both evoked and miniature potentials (del Castillo and Katz, 1954). They noticed that, when the concentration of calcium was lowered, the amplitude of evoked events was decreased, however, the frequency (but not amplitude) of spontaneous miniature events was decreased. Moreover, the fluctuations in the amplitude of the evoked events occurred at multiples of the mean amplitude of the spontaneous events. This lead to the conclusion that spontaneous events represent the minimum units of release, termed 'quanta'.

This knowledge has formed the basis of our current understanding of neurotransmitter release mechanisms. In a later series of studies by Heuser in the 1970's, electron microscopy confirmed that each quantum that is discharged correlates to the neurotransmitter contained within one vesicle undergoing exocytosis (Heuser et al., 1979, Heuser and Reese, 1973). Spontaneous release of neurotransmitter was proportional to intracellular calcium levels, yet it could occur independently of action potentials. Moreover,

recent molecular studies hint towards differences in vesicle fusion between evoked and spontaneous release in terms of their presynaptic machineries, neuromodulation and second messenger pathways (Melom et al., 2013). The existence of these seemingly two non-mutually exclusive mechanisms for transmitter release would point toward a distinct role for spontaneous transmitter release. However, the exact physiological roles of these synaptic events remain unclear, though are thought to have relevance to synaptic plasticity and neurodevelopment (Kavalali, 2014). For the purpose of this thesis, these autonomous events are used as a selective substrate for the investigation of spontaneous neurotransmitter release in the rat medial entorhinal cortex (MEC).

1.2 The Entorhinal Cortex

The EC (Brodman area 28), meaning 'inside rhinal', is so called as a result of it being partially enclosed by the rhinal (olfactory) sulcus. It is the largest cortical field in the parahippocampal region. This region also consists of the perirhinal areas 35 and 36, the parahippocampal cortex, the presubiculum and the parasubiculum (Furtak et al., 2007, Pereira et al., 2016), (Witter et al., 2017). Although we need to be cautious when making anatomical comparisons between species, the parahippocampal cortex is comparable to the 'postrhinal' cortex in the rat (Burwell and Amaral, 1998a, Furtak et al., 2007). Interest in the entorhinal cortex arose at the turn of the 20th century when it was described by Ramon y Cajal in his ground-breaking studies on the anatomy of the nervous system. Cajal was intrigued by this 'peculiar' part of the posterior temporal cortex and noted the prominent connections to the hippocampal formation, which consists of the dentate gyrus, fields CA3, CA2 and CA1, and the subiculum. We now know that the EC is the nodal point between the hippocampal formation and many association areas of the cortex, such as the parietal, temporal and frontal cortices (Fig. 1.1). This unique positioning of the EC allows it to act as a gateway between cortical and subcortical areas, where multimodal sensory and highly processed unimodal inputs converge, and can be bi-directionally conveyed to the hippocampal formation (Dickerson and Eichenbaum, 2010).
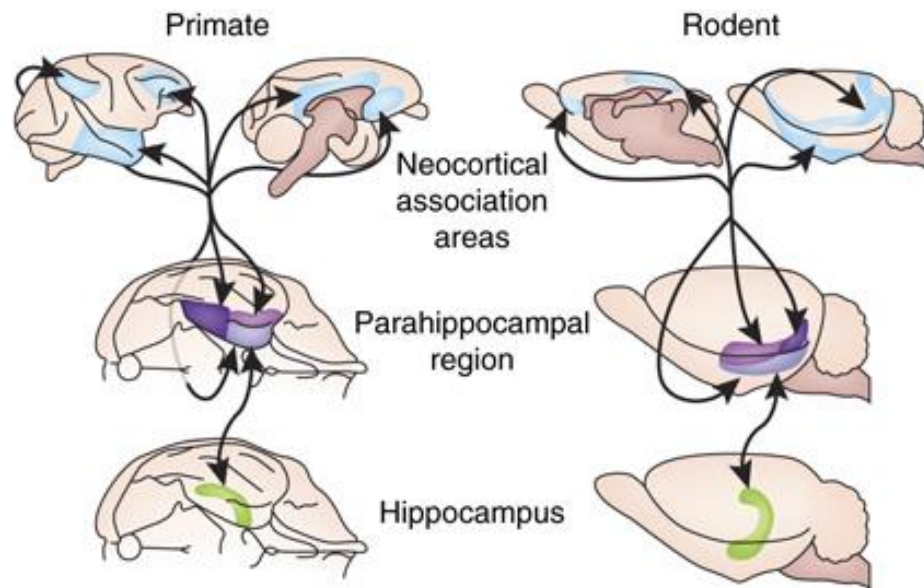
Figure 1.1: Positioning of the EC within the medial temporal lobe. *Figure shows position of the EC in light purple, ideally located to receive and convey information between neocortical association areas (blue) and the hippocampus (green). Purple: the perirhinal cortex, dark purple: the parahippocampal cortex. From (Dickerson and Eichenbaum, 2010).*

On a larger scale, the hippocampal and parahippocampal regions are a part of the 'Papez circuit', later termed the limbic system, after scientist James Papez injected rabies virus into the cat hippocampus (HC) and traced its progression (Bard, 1933). The circuit begins and ends with the hippocampal formation, passing through the following structures: the fornix, mammillary bodies, mammillothalamic tract, anterior thalamus nucleus, cingulum, parahippocampal gyrus and EC. The limbic system has major roles in a variety of cognitive functions, particularly regarding emotion and memory, but also sexual behaviour, motivation and olfaction (Papez, 1937). Systems that specifically involve the EC are pivotal for the storage of new memories. More recently, the role of the EC in cognitive behaviours such as spatial navigation has been emphasised (Moser et al., 2008). Cognitive deficits apparent in neurological disorders such as Alzheimer's disease (AD), Parkinson's disease and schizophrenia, have been attributed to neuropathological changes in these regions, especially in the EC (Zhou et al., 2016, Baiano et al., 2008, Kovari et al., 2003) Moreover, dysfunction of the EC has strong implications in the development of temporal lobe epilepsy (TLE) (Bartolomei et al., 2005, Du et al., 1993, Vismer et al., 2015) .

1.2.1 Anatomical organisation

1.2.2 Extrinsic connectivity

Using retrograde tract tracing experiments, where tract tracer injections were placed in the EC, extrinsic connectivity of the MEC has been identified by quantifying retrogradely-labeled cells in hippocampal, cortical and sub-cortical structures.

For the purpose of these following sections, the MEC is characterised into three divisions to identify the specific areas of afferent and efferent connectivity, namely medial, intermediate and lateral MEC bands (Fig. 1.2).
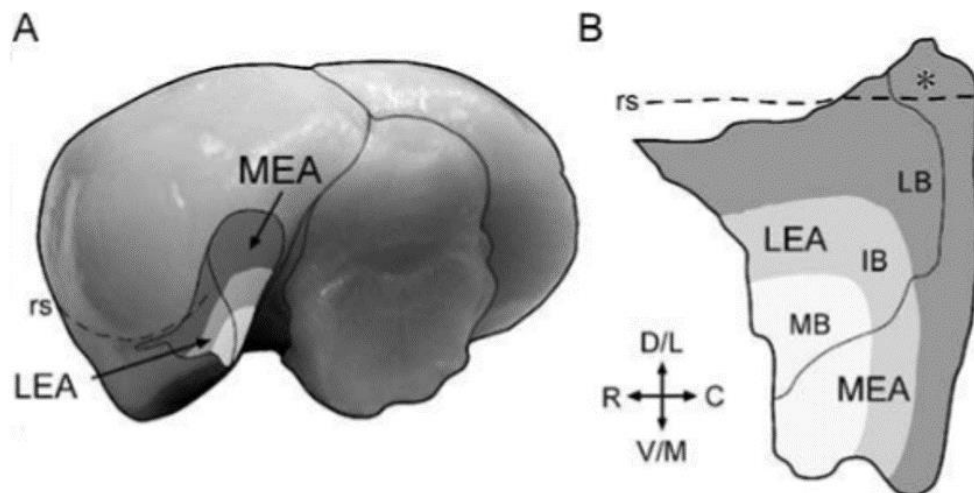
Figure 1.2: The entorhinal cortex in the rat. A: Ventral posterior view of the rat brain with the cerebellum removed. A schematic overlay shows the position of the lateral (LEA) and the medial (MEA) areas of the entorhinal cortex. In each panel, the lateral band (LB) is shown in dark grey, the intermediate band (IB) in medium grey, and the medial band (MB) in light gray. B: An unfolded map of the pial surface of the entorhinal cortex. The asterisk is located in the dorsocaudal MEA, the location in which grid cells have been described. Other abbreviations: C, caudal; D, dorsal; L, lateral; M, medial; R, rostral; rs, rhinal sulcus; V, ventral. (Adapted from Kerr et al. 2007).

1.2.2.1 Hippocampal connections of the MEC

The EC has prominent reciprocal connections with the HC and acts as a gateway between this structure and the neocortex. In fact, almost half of the afferent inputs to the MEC arise

from other areas of the hippocampal system, with the heaviest input being from the parahippocampal region. Specifically, the three main MEC afferents arise from, in order of strongest connectivity, the caudal parasubiculum, dorsal presubiculum and postrhinal cortex, and are directed to the lateral portion of the MEC. Afferents from the hippocampal formation also exist though are not as strong as from the parahippocampal region. They include the dorsal CA1 field, which projects to the lateral MEC, and the ventral CA1 and subicular area, which have inputs to the medial MEC (Canto et al., 2008, Witter and Amaral, 2004).

The MEC also has efferent connections to the hippocampal system. The strongest projections arise in the lateral and intermediate bands of the MEC and input heavily to areas of the hippocampal formation, including the dorsal dentate gyrus and dorsal CA1 field. These bands of the MEC also have connections to other areas of the hippocampal formation, though are less prominent, and include the ventral HC, dentate gyrus, fields CA3 and CA1 and the subiculum. However, as with the MEC afferent inputs, efferent connections from the MEC are much stronger to the parahippocampal region. All connections arise in the medial and intermediate bands of the MEC and preferentially input to the perirhinal, although the postrhinal connection is also strong. Moderate efferent outputs from MEC also project from the pre- and parasubiculum (Witter et al., 2017, Canto et al., 2008).

The main connectional route from the EC to the HC is via the perforant pathway (Cajal, 1893). This unidirectional pathway predominantly arises from stellate neurones (SC) in LII of the MEC, although a minor component comes from LV and LVI (Steward and Scoville, 1976, Köhler, 1985). Axons project to the middle third of the molecular layers of the dentate gyrus, where 85% of the total synapses originate from the EC. Their primary contacts are excitatory and are on the dendritic spines of dentate granule cells (DGC), carrying highly processed polymodal sensory information (Hjorth-Simonsen and Jeune, 1972).

The perforant pathway is the first relay of the tri-synaptic loop, a polysynaptic circuit with a well-established role in information processing, and consists of: 1) the perforant pathway

(above), 2) the mossy fibre pathway, where DGCs project via their axons (the mossy fibres) onto the proximal apical dendrites of CA3 (PC) neurones, 3) the Schaffer collateral-commissural pathway, consisting of CA3 (and contralateral CA1) PCs synapsing onto CA1 pyramidal cells. The loop is completed when outputs from the CA1 return to the MEC, via the subiculum where they terminate in LV (Witter, 2007).

The final pathway to mention is the temporo-ammonic input to the hippocampal CA1 field. Here, the distal apical dendrites of CA1 pyramidal neurones receive information directly from LIII cells of the EC, forming a one-to-one, monosynaptic connection. The pathway originates from pyramidal neurones in LIII and terminates on CA1 neurones. A similar pathway originating from LII of the MEC, which terminates directly on pyramidal neurones in CA3, has also been identified (Hjorth-Simonsen and Jeune, 1972, Steward, 1976). Entorhinal fibres most often synapse on the spines of dendrites on excitatory principal cells, though they also form both excitatory and inhibitory synapses on the dendrites of interneurones (Baks-te Bulte et al., 2005, Kajiwara et al., 2008).

1.2.2.2 Cortical and sub-cortical connections of the MEC

One fifth of the total afferent inputs arise from the neocortex either directly, or indirectly via the perirhinal cortex. The perirhinal and parahippocampal (postrhinal, for rodent cortices (Koganezawa et al., 2015)) provide the main cortical links to the EC (Van Hoesen and Pandya, 1975). Other inputs to the MEC include those from the pre- and parasubiculum (Caballero-Bleda and Witter, 1993), as well as from olfactory related structures, such as the olfactory bulb and the anterior olfactory nucleus. The piriform and other cortices related to sense of smell dominate input to the superficial layers of the MEC, which is reciprocated by similarly strong outputs from the MEC to the olfactory domains. Cortical inputs to the MEC also arise from frontal (Kondo and Witter, 2014), cingulate, retrosplenial, insular, parietal and visual areas. Superficial layers of the lateral MEC also receive moderate input from the orbitofrontal cortex (Kondo and Witter, 2014), postrhinal cortex (Koganezawa et al., 2015) and pre- and parasubiculum (Caballero-Bleda and Witter, 1993).

As already mentioned, afferents to the MEC are largely distributed to the superficial layers. Interestingly, there is a growing body of evidence suggesting these inputs are also

influencing neurones in LV MEC, as well as the superficial layers, suggesting that LV could be acting as an integrator of EC inputs (Canto and Witter, 2012). In fact, many other cortical inputs have been shown to project to LV from regions such as the infralimbic, prelimbic and retrosplenial cortex, as well as from the visual cortex (Olsen et al., 2017).

Cortical efferents are widespread and are mainly represented by return reciprocal afferent connections to the MEC. It is important to note that most entorhinal to cortical projections arise from pyramidal neurones from LV of the MEC, although the infralimbic and olfactory structures have additional projections from LII and LIII (Vertes, 2004).

Sub-cortical connectivity of the MEC has also been identified in areas such as claustrum, amygdala, basal ganglia, thalamus, hypothalamus and brainstem. However, by far the strongest efferent connection is to the basal ganglia, specifically the caudate-putamen and, to a lesser extent, the nucleus accumbens (Insausti et al., 1987). There is evidence for these connections arising from both LII and LV of the MEC (Pereira et al., 2016). Reciprocal connections between the amygdala and the MEC are also evident, with most studies pointing towards amygdala afferents terminating in LIII, and return projections originating in cells from LV (McDonald, 1998). Finally, thalamic and hypothalamic sub-cortical connections have also been identified in the MEC, although details about these pathways are not yet unravelled (Kerr et al., 2007).
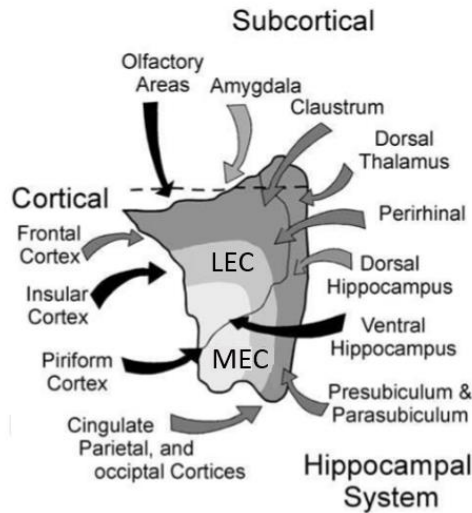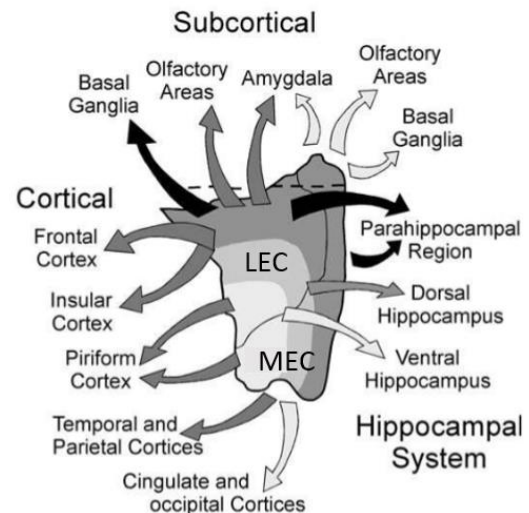
Figure 1.3: Summary of the major connections of the LEC and MEC. *Strong, moderate and weak connections are indicated by black, dark grey and light grey arrows, respectively. This thesis focuses on the MEC only.*

1.2.3 Intrinsic organisation and morphology of the MEC

The entorhinal network comprises elements receiving input and providing output, but also elements contributing to its intrinsic organisation. As mentioned, the EC can be divided into 6 layers, although LIV (lamina dissecans) is acellular and often referred to as the plexiform layer, which separates the deep and superficial layers. Similarly, LI contains mostly fibres and few neuronal cell bodies. The cells that do reside here are either spinous multipolar or horizontal cells with local connections. The remainder of this section will focus on the layers central to this thesis, namely LII and LV.

1.2.3.1 Layer II morphology

The first description of MEC neurones was published in 1933 when Lorente de Nó used the 'Golgi' stain to determine their morphology (Bard, 1933). Since then, much effort has gone into defining the intrinsic organisation of the MEC. LII is densely packed with large and medium sized pyramidal cells (PCs) and stellate cells (SCs), which are defined chemically with calbindin and reelin positive staining, respectively (Winterer et al., 2017). However, intermediate PCs (IMPC) and SCs (IMSC) that show combinations of co-expression of

calbindin and reelin have also been identified and classified into separate subgroups. IMSCs are all reelin positive with a few sub-types also co-expressing calbindin. IMPCs are generally calbindin positive but more diverse variations can include reelin positive, as well as calbindin and reelin positive co-expression (Witter et al., 2017). These four sub-groups of excitatory principal neurones in the MEC appear to have distinct individual electrophysiological profiles (Fuchs et al., 2016, Canto and Witter, 2012).

SCs are the most abundant cell type in LII, residing preferentially in the superficial and middle area of the layer. Their defining morphological characteristics include the presence of multiple, and roughly equally sized, primary spiny dendrites with wide reaching branches, often projecting to the dentate gyrus via the perforant path. PCs are so called due to their triangular, or pyramidal, shaped soma, and seem to reside in the deep parts of LII. They possess a prominent, thick and long spiny apical dendrite branching at the border of LI, and thin and short basal dendrites which branch at the border of LIII (Klink and Alonso, 1997). SCs and PCs can also be defined in terms of their electrophysiological profiles. SCs display prominent sag potentials mediated by a hyperpolarising current (I_h) (Jones, 1994) along with intrinsic theta-like (4-10 Hz) membrane potential activity and resonance properties that are not evident in PCs (Pastoll et al., 2012, Burgalossi and Brecht, 2014).

Inhibitory interneurons present in LII can be classified into three main sub-groups: parvalbumin (PV), somatostatin (SOM) and 5-HT3a expressing cells (Rudy et al., 2011). By far the most abundant are the PV containing basket cells, which constitute about half of the total interneurone population. PV-containing interneurones innervate and surround both reelin and calbindin positive principal cells, and have fast-spiking physiological profiles (Jones and Bühl, 1993, Armstrong et al., 2016). Interestingly, a clear gradient of PV staining is apparent in the MEC, with stronger expression in portions close to the rhinal fissure compared to ventral portions. SCs receive strong local inhibition from presynaptic PV-positive interneurones, and the dorsal-ventral inhibitory gradient has major implications for changing network oscillations along this axis (Beed et al., 2013). Another sub-type of basket cell present in LII expresses cholecystokinin (CCK), and falls under a sub-group of the 5-HT3a category of interneurone. These interneurones preferentially innervate calbindin-positive principal cells. Generally, basket cells have a small, spherical cell body, sparse spiny

dendrites, and an extensive axonal arbor, which appear to be confined to LII (Klink and Alonso, 1997). They form complexes around the cell somas of principal neurones, which they locally inhibit.

The second type of interneurone commonly found in LII is the called chandelier cell, reflecting the specific shape of its axon arbor. These are also PV-positive but are defined morphologically by vertical, as well as horizontal, aggregations of axonal boutons, known as 'candles'. Chandelier axon branches are confined to LII and LIII of the MEC and synapse onto the initial segments of principal cells (Soriano et al., 1993).

There is limited and conflicting knowledge available on the distribution of SOM interneurones in the MEC, although immunoreactivity experiments do confirm they are present in LII (Wouterlood and Pothuizen, 2000). In terms of morphology, they are generally multi-polar and have a low threshold for spiking.

Lastly, there are many interneurones in sub-groups of the 5-HT3a group that reside in LII. They have diverse morphological and physiological profiles and include: calretinin-, Vasoactive intestinal peptide (VIP) and CCK-expressing cells (Witter et al., 2017).

1.2.3.2 Layer II intrinsic organisation

The SC microcircuit in the superficial layers of the MEC has been well-established using *in vitro* patch clamp techniques. Interestingly, it appears that communication between SCs is not through monosynaptic connections, but via an intermediate inhibitory interneurone (Couey et al., 2013). In this network, activation of one or more SCs leads to inhibitory currents in neighbouring SCs, a mechanism which seems to be mediated by PV-containing interneurones (Buetfering et al., 2014). Similarly, PCs in LII have sparse monosynaptic connections, and generally communicate via inhibitory interneurones, though in this case, exclusively from the 5-HT3a expressing population (Fuchs et al., 2016). As such, inhibition dominates the microcircuits of SCs and PCs in LII (Berretta and Jones, 1996, Greenhill et al., 2014, Woodhall et al., 2005).

Information on the connectivity between PCs and SCs themselves is limited and conflicting. Some experimental evidence points towards minimal recurrent excitatory connectivity between SCs and PCs (Couey et al., 2013, Pastoll et al., 2013a, Fuchs et al., 2016). This would be indicative of two independent microcircuits in LII of the MEC, whereby the information relayed by SCs to the dentate gyrus is processed separately from the information relayed to downstream areas, such as the CA1, by PCs. On the other hand, a recent study, using eight simultaneous patch clamp recordings, suggests there is a prevalent feed-forward excitation from PCs (in both LII and LIII) onto SCs in LII of the MEC (Winterer et al., 2017). Nevertheless, more work is needed to identify the functional implications of the remarkable cellular diversity of LII, including the roles of intermediate PCs and SCs in the MEC network, as its plausible they could be co-ordinating the two microcircuits (Witter et al., 2017).

1.2.3.3 Layer V morphology and intrinsic organisation

It is generally accepted that LV of the MEC can be further sub-divided into LVa and LVb due to their differing molecularly defined circuitry. LVa lies adjacent to LIV (lamina dissecans), and is therefore more superficial than LVb. LVa is mainly comprised of large neurones with rounded somata, known as superficial PCs, which can be further sub-divided depending on their basal dendritic trees: multidirectional or horizontal sparsely spiny (Lorente de No, 1933, Canto and Witter, 2012). Superficial PCs generally have one distinct spiny apical dendrite that reaches towards the pial surface, firstly branching close to the soma, sometimes extending into the lamina dissecans, before extending up to LII and LI. The basal dendritic tree is spiny to sparsely spiny and extends in all directions in LV, and occasionally LVI (Canto and Witter, 2012).

Deep PCs residing in layer Vb, on the other hand, have smaller somata and a sparsely spiny apical dendrite that extends to the pia, branching profusely in LV, LII and LI. Basal dendrites generally leave the soma in all directions, and project deeper towards LVI.

The third type of neurones found in LV, generally LVb, are bipolar PCs with spindle-like somas. They possess a sparsely spiny apical dendrite that branches near the soma and continues to branch along the way to LI, where they display an apical tuft.

The last morphological neurone group consists of multipolar and horizontal principal cells, the latter comprising a distinctive polygonal shaped soma. They both have sparsely spiny dendritic trees that are mainly confined to the deep layers, avoiding the superficial layers. Whereas multipolar PCs have dendrites that are of a similar length spreading in all directions, horizontal cells have one main dendrite which spreads horizontally to the border with, and often extending into, LVI. Of note, any LV pyramidal neurones located near the border of the parasubiculum have the potential for their dendrites to extend into this area (Canto and Witter, 2012).

The different molecularly defined circuitry in LVa and LVb also reveals input-output segregation. Layer Va principal neurones appear to be the major outputs projecting to diverse cortical and sub-cortical structures, whereas LVb principal neurones are selectively targeted by outputs originating from the hippocampus, specifically the CA1 field and the subiculum, as well as from LVa, LIII and LII of the MEC itself. The principal neurones in LII that project to LVb of the MEC have been identified as reelin-positive SCs. These cells are ideally suited to integrate inputs from the superficial MEC and the hippocampus, as well as forming a major component of the intrinsic deep to superficial circuits (Sürmeli et al., 2015, Witter et al., 2017). Generally, inhibitory interneurones are sparsely distributed in LV MEC, which contributes to the weak overall synaptic inhibition in this layer compared to more superficial layers (Woodhall et al., 2005, Greenhill et al., 2014).

The electrophysiological profiles of neurones in the deep layers of the MEC are less understood, but they appear to have a notably high input resistance compared to all other layers, reflecting low conductance and therefore an increased amount of closed channels (Fransén, 2010, Jones and Woodhall, 2005, Dhillon and Jones, 2000) . The deep layers also show much less grid cell activity, and no theta modulation, compared with LII neurones (Burgalossi et al., 2011).
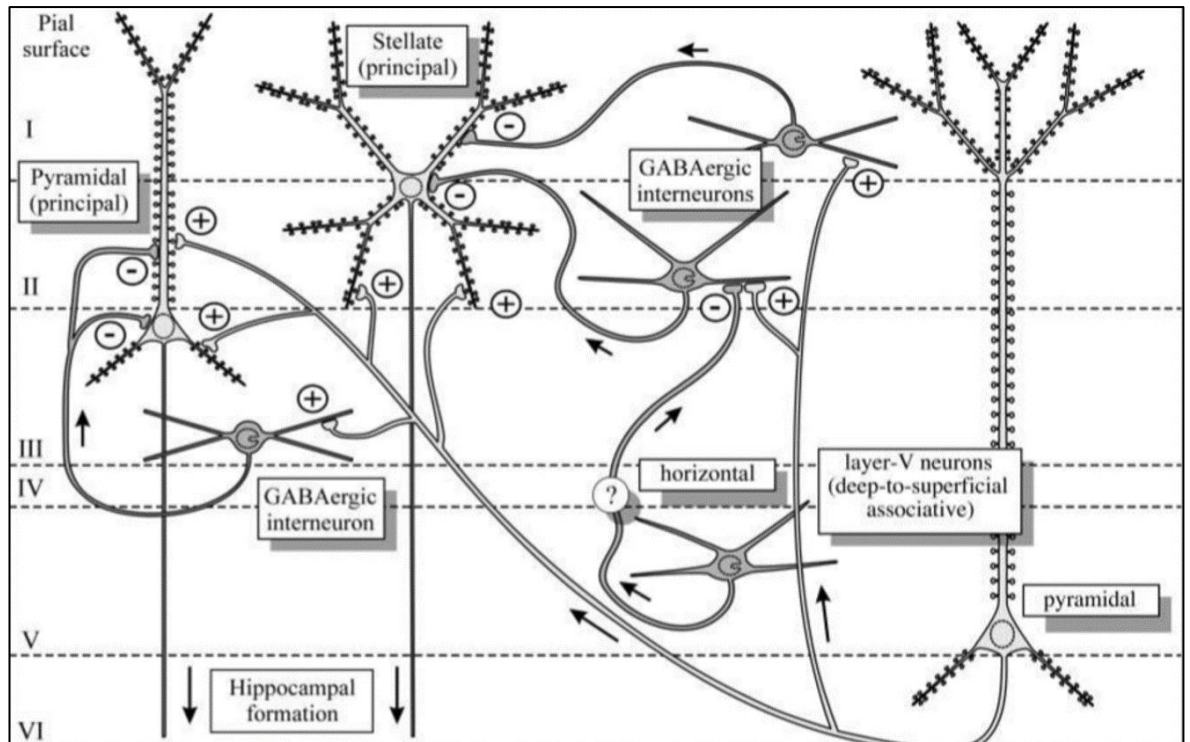
Figure 1.4: Connectivity of the EC. Diagram depicts the different cell types and morphology of each layer of the MEC, along with their intrinsic connectivity. Principal neurones are largely pyramidal neurones in LIII and LV, whereas SCs reside in LII MEC. Superficial layers are subject to increased inhibitory control. Adapted from (van Haeften et al., 2003).

1.2.4 The EC in memory

One of the first associations between the EC and cognition, particularly memory, was made by surgeon Wilder Penfield in 1937. During neurosurgery in patients with TLE he observed that with mild stimulation of the medial temporal lobe (MTL), patients could recall precise personal experiences that had previously been forgotten (Penfield and Boldrey, 1937). The second association came from the famous patient, H.M, who became severely amnesic following an experimental bilateral medial temporal lobectomy (including the EC), to treat incapacitating and refractory seizures (Penfield and Milner, 1958). It was striking that although declarative memory formation (conscious, intentional recollection of factual information, previous experiences and concepts) was severely impaired, all other cognitive functions were retained, including general intelligence and perception, suggesting memory is a distinct cerebral function (Scoville and Milner, 1957). These studies heralded the modern era of memory research.

The MTL consists of the perirhinal cortex, parahippocampal cortex and the hippocampus. Recent evidence from neuroimaging and fMRI studies has shown that these structures, including the EC, engage with many aspects of memory, including memory encoding and retrieval (Kirwan and Stark, 2004, Bellgowan et al., 2009), as well as associative learning (Hargreaves et al., 2012), episodic (Maass et al., 2014) and working memory (Schon et al., 2016). Hence, at an anatomical level we can associate the EC with cognition, but a functional representation of cognition at the molecular level is not yet fully understood. Despite this, certain observable phenomena at the synaptic and network level are thought to be important.

Donald Hebb initially formulated the conception of synaptic plasticity, a rule whereby neuronal assemblies are brought together on the basis of temporal relations among them (Morris, 1999). Essentially, activity-dependent changes in the strength of synapses are thought to provide a cellular basis of learning and memory. Still, single synapses cannot be viewed in isolation because neurones are a part of an extensive network with co-ordinated, or synchronised, patterns of activity. Synchronised neuronal activity is known as a network oscillation and is thought to be intimately involved in the formation of new memories, though the exact mechanisms are still debated. Nevertheless, a recent study has shown a particular oscillation (gamma frequency, also found in the EC) strengthens excitatory synapses in the hippocampus, allowing future signals to be transmitted more easily (Zarnadze et al., 2016). This provides insights into how synaptic strengthening and synchronised network activity could underlie memory formation in the EC, through synaptic plasticity mechanisms such as long-term potentiation.

1.2.5 The EC in spatial navigation

The EC has recently been recognised as a fundamental contributor to the process of spatial navigation (Squire and Zola-Morgan, 1991, O'Keefe and Dostrovsky, 1971, Hafting et al., 2005). In 2005, grid cells were discovered in the MEC. These cells fire at similar spacing and orientation in response to location in an environment (Hafting et al., 2005). The distinctive firing pattern of grid cells supports the role of the MEC in the representation of space, and

is thought to arise from neural dynamics that depend on the local microcircuitry (Winterer et al., 2017).

The representation of space is not achieved by grid cells alone, but multiple functional cell types. The first spatial cell type to be described was found in the adjacent hippocampus, called the 'place' cell, discovered by John O'Keefe in the 1970s in freely moving rats (O'Keefe and Dostrovsky, 1971, O'Keefe, 1976). These cells fire selectively when animals are at a specific location in the environment. The discovery of grid cells in the MEC, one synapse upstream of place cells, came 30 years later by Edvard and May-Britt Moser in 2005, who also identified other spatial selective cells in the MEC including head-direction and border cells (Hafting et al., 2005, Sargolini et al., 2006, Giocomo et al., 2014). Unlike place cells, which change their firing fields unpredictably in differing environments, grid cells maintain their positional relationship and therefore act as a metric of local space, reflecting the structure of that space independently of specific contextual details about the environment itself (Fyhn et al., 2007, Moser et al., 2008). Although grid cell firing patterns are fixed between environments, the spacing of the grid does increases topographically along the dorsal-ventral axis of the MEC, mirroring the scale expansion also observed in place cells in the hippocampus (Hafting et al., 2005, Brun et al., 2008, Jung et al., 1994). The discovery of these cells garnered attention to the EC beyond the neuroscientific community when John O'Keefe, May-Britt Moser and Edvard Moser won the Nobel Prize in Physiology and Medicine, in 2014.

Information about the development of grid cell firing patterns is mainly theoretical. However, *in vivo* experiments have shown that the firing fields of neighbouring grid cells share similar spacing and axes of orientation, suggesting these patterns are interdependent and mediated by the local microcircuit (Couey et al., 2013). Moreover, computational studies on the development of grid cell firing fields hypothesise the involvement of an attractor network, with specific local connectivity of both excitatory and inhibitory connections (Burak and Fiete, 2009).

Grid cells are principal neurones residing mainly in LII of the MEC, and can be either PCs or SCs (Tang et al., 2014, Pastoll et al., 2012). Recent studies aiming to delineate microcircuits

of the MEC suggest that calbindin-positive grid cells (mainly PCs) tend to cluster into islands, arranged in a hexagonal grid, and often project to the CA1 field of the hippocampus. Conversely, calbindin-negative border cells (mainly SCs) are homogenously distributed throughout layer II, avoiding the islands, and propagate spatial input to the dentate gyrus. Moreover, PC discharges showed over two-fold stronger spike locking to the theta oscillation compared with SCs (Ray et al., 2014). This is suggestive of two distinct principal cell networks contributing to grid cell activity in LII MEC.

The mechanisms underlying the brains representation of space are more recently being linked to those underlying memory formation and sensory processing (Doeller et al., 2010, Eichenbaum and Cohen, 2014). Buzsaki and Moser (2013) identified parallels between declarative memory and navigation, suggesting they could share the same fundamental mechanism, providing an overarching functional picture of the hippocampal formation (Buzsaki and Moser, 2013). In addition, studies on patients with EC deficits show not only memory, but also spatial impairment, often coexistent with abnormal oscillatory activity. Again, until recently, these lines of research have been studied separately, but are beginning to converge (Buzsaki and Moser, 2013).

1.2.6 The EC in CNS disorders.

1.2.6.1 Epilepsy

The EC is commonly implicated in the pathology of TLE, which is a chronic, debilitating neurological disorder affecting over 65 million people worldwide. It can be caused by numerous factors including genetic mutations, developmental disorders or by an insult to the brain, although the majority of cases are idiopathic/cryptogenic (Banerjee et al., 2009). The primary characteristic of epilepsy is the onset of recurrent spontaneous seizures that arise due to aberrant changes in neuronal activity, involving massively increased synchronisation of neuronal firing. Epilepsy can be subdivided into over 40 different syndromes, of which, TLE is the most common form. There is currently no known consistent mechanism underlying the various epilepsies, but decades of experimental work conclude that, in the broadest sense, it arises due to an imbalance of the normal excitation and inhibition within the neuronal network (Staley, 2015). With the multitude of ways the CNS

acts to maintain this balance, including at the level of ions, neurones, synapses and networks, an overarching mechanism for epilepsy may not be feasible. However, the imbalance in excitability is exemplified with clinical examples such as the marine toxin, domoic acid, and the pesticide, strychnine, which act to increase excitation, and decrease inhibition, respectively, both resulting in the generation of seizures (Jett, 2012). Currently available treatments broadly act to equalise the imbalance within the network. Whilst this approach is effective, around 30% of patients are refractory to treatment, so there remains a clinical need for a novel pharmacological target in this disorder (Laxer et al., 2014).

In cases of TLE where treatment is refractory, a partial temporal lobectomy is carried out as a last resort to remove the epileptogenic tissue. Interestingly, retrospective studies suggest that removal of the EC is correlated to a good postoperative outcome, and studies on resected tissue from patients with TLE have identified significant atrophy of the EC (Bonilha et al., 2007, Siegel et al., 1990). Moreover, a number of MRI studies have identified significant atrophy in the EC in patients with TLE (Bernasconi et al., 1999, Bernasconi et al., 2001, Salmenperä et al., 2000).

Many animal models of epilepsy (see (Löscher, 2017), which are required for the identification of novel therapeutic agents, have also identified the EC as the site of initiation and maintenance of epileptiform activity (Lopantsev and Avoli, 1998, Avoli et al., 2002, Ben-Ari et al., 1981, Walther et al., 1986, Jones and Lambert, 1990). Rat models have implicated both LII and LV as having an increased susceptibility to epileptiform activity, due to reduced inhibition and increased excitability, respectively (Kobayashi et al., 2003, Bragin et al., 2009, Greenhill et al., 2014).

Although the underlying pathology of TLE is unclear, one possibility is that the brain recapitulates developmental processes, inappropriately, in the adult brain (Scharfman, 2007, Ben-Ari, 1985, Represa et al., 1990, Yang et al., 2006). This could lead to changes in expression of proteins that control this delicate balance between excitation and inhibition, and even create new synaptic connections. Essentially, the resulting enhanced connectivity could lead to a hyper-synchronous state and the onset epileptiform activity.

A common animal model of epilepsy uses the drug KA, a potent excitotoxin, which activates KARs. KARs are heavily implicated in the synchronisation of neuronal network activity and the pathophysiology of TLE, and will be discussed in section 1.3.

1.2.7 The EC in development

1.2.7.1 Embryonic development

During early embryonic development of the human brain, three primary brain structures are formed: the prosencephalon (forebrain), the mesencephalon (midbrain) and the rhombencephalon (hindbrain). From the forebrain, two structures develop: the telencephalon and the diencephalon (Roxo et al., 2011). The dorsal telencephalon eventually develops into the cerebral cortex consisting of the more familiar cortices: frontal, parietal, temporal and occipital. The main functions of the cortex can be characterised as sensory, motor or associative. The neocortex constitutes the majority of the cerebral cortex, but the smaller, and phylogenetically oldest, area of the cerebral cortex is called the 'allocortex'. The EC is a subdivision of the allocortex known as the periarchicortex, a transitional, non-neocortical zone between the allocortex and the neocortex. It is distinguished morphologically from the typical six layers of neurones in the neocortex by its lack of a true cellular layer IV (Greene, 1996). It is located in the medial temporal lobe and is curved around the rostral surface of the hippocampus, a structure that is also intricately involved in memory processing. The anterior, inferior and lateral surfaces of the EC are surrounded by the perirhinal cortex, which is a structure that receives highly processed sensory information regarding visual perception and memory (Devlin and Price, 2007, Murray and Richmond, 2001). Indeed, sensory information does not directly penetrate the allocortex, but arrives via the thalamus or neocortex.

1.2.7.2 MEC microcircuitry development

An eloquent study detailing a temporal profile of maturation across the EC-hippocampal circuit was published earlier this year (Donato et al., 2017). Using pharmacogenetic approaches, this study described a linear, uni-directional developmental sequence whereby excitatory activity was critical for the maturation of downstream areas of the EC-

hippocampal network. This excitation originated in LII, and the progression of maturation followed, a recapitulation of information flow in adult circuits, from: LII MEC, CA3, CA1, dentate gyrus, subiculum, LV MEC and LEC and finally LII LEC. Remarkably, the excitation stemming from LII MEC originated specifically from SCs, which are the first cell type to develop to maturity in this region. Cell-type specific silencing of LII SCs, and not PCs, prevented the maturation of the rest of the EC-hippocampal circuit, indicating that instructive excitatory activity originates from these cells. The functional maturation of pyramidal neurones is delayed compared with SCs. Interestingly, the maturation of SCs themselves was independent of local excitation, but correlated with the birth date of the cell, functioning as an "autonomous" (genetic) intrinsic driver of neurogenesis at the top of the developmental hierarchy. These targets subsequently exert an excitatory driving force onto downstream areas, resulting in a stage-wise maturation of the EC-hippocampal network (Donato et al., 2017). The precise nature of the excitatory instructive signal is unknown, but is suggested to involve large-scale oscillatory calcium waves which have been observed in the immature cortex (Garaschuk et al., 2000, Goodman and Shatz, 1993).

The developmental progression of neurogenesis and maturation follows a gradient along the dorso-ventral axis of the MEC. Microcircuits mature first in the dorsal MEC, followed by the ventral MEC, where smaller and larger spatial scales are represented by grid cells, either SC or PC with the latter presenting at around the onset of exploratory behaviour (Ray and Brecht, 2016). Interestingly, local inhibitory circuits in the MEC also follow a gradient along the dorso-ventral axis, specifically regarding inhibitory inputs onto SCs, imposing a strong regulatory role on these cells. It appears that the dorsal MEC (with smaller spatial scales) is under greater inhibitory control compared to the ventral MEC (with larger spatial scales) (Beed et al., 2013). Inhibitory GABAergic neurotransmission also contributes to the maturation of the cortex, with roles in plasticity and network activity during pre- and post-natal development, acting to pace immature networks. Accordingly, aberrant maturation of inhibitory mechanisms has been implicated in the aetiology of many neurodevelopmental disorders, including autism and schizophrenia (Le Magueresse and Monyer, 2013).

The development of MEC microcircuits is currently receiving much attention after the discovery of grid cells, because this area represents one of the first examples where we can begin to understand how network topology directly supports higher cognitive functioning. This thesis will contribute to this work by carrying out a comprehensive electrophysiological profile of both excitatory and inhibitory neurotransmission in principal cells, during development, in LII - at the top of the developmental hierarchy, and LV - near the end of the developmental hierarchy.

1.2.7.3 Relevance to human brain development

Ontogenetic characteristics of brain development are shared among mammalian species. For example, adolescence appears to be a highly conserved developmental stage and species share many similar neurobehavioural and physiological characteristics. This supports the use of animal models as tools in studies of human brain development and associated diseases (Spear, 2004). In general, adolescence is the period of transition from childhood to adulthood, not to be confused with puberty, which refers to the attainment of sexual maturity. Comparing stages of development in rodents and humans can be variable, but generally there is a consensus that peak adolescence in rats occurs at ~4-5 weeks old, correlating to roughly 12-18 years old age span in humans (Spear, 2004).

The rat brain has no direct correlate to the human medial temporal lobe. As such, the rat EC is located at the most caudal, ventral and lateral aspects of the brain. It can be sub-divided into the lateral EC (LEC) and MEC based upon their different functional architecture. For example, functional studies show that the MEC significantly contributes to spatially specific information, whereas neurones in the LEC are more heavily, but not strictly, implicated in non-spatial processes, though these aspects likely work together (Van Cauter et al., 2013, Save and Sargolini, 2017).

1.3 Kainate Receptors

The existence of a new type of glutamate receptor emerged from the discovery of KA, a potent excitotoxin. The word 'kainic' is derived from the word *kaininso,* meaning 'the ghost of the sea', as it was first isolated from the seaweed *Digenea simplex* in 1953. The excitatory and neurotoxic actions of KA were recognised by the mid-1970s, and the hypothesis that KA was acting on a specific set of receptors was made (J C Watkins and Evans, 1981). It was not until the early 1990s that KARs were shown to indisputably exist after the cloning of KAR subunits (Bettler et al., 1992, Hollmann and Heinemann, 1994), and the identification of the first KAR subunit gene (Bettler et al., 1990). These break-through discoveries formed the foundation upon which much progress understanding the biophysical and functional properties of KARs has been made over the last two decades.

We now know KARs are expressed ubiquitously in the central nervous system (CNS) and respond to the endogenous agonist, glutamate. Unusually, they can act both ionotropically, through the action of ion channels, and metabotropically, through the action of G-proteins. The metabotropic mechanism of KARs is not well understood and is still somewhat controversial, but appears to involve the activation of G-proteins and second messenger pathways involving protein kinase C or phospholipase C. For example, KARs have been shown to downregulate GABA release from hippocampal CA1 interneurones via a pertussis toxin-sensitive metabotropic process (Jin and Smith, 2007). Intriguingly, a more recent study revealed a role for postsynaptic KARs in the induction of a type of functional and structural plasticity in the hippocampus, which was also attributed to a metabotropic action (Petrovic et al., 2017), also see (Rodrigues and Lerma, 2012) for a full review.

However, KARs are most commonly associated with an Ionotropic mechanism. Ionotropic glutamate receptors (iGluRs) are ion channels that open in response to glutamate binding and are permeable to Na^+, K^+ and (depending on the receptor) Ca^{2+}. There are three classes of iGluRs based on their sequence homology and preferred agonist: N-methyl-d-aspartate (NMDAR), α-amino-3-hydroxy-5-methyl-4-isoxazolepropionate (AMPAR), KA (Traynelis et al., 2010). Knowledge of the role of KARs has lagged behind the other subtypes due to a

paucity of good specific pharmacological tools to study them, but recent advances have meant that the field is catching up quickly.

1.3.1 Structure and characterisation of KARs

KARs have a tetrameric conformation formed from a combination of five subunits: the low affinity GluK1-3 and the high affinity GluK4/5. The GluK1-3 subunits can form functional homomeric receptors whereas the GluK4 and GluK5 subunits must co-assemble with their lower affinity counterparts, GluK1-3, to form functional heteromeric complexes.

Different subunit compositions can influence glutamate sensitivity, for example, homomeric GluK1 or GluK2 KARs have a low affinity to glutamate (EC50 ~ 100-200 µM range). Addition of the high affinity subunits, GluK4/5, to form heteromeric KARs increases glutamate sensitivity 3-50x. A summary of the known glutamate sensitivities at recombinant KARs with various subunit combinations can be seen in the table below.

	GluK1	GluK2	GluK3	GluK4	GluK5
GluK1	47 ± 4 (Alt et al., 2004)	48 ± 7 (Alt et al., 2004)	-	-	19 ± 1 (Alt et al., 2004)
GluK2	-	9 ± 1 (Alt et al., 2004)	-	-	8 ± 1 (Alt et al., 2004)
GluK3	-	-	5900 (Schiffer et al., 1997)	-	-

Table 1.1 Glutamate activity at recombinant KARs. *EC50 (µM) values ± SEM obtained from published data. Alt et al (2004) determined agonist-induced calcium influx in HEK293 cells expressing human KARs. Schiffer et al (1997) (Schiffer et al., 1997)determined EC50 values from HEK293 cells expressing rat GluK3a KARs.*

The GluK1 subunit is highly expressed in the developing brain with potential roles in the maturation of neurones, at least in the hippocampus (Lauri et al., 2005, Lauri et al., 2006). The GluK2 subunit has most commonly been associated with post-synaptic responses at the most fiber-CA3 synapse, also in the hippocampus. It is widely expressed in the brain, and most commonly forms a heteromeric structure with GluK5 (Perrais et al., 2010). On the

other hand, the GluK3 subunit often forms heteromeric complexes with GluK2 with low glutamate sensitivity, and are thought to contribute to presynaptic KAR activity (Pinheiro et al., 2007). GluK4 is expressed mainly in the hippocampus whereas GluK5 is ubiquitously expressed in the brain. Both subunits must form heteromers with GluK1-3, and in doing so they can dramatically change the functional and pharmacological properties of recombinant receptors, such as an increase in glutamate sensitivity and slower deactivation and desensitisation kinetics (Mott et al., 2010, Fisher and Mott, 2011). All subunits contain an agonist binding site and therefore has the ability to influence channel activation and gating properties (Fisher and Fisher, 2014).

All five subunits share some sequence homology with both AMPAR (~30%) and NMDAR (~10%) subunits. The GluK1 KAR subunit was the first to be cloned in 1990, displaying ~40% sequence homology with the GluR1 AMPAR, but with a significantly increased affinity for KA over AMPA (Bettler et al., 1990, Sommer et al., 1992). The cDNA of the GluK2 and GluK3 subunits were subsequently cloned, showing 75-80 % sequence homology with the GluK1. When expressed as homomeric receptors in *Xenopus* oocytes they were activated by KA, but not by AMPA, and also showed a higher affinity for KA than for AMPARs (Egebjerg et al., 1991, Bettler et al., 1992). Finally, the cDNA of two further KAR subunits were identified in 1992, which are now referred to as GluK4 and GluK5 (previously KA1 and KA2), and show 68 % sequence homology to each other. Unlike GluK1-3, these subunits are unable to form functional homomeric structures when expressed in heterogenous systems, however, co-expression with GluK1/2 produces channel activity with novel pharmacological properties (Herb et al., 1992). The GluK4/5 subunits are also unable to form heteromeric structures with AMPAR subunits and, again, show little to no affinity for AMPA (Wenthold et al., 1994).
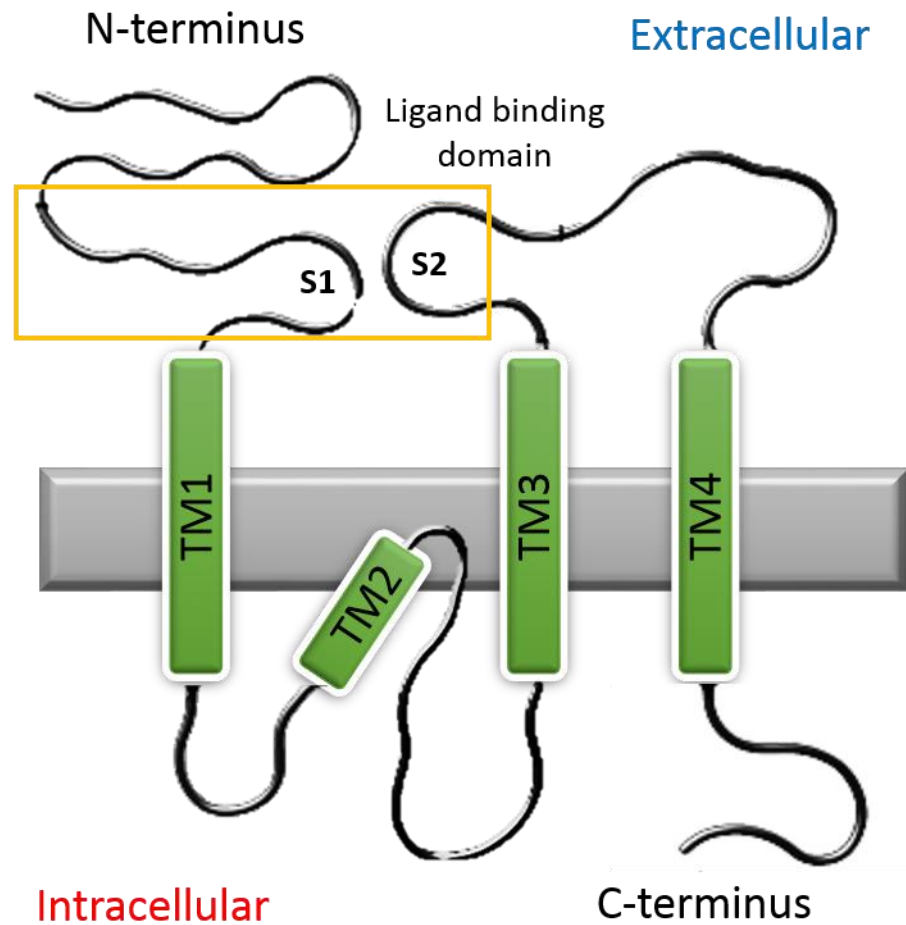
Figure 1.4: Schematic representation of the general structure of an ionotropic glutamate receptor subunit. *The S1 and S2 domains form the ligand binding domain.*

The precise topology of the iGluRs in the plasma membrane was determined by two groups in 1994, both reporting a secondary structure distinct from that of other ligand gated-ion channels, with each subunit consisting of a large extracellular N-terminus, a transmembrane domain (TM1), re-entrant loop (TM2), another transmembrane domain (TM3), a large extracellular loop, and a final transmembrane domain (TM4), followed by a cytoplasmic C-terminal domain (Wo and Oswald, 1994, Hollmann et al., 1994). TM2 is composed of hydrophobic residues that dip into the membrane forming a hairpin-like structure. Two discontinuous segments of approximately 150 amino acid residues each, one before the TM1 domain (S1), and the loop between TM3 and TM4 (S2), together form the ligand binding domain, and therefore control the agonist pharmacology of the iGluRs

(Stern-Bach et al., 1994). The S1 and S2 segments share sequence similarities with a bacterial periplasmic amino acid binding protein, which could suggest an evolutionary structural relationship (Kuusinen et al., 1995). More recently, native KARs were found to be accompanied by gain-of-function auxiliary proteins, known as Netos, which act to support the receptors' extracellular loop domains by bringing them into closer proximity and influencing a more active conformation (Litwin et al., 2017).

There are no full-length crystal structures of KARs reported to date, unlike the AMPAR, GluA2 and the NMDAR, GluN1/GluN2B (Meyerson et al., 2016, Karakas and Furukawa, 2014). However, a full-length electron microscopic structure of a tetrameric GluK2 in its bound confirmation with an agonist was published in 2014 (Meyerson et al., 2014). Furthermore, the crystal structures of over 80 soluble constructs have since been identified, particularly from the GluK1-3 subunits (Mollerud et al., 2017). More work is needed to determine the full-length crystal structures of KARs in different conformations to help understand KAR functions at the molecular level.

1.3.2 RNA editing and alternative splicing at KARs
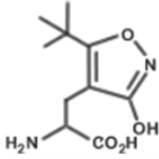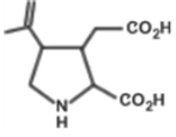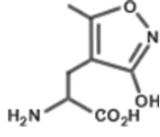
RNA editing is a molecular process whereby discrete alterations are made to the sequence of nucleotides in the RNA, encoding a KAR (for example), and can alter the characteristics of that receptor. One of the most important sites of mRNA editing encodes the GluK1 and GluK2 subunits. Editing at these sites, with an RNA deaminase, determines the alternative incorporation of an amino acid in the channel pore-forming P-loop (QR-site). Receptors with edited QR sites have functionally distinct characteristics, namely decreased divalent cation permeability, particularly Ca^{2+}, and very low single channel conductance (Egebjerg and Heinemann, 1993, Swanson et al., 1996). Another important editing site of KARs is in the first transmembrane domain (TM1) of the GluK2 subunit, and influences ion selectivity of the receptor (Köhler et al., 1993). A considerable amount of highly controlled KAR subunit editing occurs throughout development, but the physiological relevance of these changes is still uncertain.

Various isoforms of KARs can also be derived from alternative splicing, giving rise to further receptor diversity regarding their trafficking and channel properties. Alternative splicing of
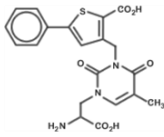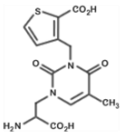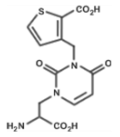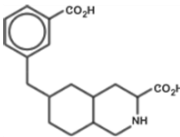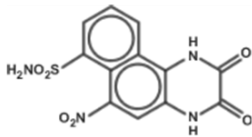
the extracellular N-terminal domain of the GluK1 subunit results in two variants: $GluK1_1$ and $GluK1_2$ (Bettler et al., 1990), and the latter can be further spliced into $GluK1_a$, $GluK1_b$ and $GluK1_c$ (Sommer and Seeburg, 1992). Alternative spicing can also occur at the C-terminal of the GluK2 subunit (GluK2a/GluK2b) and the GluK3 subunit (GluK3a/Gluk3b) (Jaskolski et al., 2004, Schiffer et al.). Thus, KARs comprise a diverse combination of subunits with varying protein interactions and surface expression which influence receptor function.

1.3.3 Pharmacology

The study of KARs has been hindered by the lack of selective ligands, particularly a previous lack of pharmacological discrimination between KARs and the more abundant AMPAR, obscuring the involvement of a clear KAR mediated component. Competitive antagonists, such as CNQX, have shown little selectivity between KAR and AMPAR, but a related compound, NBQX, had ~100-fold selectivity for AMPAR than KAR. The study of KARs was helped further with the development of AMPAR selective non-competitive antagonists, such as GYKI 53655, however, many drugs have not been tested against all heteromeric subunit combinations of KARs, which complicates the assessment of pharmacological properties (Paternain et al., 1995, Wilding and Huettner, 1996, Pinheiro and Mulle, 2006). Agonist binding to KARs involves the N-terminus and the extracellular loop, which connects TM3 and TM4. Different subunits have slight differences in the residues comprising the binding site. This is of particular importance to the development of selective KAR agonists or antagonists. For example, the GluK2/3 subunit possesses a larger residue that exposes many ligands to steric hindrance, which is why obtaining a GluK1 selective agonist, e.g. UBP-310, has proven easier (Mayer, 2005, Møllerud et al., 2017). See table 1.2 and 1.3 for a list of various KAR ligands and subunit selectivity.

Compound (Agonists)	ATPA	Kainic Acid	AMPA
Structure			
GluK1	EC50=0.33±0.05µM	EC50=4.9±0.4µM	EC50=208±42µM
GluK2	NA	EC50=1.1±0.1µM	NA
GluK3	-	-	-
GluK1/2	EC50=0.80 ± 0.07	EC50=7.4±1.1µM	EC50=154±19µM
GluK1/5	EC50=0.38 ± 0.04	EC50=1.5±0.1µM	EC50=123±5µM
GluK2/5	EC50=106 ± 16	EC50=0.6±0.1µM	EC50=137±9µM
References	(Moldrich et al., 1999, Clarke et al., 1997, Alt et al., 2004)	(Alt et al., 2004)	(Alt et al., 2004)

Table 1.2: KAR agonists and subunit selectivity

Compound (Antagonists)	ACET	UBP310	UBP304	LY382884	NBQX
Structure					
GluK1	Kb=7±1nM	Kb=10±1nM	Kb=120±30nM	IC50=2±1µM	IC50=25±4µM
GluK2	-	-	-	-	IC50=21±6µM
GluK3	IC50=92±9	IC50=23±2nM	Kb=111±38nM	-	Kb=18±8µM
GluK1/2	-	-	Kb=120±10nM	IC50=4±1µM	IC50=18±8µM
GluK1/5	Kb=5±1nM	Kb=8±2nM	Kb=180±20nM	IC50=4±1µM	IC50=26±7µM
GluK2/5	-	-	-	-	IC50=87±90µM
References	(Dargan et al., 2009, Dolman et al., 2007)	(Mayer et al., 2006, Dolman et al., 2007, Perrais et al., 2009)	(Dolman et al., 2006)	(Alt et al., 2004)	(Alt et al., 2004, Dolman et al., 2005)

Table 1.3 KAR antagonists and subunit selectivity

1.3.4 Localisation of KARs

Due to the lack of specific antibodies for some KAR subunits, a comprehensive localisation at the synaptic and sub-synaptic level has not yet been established. Functional localisation studies have been carried out using electrophysiological approaches, which have shown pre-synaptic KARs modulating neurotransmitter release, and postsynaptic KARs mediating direct excitatory neurotransmission. Postsynaptically, KARs mediate EPSCS with characteristic small amplitude and slow decay kinetics (Castillo et al., 1997), which have more recently been attributable to the KAR auxiliary subunits, Neto1 and Neto2 (Zhang et al., 2009). These auxiliary proteins interact directly with KARs and modify the biophysical features of the receptor, for example, Neto1 and Neto2 increase channel function by

modulating gating properties (Copits et al., 2011, Fisher, 2015, Fisher and Mott, 2013). In the hippocampus, cortex, amygdala and EC (see below), KARs have been identified on both GABAergic interneurones and excitatory principal cells, particularly at hippocampal mossy fibre synapses on CA3 PCs (Schmitz et al., 2001a, Schmitz et al., 2000). Presynaptically, KARs have also been identified at both GABAergic and glutamatergic synapses where they act to facilitate or inhibit neurotransmitter release. At excitatory synapses, presynaptic KAR activation has been linked to synaptic plasticity processes (Kamiya, 2002, Contractor et al., 2001). In particular, KARs, thought to be GluK2/3 heteromers, have been shown to act as autoreceptors at synapses on the mossy fibre-CA3 pathway, where they exert frequency dependent facilitation of glutamate release (Pinheiro et al., 2007). Activation of presynaptic KARs at inhibitory synapses have a dual influence on GABA release.

In the hippocampus, activation of heteromeric GluK1/2 KARs leads to a depression of evoked IPSCs in CA1 PCs (Clarke et al., 1997, Mulle et al., 2000). Further to this, using paired recordings in at interneurone-PC synapses in the CA1 region, GluK1 KARs appear to have a biphasic effect, where low concentrations of KA (300 nM) facilitated GABA release at synapses where the release probability was low, but depressed GABA release at high release probability synapses at high concentrations (5 μM(Jiang et al., 2001). In this respect, it is thought that ambient or spillover glutamate released from excitatory synapses can modulate nearby presynaptic KARs at inhibitory synapses to protect over-excitation of local circuits. It has also been suggested that the biphasic effects could involve a metabotropic signalling pathway, but since the topology of the KAR is unlike that of the usual G-protein coupled receptors, this theory remains controversial (see (Rodríguez-Moreno and Sihra, 2007). Nonetheless, Rozas et al. (2003) suggested that KARs containing the GluK1 (ion channel forming) subunit was able to signal through a second messenger cascade, indicating a non-canonical pathway. However, it is also important to mention that high concentrations (e.g. 5 μM) render KA non-specific for KAR, therefore the apparent biphasic effect on inhibitory neurotransmission could be due to its interactions with other receptors, or due to neurotoxin effects on the cells they reside on.

1.3.4.1 KARs in the MEC

In situ hydridisation studies have revealed KAR mRNA in neurones of the rat MEC, but the functional presence and roles of KARs in this area are only beginning to be revealed. One study revealed that evoked EPSCs in the superficial layers of the MEC had a slow component mediated by KARs, most prominently in LIII pyramidal neurones, though also present in SCs (West et al., 2007).

A recent comprehensive study from this laboratory has identified the location and function of KARs in LIII of the MEC. Chamberlain et al. (2012) identified KARs containing the GluK1 subunit as facilitatory autoreceptors at glutamatergic synapses on pyramidal neurones. In addition, the same receptors also mediated an excitatory drive at glutamatergic synapses on GABAergic interneurones. In contrast, a KAR, likely containing the GluK2 subunit, mediates a slow post-synaptic excitation at glutamatergic synapses on principal neurones, and is likely to also be act as a presynaptic heteroreceptor, facilitating GABA release at inhibitory terminals on principal neurones.

These studies emphasise the diversity of KAR expression and function, and show KARs contribute to network function at multiple levels in LIII in the MEC. The role of KARs in synaptic and network function in other areas of the MEC is currently unknown. Thus, a primary aim of the experimental work in this thesis was to dissect out the localisation and functions of KAR in LII and LV of the rat MEC.

The study by (Chamberlain et al., 2012), also showed that in conditions of low Mg^{2+} there was an enhancement in both GABA and glutamate release which showed rhythmic periodicity, dependent on KARs containing the GluK1 subunit, which has implications for regulation of KAR-dependent slow network oscillations and putative role for the receptors in oscillogenesis in the MEC. Indeed, KARs are likely to pay a major role in the generation and maintenance of synchronised neuronal network activity in the MEC (see below) particularly slow wave oscillations (SWO) and GFO. In addition, KARs have been identified as potential targets underlying the pathophysiology of disorders involving abnormal network synchrony, including schizophrenia and epilepsy (Porter et al., 1997, Tucholski et al., 2013).

1.3.5 KAR and network synchronisation

KARs are thought to be involved in both normal and pathological synchronisation of neuronal networks. The distinctive slow kinetics associated with KAR-mediated synaptic events enable temporal summation and the generation of oscillations at various frequencies. For example, oriens lacunosum moleculare (O-LM) interneurones within the hippocampus are tuned to operate at theta frequencies, which can be witnessed pharmacologically (*in vitro*) or locally (*in vivo*), but both rely on the activation of post-synaptic KARs, in addition to the membrane properties of the O-LM cells themselves (Goldin et al., 2007). Further to this, EEG and single unit recordings in freely moving rats showed a significant decrease in the frequency of the theta modulation after bilateral intracerebroventricular injection of a GluK1 specific antagonist, UBP-304. Again, the root of the affect appeared to be due to a decrease in hippocampal interneurone discharges that were setting the pace for the theta oscillation (Huxter et al., 2007). This suggests GluK1 KARs have an important role in modulating theta activity through their effects on interneurones.

KARs have also been linked to SWO, spontaneous neuronal activity in the form of slow (<1 Hz), synchronised network state transitions. Of particular interest, in an *in vitro* study, Cunningham et al (2006b) showed that activation of KARs was sufficient to induce the rhythmic bi-stability necessary for the generation of SWO within the network, likely due to the temporal summation enabled by the slow KAR-mediated excitatory events (Cunningham et al., 2006b). This suggests KARs could play a prominent role in the manifestation of SWO in the MEC.

The most common type of oscillation associated with KAR activation is the GFO (30-80 Hz), thought to underlie important aspects of cognition relative to the area of the brain in which they occur. Importantly, these fast network oscillations can be induced in the MEC, independently of the hippocampus, with nanomolar doses of KA (Cunningham et al., 2003, Cunningham et al., 2004a). A further study showed that the generation and maintenance of these gamma oscillations in the MEC is critically reliant on KARs containing the GluK1 subunit (Stanger et al., 2008), which, interestingly, is in contrast to the same oscillations in the hippocampus. Other region specific properties of KA-induced GFO have been observed

in the MEC. Middleton et al. (2008b) revealed two types of KA-induced GFO that differed in frequency with distinct underlying mechanisms defined by the type of interneurone recruited into the rhythm, either basket interneurones or goblet cells, which were dependent, or independent, on NMDAR drive, respectively (Middleton et al., 2008b).

Despite this, more work is needed to determine the precise nature of KA-induced oscillations in the MEC, which was a specific aim of the work in this thesis. What is especially interesting about the use of KA in this model is that, whilst low concentrations induce a GFO, high concentrations push the network into a state of epileptogenesis, a phenomena which has been replicated *in vivo.* KAR activation is therefore a useful model of both oscillogenesis and epileptogenesis (Victor Nadler, 1981, Ben-Ari, 1985, Fisahn, 2005).

1.3.6 KAR and epilepsy

KARs have been associated with the generation of epileptogenic activity since the discovery of KA. It was soon realised KA is a potent analogue of glutamate with the ability to depolarise neurons, causing hyper-excitability and eventual cell death. It is these properties that make KA a viable and widely used tool for researching TLE, as they mirror pathophysiological aspects of the disorder in animal models. The discovery of KA actually pre-dated the discovery of the high affinity KARs to which it binds, which were later shown to distribute in areas that are susceptible to seizures, such as the hippocampus and the MEC (Monaghan and Cotman, 1982, Represa et al., 1987). Nowadays, it is well established that activation of KARs generates seizures in the limbic system (Ben-Ari, 2010). Research regarding KARs in the MEC is lagging behind other areas of the limbic system, so examples of their involvement in epileptogenesis can be drawn from these areas. Despite the delay in availability of pharmacologically specific agents, which has hindered research in this field, genetic and electrophysiological approaches have helped to identify two subunits as playing major roles in the context of hyperexcitability and epilepsy, namely the GluK1 and the GluK2 containing KARs. Firstly, transgenic GluK2 knockout mice showed a greatly reduced susceptibility to seizures, and hippocampal pyramidal neurones in the CA3 region became much less sensitive to the effects of systemic KA administration (Mulle et al., 1998). On the other hand, Cossart et al (1998). showed that GluK1-containing KARs were expressed mainly on interneurones in the hippocampal region, and therefore decreased

the excitability of principal cells due to an increase in tonic/phasic inhibition (Cossart et al., 1998, Khalilov et al., 2002). These studies are indicative of pro- and anticonvulsive actions of KARs containing the GluK2- and GluK1- subunits, respectively.

The main characteristic pathologies associated with TLE, in both animal models and human patients (post-mortem studies), include the reorganisation of the affected neuronal network, with some neurones' fate being cell death, and others sprouting new, but aberrant, connections. Of significance, injection of KA in rodent models of TLE not only leads to the onset of recurrent seizures, but also sprouting of recurrent excitatory connections, specifically of mossy fibres onto CA3 pyramidal neurones and DGCs in the dentate gyrus. These profound rearrangements, due to activation of KARs, lead to increased excitation of these cell types via a form of frequency facilitation dependent on presynaptic KARs activation. In fact, long lasting KAR mediated synaptic currents (EPSC$_{KA}$), originating from aberrant, recurrent mossy fibre synapses, have been recorded in chronically epileptic rats, which do not exist in naïve conditions. Hypothetically, the formation of aberrant mossy fibre synapses onto DGCs, after application of KA, leads to the formation of functional KAR operated synapses mediating the EPSC$_{KA}$, which contributes to evoked, spontaneous and miniature glutamatergic synaptic transmission in chronically epileptic, and not naïve, rats (Sloviter et al., 2006, Stafstrom, 2006, Epsztein et al., 2005). Of note, dual LFP recordings in the EC and dentate gyrus of freely behaving mice showed a significant de-synchronisation of theta oscillatory activity after injection with KA, compared to controls, suggesting that on-going pathologic dynamics in epilepsy can affect physiological oscillations, beyond acute epileptiform activity (Froriep et al., 2012).

Finally, autoradiography studies have also shown there to be an increase in KA binding sites in the CA3 region of the hippocampus of humans with TLE compared to controls, suggesting that this KAR mediated anatomical plasticity is not restricted to animal models (Represa et al., 1989). These connections have been identified due to the well-defined architecture of this pathway, but it is not unrealistic to suggest a similar contribution of KARs to the generation of seizures could be prevalent in the MEC, especially as seizure generation is often initiated in the MEC. Studies looking specifically at the MEC have reported neuronal

cell loss and alterations in synaptic connectivity in the superficial layers of both human patients and KA-induced animal models of TLE (Tolner et al., 2007, Tolner et al., 2005).

1.3.7 Desensitisation

KAR-mediated synaptic responses have two main intrinsic characteristics distinguishing them from AMPAR-mediated currents: they are smaller in amplitude, and have slower deactivation kinetics. Furthermore, two distinct agonist binding affinities are apparent: 1) high affinity agonist binding leading to ion channel opening and 2) low affinity agonist binding site leading to a strong desensitisation (Mott et al., 2010). In the former mechanism, deactivation of the KAR commences following ligand unbinding and subsequent closing of the ion channel, whereas following desensitisation the agonist remains bound. In fact, some KAR agonists, e.g. SYM2081, induce such a fast desensitisation that they essentially act as an antagonist at these receptors (Zhou et al., 1997). The relative contribution of deactivation and desensitisation rates to the time course kinetics of the synaptic current is related to the time course of glutamate in the synaptic cleft (Clements, 1996). For example, in brief (~1 ms) periods of glutamate elevation, deactivation kinetics will dominate, whereas after prolonged exposure to glutamate, desensitisation will act to limit the excitability of the receptor. The desensitisation time constants of KARs are approximately 10-fold slower than those of AMPARs and constitute a defining characteristic of this receptor. Pharmacological manipulation with concanavalin A relieves desensitisation of KARs containing the GluK1 and GluK2, but not the GluK3 subunits, suggesting differences in glycosylation sites between receptor subtypes (Schiffer et al., 1997). Moreover, the GluK1 subunit has been associated with slower desensitisation responses compared with the GluK2 subunit (Swanson et al., 1996). The significant desensitisation and slow kinetics associated with KAR currents are critical factors determining the frequency and amplitude of excitatory responses, and may underlie a protective mechanism to prevent excitotoxicity (Jones and Westbrook, 1996).

1.3.8 KARs and development

A distinctive feature of a number glutamate receptors, including KAR, is a change in expression and function during early development. Unpublished data from Professor Elek

Molnar's laboratory in Bristol has shown that GluK1 and GluK2 receptors in the hippocampus and other areas show a distinctive developmental profile, being low at birth and rising steadily during early development in juveniles but regressing to lower levels in full adult animals (Fig.1.6). A developmental profile of functional effects of KARs in the MEC has not yet been fully addressed, and is one of the main aims of this thesis. We are still hindered by the lack of pharmacological tools to study KAR subtypes, and so the focus is mainly on the GluK1-containing KARs, for which specific agonists and antagonists are available. The current available data on KAR expression focuses on either whole rat brain gene expression studies without lamina differentiation in the MEC, or functional electrophysiological studies on the immature rat hippocampus. In the former, the distribution of high-affinity KAR transcripts in the developing rat brain were examined, and flagged up some potentially interesting differences between expression patterns in embryonic and postnatal development compared with adult KAR subunit expression patterns, particularly regarding KARs containing the GluK1 subunit. In particular, there seemed to be a brief developmental increase in the expression of GluK1-containing KARs at around postnatal day (P) 12, which then decreased in expression into adulthood (Bahn et al., 1994). In support of this, immunohistochemical studies (unpublished) in the laboratory of Professor Elek Molnar at the University of Bristol established a differential developmental profile of KAR subtype expression in hippocampal areas of the rat brain, seeing a peak expression of the GluK1 subunit at P14 (Fig 1.6).

Functionally, KARs have been postulated to play important roles in the development and maturation of neuronal circuits. Attention has focused on KAR control of glutamate release at immature MF-CA3 synapses. KARs on MFs are thought to act as auto-receptors that are tonically and constitutively activated by ambient glutamate which is present in higher concentrations in neonate neurones (Lauri et al., 2005, Lauri et al., 2006). Differences in KAR function have been identified in the hippocampus throughout development. In the immature hippocampus, KARs increase glutamatergic inputs to interneurones and, in doing so, encourage synchronised network activity. These precise mechanisms are developmentally downregulated in the mature hippocampus, and replaced by alternative modes to regulate such activity, attributed to somatodendritic KARs on interneurones (Lauri et al., 2005). It is becoming increasingly apparent that the differences in expression,

activation and signalling of KARs during postnatal development accommodate their differential roles in the maturation of synapses and adult neurotransmission. These developmentally regulated KARs are thought to reside presynaptically, and act to fine tune neuronal circuitry by influencing what synapses are strengthened or eliminated in an activity dependent manner (for review see (Lauri and Taira, 2012)). Of course, this research has been conducted in the hippocampus, but it is not unrealistic to hypothesise a similar role for KARs in the MEC given their expression and role in network synchrony in this region. Clearly, there is a gap in the research vis-à-vis the function of KAR during development, especially lamina differences in the MEC, which this thesis will aim to address. Understanding KARs at a synaptic and network level will provide a basis for possibilities of pharmacological manipulations to control hyper-excitability and pathological synchronisation within brain circuits.

To assess the state of functional activity at KARs in the EC we have taken advantage of the ability of KAR activation to induce GFO when applied at low concentrations, as described previously in a number of preparations (Cunningham et al., 2003, Hormuzdi et al., 2001, Cunningham et al., 2004a). This allows us to use GFO as a functional measure of overall network activity of KAR and monitor changes throughout development.
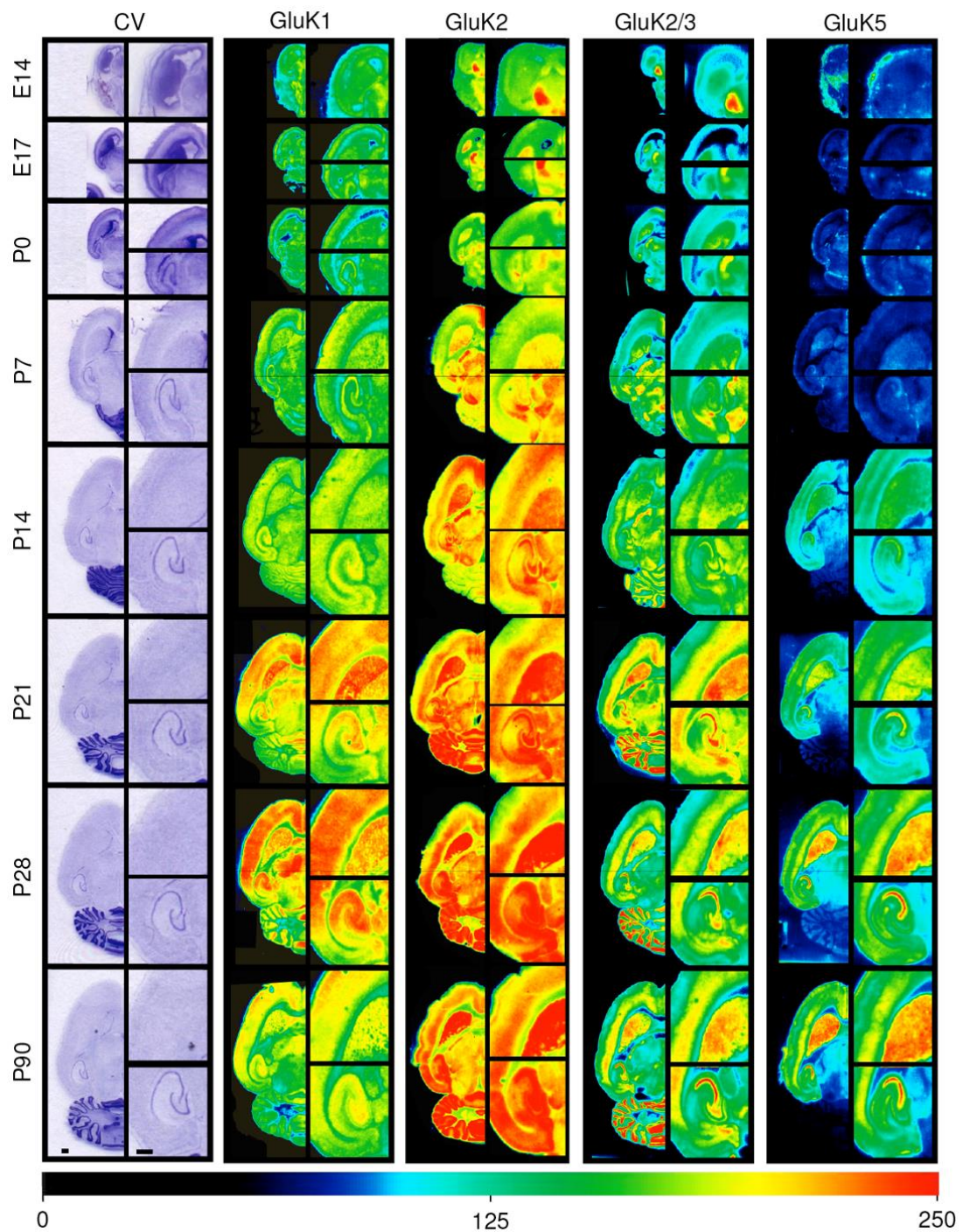
***Figure 1.5: Localisation of KAR subunits GluK1, GluK2, GluK2/3 and GluK5 immunoreactivity at 8 stages of development in the rat hippocampus and MEC**. Horizontal brain slices were immunostained with anti-GluK1, GluK2, GluK2/3 and GluK5 antibodies. Note the increased expression of the GluK1 subunit in the P14 MEC. Work (unpublished) from studies conducted in the laboratory of Professor Elek Molnar at the University of Bristol.*

1.4 Oscillatory Activity

1.4.1 The EEG

Synchronised rhythmic electrical activity in populations of neurones is known as oscillation. The electrical nature of the brain was discovered by Richard Caton in 1875, when he observed electrical currents from the skulls of living rabbits and monkeys (Caton, 1875). This pioneering observation laid the groundwork for psychiatrist, Hans Berger, to discover and record "brain waves" in humans, after his invention of the electroencephalogram (EEG), which is a method of recording electrical activity in the brain by placing electrodes on the scalp. The EEG is regarded as one of the most remarkable and momentous developments in the history of neurobiology and, along with magnetoencephalography (MEG) recordings, have empowered the detection of neuronal oscillations at different frequencies, namely: SWO, theta (θ), alpha (α), beta (β) and gamma (γ). Rhythmic activity within the brain is on-going, yet transient, and different frequencies often exist in parallel, with some rhythms being nested within others through relations between their amplitudes and phases. In these instances, the EEG signal can be filtered to focus on the desired oscillation, to gain information on the functional significance of that particular frequency of activity. Generally, states of sleep give rise to large amplitude but low frequency rhythmic activity, whereas states of attentiveness are characterised by low amplitude, high frequency rhythms. Essentially, it is thought that neuronal oscillations enable the brain to generate and sense temporal information, which acts as a prerequisite for ensuing actions and cognition.

1.4.2 Neuronal oscillations

Neuronal oscillations are coordinated electrical activity within a group of neurones and are thought to underlie important aspects of cognition and behavioural states across multiple systems (Whittington et al., 2011). The underlying mechanisms of these rhythms are therefore of great importance to understand the physiological basis of cognition. Dissecting out these mechanisms is not possible in humans using EEG, but the development of both *in vivo* and *in vitro* rodent models has allowed us to gain information about aspects of the local circuits contributing to various brain rhythms. Indeed, *in vitro* brain slice

electrophysiology allows for the reproduction of EEG-like oscillations in small, isolated sections of brain, which can be pharmacologically manipulated and observed at both a cellular and local network level. In general, endogenous oscillations enable the precise timing of neuronal action potentials, which is important for coding information specific to different brain regions and frequencies.

The EC-hippocampal system is critically important for the formation and storage of memories, but this system is also fundamental in spatial navigation (Sasaki et al., 2015). The underlying mechanisms of both memory and spatial navigation have been separately associated with neuronal oscillations. An emerging idea is that this common mechanism could in fact converge these disparate directions and provide an overarching, coherent and functional picture of the MEC-hippocampal system. Whilst many frequencies of neuronal oscillations co-exist, the ones of particular importance to the MEC are SWO, theta, beta and gamma.

1.4.3 Slow wave oscillations

SWOs are forms of slow (<1 Hz), synchronous network state transitions expressed in the thalamus and the cortex, including the MEC, and are conserved between species (Zhu et al., 2006). These state transitions fluctuate between periods of intense, large amplitude neuronal activity (up-states), and almost complete silence (down-states). It is the cycling between these states that constitute the slow oscillation. SWOs are a prominent feature of deep sleep, in the absence of sensory stimulation, that occur as a consequence of recurrent excitation and local inhibitory connections in the areas they reside, which initiate and support patterned network activity (Neske, 2015). At the cellular level, up and down states have been attributed to fluctuations between depolarisation and hyperpolarisation of the membrane potential, and they have been identified in the MEC, *in vitro.* (Cunningham et al., 2006b). SWOs in the MEC have been linked with slow EPSPs mediated by KARs, were unaffected by NMDAR blockade in adult rat MEC, and were influenced by metabolic demand via the fluctuations in membrane potential mediated by ATP-modulated potassium channels (Cunningham et al., 2006b). Previous work by this research group has also investigated SWO in the MEC at the cellular level in immature animals (P9-13). Using intracellular recording, Jones and Heinemann (1989) showed that neurones in LII of the

MEC exhibited spontaneous synaptic activity that often summated into large depolarising events, similar to the 'up-states' described in the MEC much later (Jones and Heinemann, 1989). In the immature EC, the synaptic events were abolished by NMDAR blocker, AP5, an effect that has been confirmed by work in this thesis, and also in similar network activity recorded from the neighbouring neocortex (Castro-Alamancos and Favero, 2015). Interestingly, the presence of these large NMDAR dependent events was inversely correlated to the age of the rat, which could be a result of a decrease in NMDAR population throughout development (Sucher et al., 1995). This could explain the difference in NMDAR sensitivity between the studies of Jones and Heinemann and (1989) Cunningham et al. (2006) as they were conducted in neonatal (P9-13) and adult rats, respectively. Nonetheless, the presence of SWO in the MEC is indisputable. The regional and functional roles of such oscillations are unclear, but are thought to involve aspects of learning and plasticity, particularly declarative memory consolidation during sleep, as well as being linked to neuronal metabolism and development (Cunningham et al., 2006b). Of note, SWOs have also been suggested to act as a "base frequency" that groups and modulates other oscillations, including beta/gamma activity (see (Neske, 2015, Takeuchi et al., 2015).

1.4.4 Theta Oscillations

Theta oscillations are a prominent rhythm observed in the hippocampus and its surrounding limbic structures, including in the MEC, during exploratory behaviour and REM sleep, in both humans and rodents (Lega et al., 2012, Ekstrom et al., 2005). EEG studies suggest that the frequency of theta rhythms in humans (1-4Hz) is slower than that of rodents (4-10 Hz) (see (Jacobs, 2014)). Functionally, this rhythm is believed to have roles in the formation and retrieval of episodic, associative and spatial memories (Stella and Treves, 2011, Backus et al., 2016, Hanslmayr et al., 2016). Despite this, the exact relationships to behaviour are still being delineated, but the theta oscillation could constitute a mechanism that underlies and links together these behavioural states (Hasselmo, 2005).

The theta oscillation has most commonly been recorded from place cells in the hippocampus, but the MEC is garnering more attention following the discovery of grid cells. In the MEC, it is thought that spatial information is encoded, at least partly, by the precise timing of grid cell spiking relative to the phase of the theta cycle. Principal cells in LII are

most strongly modulated by the theta rhythm, however, interneurones from all layers fire relatively synchronously within the theta cycle (Quilichini et al., 2010). It is becoming increasingly apparent that the generation of the theta rhythm involves interactions from multiple brain regions, especially the medial septum-diagonal band of Broca (Stewart and Fox, 1990). More importantly, recent studies suggest the temporal organisation of hippocampal neuronal activity, particularly theta cycle rhythmicity and its associated spatial firing, is critically dependent on inputs from the MEC (Schlesiger et al., 2015, Fernández-Ruiz et al., 2017). The theta phase timing is therefore likely to be comprised of the interactions of upstream inputs with local mechanisms, which support memory and spatial navigation, and so cannot be fully explained by local *in vitro* models (Wang, 2010). For this reason, the circuit mechanisms of theta oscillations in the MEC are still unclear, but a prominent feature is their co-ordination with GFO. Indeed, this faster gamma rhythm (30-80 Hz) appears to be nested within, and modulated by, the slower theta rhythm. It is thought this allows more effective activation of downstream neuronal targets in the hippocampus (Fries, 2009), as well as allowing multiple 'items' to be encoded on each gamma cycle (Lisman, 2005). The mechanisms linking theta-nested GFO and grid-cell firing patterns are receiving increasing amounts of attention, but are still up for debate. The most consistent model involves local feedback inhibition between SCs, in the absence of recurrent excitation, that can simultaneously generate grid cell firing fields through network attractor states (Pastoll et al., 2013b).

1.4.5 Gamma Oscillations

GFO occur during both awake and sleep states throughout the cortex, hippocampus and striatum, and appear to be modulated by sensory input (Lowet et al., 2015, Saleem et al., 2017). It was this observation that lead scientists in the late 1980s to postulate that GFO could represent a mechanism that links the activity of single neurones, which fire synchronously in an assembly, to the nature of a sensory stimulus. In theory, oscillations can efficiently bind together outputs of neurones that encode different features of a single perceptual entity (see (Singer and Gray, 1995)). Donald Hebb (1950) coined the term 'cell assembly' to describe a network of neurones which are repeatedly activated, in a near-synchronous manner, in response to a certain sensory input (Maldonado and Gerstein,

1996). The excitatory connections will be strengthened together thereafter, a mechanism which has implications for many cognitive processes in general (Hebb, 1950). GFO have been particularly related to sensory processes linked to attention (Tallon-Baudry et al., 2005) and working memory (Howard et al., 2003).

Whereas theta oscillations appear to have a large input dependence from other structures, the faster gamma rhythm can be generated in local circuits. This means that *in vitro* models of gamma generation can be transferred to different brain structures, e.g. the hippocampus and the MEC, and the underlying and regional mechanisms maintaining the rhythm can be studied using pharmacological and genetic manipulations (Traub et al., 2004). Experimental work has also informed computational modelling, which aims to identify properties determining the synchronisation and frequency of such oscillations (Whittington et al., 2000). GFO can be generated reliably *in vitro*. There are three main modes, which differ in their mechanisms of interneurone excitation, or recruitment, into the rhythm and will be discussed in the following sections. Of note, although it is not the whole picture, it is generally accepted that the type of interneurones involved in GFO are the perisomatic targeting parvalbumin-containing basket cells due to their fast kinetics and inputs to target cells close to the action potential initiation site (for review see (Whittington et al., 2011).

1.4.5.1 Interneurone network gamma

As suggested by its name, interneurone network gamma, or ING, relies solely on the excitation of inhibitory neurones. This mechanism was described when Whittington et al. (1995) evoked GFO in hippocampal slice preparations by applying afferent stimulation. The emergent IPSP oscillation was driven by activation of inhibitory neurones by a metabotropic mechanism. In this model, GFO are mediated by $GABA_A Rs$ (and possibly gap junctions (Traub et al., 2001)) between interneurones, which are pharmacologically disconnected from pyramidal neurones by blockade of ionotropic glutamate receptors (Whittington et al., 1995). In a network of tonically active interneurones, the IPSP impinging on each cell is intrinsically linked to the activity of the interneurone it is connected to. In its most stable model, interneurones that are mutually coupled with GABAergic synaptic input will rhythmically synchronise their firing to each other, and can only generate an IPSP when the input to that cell is at a minimum, and then the cycle continues. The frequency of the

IPSP is therefore determined by the GABA$_A$R feedback kinetics, specifically their conductance, decay time and the initial excitatory drive delivered to the interneurone, but also the GABA$_A$R subunit composition. The maximum frequency of the gamma oscillation is inversely proportional to the decay time constant of the IPSP (Whittington et al., 1995). As this model relies on the activity of interneurones without excitation from other cells, the intrinsic properties of the interneurones themselves must have enough drive to fire, even in the presence of the reciprocal inhibition. For this to work, the natural firing rates of the interneurones must be greater than that of the gamma rate. Further to this, although synaptic input from pyramidal neurones is not required for the ING model, the network of interconnected interneurones can generate a GFO in PCs by entraining their firing. In this way, PCs fire periodically when the IPSPs have decayed to their weakest point. For this to occur through an ING mechanism, which, remember, has no input from pyramidal neurones, the drive of the latter must be high enough to fire during moments of low inhibition, but not so high that they fire prior to the interneurones, as this would be contributing to the rhythm.

Whilst it is possible the ING mechanism contributes to gamma activity *in vivo,* and it provides conceptually useful information, it is unlikely to have physiological relevance existing in isolation.

1.4.5.2 Pyramidal-interneurone network gamma

Unlike the ING model, pyramidal-interneurone network gamma, or PING, as its name suggests, involves a network containing populations of excitatory, as well as inhibitory, neurones, which are reciprocally connected to each other (Wilson and Cowan, 1972, Whittington et al., 2000). This model of GFO is a more relevant approach because local circuits throughout the brain generally exhibit dense reciprocal connections between interneurones and principal cells. A single basket cell can receive inputs from over 1000 PCs (Andersen et al., 2006). The PING model is essentially an adaptation of ING, where the reciprocal interneurone connectivity remains the same, but with the addition of fast, AMPAR-mediated phasic excitatory projections onto the inhibitory population. This fast excitation of interneurones, in turn, provides fast inhibition back onto the excitatory principal cells and to reciprocal interneurones, silencing both populations via GABAergic

synapses. This interplay influences the network into an oscillatory state, but for this cyclic behaviour to occur, the amount of excitation and inhibition should be balanced. The presence of PCs seems to increase the stability of the network, as inferred by the degree of frequency attenuation in each model after pharmacological manipulation of $GABA_A$Rs (Whittington et al., 1996). Moreover, the participation of pyramidal neurones, and the subsequent AMPAR-mediated fast EPSPs in interneurones, can theoretically lead to presence of spike doublets, or bursts, which allow long range synchronisation of spatially separate, but interconnected, brain regions, despite long conduction delays (Whittington et al., 1997b, Traub et al., 1996b). Unlike the ING model, PING requires excitatory input from pyramidal neurones, therefore the latter must recover from inhibition faster than the interneurones to provide this drive. The synaptic delay and axonal conductance between the EPSP and the resulting IPSP spikes, determine the properties of the rhythm (Ermentrout and Kopell, 1998, Leung, 1982). GFO where frequency is determined by the above factors are a prominent feature of both *in vivo* and *in vitro* rhythms (Bragin et al., 1995, Csicsvari et al., 2003, Mann et al., 2005).

Both ING and PING models are critically dependent on the action and involvement of reciprocally connected GABAergic interneurones. The participation of either mechanism in the generation and/or maintenance of GFO is likely to be region and species specific. However, the critical differences between these mechanisms is that the specific type of neurones involved possess the intrinsic properties to pace the network into either rhythm e.g. whether neurones exhibit sub-threshold or threshold membrane potential oscillations (Whittington et al., 2011, Gloveli et al., 2005). Moreover, depending on the levels of excitation of either population of neurones, the ING and PING mechanisms can be interchangeable.

1.4.5.3 Persistent gamma

Persistent gamma (PG) oscillations can be generated in a stable fashion *in vitro,* lasting for several hours, by bath application of appropriate pharmacological agents, including: KA (nanomolar concentrations), carbachol (tens of µM) and dihydroxyphenylglycine (DHPG). These agents induce a stable GFO via tonic activation of KAR, muscarinic and mGlu receptors, respectively. It was first observed in the hippocampus (Fisahn et al., 1998), but

has since been described in other regions including: the cerebellar cortex (Middleton et al., 2008b), the neocortex (Traub et al., 2005), the basolateral amygdala (Randall et al., 2011) and, most importantly for this thesis, the MEC (Cunningham et al., 2003, Cunningham et al., 2004a). *In vivo*, PG appears at first to be following a PING mechanism, where interneurones are not tonically active but receive stimulation via large compound phasic excitatory inputs from principal cells at a gamma frequency (Bragin et al., 1995). However, several mechanistic differences have been recognised in PG, the main one being its high dependency on conductance between gap junctions, the phylogenetically oldest form of neuronal communication (Draguhn et al., 1998, Traub and Bibbig, 2000). Indeed, bath application of the gap junction blocker, carbenoxolone, abolished PG rhythms (Traub et al., 2000, Cunningham et al., 2003). The maintenance of PG therefore depends on chemical synapses and electrical coupling between both principal cells (axonal) and interneurones (dendritic) (Traub et al., 2001). Gap junctions connecting the axons of principal neurones form the axonal plexus, through which action potentials can propagate (Traub et al., 1999). As mentioned, the PG mechanism critically depends on large phasic EPSPs onto interneurones, however, the somatic spike rates (0-4 Hz) of principal cells converging onto these cells are too low to account for this amount of excitation. This discrepancy can perhaps be partially explained by gap junctions, because action potentials can propagate through gap junctions to other cells, producing activity in these cells without direct synaptic input. Interestingly, models of PG often have very fast oscillations, (100-200 Hz), nested within the gamma rhythm, including in the MEC (Cunningham et al., 2004a), which has also been attributed to the presence of gap junctions in computational models in other brain regions (Traub et al., 1999, Traub et al., 2008).

The model of PG relevant to this thesis is induced by activation of KARs by bath application of nanomolar concentrations of KA to the MEC-hippocampal brain slice. A lamina profile of KA-induced GFO in the MEC was determined by Cunningham et al. (2003). They found a general increase in gamma power in the superficial compared to the deep layers, with the highest power residing in LIII. In all layers, the strength of the gamma power peaked in the medial portion of the MEC, and diminished as the electrodes were moved laterally. Microlesions between the MEC and the hippocampus had no effect on the gamma power, despite the robust and extensive reciprocal connections. A pharmacological profile of MEC

GFO was also determined and revealed that, as in studies in the hippocampus, GFO is highly dependent on the synchronised output of interneurones, and phasic excitation onto such interneurones (Cunningham et al., 2003). Additional studies have also shown KA-induced GFO in the MEC to be dependent on the GluK1-containing KAR receptor, using a subunit specific antagonist, UBP302 (Stanger et al., 2008).

1.4.6 GFO and CNS disorders

1.4.6.1 Schizophrenia

Alterations in GFO have been associated with various CNS disorders in humans and animal models of disease, particularly AD and schizophrenia. Combinations of clinical electrophysiological, MRI-based and post-mortem studies on patients with schizophrenia have identified abnormal gamma band activity that has been attributed to impaired GABAergic neurotransmission, particularly relating to PV-containing interneurones (Gloveli et al., 2005, Hashimoto et al., 2003). Convergent evidence suggests impairment in GFO could underlie many of the symptoms and fundamental cognitive deficits witnessed in patients with schizophrenia (Uhlhaas and Singer, 2010). Gamma activity is thought to allow feature binding, whereby sensory inputs are united to perceive information correctly. To do this, the inputs must be discharged synchronously, but in patients with schizophrenia there are problems regarding integration of the sensory information, which perhaps leads to symptoms of hallucinations, thought disorder and disorganisation (Taylor et al., 2013).

As well a deficit in PV-containing interneurones themselves, deficits in the glutamatergic input to this subset of cells have been proposed to play an upstream role in the pathophysiological mechanisms underlying abnormalities in GFO in schizophrenia. NMDAR hypofunction on inputs to PV-containing interneurones appear to mimic aspects of the disorder in healthy subjects, and exaggerate symptoms in schizophrenia patients (Coyle, 1996, Krystal et al., 1994). Moreover, schizophrenia-associated genetic loci have been identified, and appear to be associated with glutamatergic, and not GABAergic, neurotransmission (Schizophrenia Working Group of the Psychiatric Genomics, 2014). In line with this, animal models of the disease have implicated PV-containing interneurones with a large NMDA receptor expression in the underlying neurobiology of abnormal gamma

activity. In particular, a study by Cunningham et al. (2006a) found a significant reduction in the power of gamma activity in both a genetic (LPA1-decicient mice) and an acute (NMDAR antagonism) animal model of schizophrenia. What is particularly interesting about these models is that the observed deficits in PV-containing interneurones, and the resulting reduction in gamma activity, was specific to LII of the MEC, and showed no deficits in the hippocampus (Cunningham et al., 2006a). This suggests abnormal GFO residing in the superficial layers of the MEC may be involved in the network dysfunction leading to the onset of schizophrenia. Caution should be taken when looking at models of schizophrenia-like symptoms, however, because they show variable effects on gamma rhythms which depend on the brain region studied and the source of excitation initiating the oscillation (Cunningham et al., 2006a, Hunt et al., 2017). Models of schizophrenia are often based on post-mortem markers, for example parvalbumin immunopositive cell number and GAD67, the latter of which is also expressed in somatostatin and calretinin-containing interneurones, thus calling into the reliability of such models.

In addition, evidence for disruptions in network oscillations specifically at a gamma frequency is not a consistent pathology across all patients with schizophrenia, but rather disruptions across multiple bandwidths are evident, especially delta and theta oscillations, though again, not consistently. Indeed, interdependent rhythms often nested within each other and can dynamically and mechanistically influence each other and the co-ordinated activity between brain regions. It has therefore been proposed that the disruption of broader, pathway-specific cross-frequency oscillatory activity may more accurately link network dysfunction to the underlying pathology of schizophrenia. See Hunt et al. for a review on 'aberrant network activity in schizophrenia' (Hunt et al., 2017). Nevertheless, abnormal network synchrony is prevalent in both patients and models of schizophrenia, so understanding the physiological development of gamma oscillations in the cortex could provide region-specific insights into the development of cognition and associated diseases.

1.4.7 Neuronal synchrony and development

Neuronal oscillations are thought to have major roles in shaping the maturation of cortical networks during many stages of development by a process known as spike timing dependent plasticity (STDP), the precise temporal correlations of pre- and postsynaptic

activity which leads to the modification of synapses. Stimulation of neurones during the peak or the trough of theta or GFO, for example, can determine whether a synapse is strengthened or weakened, respectively. Presentation of aberrant neural oscillations at critical points of development could, therefore, lead to imprecise STDP and the pathological modification of neuronal networks (Uhlhaas and Singer, 2010).

During normal development, a significant increase in theta and gamma band activity, and long-range synchronisation, has been identified at the stage of early adulthood. This is followed by a significant decrease in beta and gamma band activity during late adulthood, which is thought to represent a transient destabilisation period of development occurring prior to the emergence of a mature cortical network (Uhlhaas et al., 2009). Perhaps then, in a network unable to support such changes in gamma activity, a break-down in the temporal dynamics of the network during these critical periods of development could lead to abnormal cognitive functioning, as seen in schizophrenia. Normal brain development relies on the dynamic interplay between developmentally directed gene expression and brain activity itself, either of which could be affected by intrinsic errors or even external factors. For example, chronic early life stress is a risk factor for many psychiatric illnesses including bipolar disorder, depression and schizophrenia, and has been recently correlated to a disruption in the maturation of GFO in the hippocampus (Dricks, 2016). Again, post-mortem studies in chronically stressed rats, and in humans with schizophrenia, show a reduced number of PV-containing interneurones. Basket cells are the proposed cellular substrate underlying GFO, and postnatal development of such cells promotes striking changes in their morphological, intrinsic and synaptic properties. Most importantly, the maturation of basket cells leads to a conversion from slow into fast IPSCs, thus promoting coherent activity in the gamma frequency band (Doischer et al., 2008).

Clearly, disruption of the excitatory-inhibitory balance will affect the precise timing of synchronised network activity, such as a GFO, which, if occurring at critical points during development, will have detrimental effects on the development of cognitive processing. Although there is a comprehensive developmental profile of the maturation of GFO in the hippocampus (Tsintsadze et al., 2015), there is currently no such profile in the MEC, and establishing this was a major aim of this project. Knowing the normal physiological

development of GFO in the MEC will help us understand the development of cognition, but also understand the roles of such rhythmic activity in structuring the development of this area of the brain. Furthermore, this knowledge can be applied to help understand neurodevelopmental disorders, which could be related to pathologically synchronised networks.

Chapter 2

Materials and Methods

2.1 General methods

This project has investigated of role of KARs in network activity in LII and LV of the rat MEC *in vitro* using recordings from both single neurones (whole-cell patch clamp) and population activity (local field potentials). The focus has been on developmental changes and both approaches have been applied in brain slices from rats aged P8 to P27.

2.1.1 Animals

All experiments were performed *in vitro* using brain slice preparations from both male and female Wistar rats (aged 8-28 days old and weighing ~20-110 g) bred in the Biosciences Service Unit at the University of Bath. The rats were group-housed in cages on a 12-hour light-dark cycle (07:00-19:00 lights on) and provided with food and water *ad libitum.* Animals aged P23-27 were weaned but all animals under this age remained with the maternal parent until required for use, and were not cross-fostered. Careful note was taken of animal age, weight, sex (no conscious effort was made to select either males or females), and whether eyes were open or not at time of use.

Male and female rats attain sexual maturity at approximately >P50 (Zemunik et al., 2003) and >P38 (Rivest, 1991). Therefore sex specific physiological influences on brain activity, for example the effects of neurosteroids on GABAergic neurotransmission (Gunn et al., 2011), will not contribute to variability in this study, and justifies the use of both male and female rats (Becker et al., 2016, Beery and Zucker, 2011). Animals were removed from the animal facility and transferred in a covered cage to the experimental laboratory on the day required.

2.1.2 Ethics Statement

All experiments were performed under a home office license in accordance with the U.K. Animals (Scientific Procedures) Act 1986, European Communities Council Directive 1986 (86/609/EEC) and conformed with the ethical review procedures of the University of Bath. Every effort was made to ensure that only the minimum number of animals was used and that suffering and stress was reduced with appropriate precautions and due and careful

consideration of 3Rs guidelines. The use of animal tissue for research at the University of Bath requires a consideration of ethical implications by both the principal investigator, and second assessor, external to the group, plus a review and approval from the Head of Department, preceding further review by the a Research Ethics Officer. A report has to be submitted to the University Ethics Committee before experimental work is allowed to proceed, ensuring that ethical implications and processes for managing ethical issues and animal welfare have been properly considered. All experiments in this thesis were conducted on brain tissue removed following Schedule 1 procedures (cervical dislocation preceding decapitation). The experimenter was required to be trained by in-house staff in the animal facility and deemed competent in these procedures before engaging in animal usage.

2.2 Slice preparation

Combined MEC-hippocampal slices were obtained from either male or female Wistar rats (as above) using an approach described previously (Jones and Heinemann, 1988). Cervical dislocation was followed by decapitation and rapid removal of the brain into ice-cold (4˚C) oxygenated (carbogen gas - 95% O_2, 5% CO_2) sucrose-based ACSF (see section 2.4 for composition). The cerebellum was removed and the cerebral hemispheres were separated using a scalpel blade. A small amount of tissue was then removed from the dorsal surface of the two hemispheres, cutting parallel to the base of the brain, to create a flat surface prior to gluing the hemispheres onto a metal slicing block using cyanoacrylate glue with ventral side upwards. The block was then rapidly loaded into the slicing chamber of a Camden Vibroslice (CI7000 SMZ2) filled with chilled, oxygenated sACSF (for composition see Section 2.4).

400 µM thick horizontal slices (Fig. 2.1) were cut automatically at ultra-slow advance speed (0.15 mm/sec) using a vibration frequency of 80 Hz and displacement of 2 mm. The slice thickness permits a good compromise between maintaining both the local circuitry needed to generate oscillatory activity and sufficient oxygenation of the tissue. The cutting parameters were selected on the basis of test experience to give the best tissue preservation, viability of slices and quality of recordings.

Slices were cut and discarded until the ventral portion of the hippocampus and rhinal fissure were visible. Slices thereafter were trimmed with a scalpel to leave the MEC-hippocampus slice containing the following brain areas: ventral hippocampus, dentate gyrus, parahippocampal regions (subiculum, presubiculum, and parasubiculum), the entorhinal and the perirhinal cortices (Fig. 2.1).
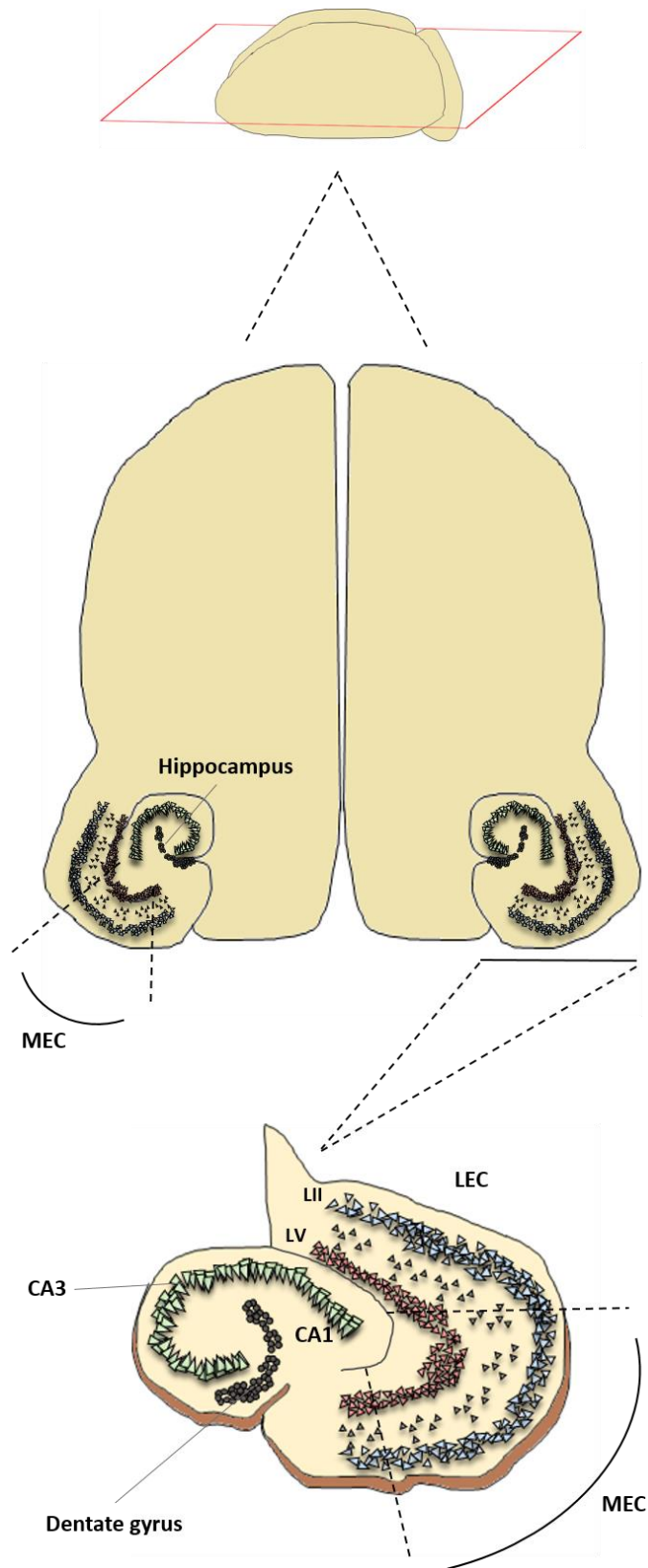
Figure 2.1: The horizontal brain slice preparation. *The rat brain was cut along the horizontal plane (top picture). Slices containing were trimmed to contain the MEC and HC (bottom picture).*

2.3 Slice maintenance and storage

Following dissection, slices were immediately transferred to a holding chamber (BSC-PC, Warner Instruments) containing ACSF (see 2.4 for composition) at room temperature. The chamber was bubbled continuously with carbogen gas producing a circular flow of oxygenated ACSF to the slices, which retained excellent viability for up to 8 hours. Slices were left to equilibrate for at least one hour before use in the holding chamber and were then transferred individually to the recording chamber when required (Fig. 2.2).

Top view

Side view
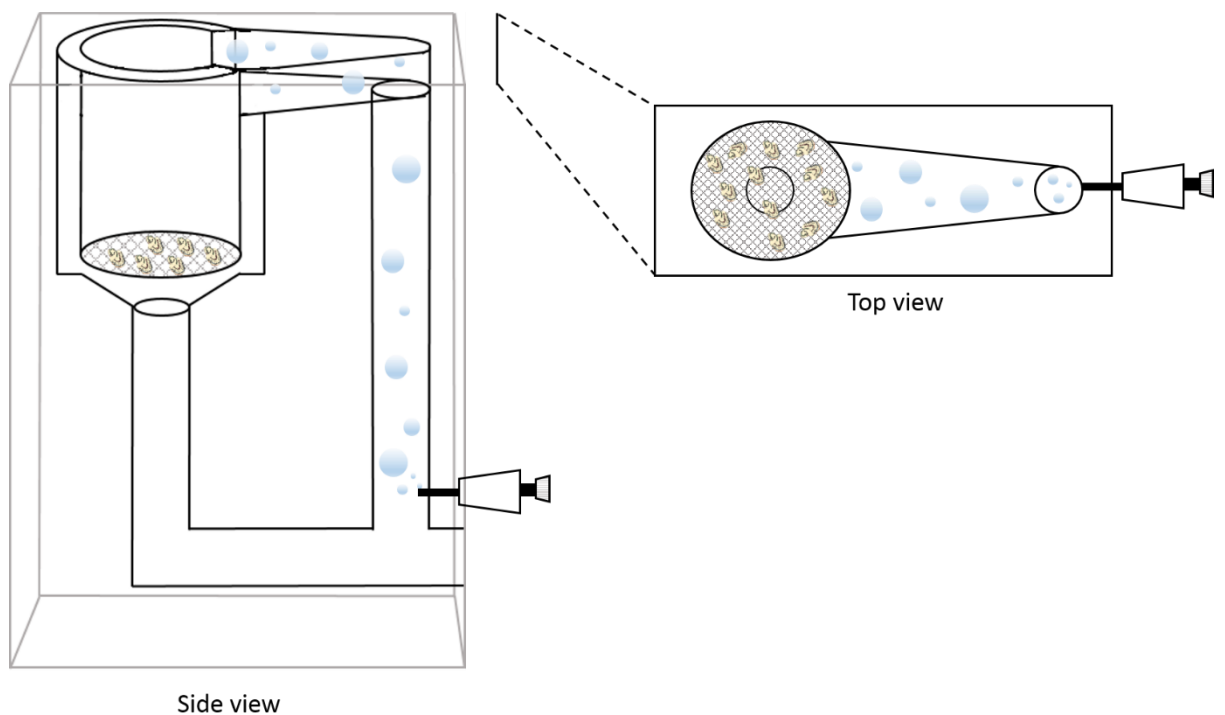
Figure 2.2: Schematic diagram of the BSC-PC slice holding chamber

2.4 ACSF

The core artificial cerebrospinal fluid (ACSF) used for recording was a Krebs bicarbonate buffer composed of (in mM) NaCl (126), KCl (4), $MgSO_4$ (1.25), NaH_2PO_4 (1.4), $NaHCO_3$ (24), $CaCl_2$ (2), D-glucose (10). In addition, sodium pyruvate (5), creatine monohydrate (5),

taurine (1), ascorbic acid (0.57) were added to maintain cellular metabolism and increase cell survival and viability.

Two variations of this recipe were used during the dissection and when storing the slices in the holding chamber. To store the slices, normal ACSF (above) was used with the addition of the anti-oxidant, n-acetyl cycsteine (6 μM) and the nonsteroidal anti-inflammatory drug indomethacin (45 μM), again to facilitate neuronal survival and slice viability.

During the brain dissection and slicing procedure a modified and protective sucrose based ACSF (sACSF) was used, composed of (in mM) sucrose (206), KCl (2), MgSO$_4$ (1.6), NaH$_2$PO$_4$ (1.25), NaHCO$_3$ (26), CaCl (2.25), glucose (10) and sodium pyruvate (5). In sACSF, NaCl was replaced by an equimolar concentration of sucrose to reduce the activity of Na$^+$/K$^+$ pumps, metabolic demand and general excitotoxic damage which leads to swelling and pyknosis. Additionally, n-acetyl cycsteine (6 μM), indomethacin (45 μM), the NMDAr channel blocker, ketamine (150 μM) and the ATP-gated P2X(7) receptor blocker, Coomassie Brilliant Blue (250 nM), were added as they provide notably improved neuronal preservation. We have previously established that the additives that we have used in our solutions facilitate production of viable, robust and high quality slices, but have no apparent direct effects on the pharmacology of glutamatergic or GABAergic transmission (Jones R.S.G. and Woodhall, G.L. unpublished observations).

All ACSF solutions had osmolarities between 300-310 Osm. The ACSF solution used for recording had a pH of 7.3-7.4 at 31$\pm$1°C. A summary of the composition of the three ACSF solutions and details of the additives are in table 2.1.

	Normal ACSF	Dissection ACSF	Storage ACSF
Sucrose	-	206 mM	-
NaCl	126 mM	-	126 mM
KCl	4 mM	2 nM	4 mM
$MgSO_4$	1.25 mM	1.6 mM	1.25 mM
NaH_2PO_4	1.4 mM	1.25 mM	1.4 mM
$NaHCO_3$	24 mM	26 mM	24 mM
$CaCl_2$	2 mM	2.25 mM	2 mM
D-glucose	10 mM	10 mM	10 mM
Ascorbic acid	570 µM	-	570 µM
Creatine monohydrate	5 mM	-	5 mM
Sodium pyruvate	5 mM	5 mM	5 mM
Indomethacin	-	45 µM	45 µM
N-acetyl cycsteine	-	6 µM	6 µM
Coomassie brilliant blue	-	250 nM	-
Ketamine	-	150 µM	-

Table 2.1: Composition of ACSF solutions

2.5 Whole cell patch clamp recording

2.5.1 General details and usage

At the single cell level, the ability of KARs to modulate the release of the neurotransmitters, glutamate and GABA, from synaptic terminals has been determined. To monitor transmitter release, whole-cell voltage clamp recording of spontaneous synaptic currents was used (Fig. 2.3). A high resistance electrical seal is formed between the patch clamp pipette and the cell membrane of the neuronal cell soma. This is achieved by pressing the glass pipette against the cell surface and applying negative pressure to form a gigaseal. The membrane under the tip of the patch pipette is then ruptured by increasing the negative pressure. By this means the recording pipette essentially becomes electrical continuous

with the membrane of the neurones allowing the recording of individual synaptic currents across the whole surface of the cell body and dendritic tree with high resolution and low noise. Currents with amplitudes as small as 2-3 pA can be reliably recorded this way. Additionally, the neuronal cytosol and the electrolyte solution in the pipette reach a diffusional equilibrium.
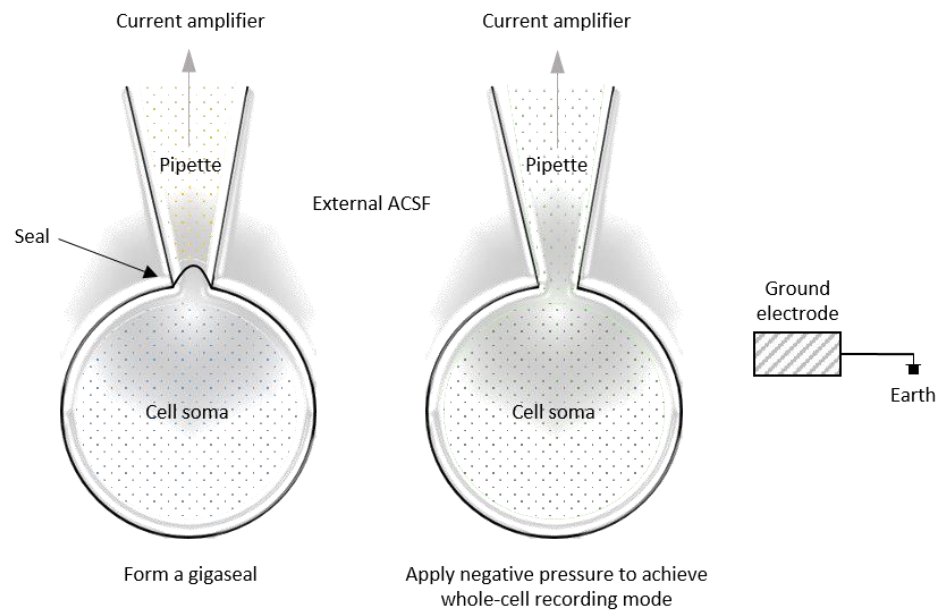
Figure 2.3: Whole-cell patch clamp. *A tight contact, or gigaseal, is formed between the pipette and the plasma membrane (left). In whole cell configuration, negative pressure is applied to achieve access into the neurone and a diffusional equilibrium is reached with the solution in the pipette and the interior of the cell.*

In voltage clamp mode the current passing through open ion channels on the postsynaptic cell, as neurotransmitters spontaneously released from presynaptic terminals interact with postsynaptic receptors, can be recorded. In most cortical neurones these comprise both spontaneous excitatory postsynaptic currents (sEPSCs) and spontaneous inhibitory postsynaptic currents (sIPSCs) mediated by glutamate or GABA, respectively.

Recording spontaneous synaptic currents provides a means of looking at both pre and postsynaptic changes at GABA and glutamate synapses. Alterations in time course and amplitude of spontaneous events are generally an indication that the postsynaptic receptors are being affected. On the other hand, if the frequency of the spontaneous

activity is altered in the absence of an overt change in amplitude, it can be concluded that presynaptic release properties are being targeted.

Spontaneous neurotransmitter release is comprised of two components. Firstly, spontaneous events can arise as a consequence of action potentials, generated in the soma or axon of the presynaptic neurone, invading the presynaptic terminal and opening voltage gated calcium channels (VGCC) initiating release that is usually multi-quantal. The second component is independent of action potentials and extracellular calcium, although there is still debate over how absolute the latter property is. These events reflect mono-quantal release of transmitter, and may depend on calcium sources inside the terminal. Experimentally, the action potential-dependent component can be removed by blocking voltage gated sodium channels (VGNC) with TTX, thus isolating the action potential-independent events. These are usually referred to as "miniature" events, and can be seen at both excitatory glutamate (mEPSCs) and inhibitory GABA synapses (mIPSCs). The advantage of recording mPSCs is that it rules out drug effects at pre-terminal areas, eliminates the possibility of network driven activity, and identifies sites of action as directly on the synaptic terminal.

These approaches have been used here to pharmacologically dissect out the contribution, location and function of KARs to modulation of neurotransmitter action at both excitatory and inhibitory synapses in the rat MEC. To achieve this, various agonists and antagonists for ligand gated ion channels were used (see section 2.7).

2.5.2 Neurones recorded

All experiments were conducted on neurones in layer II or layer V of the MEC. Specifically identifying neurones by morphology after dye injection was not attempted. However, the neurones were selected on the basis of roughly identifiable PC or SC morphology when viewed with DIC and are believed to be largely glutamatergic principal neurones. Neurones were selected for whole cell patch clamp based upon healthy, undamaged appearance. It is possible that occasional neurones recorded were interneurones, but these generally have very high baseline frequencies of synaptic currents, and any abnormal recordings were excluded from analysis.

2.5.3 Experimental details

For patch clamp recordings, individual slices were transferred from the holding chamber to a recording chamber where they were submerged in a continuous flow (2ml/min) of oxygenated (95% O_2, 5% CO_2) ACSF re-circulated from a small reservoir. Slices were held in place in the chamber with a slice anchor constructed from a thin U-shaped piece of stainless steel with several very thin strands of nylon thread glued across it. The ACSF was maintained 31 ± 1 °C using an inline heater (SH-27B, Warner Instruments) and a feedback power supply (TC-324, Warner Instruments). This temperature establishes a good physiological environment without compromising the longevity of the tissue. The whole circulating volume, including the reservoir, was ~10 ml and the volume of the recording chamber was ~0.5-1.0 ml. Slices were allowed to equilibrate at the recording temperature for at least 30 minutes under these conditions before recording commenced.

The recording chamber was mounted on an upright BX50WI Olympus microscope and neurones were visualised using a CCD infrared video camera (KP-M1E/K, Hitachi Kokusai Electric Inc.) and differential interference contrast (DIC) optics. Visual contrast was enhanced by use of an SP-11 video processor (Kramer Electronics Ltd; Israel). All neurones in this thesis were recorded in LII and LV of the MEC (unless stated otherwise) using an Axopatch 200B amplifier in voltage clamp configuration. A silver pellet electrode was placed in ACSF at the inlet to the recording chamber to act as a reference zero ('ground') current level. Whole cell patch-clamp pipettes were pulled from borosilicate glass pipettes (PG120, 1.2mm O.D x 0.93 mm I.D., Harvard Apparatus), with an open tip resistance of 1-4 MΩ, using a Flaming/Brown microelectrode puller. The pipettes were filled with the appropriate intracellular solution optimised for the desired postsynaptic current (PSC) recordings (see below). The filled pipettes were then inserted onto a microelectrode holder, forming an electrical connection via a chlorinated silver wire, and then loaded onto the head stage of the amplifier.

When a suitable neurone was identified a seal test was applied and the patch pipette was advanced under visual control and with positive pressure applied, to make contact with the surface. Negative pressure was then applied to attempt to achieve a gigaseal whilst monitoring the seal test. The recording was left to settle for 5-10 minutes after sealing,

before further negative pressure was applied to rupture the patch. Neurones were then voltage clamped at -60 mV and the recording allowed to equilibrate for 15-20 minutes before data was acquired. Access resistance was monitored at 5-minute intervals throughout recording and if it varied by greater than 15% neurones were excluded from analysis. Series resistance compensation was not used. Input resistances for the neurones recorded in these studies were of the order 500-700 MΩ.

Drugs were added directly to the perfusion ACSF reservoir and each treatment was applied for at least 15-20 minutes before washing out.

2.5.4 EPSCs

To record sEPSCs, patch pipettes were filled with a Cs gluconate-based patch solution containing (in mM) D-gluconate (100), HEPES (40), QX-314 (1), ethylene glycol tetracetic acid (0.6), NaCl (2), MgCl2 (5), tetraethylammonium-CL (5), phosphocreatine (10), ATP-Na (4), GTP-Na (0.3). The pH was adjusted to pH 7.3 with CsOH and diluted to 275-295 mOsm before use. To improve space clamp and to allow resolution of small events generated at distal dendritic sites, Cs and QX-314 were included in the patch solution to block potassium channels and VGNC, respectively.

In neurones clamped at -60 mV sEPSCs were recorded as inward currents. These are primarily mediated by sodium ions passing through AMPA receptors activated in response to spontaneous glutamate release from presynaptic terminals (see Berretta and Jones 1996). Action potential-independent events, or mEPSCs, were recorded by blocking VGNC with bath perfusion with TTX (1 μM).

2.5.5 IPSCs

To record sIPSCs, patch pipettes were filled with a Cs-based patch solution containing (in mM): CsCl (100), HEPES (40), QX-314 (1), EGTA (0.6), TEA-Cl (10), $MgCl_2$ (5), ATP-Na (4), and GTP-Na (0.3). The pH was adjusted to pH 7.3 with CsOH and diluted to 275-295 mOsm before use. In neurones clamped at -60 mV, IPSCs were recorded as outward currents (high Cl^- in internal solution), which were primarily mediated by chloride (Cl^-) ions passing

through GABA$_A$Rs consequent upon their activation by GABA, spontaneously released from presynaptic terminals. SYM2206 (20 µM) and DL-AP5 (40 µM) were added to the perfusion ACSF to block AMPAR and NMDAR receptors, respectively, and permit recording of sIPSCs uncontaminated by the presence of glutamatergic sEPSCs. Activity-independent mIPSCs were isolated by the addition of TTX (1 µM).

2.5.6 Data acquisition and analysis

Signals were filtered at 2 kHz and digitized at 50 kHz using a Digidata 1440A A-D converter (Axon Instruments). Data were recorded direct to computer hard drive using AxoScope software. PSCs were analysed off-line. Minianalysis software (Synaptosoft, Decatur) was used to detect PSCs using a threshold-crossing algorithm. Threshold varied from neurone to neurone but was maintained at a constant level once set for any individual neurone analysis. Threshold was usually set at a level around 2.5 times the baseline noise. As a general rule, at least 200 events were accumulated and analysed in any given situation (control v drug) although in neurones with low baseline rates this was not always possible. In these cases the number of events in control and drug situations was matched as closely as possible.

Miniature and spontaneous EPSCs and IPSCs were detected using a threshold of 3-7 pA and all records were manually inspected to eliminate clearly or suspected non-biological events from analysis. The following parameters were detected: frequency, assessed as events per minute, amplitude (pA), decay time (ms), rise times (ms) and holding current (pA) and were analysed via the nonparametric Kolmogorov-Smirnov test (KS-test) of the cumulative probability distribution, constructed from ~200 events from each neurone. Significant differences from control obtained via KS-tests are represented as asterisks on histograms and assigned when $p \leq 0.01$. EPSC/IPSC rise times were calculated as time between 10 – 90 % of maximum current while decay times taken as time for current to decay 33.3%.

Pooled data for each treatment group were compared using the means of each parameter in each neurone. Data are presented as a percentage change from control level before drug application. Errors represent the standard error of the mean (SEM). Statistical comparisons were made using repeated measures one-way ANOVA and paired t-tests when comparing

data which had been derived from the same slice or cell i.e. before and after addition of drugs. Two-way ANOVA analysis was used when comparing groups that were influenced by two different independent variables (e.g. time and age). Between slice changes were assessed using a Mann Whitney rank sum test. Significance was set at a level of $P < 0.05$ and signified by an asterisk.

2.6 Local field potential recordings

2.6.1 General details and usage

To monitor functional changes in KARs in network activity within local MEC circuitry, throughout development, we used KA to induce oscillatory activity in neuronal networks. These oscillations represent synchronous population activity in thousands of neurones and the electrical events reflect the extracellular voltage changes occurring as the summed, or 'net', electrical current flow in multiple neurones. They were recorded extracellularly as local field potentials (LFP) using low resistance glass microelectrodes filled with ACSF and inserted into the specific areas of interest.

2.6.2. Experimental details

Slices were prepared and stored in exactly the same way as for the whole-cell patch clamp experiments. In most experiments, two slices were placed on a layer of lens paper in an interface-type recording chamber (BSC2, Digitimer Ltd. UK), where they were maintained at the interface between a continuous perfusion (1.2-1.4 ml/min) of oxygenated (95% O_2, 5% CO_2) ACSF and warm humidified carbogen gas. The perfusion solution was recirculated from a storage reservoir (50 or 100 ml) in a water bath maintained at 25±1°C.

Extracellular LFP recordings were made using microelectrodes pulled from borosilicate glass pipettes (PG120, 1.2mm O.D x 0.93 mm I.D., Harvard Apparatus) with a resistance of 1-4 MΩ, using a Flaming/Brown microelectrode puller. The pipettes were filled with normal ACSF. Separate electrodes were placed in LII and LV MEC of the same slice under visual control using a Leica MZ8 binocular microscope (Fig. 2.4), and using Narishige micromanipulators. Slices were left to equilibrate for at least 30 minutes at room

temperature in the interface chamber before being warmed gradually to 31±1°C using a PTCO3 temperature controller (Digitimer Ltd. UK) which warmed a water reservoir in the bottom of the recording chamber through which the perfusion ACSF was circulated.
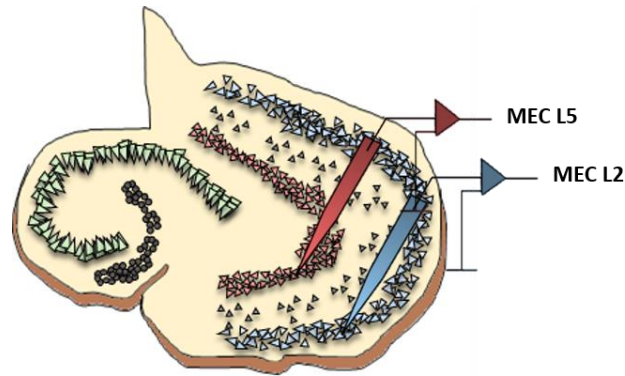
Figure 2.4: Diagrammatic representation of the combined MEC-HC brain slice. *Figure shows the positioning of the electrodes for LFP recordings in layer II and V MEC.*

2.6.3 Generation of oscillatory activity

Control recordings of baseline activity were made for at least 20 min prior to the addition of any pharmacological agents to ensure the oscillatory activity was a result KAR activation, and not spontaneous network activity. Oscillatory activity was induced by perfusion with KA (400 nM) bath applied via the circulating reservoir of ACSF. One-minute epochs of activity were recorded at 15 min intervals during the establishment and maintenance of oscillatory activity, and analysed immediately for amplitude and frequency. Drug treatments were only applied when the oscillatory activity had stabilised i.e. the amplitude and frequency was within 15 % variability in 3 consecutive recordings.

2.6.4 Data acquisition and analysis

LFPs were recorded using an EXT-02 extracellular amplifier (NPI Electronic). Signals were low pass filtered at 0.5 kHz and digitised at 10 kHz using a Minidigi 1B digitizer (Molecular Devices). Raw data were recorded straight to a computer hard disk using AxoScope software.

LFP recordings were quantified on the amplitude of the modal peak and the peak frequency of the oscillation. Power spectra were created from 1-minute epochs of raw data using a fast Fourier transformation (FFT) algorithm, from which measurements of amplitude and frequency could be determined directly from the peak. FFTs convert the time domain of the original signal into a representation in the frequency domain by deconstructing the waveform of the oscillation into a series of sine and cosine functions. The phase information inherent in the analysis was removed, and the magnitude squared for each frequency component was used to determine the power distribution. The amplitude is expressed as the sum of the voltage squared at each frequency band (μV^2/Hz), which, in this thesis, were theta (4-10 Hz), beta (12-30 Hz) and gamma (30-80 Hz).

Pooled data for each treatment group were compared using the means of each parameter in each slice. Data are presented as a percentage of control level (before drug application). Error bars represent the SEM and 'within slice' comparisons were made using ANOVA and Student's paired t-test. Comparisons made between different slices and age groups were made using the non-parametric Mann-Whitney test.

2.7 Drugs and solutions

All ingredients for patch solutions were obtained from Sigma, and ACSF salts were obtained from Sigma or Fisher Scientific. Ketamine was purchased from Dodge Animal Health Ltd.

Drugs were made up as stock solutions, either distilled water (dH_2O) or dimethyl sulfoxide (DMSO; Sigma, UK), stored in aliquots at -20 ˚C and diluted to the desired concentration the ACSF reservoir immediately prior to perfusion

ATPA: ((RS)-2-Amino-3-(3-hydroxy-5-tert-butylisoxazol-4-yl) propanoic acid), Tocris, UK. dH_2O stock solution. Selective GluK1 agonist.

Bicuculline: ([R-(R*,S*)]-6-(5,6,7,8-Tetrahydro-6-methyl-1,3-dioxolo[4,5-g]isoquinolin-5-yl)furo[3,4-e]-1,3-benzodioxol-8(6H)-one) Tocris, UK. DMSO stock solution. Selective $GABA_A$R antagonist.

DL-AP5: (DL-2-Amino-5-phosphonopentanoic acid), Tocris, UK. dH_2O stock solution. Selective, competitive NMDAR antagonist.

GYKI 52466: dihydrochloride (4-(8-Methyl-9H-1,3-dioxolo[4,5-h][2,3]benzodiazepin-5-yl)-benzenamine dihydrochloride). Tocris, UK. DMSO stock solution. Selective, non-competitive AMPAR antagonist.

KA: (Kainic acid), Tocris, UK. dH_2O stock solution. Agonist at KAR.

SYM 2206 ((±)-4-(4-Aminophenyl)-1,2-dihydro-1-methyl-2-propylcarbamoyl-6,7-methylenedioxyphthalazine). DMSO stock solution. Tocris, UK. Non-competitive AMPAR antagonist.

TTX (Tetrodotoxin), Alomone Labs., Israel. dH_2O stock solution

UBP-310: ((S)-1-(2-Amino-2-carboxyethyl)-3-(2-carboxy-thiophene-3-yl-methyl)-5-methylpyrimidine-2,4-dione), Tocris, UK. DMSO stock solution. GluK1 receptor antagonist.

Chapter 3

A comparison of spontaneous excitatory transmission in LII and LV in neonate and juvenile rats

3.1 Introduction

A surge of attention has focussed on the pathological role of the MEC in a number of psychiatric and neurological disorders. Neurones in LII have a selective vulnerability to aging and AD, showing the earliest evidence of regional atrophy which is associated with age-related memory dysfunction (Stranahan and Mattson, 2010). Both LI and LV are functionally implicated in the development of TLE in both patients and animal models (Pilli et al., 2012, Armstrong et al., 2016). MRI studies have shown abnormally decreased volumes of the EC in patients with schizophrenia, which is not apparent in the hippocampus or in healthy controls (Baiano et al., 2008). Enhanced understanding of the development of the MEC can inform the interpretation of the predisposition of MEC neurones to many psychiatric disorders, including AD, epilepsy and schizophrenia, which can be used to develop more targeted therapeutics.

The aim of this chapter was to compare the baseline characteristics of sEPSCs in LII and LV, in both neonatal and juvenile Wistar rats, using whole cell patch clamp. The synaptic potentials mediated by spontaneous neurotransmitter release impinging on their somata and dendrites have two components; they can be driven by action potentials arriving at the terminals (activity dependent; sEPSCs), or by mono-quantal neurotransmitter release (activity independent; mEPSCs), and these two components can be recorded in the absence or presence of TTX, respectively. Spontaneous background currents, or synaptic 'noise', are important in signal detection and determine overall excitability of the network (Jones and Woodhall, 2005). The properties of EPSCs assessed in this chapter included the frequency (in events per minute), amplitude (pA), decay time (ms) and rise time (ms).

Previous work in this laboratory conducted a study of the characteristics of EPSCs in principal neurones in LII and LV of adult Wistar rats (Berretta and Jones, 1996). In summary, the studies showed that the frequency of sEPSCs was similar in LII and LV, but that the events in the LV had a greater average amplitude, and this was attributed to the existence of a population of larger events not present in LII. sEPSCs in LV had faster rise and decay times. When action potential driven release was blocked, the frequency of EPSCs was decreased by 15-20% in both layers, but a decrease in amplitude was noted in LV (as a

result of blockade of the larger amplitude events), but not in LII. Finally, the majority of events in both layers were mediated by activation of postsynaptic AMPARs, but occasional events were recorded that were the result of activation of postsynaptic NMDARs, and these were seen relatively more frequently in LV. The animals used in these studies were considerably older (6-8 months) than those used in the present study (P8-28), and experimental parameters and conditions in this laboratory have changed considerably since these initial studies were published (e.g. use of neuroprotective and other additives, more sophisticated cutting equipment). In order to provide a baseline for the current studies of developmental changes in KAR activation, it was deemed necessary to repeat some of this comparison in the current experimental conditions and in younger animals. This study is concerned with early postnatal development, comparing sEPSCs in two groups of rats aged P8-11 and P21-28 which will be referred to as neonate and juvenile aged rats hereon in. The rationale for choosing these age groups stems from the preliminary immunohistochemical data from the lab of Prof. Elek Molner, showing a clear change in KAR expression between these age groups, and delineating the functional consequence of this was ultimately the aim of this thesis.

A further series of experiments in this lab recorded the properties of sEPSCs in LIII (Chamberlain, 2009, Greenhill et al., 2014). Again, these were done in slices from Wistar rats that older than the animals used in the present study (P28-40), although were more comparable to those used here. A comparison between sEPSCs neurones in LIII and properties reported in older animals (Berretta and Jones, 1996; Greenhill et al 2014) showed the following main differences: a much higher frequency in LIII, a similar amplitude to events in LII, but similar rise and decay times to LV. There was a much higher contribution of action potential dependent release in LIII (around 60-70%), but, as in the other layers, the vast majority of sEPSCs were mediated by AMPARs, with occasional events mediated by postsynaptic NMDARs (Greenhill et al., 2014, Chamberlain, 2009).

Thus, the aims of the current study were principally

1. To provide a detailed picture of the properties of sEPSCs in LII and LV of juvenile animals (of a similar age to those used in studies in LIII; Chamberlain, 2009; Chamberlain et al., 2012; Greenhill et al., 2014).

2. To compare the properties of sEPSCs in LII and LV neurones during early development as a basis for subsequent investigations in to developmental roles for KAR in excitatory transmission.

3.2 Methods

Experiments were conducted on combined slices of EC and hippocampus, as described in Chapter 2, from neonatal (P8-11; 20-35 g) and juvenile (P20-28; 50-100 g) Wistar rats. Whole cell voltage clamp recordings of sEPSCs and mEPSCs were made from principal neurones in LII and LV in the MEC. Neurones were voltage clamped at -60 mV. Cells were selected with good access resistance that remained stable for the duration of the recording.

Mean values for frequency, inter-event interval (IEI; inverse of frequency), amplitude, rise times and decay times were determined from a sample of at least 200 events during a continuous recording period for each neurone. EPSC/IPSC rise times were calculated as time between 10 – 90 % of maximum current while decay times taken as time for current to decay 33.3%. Statistical comparisons were made using a non-parametric (Mann Whitney) test and KS-tests for average mean data and cumulative probability distributions (constructed using 200 events from each neurone), respectively. Statistical significance was defined when $P < 0.05$, except for KS-analysis, where significance was reached if $P < 0.01$ due to the sensitivity of the test.

To facilitate comparisons between groups and gain an overall indication of integrated excitation we calculated an arbitrary charge transfer number for each neuronal population at the different age levels. This is approximately related to the area under the curve of the EPSC. Thus, from the mean value of parameters for the sEPSC populations we calculated the sum of the rise and decay times, and determined the product of this and the mean amplitude and frequency.

3.3 Results

3.3.1 Characterisation of sEPSCs in layers II and V of the MEC in juvenile rats

3.3.1.1 Amplitude and Frequency of sEPSCs

Whole-cell recordings from LII (n = 32) and LV (n = 19) juvenile (P20-28) neurones, at a holding potential of -60 mV, exhibited continuous synaptic activity reflected as sEPSCs. They were mediated by primarily by activation of AMPARs as they could be blocked by NBQX (Fig. 3.1)
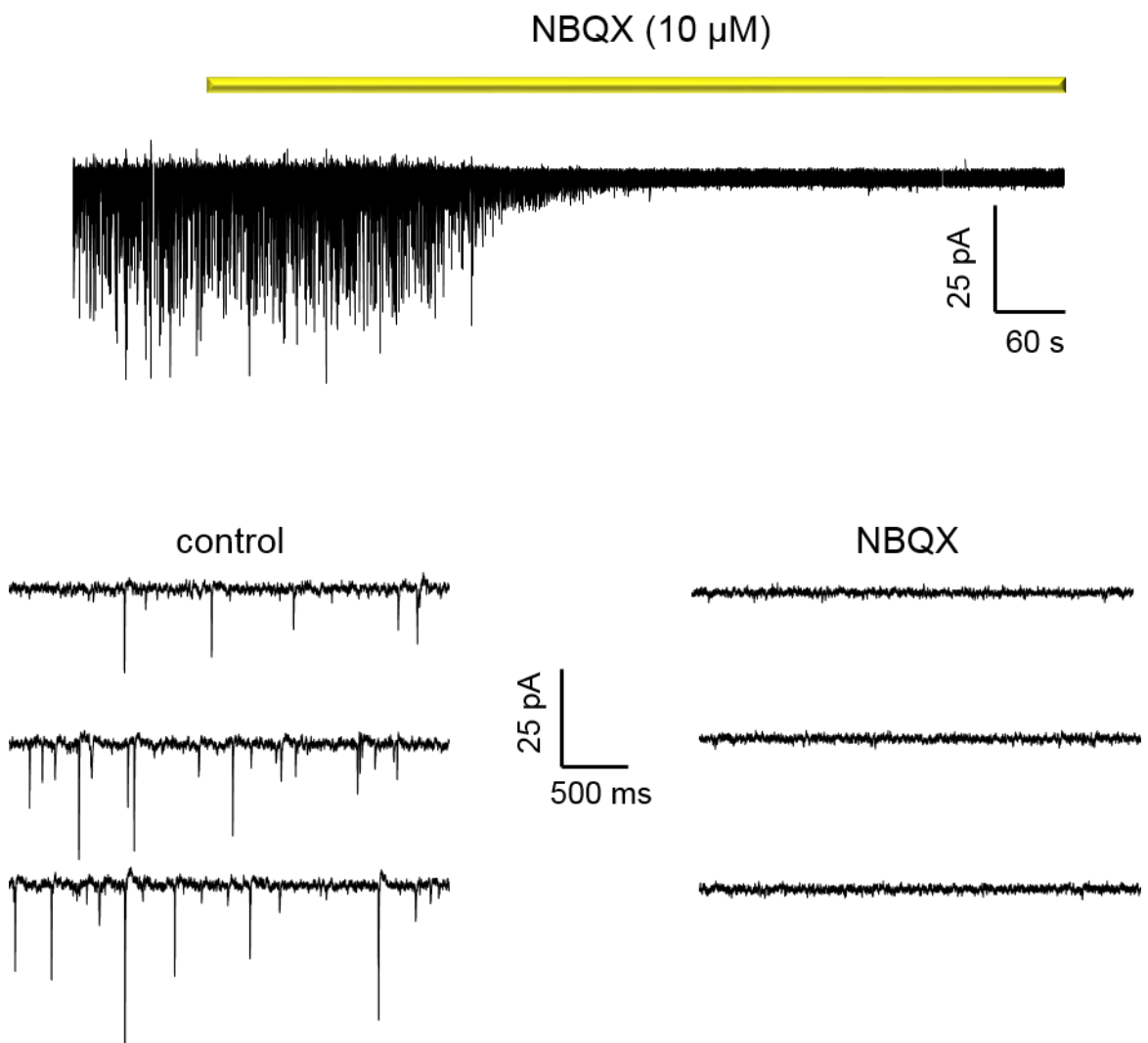
Figure 3.1: Pharmacology of sEPSCs in MEC neurones. *The traces show the typical response of neurones in the MEC before and after the addition of NBQX (10 µM). NBQX (10 µM) effectively abolished sEPSCs.*

sEPSCs occurred at a significantly higher frequency in LII (195.7 ± 22.6 events/min) compared to LV (123.6 ± 31.2 events/min; P < 0.05). The cumulative probability plot of the IEI shows LII neurones have a significantly smaller IEI compared to LV (P<0.0001; KS-test), with no LII neurones IEI exceeding 15.5 seconds compared with a maximum of 40.4 seconds in LV. Berretta and Jones (1996) reported frequencies of ~85 events/min in both LII and LV, which is comparable to LV, but not LII, in this study.

The mean event amplitudes of sEPSCs were similar in both LII and LV principal neurones at 9.4 ± 0.6 pA and 10.5 ± 0.7 pA. These values were lower than in the older animals reported by Berretta and Jones (1996) and although there was still a slight skew towards larger amplitude events in LV, the difference in mean amplitude between the two layers was not significant. Summary data for frequency and amplitude of sEPSCs in juvenile rats are summarised in Fig. 3.2.
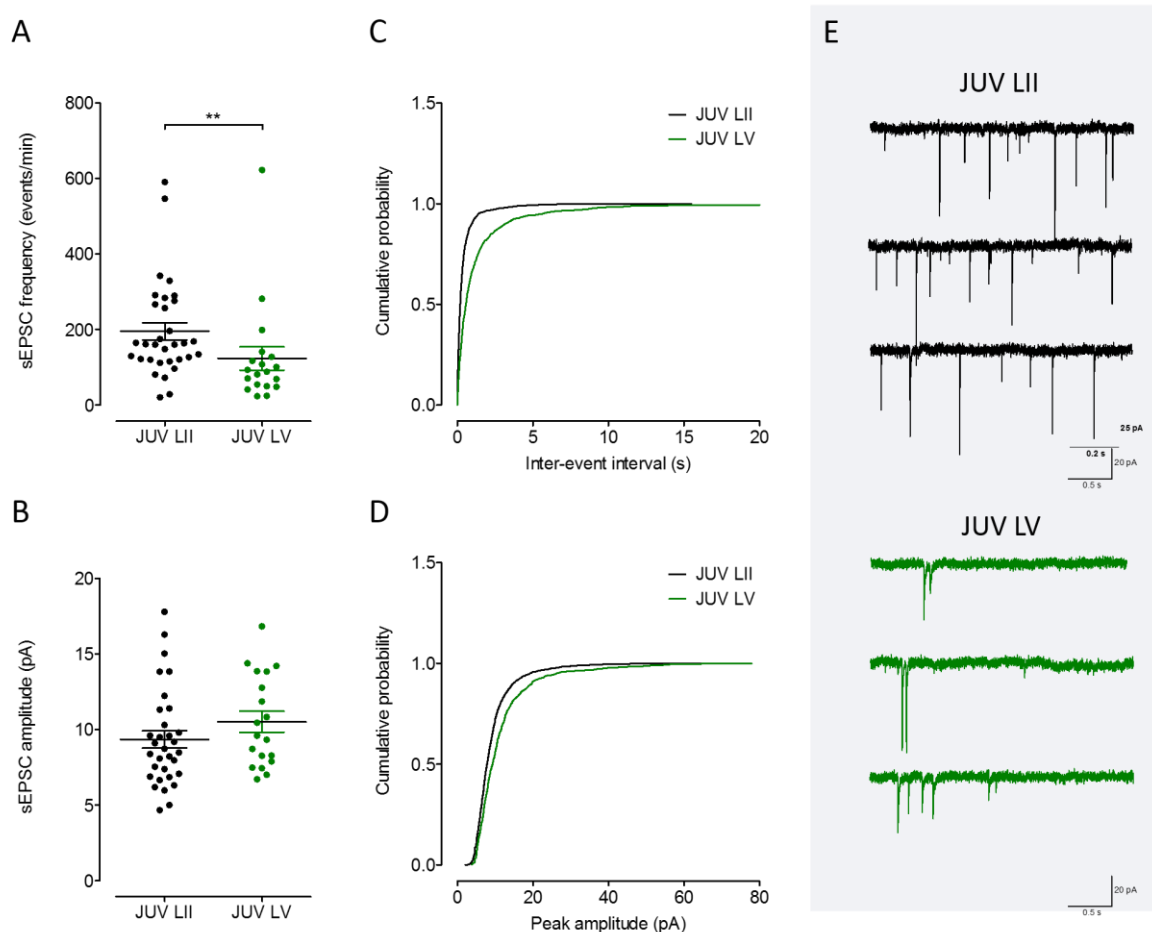
Figure 3.2. Comparison of sEPSC frequency and amplitude in LII and LV MEC principal neurones in juvenile rats. *(**A**) Average sEPSC frequency and (**B**) sEPSC amplitude data from 32 LII (black) and 19 LV (green) principal neurones. Average frequency of sEPSCs was significantly greater in LII neurones (P < 0.001; Mann Whitney test). (**C**) Cumulative probability distribution of the IEI and (**D**) peak amplitude of events (> 30) collected and pooled from each neurone in LII and LV. Cumulative probability distributions show the smaller IEI in LII neurones (P < 0.0001; KS-test) (**E**) sEPSCs recorded in a LII and sEPSCs recorded in a LV neurone. Three traces are consecutive recordings of spontaneous activity.*

3.3.1.2 Kinetics

sEPSCs recorded in LII (n = 32) had an mean rise time of 3.9 ± 0.3 ms and mean decay time of 3.6 ± 0.2 ms, whereas in LV (n = 19) the average rise and decay time was 2.7 ± 0.3 ms and 2.9 ± 0.2 ms (Fig. 3.2). Both rise and decay times were significantly faster in sEPSCs of LV neurones compared with LII neurones (P = 0.01 and P = 0.03; Mann Whitney test), agreeing qualitatively with the studies of Berretta and Jones. However, the absolute values for rise times were faster (LII: 2.5 ± 0.1 ms and LV: 1.87 ± 0.1 ms) and the average decay time was much slower (LII: 8.0 ± .0.4 and LV: 5.7 ± 0.3). We cannot be sure that any of the

differences noted here compared to the older studies are real in the absence of comparisons made under identical conditions, but they do emphasise the importance of comparing data within the same experimental conditions and preparation, for example, when comparing this data to neonatal sEPSCs. The cumulative distribution analysis clearly confirms that sEPSCs in juvenile LV neurones had significantly faster rise and decay times compared to LII neurones (P < 0.0001 for both plots C & D, KS-test).
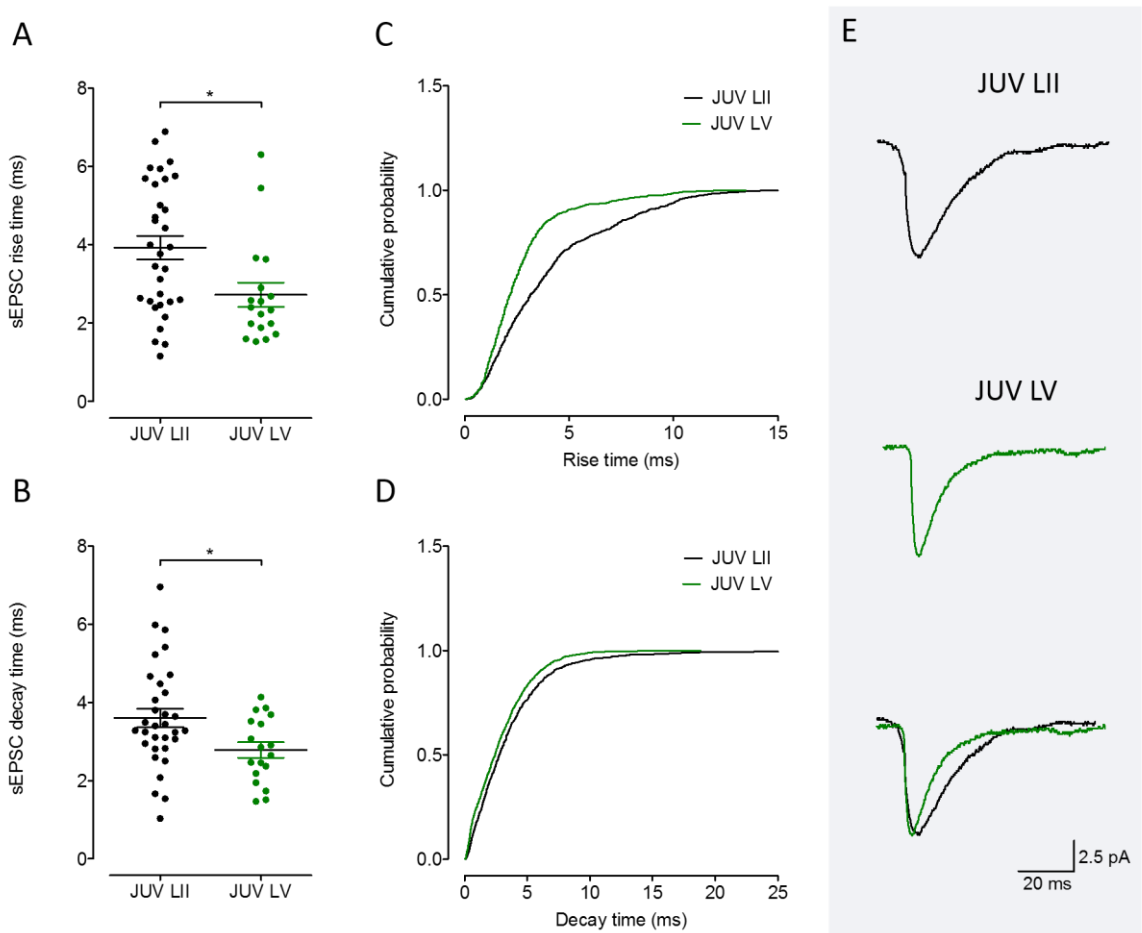
Figure 3.3. Comparison of sEPSC decay and rise time in LII and LV MEC principal neurones of juvenile rats. (***A***) *Scatter plot of sEPSC rise time and (**B**) sEPSC decay time data from 32 LII (black) and 19 LV (green) principal neurones. The average rise time of sEPSCs was significantly faster in LV neurones (P = 0.01; Mann Whitney test). (**C**) Cumulative probability distribution of the rise time and (**D**) decay time of events (>30) collected and pooled from each neurone in LII and LV. Cumulative probability distributions show the faster rise and decay times in LV neurones (P < 0.0001; KS-test, both plots). (**E**) Averaged sEPSCs of a LII (top; black) and a LV (middle; green) neurone are shown (bottom: superimposed events).*

3.3.1.3 Effect of TTX on sEPSCs

mEPSCs recorded in the presence of TTX are considered to reflect the release of single quanta from individual release sites, independently of action potentials (Arancio et al., 1994). Spontaneous glutamate release in the presence and absence of TTX in LII and LV principal neurones is summarised in Fig. 3.3 and 3.4, respectively. Pooled cumulative distributions of the IEIs of sEPSCs in LII and LV (Fig. 3.5) showed a slight shift to the right in the presence of TTX, indicating an increase in the IEI (decreased frequency) of events in both layers (P < 0.0001 for both plots, KS-test). TTX (1 μM) reduced the frequency of sEPSCs in both layers by ~28-30 %, from an average of 195.7 ± 22.6 (n = 32) to 139.7 ± 19.8 events/min (n = 17) in LII and 123.6 ± 31.2 (n = 19) to 83.9 ± 16.1 events/min (n = 14) in LV. These results are comparable with the Berretta and Jones (1996) study, which showed TTX (0.5 μM) reduced the frequency of sEPSCs in both layers by 15-20%. This is in contrast to previous work on LIII, done at comparable ages and conditions to the present experiments, which showed that TTX had a much larger effect on sEPSCs (decrease in frequency of -85 %), signifying the majority of events in LIII are action potential-dependent (Chamberlain, 2009). Unlike in LIII, most of the sEPSCs in LII and LV of the MEC are therefore miniature events, mediated by spontaneous release of single quanta from presynaptic sites. This may be associated with a greater preponderance of recurrent excitatory connections between neurones in LIII compared to LII and LV (Dhillon and Jones, 2001)

TTX had differential effects on the amplitude of sEPSCs. In LII, there was no change in the average amplitude (9.4 ± 0.6 pA vs 8.9 ± 0.6 pA) or the cumulative amplitude distribution (Fig. 3.3). However, in LV there was a significant decrease in the average amplitude of sEPSCs from 10.5 ± 0.7 pA (n = 19) to 8.3 ± 0.8 pA (n = 14) in the presence of TTX (P = 0.01, Mann Whitney test). The plot in Fig. 3.5 shows that the change in the amplitude distribution was mainly due to the loss of larger amplitude sEPSCs in LV (P < 0.0001; KS-test), whereas in LII the cumulative amplitude distribution was unaltered, again in accordance with the previous studies (Berretta and Jones, 1996).

There was no difference between the mean kinetics of sEPSCs and mEPSCs in LII (rise time 3.9 ± 0.3 ms vs 4.2 ± 0.4 ms and decay time 3.6 ± 0.2 ms vs 3.5 ± 0.2ms) and in LV (rise time

2.7 ± 0.3 ms vs 2.4 ± 0.2 ms and decay time 2.9 ± 0.2 ms vs 2.8 ± 0.2ms) principal neurones. The effects of TTX on sEPSCs in LII and LV MEC are summarised in table 3.1.
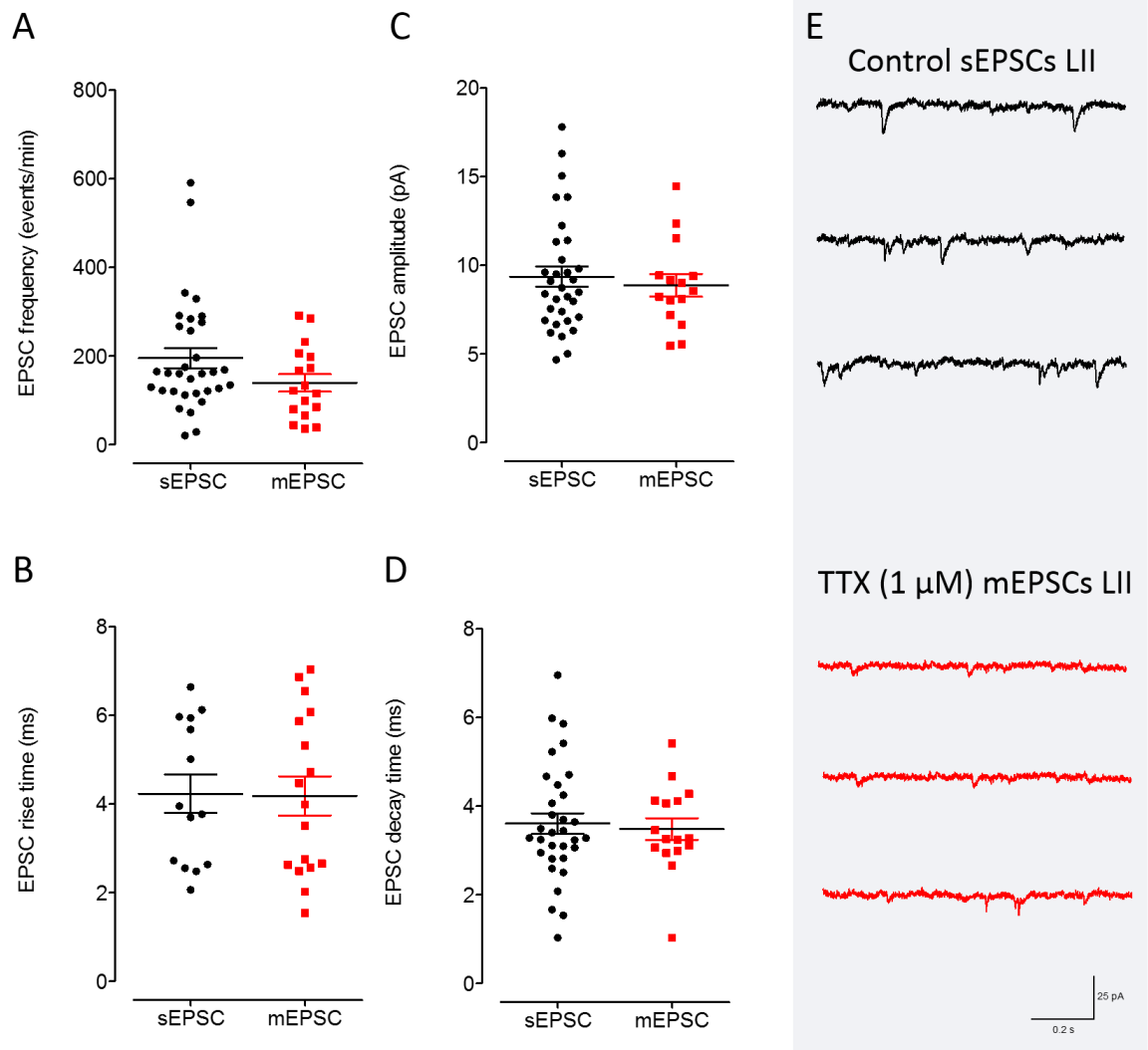
Figure 3.4: Comparison of sEPSCs and mEPSCs in LII neurones of juvenile rats. Voltage clamp recordings were made from LII neurones in the absence (sEPSCs; n = 32; black) and presence (mEPSCs; n = 17; red) of TTX (1 μM). (A) Scatter plots comparing the (A) frequency (events/min), (B) rise time (ms), (C) amplitude (pA) and (D) decay time (ms) of sEPSCs and mEPSCs from LII principal neurones. Note no significant differences between sEPSCs and mEPSCs of LII neurones. (E) sEPSCs and (F) mEPSCs recorded in a LII MEC neurone, before and after the application of TTX. Three traces are consecutive recordings of spontaneous activity.
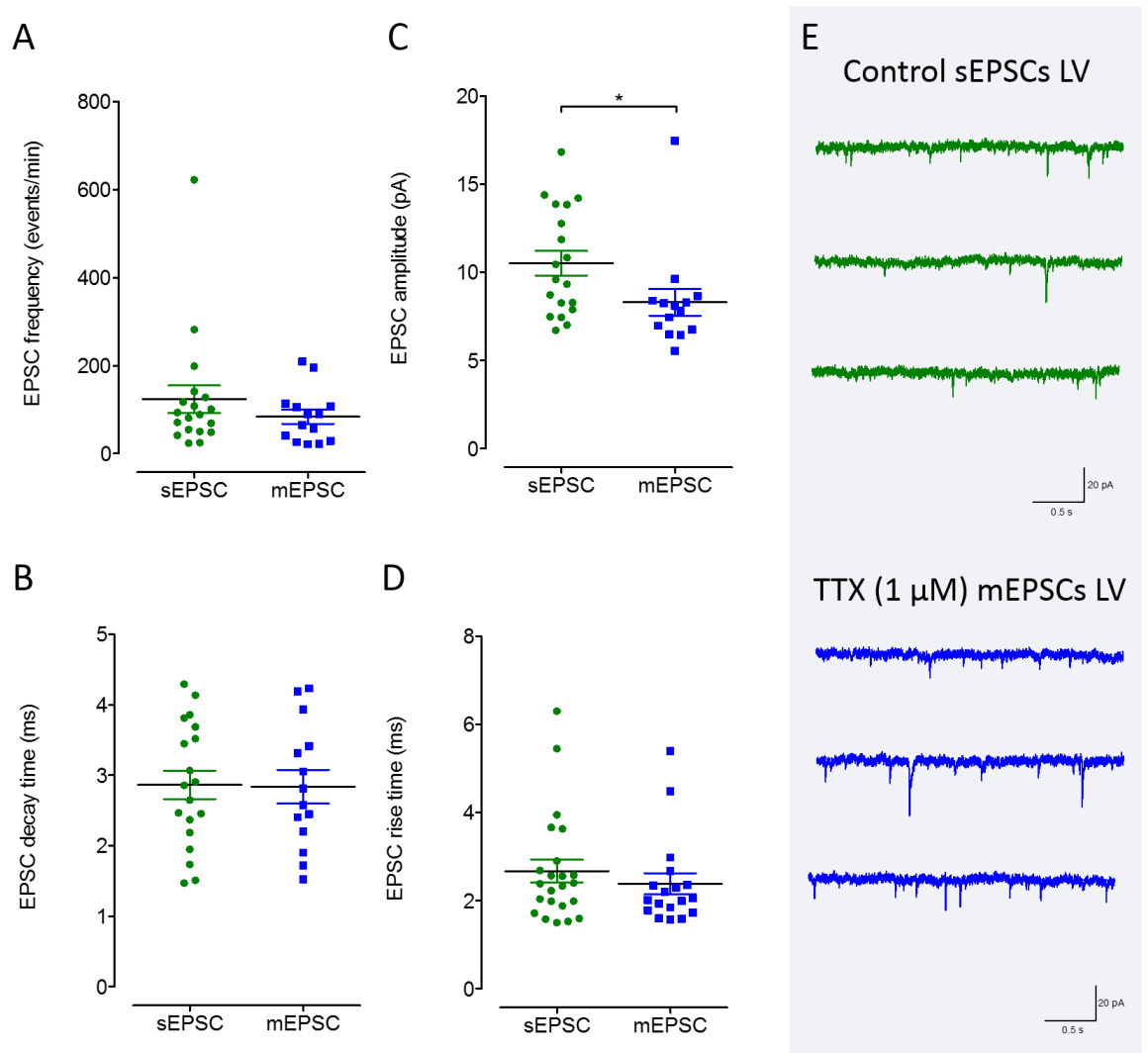
Figure 3.5: Comparison of sEPSCs and mEPSCs in LV principal neurones of juvenile rats. *Voltage clamp recordings were made from LV neurones in the absence (sEPSCs; n = 19; green) and presence (mEPSCs; n = 14; blue) of TTX (1 μM). (A) Scatter plots comparing the (A) frequency (events/min), (B) rise time (ms), (C) amplitude (pA) and (D) decay time (ms) of sEPSCs and mEPSCs from LV principal neurones. Note the decreased mean amplitude in the presence of TTX (P = 0.019; Mann Whitney test) (E) sEPSCs and (F) mEPSCs recorded in a LV MEC neurone, before and after the application of TTX (μM). Three traces are consecutive recordings of spontaneous activity.*

	Layer	N number	Frequency (events/min)	Amplitude (pA)	Rise time (ms)	Decay time (ms)
Juvenile sEPSCs	**II**	**32**	**195.7 ± 22.6**	**9.4 ± 0.6**	**3.9 ± 0.3**	**3.6 ± 0.2**
Juvenile mEPSCs	**II**	**17**	**139.7 ± 19.8**	**8.9 ± 0.6**	**4.2 ± 0.4**	**3.5 ± 0.2**
Juvenile sEPSCs	**V**	**19**	**123.6 ± 31.2**	**10.5 ± 0.7**	**2.7 ± 0.3**	**2.9 ± 0.2**
Juvenile mEPSCs	**V**	**14**	**83.9 ± 16.1**	**8.3 ± 0.8 ***	**2.4 ± 0.2**	**2.8 ± 0.2**

Table 3.1: Summary of the effects of TTX on SEPSCs in juvenile LII and LV neurones. Average frequency, amplitude, rise and decay times of sEPSCs in LII (black) and LV (green) neurones. * denotes statistically significant (P < 0.05) changes between sEPSCs and mEPSCs in the same layer. Note the smaller amplitude in LV mEPSCs compared to LV sEPSCs.

3.3.2 Characterisation of sEPSCs in layers II and V of the MEC in neonatal rats

3.3.2.1 Frequency and amplitude

Whole cell recordings from LII (n = 16) and LV (n = 18) neonatal (P8–14) neurones, at a holding potential of -60 mV, like those in juvenile animals exhibited continuous sEPSCs manifested as spontaneously occurring inward currents. sEPSCs occurred at a much higher frequency in LII (137.2 ± 21.6 events/min) compared to LV (36.3 ± 7.7 events/min; P = 0.0001, Mann Whitney test). A cumulative probability plot of IEI shows significantly shorter IEIs in LII neurones compared with LV (P<0.0001, KS-test), with no LII neurones exhibiting IEI exceeding ~15 seconds compared with a maximum of ~40 seconds in LV neonatal neurones.

The mean event amplitudes of sEPSCs were similar in both LII and LV principal neurones at 8.4 ± 0.5 pA and 9.0 ± 0.5 pA, but the cumulative distribution plots of amplitude revealed a shift towards larger amplitude events in LV compared to LII in neonatal neurones (P <

0.0001; KS-test). Amplitudes of sEPSCs in LII did not exceed 50 pA, compared with a maximum amplitude of 130 pA in LV. The frequency and amplitude of sEPSCs in neonatal rats are summarised in Fig. 3.6.

3.3.2.2 Kinetics

There was no difference between the mean kinetics of sEPSCs from LII (rise time 5.4 ± 0.2 ms; decay time 4.2 ± 0.3 ms, n = 18) and LV (rise time 5.0 ± 0.3 ms; decay time 4.8 ± 0.6 ms, n = 18) in neonatal neurones. Despite this, a skew towards faster rise times of sEPSCs in LV compared to LII neurones can be identified from the cumulative distribution plots in Fig. 3.7 C ($P < 0.0001$, KS-test). No differences significant differences in decay time were present between the two layers at this stage of development (Fig. 3.7).
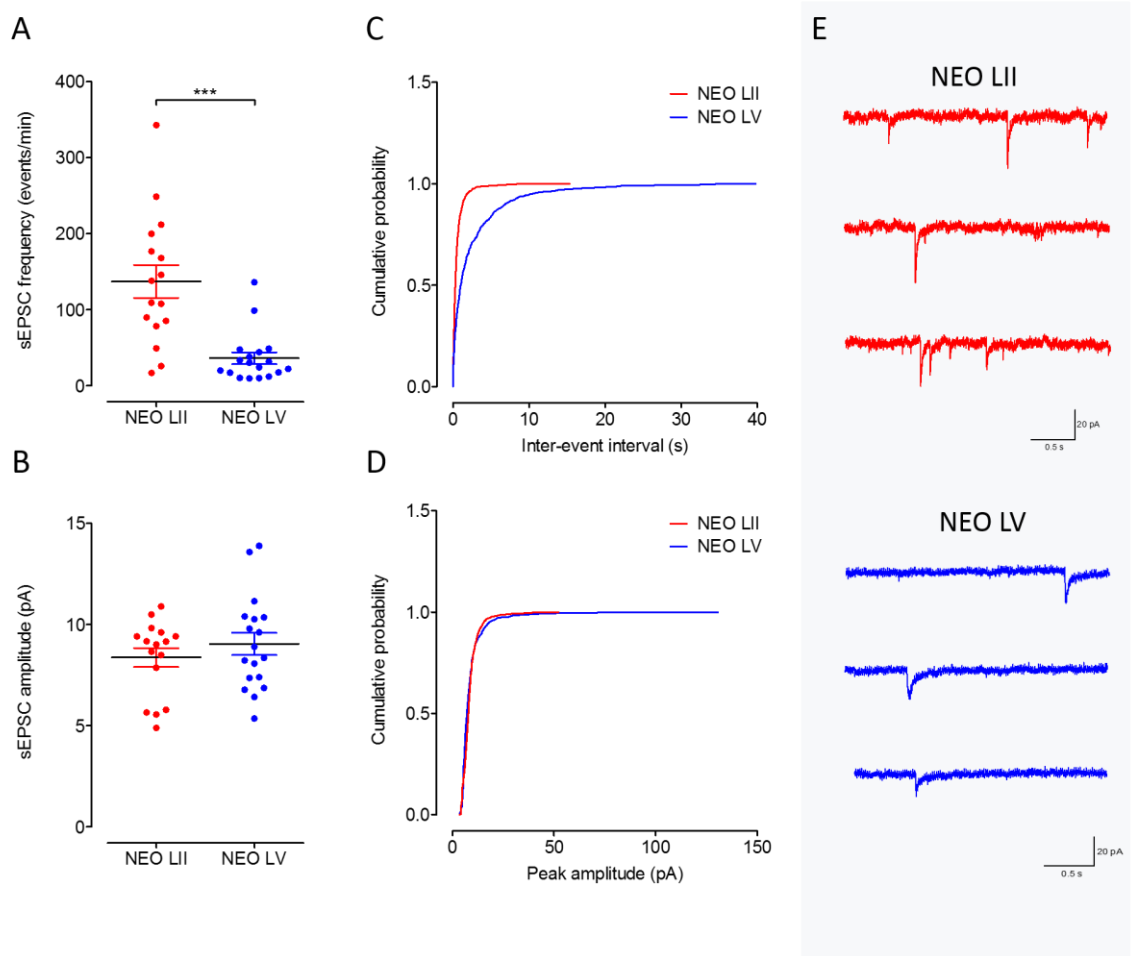
Figure 3.6: Comparison of sEPSC frequency and amplitude in LII and LV neurones of neonate rats. *(A) Scatter plots comparing the sEPSC frequency and (B) sEPSC amplitude data from 16 LII (red) and 18 LV (blue) principal neurones. Average frequency of sEPSCs was significantly greater in LII neurones (P < 0.001; Mann Whitney test). (C) Cumulative probability distribution shown of the IEI and (D) peak amplitude of events (> 55) collected and pooled from each neurone in LII and LV. Cumulative probability distributions show the smaller IEI in LII neurones (P < 0.0001; KS-test), and the presence of higher amplitude events in LV neurones. (E) sEPSCs recorded in a LII and sEPSCs recorded in a LV neurone. Three traces are consecutive recordings of spontaneous activity. Note the slow frequency of LV neonatal principal neurones.*
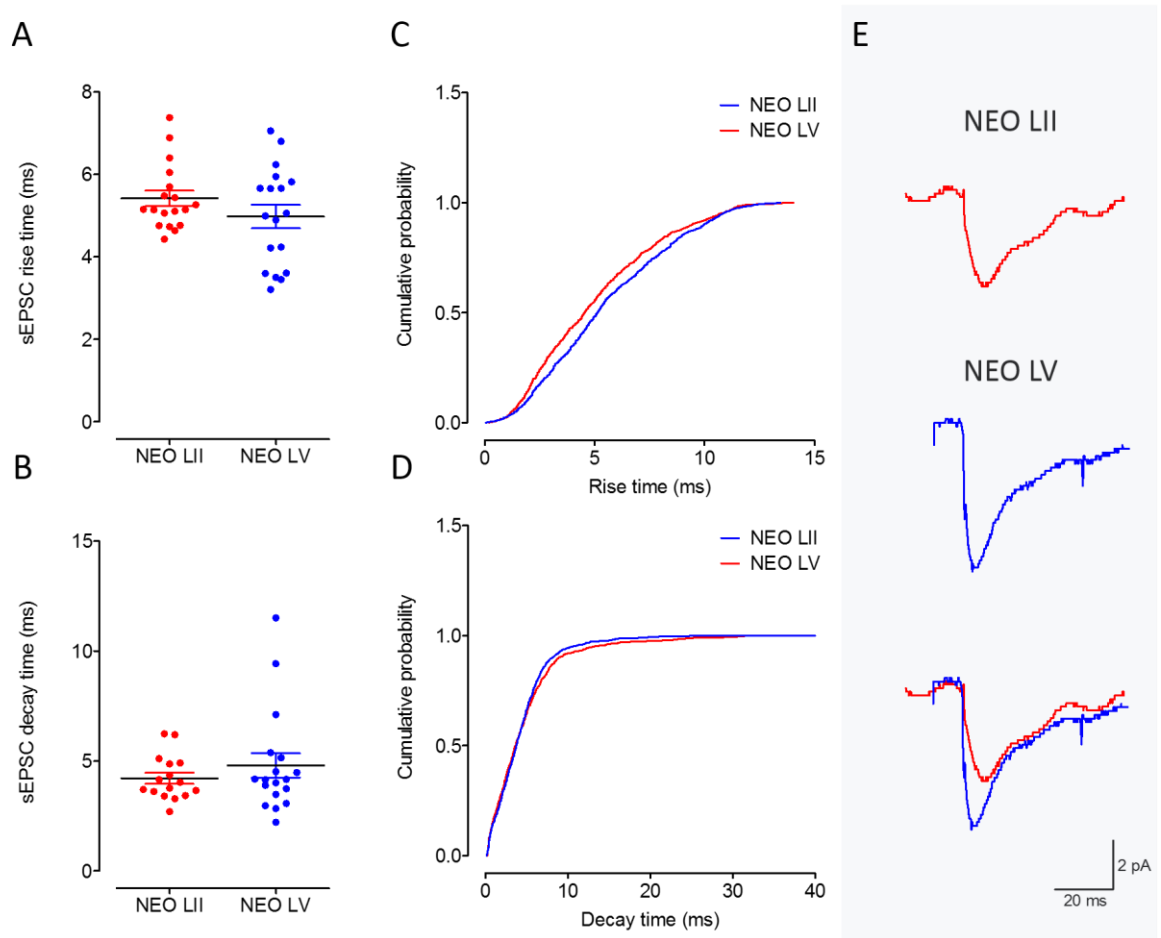
Figure 3.7: Comparison of sEPSC decay and rise time in LII and LV neurones of neonate rats. (A) Scatter plot of sEPSC rise time and **(B)** sEPSC decay time data from 16 LII (red) and 18 LV (blue) principal neurones. There were no significant differences between LII and LV mean rise or decay times. **(C)** Cumulative probability distribution shown of the rise time and **(D)** decay time of events (>55) collected and pooled from each neurone in LII and LV. Cumulative probability distributions show the faster rise time in LV neurones ($P < 0.0001$; KS-test), but no differences in decay time. **(E)** Averaged sEPSCs of a LII (top; red) and a LV (middle; blue) neonate neurone(s) are shown (bottom: superimposed events).
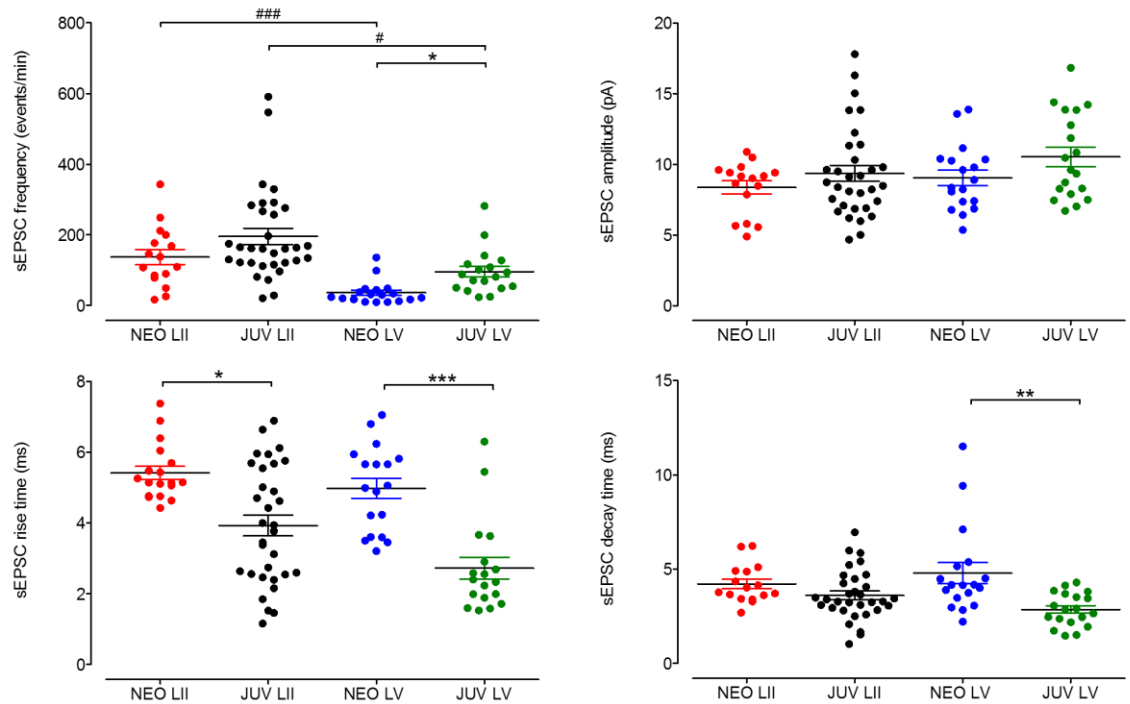
	Layer	N number	Frequency (events/min)	Amplitude (pA)	Rise time (ms)	Decay time (ms)
Neonate	**II**	**16**	**137.2 ± 21.6**	**8.4 ± 0.5**	**5.4 ± 0.2**	**4.2 ± 0.3**
Juvenile	II	32	195.7 ± 22.6	9.4 ± 0.6	3.9 ± 0.3	3.6 ± 0.2
Neonate	**V**	**18**	**36.3 ± 7.7**	**9.0 ± 0.5**	**5.0 ± 0.3**	**4.8 ± 0.6**
Juvenile	**V**	**19**	**123.6 ± 31.2**	**10.5 ± 0.7**	**2.7 ± 0.3**	**2.9 ± 0.2**

Table 3.2: Summary data of the baseline characteristics of sEPSCs in LII and LV of neonate and juvenile neurones. *Scatter plots of sEPSC frequency, amplitude, rise times and decay times of sEPSCs in neurones from neonate LII (red, n = 16)), juvenile LII (black, n = 32), neonate LV (blue, n = 18) and juvenile LV (green, n = 19). * and # denote statistically significant developmental and laminar differences.*

3.3.3 Age Comparison

3.3.3.1 Frequency and amplitude

Whole cell recordings of sEPSCs were compared in 35 neurones recorded in slices from neonatal rats (P8-14) and 51 neurones from juvenile animals (P20-28). Again events were largely abolished by CNQX in both groups, confirming their dependence on AMPAR activation (not shown).

In LII, the mean frequency of sEPSCs in neonatal (n = 16) and juvenile (n = 32) neurones was 137.2 ± 21.6 events/min and 195.7 ± 22.6 events/mins, respectively. The mean frequencies were not significantly different, although the cumulative probability plot of IEI showed a slight shift towards longer IEIs (decreased frequency) in the neonates, which was significant when compared with a KS-test (P < 0.0001). In contrast, there was a marked difference in mean frequency of sEPSCs neurones in LV in neonatal (36.3 ± 7.7; n = 18) and juvenile (123.6 ± 31.2 events/min; n = 19) slices, which was significant (P < 0.01, Mann Whitney test). This is shown by the scatter plot in Fig. 3.8. The decreased frequency in neonatal LV neurones is reinforced by the cumulative probability distribution of IEI, showing a clear rightward shift towards increased IEIs in the neonatal neurone population (P < 0.0001, KS-test).

Mean amplitudes of sEPSCs in neonatal neurones did not significantly differ from the amplitude of sEPSCs in juvenile neurones in either LII (8.4 ± 0.5 pA and 9.4 ± 0.6 pA) or LV (9.0 ± 0.5 pA and 10.5 ± 0.7 pA), the cumulative probability analyses of amplitude did show leftward shifts towards smaller amplitude events compared to neonates (P < 0.0001 for both plots, KS-test). Although there was a slight overall shift towards lower amplitude events in LV neonatal neurones, there were also occasional cells that showed much larger amplitude events in neonatal slices. sEPSC amplitude in the population of juvenile LV neurones did not exceed 80 pA, whereas in neonatal LV neurones amplitudes up to 130 pA were occasionally seen. Comparisons of frequency and amplitude of sEPSCs in juvenile and neonatal MEC principal neurones are summarised in Fig. 3.8 and 3.9.
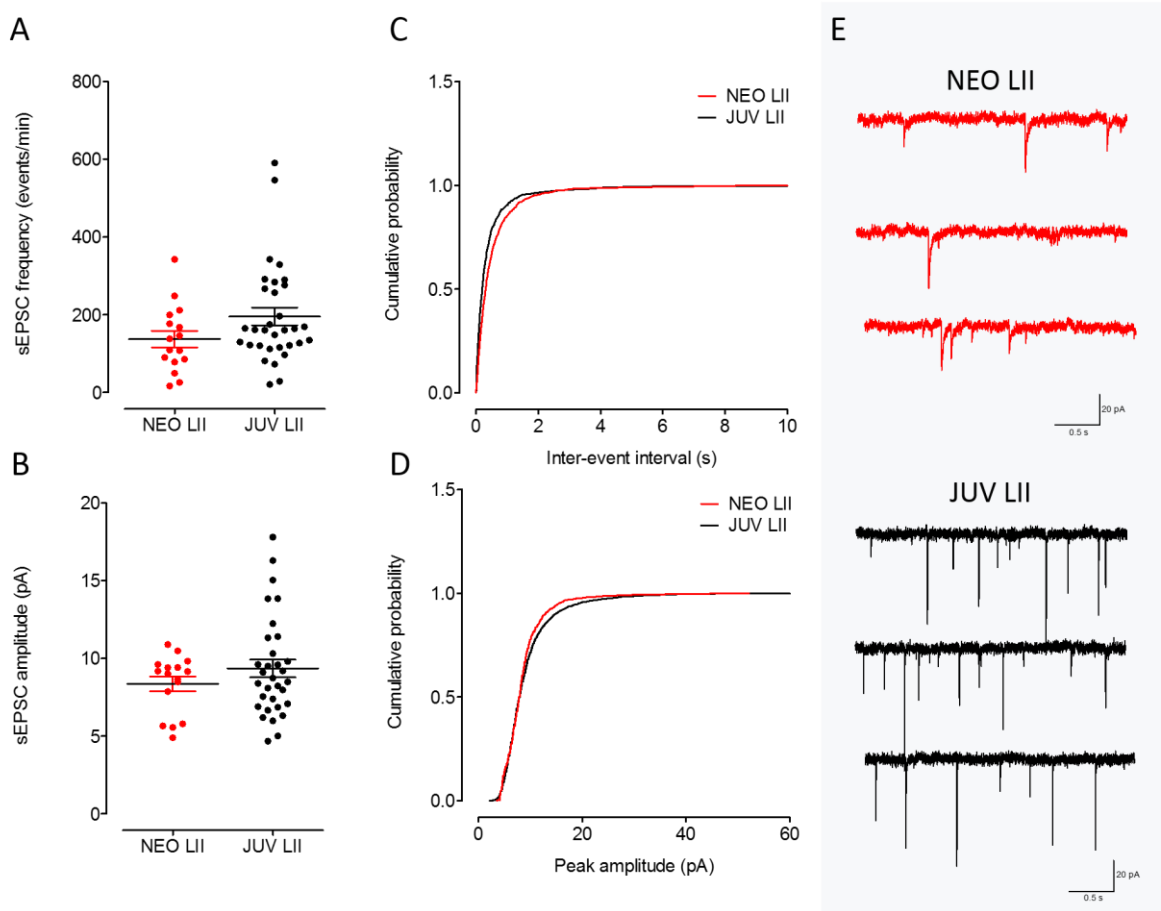
Figure 3.8: Comparison of sEPSC frequency and amplitude in neonatal and juvenile neurones in LII. (A) Scatter plots comparing the sEPSC frequency and (B) sEPSC amplitude data from 16 NEO (red) and 32 JUV (black) principal neurones. (C) Cumulative probability distribution shown of the IEI and (D) peak amplitude of events (> 55) collected and pooled from each neurone. Cumulative probability distributions show a slight skew towards increased IEI and decreased amplitude of NEO sEPSCs (P < 0.0001 both plots; KS-test).(E) sEPSCs recorded in a LII NEO and sEPSCs recorded in a LII JUV principal neurone in the MEC. Three traces are consecutive recordings of spontaneous activity
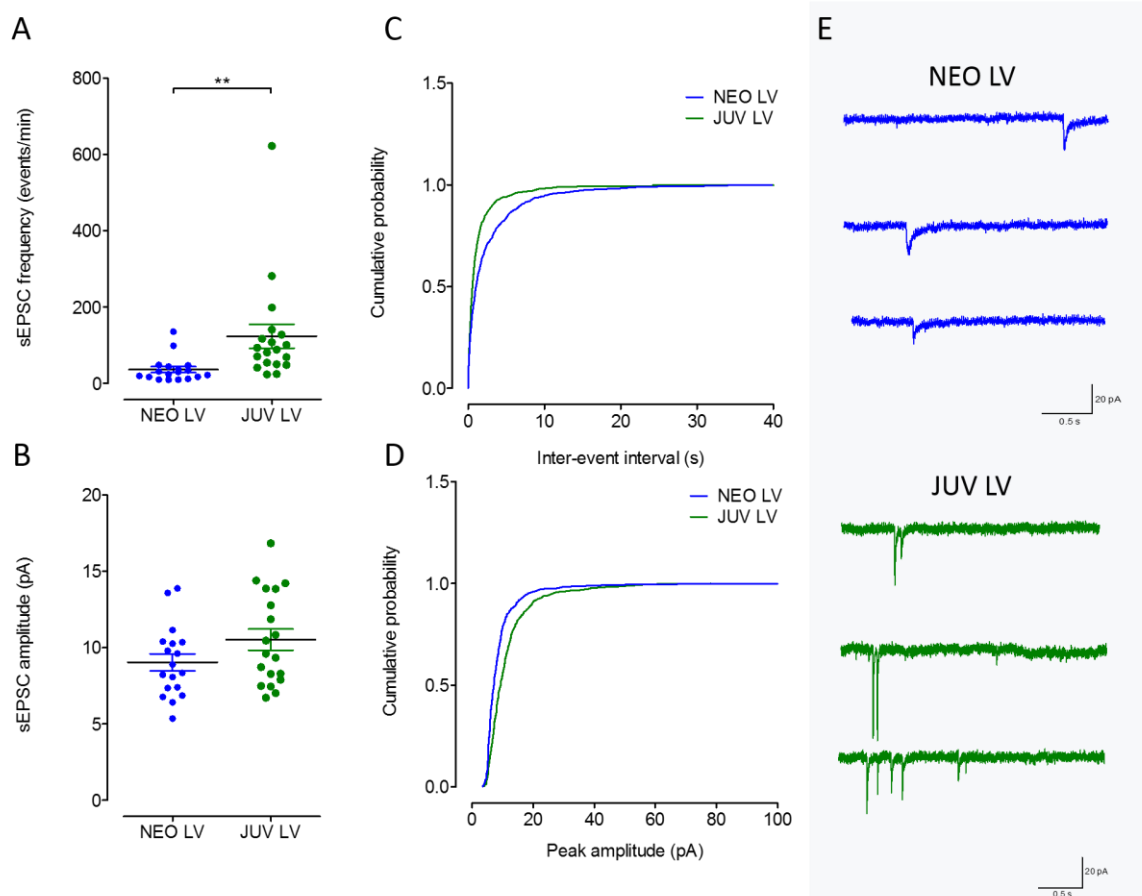
Figure 3.9: Comparison of sEPSC frequency and amplitude in neonate and juvenile neurones in LV*. (****A****) Scatter plot of sEPSC rise time and (****B****) sEPSC decay time data from 18 NEO (blue) and 19 JUV (green) neurones. Frequency of sEPSCs in LV neurones significantly increases during development. (****C****) Cumulative probability distribution shown of the IEI and (****D****) peak amplitude of events (> 52) collected and pooled from each neurone. Note the clearly increased IEI (slower frequency) in NEO compared with JUV sEPSCs (P < 0.0001, KS-test), and the presence of higher amplitude events in juvenile sEPSCs of LV MEC.). (****E****) sEPSCs recorded in a LV NEO and sEPSCs recorded in a LV JUV principal neurone*

3.3.2.2 Kinetics

The most dramatic differences between neonatal and juvenile sEPSCs occurred in their rise and decay kinetics. The average rise time of sEPSCs got significantly faster with development in LII (from 5.4 ± 0.2 ms to 3.9 ± 0.3 ms; P = 0.003, Mann Whitney test) and LV (from 5.0 ± 0.3 ms to 2.7 ± 0.3 ms; P < 0.0001, Mann-Whitney test) neurones. Similarly, mean decay times of events were significantly slower in neonatal compared to juvenile sEPSCs in both LII (from 4.2 ± 0.3 ms to 3.6 ± 0.2 ms; P = 0.04, Mann Whitney test) and LV

(from 4.8 ± 0.6 ms to 2.9 ± 0.2 ms; P = 0.0006, Mann Whitney test) neurones. These findings are reinforced by the cumulative distribution analysis (Fig. 3.10) which clearly indicate sEPSCs in LII and LV MEC neurones had significantly faster rise and decay times in the older juvenile rats (P < 0.0001 for both plots, KS-test).

Faster kinetics in the juvenile compared to neonatal sEPSCs are present in both layers, though developmental changes are more pronounced in LV MEC neurones. This seems to be due to a developmental elimination of slower sEPSCs in LV juvenile neurones, a trait not present in LII neurones. For example, no events in juvenile LV neurones exceed a decay time of 18 ms, but 2% of events in neonatal LV neurones exceed this decay time. In LII neurones, sEPSCs exceeding a decay time of 18 ms remains at 1 % in both neonatal and juvenile neurones. This can be clearly seen from the cumulative distribution plots in Fig. 3.10.
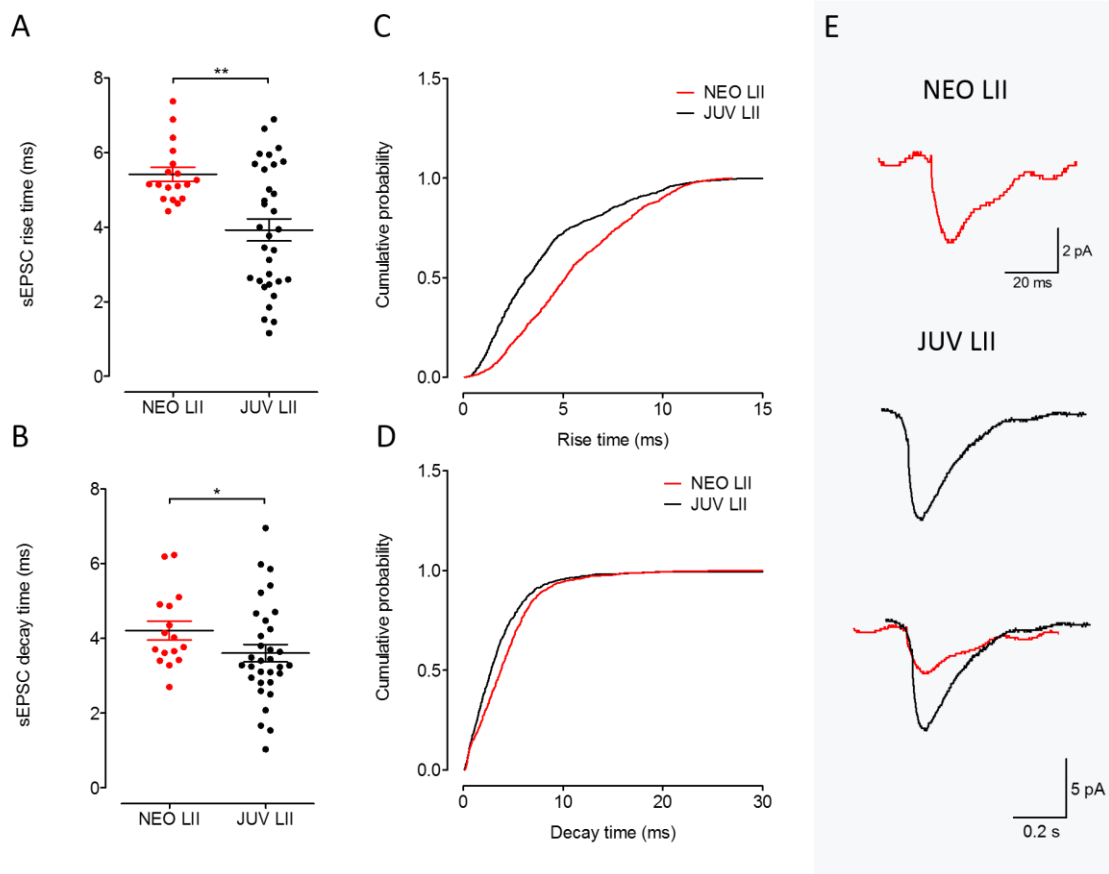
Figure 3.10: Comparison of sEPSC decay and rise time in neonatal and juvenile neurones in LII. *(**A**) Scatter plot of sEPSC rise time and (**B**) sEPSC decay time data from 16 NEO (red) and 32 JUV (black) principal neurones. Rise and decay times were significantly faster in JUV II sEPSCs compared to NEO LII sEPSCs (P = 0.003 and P = 0.04, respectively, Mann Whitney test). (**C**) Cumulative probability distribution shown of the rise time and (**D**) decay time of events (>30) collected and pooled from each neurone. Cumulative probability distributions show the faster rise and decay time in JUV neurones compared to NEO (P < 0.0001; KS-test). (**E**) Averaged sEPSCs of a NEO LII and a JUV LII neurone are shown (bottom: superimposed events).*
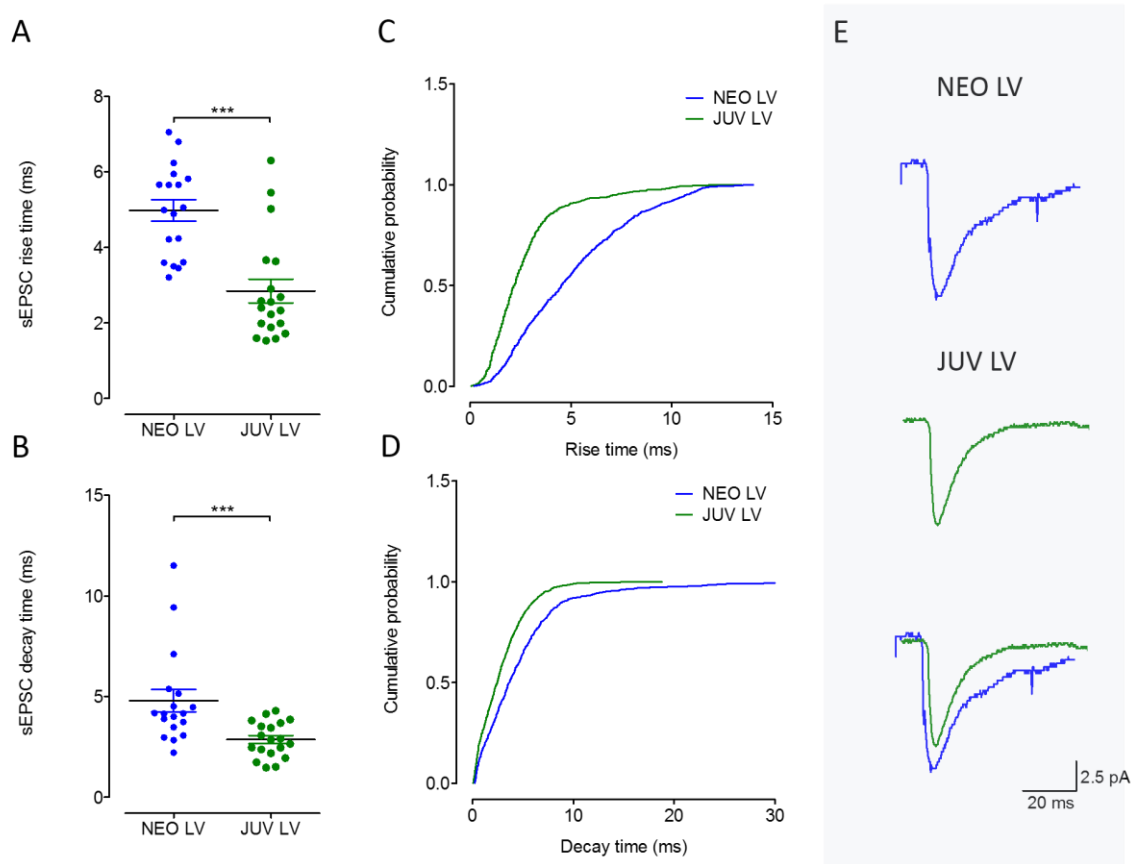
Figure 3.11: Comparison of sEPSC decay and rise time in neonate and juvenile neurones in LV. (***A***) *Scatter plot of sEPSC rise time and* (***B***) *sEPSC decay time data from 18 NEO (blue) and 19 JUV (green) neurones. Rise and decay times were significantly faster in JUV V sEPSCs compared to NEO LV sEPSCs (P = 0.0006 and P < 0.0001, respectively, Mann Whitney test).* (***C***) *Cumulative probability distribution shown of the rise time and* (***D***) *decay time of events (>52) collected and pooled from each neurone. Cumulative probability distributions clearly show the faster rise and decay time in JUV neurones compared to NEO (P < 0.0001 for both plots; KS-test).* (***E***) *Averaged sEPSCs of a NEO LV and a JUV LV neurone(s) are shown (bottom: superimposed events).*

Age group	Layer	Charge transfer (/min)	Charge transfer (/s)	Comparison	Ratio
Neonate	II	11064	184	**II:II** JUV v NEO	1.3:1
Juvenile	II	13797	230	**V:V** JUV v NEO	2.3:1
Neonate	V	3202	53	**II:V** NEO	3.5:1
Juvenile	V	7268	121	**II:V** JUV	1.9:1

Table 3.3: Charge transfer values and ratios of sEPSCs. Charge transfer values are indicative of the overall neuronal excitation, and are calculated using the following equation: Rise time + decay time x amplitude x frequency. For /sec divide by 60.

3.4 Discussion

3.4.1 Comparison of sEPSCs in juvenile compared to older animals

Previous reports of sEPSC properties in the MEC (LII, LIII and LV) have come from studies in older animals than the juvenile group reported here (Berretta and Jones, 1996, Chamberlain, 2009, Greenhill et al., 2014). Attempts to make comparisons between these studies must involve caution, and until equivalent studies have compared all three layers in the same age groups it may be dangerous to draw too much inference from the differences in terms of developmental effects. Nevertheless, and notwithstanding differences in experimental approaches and procedures in different studies, it is instructive to consider first how the juvenile and adult sEPSCs may differ, but perhaps more importantly how the two age groups studied together here, may also differ.

Despite considerable variability in sEPSC frequency from cell to cell, and within different studies, sEPSCs in LIII MEC seem to have the highest frequency (276 ± 60.0 events/min), followed by LII (195.7 ± 22.6 events/min) and LV (123.6 ± 31.2 events/min), in juvenile rats. Previous work (Berretta and Jones, 1996; Greenhill et al, 2014) shows little difference in sEPSC frequency in LII and LV, but this work was conducted on adult rats. In the studies presented here, sEPSC frequency is considerably higher in LII compared to LV in both neonatal and juvenile principal neurones.

Other parameters of sEPSCs were qualitatively similar in the juvenile and older rats. Amplitudes of sEPSCs in LII and LV were approximately the same in LII and LV in juvenile (present study) and older rats (Berretta and Jones, 1996; Greenhill et al, 2014), but in juveniles they were slightly lower than those previously recorded. Again, it is difficult to draw inferences from this as the differences may be attributed to differences in experimental set up and procedures. It is noteworthy that there was a small population of sEPSCs with large amplitude, in LV neurones, rarely seen in LII in adult or juvenile neurones, which, interestingly, was also present in neonatal neurones. This may reflect a high preponderance of recurrent excitatory connections in LV compared to an almost complete absence of such connections in LII (Dhillon and Jones, 2000). Interestingly, there appeared to be a small increase in the population of larger amplitude events in LV during

development, which potentially could underlie the development of recurrent collateral excitation. The effect of TTX on sEPSCs suggests that the larger amplitude events in LV could be due to differences in the activity-dependent component of spontaneous transmitter release, such that the amplitude distribution of sEPSCs was unaffected by TTX in LII neurones, but the larger amplitude events in LV were abolished. This could indicate both activity-dependent and independent events in LII are mediated by the release of single quanta of transmitter, whereas in LV, activity dependent release can also be mediated by the release of multiple quanta.

Rise times of sEPSCs in juvenile animals in this study were slower than those previously reported (Berretta and Jones, 1996) but the general trend of significantly faster rise times in LV compared to LII neurones was present in both data sets. Berretta and Jones (1996) attributed these differences, at least in part, to dendritic filtering in the less electronically compact LII neurones. Interestingly, rise times in the neonate animals (see below) were slower than in Juvenile animals. Speculatively, the progressive decrease in rise time seen in both layers from neonate through juvenile to old animals could result from increasing electrotonic compactness throughout development, perhaps occurring as a result of morphological and synaptic changes in neurones in both layers. LII principal neurones are either SCs with multiple spiny dendrites and wide-reaching branches towards the dentate gyrus, or PCs with long and thick spiny dendrites. LV neurones are generally large PCs with round somata and either horizontal or multidirectional sparsely spiny dendrites. These morphological and electrical properties characteristic of principal neurones in each layer of the MEC could, in part, account for the slow sEPSC kinetics in LII, relative to neurones in LIII and LV.

3.4.2 Developmental changes in sEPSCs

In these experiments we conducted equivalent examinations of sEPSCs in neonate and juvenile animals, so were able to directly compare changes in properties of spontaneous excitation over the developmental period. As noted above, and summarised in table 3.1 there were a number of lamina specific differences within and across the two age groups.

Frequencies of sEPSCs were consistently higher in LII compared to LV in both neonate and juvenile groups. This difference was particularly marked in the younger animals where sEPSC frequency in LV was very low. In terms of development, the frequencies increased in both layers as animals got older, which could indicate that the probability of release was rising at synapses in both layers. Alternatively, the absolute number of synaptic contacts could be increasing as a result of synaptogenesis. The relative frequency increased markedly in LV (to about 340% of control) compared to LII (~140%) but although the differential sEPSC frequency between the layers decreased with development, it was still in favour of a higher level in LII in the juvenile animals.

Amplitudes of sEPSCs (~8-10 pA) were fairly constant between age groups and were similar in each layer. One interpretation of this is that there was little change in the quantal content between layers, that the underlying postsynaptic AMPARs at the synapses were similar in number and composition in both layers, and that there was little change in these parameters as the rats approached adulthood. Unpublished immunocytochemical studies from Professor Elek Molnar's group at the University of Bristol (personal communication) has shown that the expression of some AMPAR subunits (e.g. GluA1) increases progressively from P0 to P21 in hippocampal areas but much less markedly in extrahippocampal areas. In contrast, other subunits (e.g. GluA2) show little much less change in hippocampus and virtually no change in other areas over the same period. However, a definitive study of receptor expression in the EC remains to be done.

Rise and decay times of sEPSCs were very similar in either layer, and in neonate animals, and, while both parameters became faster in both neuronal populations with development, there was no major differential apparent between layers in the two age groups. There is very little data available on morphological changes in EC with development, which could potentially help explain developing differences in kinetic parameters. However, information about dendritic growth and branching in the hippocampus is available (Dailey and Smith, 1996, McAllister, 2000). As might be expected, there is a developmental increase in the size and complexity of principal cell dendritic trees. With this in mind, it would be intuitive to think that sEPSC kinetics get slower with age due to an increase in electronic length associated with the elongation, proliferation and

ramification of basilar and apical dendrites. However, both LII and LV sEPSCs displayed faster kinetics in juvenile compared with neonatal neurones, suggesting the contribution of electronic length to sEPSC kinetics during development may be over-shadowed by other factors, or that morphological changes in the EC may result in less dendritic filtering, for example, the pruning of distal dendritic synapses.

Other factors that could influence kinetics include postsynaptic receptor composition (Conti and Weinberg, 1999) and affinity for the transmitter (Jones et al., 1998), as well as the rates and time course of desensitisation (Jones and Westbrook, 1996). Different factors become more or less important in defining the shape of EPSCs in immature versus mature neurones. For example, in immature neurones at mossy fibre-granule cell synapses, decay time depends primarily on the rate of receptor deactivation and glutamate clearance (Silver et al., 1996), however, changes to morphological complexity and the expression of glutamate transporters and receptors alter decay time throughout development. This study suggests the dominant determinant influencing faster rise and decay times of sEPSCs in mature neurones was an increase in synchrony of multi-vesicular transmitter release, and faster desensitisation, respectively. Similar developmental factors presumably play a role in the maturation of sEPSCs in the MEC. A striking feature of sEPSCs in the MEC from these results was the developmental elimination of sEPSCs with slower decay times. The presence of only fast decaying sEPSCs could push the network towards higher frequency events, with perhaps a greater potential for hyper-synchronous network activity (see Chapter 7).

3.4.3 Developmental changes in overall excitation

Whilst changes in sEPSC characteristics tell us about developmental alterations in synaptic properties, they do not provide real information about the overall level of persistent, on-going excitation in neurones and, hence, in neuronal networks. It has been argued that the integration of spontaneous excitation and persistent spontaneous inhibition are determinant in the control of intrinsic neuronal excitability and, hence, network reactivity leading to synchronisation (Woodhall et al., 2005, Greenhill et al., 2014). To measure and compare overall excitation in the developing EC we calculated arbitrary charge transfer numbers for neurones in either layer in each age group (see table 3.2). This analysis

revealed that the levels of background excitation were highest in LII in juvenile rats. The ratio to LII in neonates was 1:1.3 showing an increase in overall excitation despite decreasing rise and decay times of individual events. However, the relative increase in integrated excitation with development was even more marked in LV with a ratio of juvenile to neonate of 1:2.3 again in the face of even bigger decrease in rise and decay times.

Comparison between layers in the two age groups was instructive. In the neonates, background excitation was dramatically higher in LII than LV with a ratio between them of 1:3.3. In the older animals although the differential was qualitatively maintained in favour of LII, quantitatively it fell to a ratio of 1:1.9, tending towards an equalisation of background synaptic excitation in the deep and superficial layers.

What conclusions can be drawn from this? LII is clearly subject to higher levels of background excitation than LV both early in development and when approaching the more stable adult situation, and the relative overall change is not dramatic. Background excitatory influence on neuronal activity in LV climbs more rapidly towards that seen in LII by P20-28, but does not become equal to it. This suggests differential development of excitatory neuronal activity in the two populations. It should be noted that many of the studies here were completed in tissue from rats a little more than 3 weeks old, and it could be argued that these are still some way from adulthood, (rats becoming sexually mature at around 35-40 days, and not socially mature before 5-6 months; (Sengupta, 2013). Following changes over more extended time frames may well lead to a further narrowing of differential between layers. Indeed, back calculation of arbitrary charge transfer numbers from the results of Berretta and Jones (1994) in 3-4 month old animals establishes a ratio of excitation in LV:LII of just 1:1.2. Accepting the caveats associated with different experimental procedures and conditions, this does suggest that the two layers continue to equalise with continuing development.

It is very relevant therefore that a recent study has shown that postnatal development and maturation of the MEC and its hippocampal connections occurs in a hierarchical fashion. This starts with maturation of LII SCs at around P14-17 and proceeds linearly through the

hippocampal formation, with the full maturation of LV occurring at around P28 days (Donato et al., 2017). Thus, the delayed maturation of LV compared to LII could explain the decreased background excitation exerted by sEPSCs between the layers in neonatal *v* juvenile neurones, and the significantly greater influence of this excitation across layers, before they begin to equalise.

3.4.4 Wider picture

The results from this chapter show that excitatory events become faster and more frequently during development. The complete lack of a change in amplitude strongly implies the developmental changes observed are occurring specifically at the level of the synapse, and not a result of increased network activity. Increased synaptic 'noise' during development has been postulated to increase the range of synaptic strengths, which may support synchronised neuronal activity, such as gamma frequency oscillations, alongside multiplexed neuronal firing, such as grid cell computation (Solanka et al., 2015, Ermentrout et al., 2008). In a model of MEC neurones, Solanka et al. showed that increasing synaptic noise was beneficial to both gamma oscillations and encoding spatial locations with grid cell activity. Moreover, increases in intrinsic noise reduced the likelihood of seizures in this model, as it prevented neurones from becoming excessively synchronised (Solanka et al., 2015). The results of this chapter provide experimental evidence that synaptic excitation increases during normal development in the rat MEC. It is not unreasonable to suggest that alterations in synaptic excitation, for reasons which could include: deficits in ambient neurotransmitter (e.g. glutamate), abnormal receptor (AMPAR) expression on the postsynaptic membrane or slower receptor kinetics due to aberrant subunit composition, may have serious implications in the generation of neurodevelopmental disorders associated with the MEC, especially TLE.

What is missing from this discussion is of course how this background excitability is influenced by concurrent and persistent spontaneous inhibition and how the two integrate in overall network excitability. Development of background inhibition is presented in the next chapter.

Chapter 4

A comparison of spontaneous inhibitory transmission in LII and LV in neonatal and juvenile rats

4.1 Introduction

Numerous disease states have implicated a dysfunction of the MEC in the underlying aetiology. For example, the MEC shows structural changes in patients with TLE and animal models of the disorder (Bartolomei et al., 2005, Bernasconi et al., 1999, Salmenperä et al., 2000), and a considerable body of evidence supports changes in inhibitory synaptic organisation and neurotransmission in the generation and propagation of epileptiform activity, implicating layers II, III and V (Treiman, 2001, Bernard, 2010). Disrupted functional and anatomical arrangements of circuit selectivity in LII have been identified in animal models of TLE (Gibbs et al., 1997, Brooks-Kayal et al., 1998). Specifically, epileptic animals had a decreased contribution of inhibitory neurotransmission from presynaptic $GABA_ARs$, and an increase in direct excitatory connections between LII principal cells, leading to a net increase in excitability within the network (Armstrong et al., 2016). Alzheimer's patients show an age-dependent loss and impaired expression of functional $GABA_ARs$ (Limon et al., 2012) and GABA transporters in the EC (Fuhrer et al., 2017). A decreased expression of PV-containing interneurones, which co-localised with pathological markers has also been reported in AD (Solodkin et al., 1996). Mice specifically over-expressing tau in the MEC present with memory deficits which were preceded by impairments in synaptic plasticity and aberrant levels of inhibitory neurotransmitters (Fu et al., 2017).

A number of disorders characterised by neurodevelopmental disturbances such as bipolar disorder and schizophrenia also implicate the MEC and disease specific altered intrinsic inhibitory networks (Fung et al., 2014) in their aetiology. For example, post-mortem studies show a decreased expression of PV-containing interneurones in the superficial layers of the MEC in patients with bipolar disorder, leading to disruptions in information integration and transfer (Pantazopoulos et al., 2007).

In order to better understand the role inhibitory synaptic mechanisms in the MEC in neurodevelopmental disorders, it is necessary first to determine how inhibition may alter during normal development. In the previous chapter developmental changes in background synaptic excitation were investigated. In this chapter I have conducted similar

studies on inhibition, using characteristics of sIPSCs to monitor persistent background inhibition.

Previous work in this laboratory has compared sIPSCs in LII, LV (Woodhall et al., 2005) and LIII (Chamberlain et al., 2012) in slices from adult rats, using whole cell patch clamp. As noted in the previous chapter on sEPSCs, caution should be exercised when drawing inferences from the previous studies in comparison to the present results, as different age groups were studied and experimental conditions and procedures were also different (particularly with regard to the use additives for neuroprotection and metabolic support). Nevertheless, it is worth summarising these studies here. The frequency of sIPSCs was greatest in LII, closely followed by LIII, and both layers displayed a very high frequency (40 events/sec was not uncommon). The frequency of events was dramatically (4-5 fold) lower in LV. Interestingly, in the presence of TTX, the frequency of events in LV was almost halved, whereas layer II remained largely unaffected, suggesting a large majority of events in layer II occur independently of action potentials. LIII resembled LV, in that about 50% of sEPSCs were action potential driven and 50% were mIPSCs. Amplitudes of sIPSCs were similar in all three layers, and rise and decay kinetics were the same in LV and LIII, but slower in LII. Finally, another study in adult slices (Bailey et al., 2004) showed that GABA release was inhibited by presynaptic GABA$_B$R in both LV and LII, and this effect was tonically active in the former but not the latter.

Whilst these studies have comprehensively characterised the baseline properties of sIPSCs in the MEC, there are no studies that have addressed the changes in inhibition during development. This project focused specifically on LII and LV, due to their physiological importance in managing synaptic inputs and outputs of the hippocampal formation, and in view of potential involvement in neurodevelopmental disorders noted above. The studies aimed to reinforce our current knowledge on the characteristics of sIPSCs in juvenile rats, but to also extend this characterisation to neonatal rats, allowing the definition of developmental changes in inhibitory neurotransmission in the MEC. This knowledge can be applied to help understand the development of associated neurodevelopmental or degenerational disorders.

Thus, the aims of the current study were principally:

1. To provide a detailed picture of the properties of sIPSCs in LII and LV of juvenile animals (P20-28).

2. To compare the properties of sIPSCs in LII and LV neurones during early development (P8-11) as a basis for subsequent investigations in to developmental roles for KAR in inhibitory transmission.

4.2 Methods

All experiments in this chapter were conducted on combined slices of EC and hippocampus described in Chapter 2 from neonatal (P8-11; 20-35 g) and juvenile (P20-28; 50-100 g) Wistar rats. Whole cell voltage clamp recordings of sIPSCs and mIPSCs were recorded from principal neurones in LII and LV of the MEC. Neurones were voltage clamped at -60 mV. Cells were selected with good access resistance that remained stable for the duration of the recording. All experiments were conducted in the presence of DL-AP5 and SYM2206 to block NMDAr and AMPAr, respectively, and record sIPSCs, uncontaminated by sEPSCs.

Mean values for frequency, inter-event interval (IEI; inverse of frequency), amplitude, rise and decay times were determined from a sample of 200 events during a continuous recording period for each neurone. IPSC rise times were calculated as time between 10 – 90 % of maximum current while decay times taken as time for current to decay 33.3%.

Statistical comparisons were made using a KS-test on cumulative probability distributions constructed from ~200 events from each neurone. To facilitate comparisons between groups and gain an overall indication of integrated inhibition we calculated an arbitrary charge transfer number for each neuronal population at the different age levels. This is approximately related to the area under the curve of the EPSC. Thus, from the mean value of parameters for the sIPSC populations we calculated 50% of the sum of the rise and decay times, and determined the product of this and the mean amplitude and frequency.

4.3 Results

4.3.1 Characterisation of sIPSCs in layers II and V of the MEC in juvenile rats

4.3.1.1 Amplitude and Frequency of sIPSCs

Whole cell recordings from principal neurones in both LII (n = 15) and LV (n = 18) in slices from juvenile animals revealed frequent inward currents, which pharmacological analysis (not shown) confirmed were sIPSCs mediated by $GABA_A$Rs. These persistent events were similar to those described in older animals (Bailey et al., 2004; Woodhall et al., 2004). sIPSCs occurred at a significantly higher frequency in LII (571.0 ± 148.0 events/min; 9.5 Hz) compared to LV sIPSCs (150.7 ± 21.2 events/min; 2.5 Hz, P = 0.008). This was confirmed by the cumulative probability plot of IEI in Fig. 4.1, with no LII neurones IEI exceeding 7 seconds compared with a maximum of 16 seconds IEI in LV. This data is remarkably comparable to that reported by Woodhall et al. (2005) in adult animals (11.5 Hz and 2.5 Hz in LII and LV, respectively).

The average amplitude of events was very similar in LII (20.1 ± 6.0 pA) and LV (18.7 ± 1.8 pA) and the small difference was not significant. Again, this data is entirely consistent with the studies in adult animals (Woodhall et al., 2005; LII 24.0 ± 1.8 pA v LV 25.7 ± 3.9 pA). Although the average event amplitude was not significantly different, the cumulative amplitude plot, constructed from ~1000 sIPSCs from each data set, shows that there were more higher amplitude events in LII than in LV (P < 0.001, KS-test). Of the events sampled in the pooled data, 3% of events in LII exceeded 100 pA, compared to 1 % in LV, with maximum amplitudes of 502.5 pA and 212.4 pA in LII and LV, respectively. Frequency and amplitude of sIPSCs in juvenile rats are summarised in table 4.1.
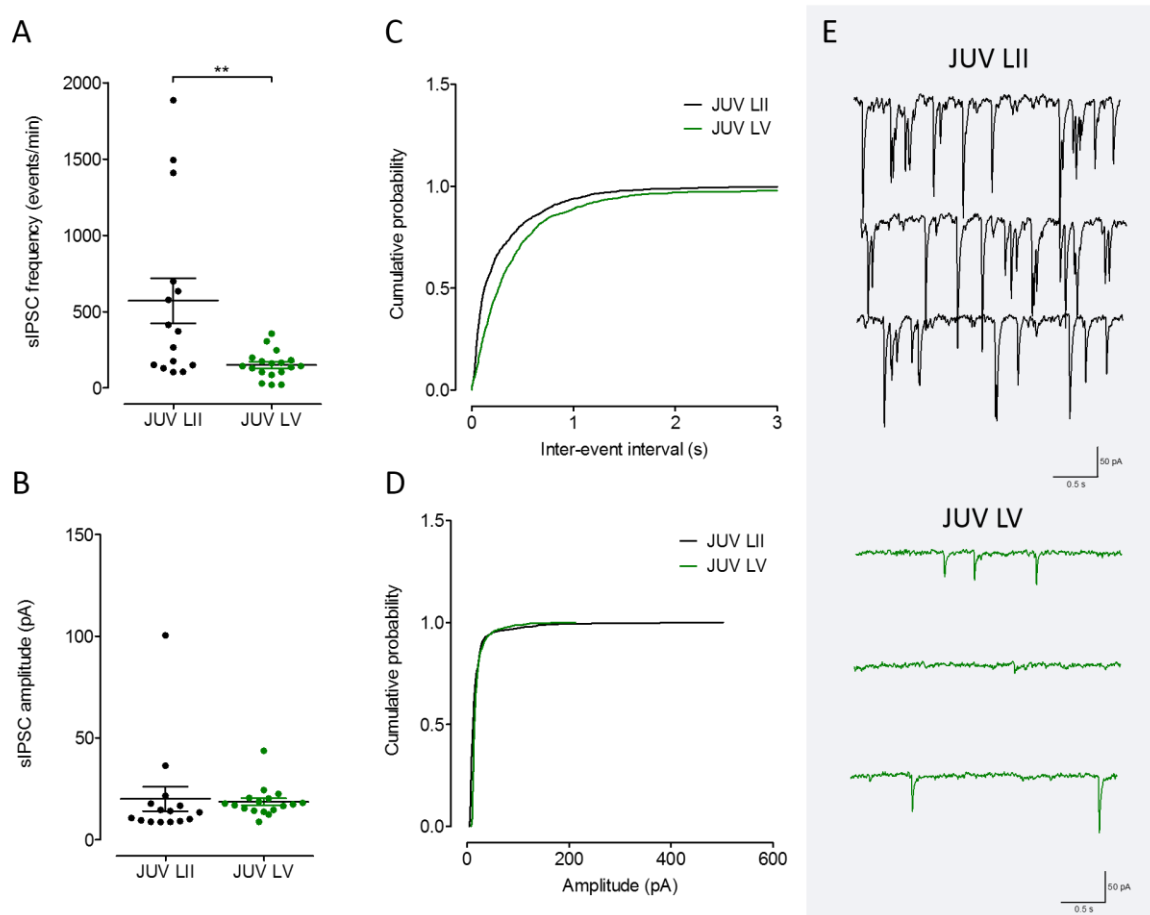
Figure 4.1: Comparison of sIPSC frequency and amplitude in LII and LV neurones of juvenile rats. ***(A)*** *Average sIPSC frequency and* ***(B)*** *sIPSC amplitude data from 15 LII (black) and 18 LV (green) principal neurones. Average frequency of sIPSCs was significantly increased in LII neurones (P < 0.01; Mann Whitney test).* ***(C)*** *Cumulative probability distribution shown of the IEI and* ***(D)*** *peak amplitude of events (> 55) collected and pooled from each neurone. Cumulative probability distributions show the smaller IEI in LII neurones (P < 0.0001; KS-test), and the presence of higher amplitude events in LII neurones.* ***(E)*** *sIPSCs recorded in a LII and* ***(F)*** *sIPSCs recorded in a LV neurone. Three traces are consecutive recordings of spontaneous activity.*

4.3.1.2 Kinetics

sIPSCs in LII (n = 15) had a mean rise time of 5.7 ± 0.6 ms and average decay time of 5.4 ± 0.9 ms, whereas in LV (n = 18) the average rise and decay time was 6.9 ± 0.7 ms and 9.9 ± 2.2 ms (Fig. 4.2). Thus, the decay time of sIPSCs was slightly faster in LII compared with LV ($P < 0.05$, Mann Whitney test), a difference which was qualitatively similar in adult animals, although Woodhall et al. (2005) reported longer decay times (8.5 ± 0.6 ms in LII and 10.1 ± 1.0 ms in LV). The cumulative distribution analysis confirms the slower decay times of sIPSCs in LV compared to LII neurones ($P < 0.0001$, KS-test). Rise times did not differ

significantly in the two layers. The rise and decay times of sIPSCs reported by Woodhall et al (2004) differ substantially from those in the present studies, but this may be as a result of different parameters of analysis so it is not worthwhile attempting to directly compare these studies.
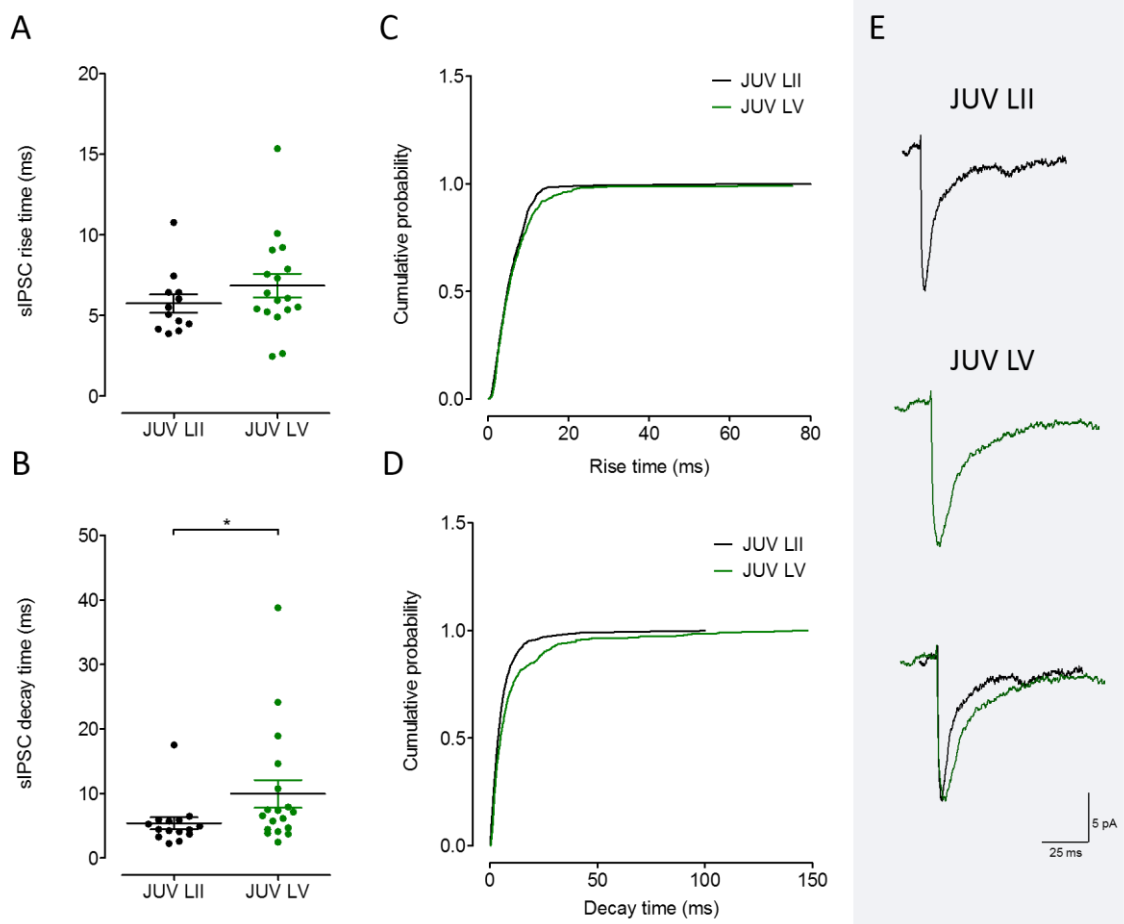
Figure 4.2: Comparison of sIPSC decay and rise time in LII and LV neurones of juvenile rats*. (**A**) Scatter plot of sIPSC rise time and (**B**) sIPSC decay time data from 15 LII (black) and 18 LV (green) principal neurones. The average decay time of sIPSCs was significantly faster in LII neurones (P < 0.05; Mann Whitney test). (**C**) Cumulative probability distribution shown of the rise time and (**D**) decay time of events (>55) collected and pooled from each neurone. Cumulative probability distributions show the faster rise and decay times in LII neurones (P < 0.0001; KS-test, both plots). (**E**) Averaged sIPSCs of a LII (top; black) and a LV (middle; green) JUV neurone are shown (bottom: superimposed events).*

4.3.1.3 Effect of TTX on sIPSCs

mIPSCs recorded in the presence of TTX largely reflect the release of single quanta of GABA from individual release sites, independently of action potentials invading the terminals. The effect of TTX on spontaneous GABA release onto principal neurones in LII and LV of juvenile rats is summarised in Fig. 4.3 and 4.4, respectively. Marked differences were noted between the deep and superficial layers in response to TTX application. It was apparent that the frequency of sIPSCs in LII is largely unaffected by blocking action potentials, a finding that has been previously documented in adult slices (Woodhall et al., 2005). In fact, none of the other parameters of sIPSCs were significantly changed after TTX, despite a tendency towards faster rise and decay times. This suggests that sIPSCs, and therefore GABA release onto principal cells in LII MEC, arises largely independently of action potentials. However, these results should be treated with caution, as mIPSPs were only recorded in 3 neurones

In contrast, bath application of TTX decreased the average frequency of sIPSCs in juvenile LV neurones by 66% from 150.7 ± 21.2 events/min (2.5 Hz) to 51.6 ± 7.6 events/min (0.9 Hz) (P = 0.002, Mann Whitney test). Again, this is comparable to the study of Woodhall et al (2005), which showed a 63 % decreased in frequency of LV sIPSCs in the presence of TTX in adult slices. Despite the change in frequency, there was no change in the mean amplitude of LV sIPSCs in the absence (18.7 ± 1.8 pA) or presence (17.6 ± 1.6 pA) of TTX. mIPSCs in LV had a faster mean rise (6.9 ± 0.7 ms to 4.1 ± 0.3) and decay time (9.9 ± 2.2 ms to 5.7 ± 0.6) with the former reaching significance (P = 0.001; Mann Whitney test).

Figure 4.3: Comparison of sIPSCs and mIPSCs in LII neurones of juvenile rats*. Voltage clamp recordings were in the absence (sIPSCs; n = 15, black) and presence (mEPSCs; n = 3, red) of TTX (1 µM). (**A**) Scatter plots comparing the (**A**) frequency (events/min), (**B**) rise time (ms), (**C**) amplitude (pA) and (**D**) decay time (ms) of sIPSCs and mIPSCs from LII principal neurones. Note no significant differences between sIPSCs and mIPSCs of LII MEC neurones. (**E**) sIPSCs and mIPSCs recorded in a LII MEC neurone, before and after the application of TTX (µM). Three traces are consecutive recordings of spontaneous activity*

Figure 4.4: Comparison of sIPSCs and mIPSCs in LV neurones of juvenile rats. Voltage clamp recordings were made from neurones in the absence (sIPSCs; n = 18, green) and presence (mIPSCs; n = 9, blue) of TTX (1 μM). (A) Scatter plots comparing the (A) frequency (events/min), (B) rise time (ms), (C) amplitude (pA) and (D) decay time (ms) of sIPSCs and mIPSCs from LV principal neurones. Note the decreased mean frequency and rise time in the presence of TTX (P = 0.002 and P = 0.001; Mann Whitney test) (E) sIPSCs and mIPSCs recorded in a LV MEC neurone, before and after the application of TTX (μM). Three traces are consecutive recordings of spontaneous activity.

4.3.2 Characterisation of sIPSCs in layers II and V in neonatal rats

4.3.2.1 Frequency and amplitude

There are currently no studies that have addressed lamina differences in the properties of sIPSCs in principal neurones in neonatal rats. Like their counterparts in adult (Woodhall et

109

al., 2004) and juvenile (above) slices, whole cell recordings from LII (n = 7) and LV (n = 12) neurones in neonate slices revealed sIPSCs that were abolished by $GABA_A$Rs antagonists (not shown). Interestingly, there was no significant difference in the mean frequency between LII (67.2 ± 20.7 events/min, or 1.1 Hz) and LV (61.2 ± 19.8 events/min, or 1.0 Hz) although cumulative probability distributions of IEI (Fig. 4.5) did show a small shift towards longer IEIs, or a slower frequency, in LV neonatal neurones compared to LII which was significant when subjected to KS analysis (P < 0.0001).

The mean amplitude of sIPSCs in LV (17.2 ± 2.4 pA) was a little larger than that in LII neurones (14.1 ± 2.4 pA), but this did not reach significance. However, again, subsequent analysis of the cumulative distribution plots did show a displacement of the amplitudes plot to the right in LV, indicating an increased presence of larger amplitude events in this layer (P < 0.0001). Despite this, LII has a much higher maximum amplitude (269.3 pA) compared to LV (177.2 pA), in fact, only one event from the pooled data in LV exceeded 100 pA (0.001%). Events exceeding 100 pA in LII were 10 fold higher than in LV. Indeed, the shift in the amplitude distribution was attributed to an increase in medium sized events between 40-100 pA, such that only 0.005% (1/864) of sIPSC in LII neonatal neurones were in this region, compared with 6% (51/864) of pooled LV events. The increased presence of medium sized amplitudes in LV and the increased presence of small and large, but not medium, sized events would explain the lack of significant differences in the overall mean amplitudes between LII and LV neonatal sIPSCs. The frequency and amplitude of sIPSCs in LII and LV of neonatal rats are summarised in Fig. 4.5.
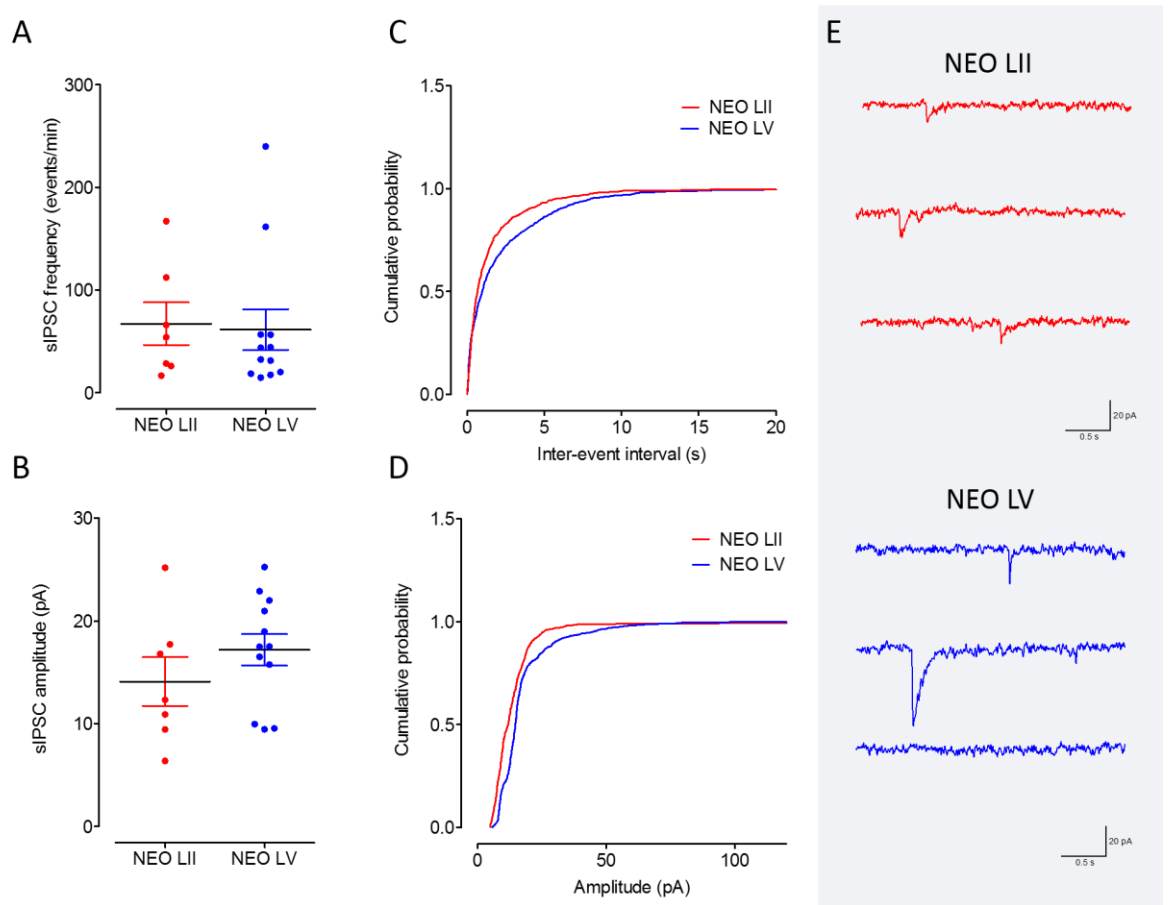
***Figure 4.5: Comparison of sIPSC frequency and amplitude in LII and LV MEC principal neurones of neonate rats**. (**A**) Average sIPSC frequency and (**B**) sIPSC amplitude data from 6 LII (red) and 12 LV (blue) principal neurones. No significant differences between LII and LV were noted in the average frequency or amplitude (**C**) Cumulative probability distribution shown of the IEI and (**D**) peak amplitude of events (> 77) collected and pooled from each neurone. Cumulative probability distributions show the smaller IEI in LII neurones (P < 0.0001; KS-test), and a skew towards higher amplitude events in LV neurones. (**E**) sIPSCs recorded in a LII and sIPSCs recorded in a LV neurone. Three traces are consecutive recordings of spontaneous activity.*

4.3.2.2 Kinetics

In neonatal neurones, the kinetics of sIPSCs were faster in LV (n = 12) compared to LII (n = 7) neurones. The mean rise time of LV sIPSCs was 6.2 ± 0.5 ms compared to 7.4 ± 0.4 ms in LII, though this did not reach significance, seemingly due to a large spread of both fast and slow average rise times, perhaps reflecting GABA release from different sub-populations of neurones (cf Woodhall et al., 2005). Further analysis using cumulative distribution plots

show a clear displacement of towards faster rise times in LV compared to LII (P < 0.0001; KS-test). The mean decay time of sIPSC in LV (5.0 ± 0.6 ms) was clearly and significantly faster than in LII (9.6 ± 1.3 ms) neurones (P = 0.004, Mann Whitney test). Again, the dramatic leftward shift of the amplitude distribution indicate the much faster decay times in LV sIPSCs relative to those in LII neurones (P < 0.0001, Mann Whitney test). The kinetics of sIPSCs in LII and LV of neonatal rats are summarised in Fig. 4.6.
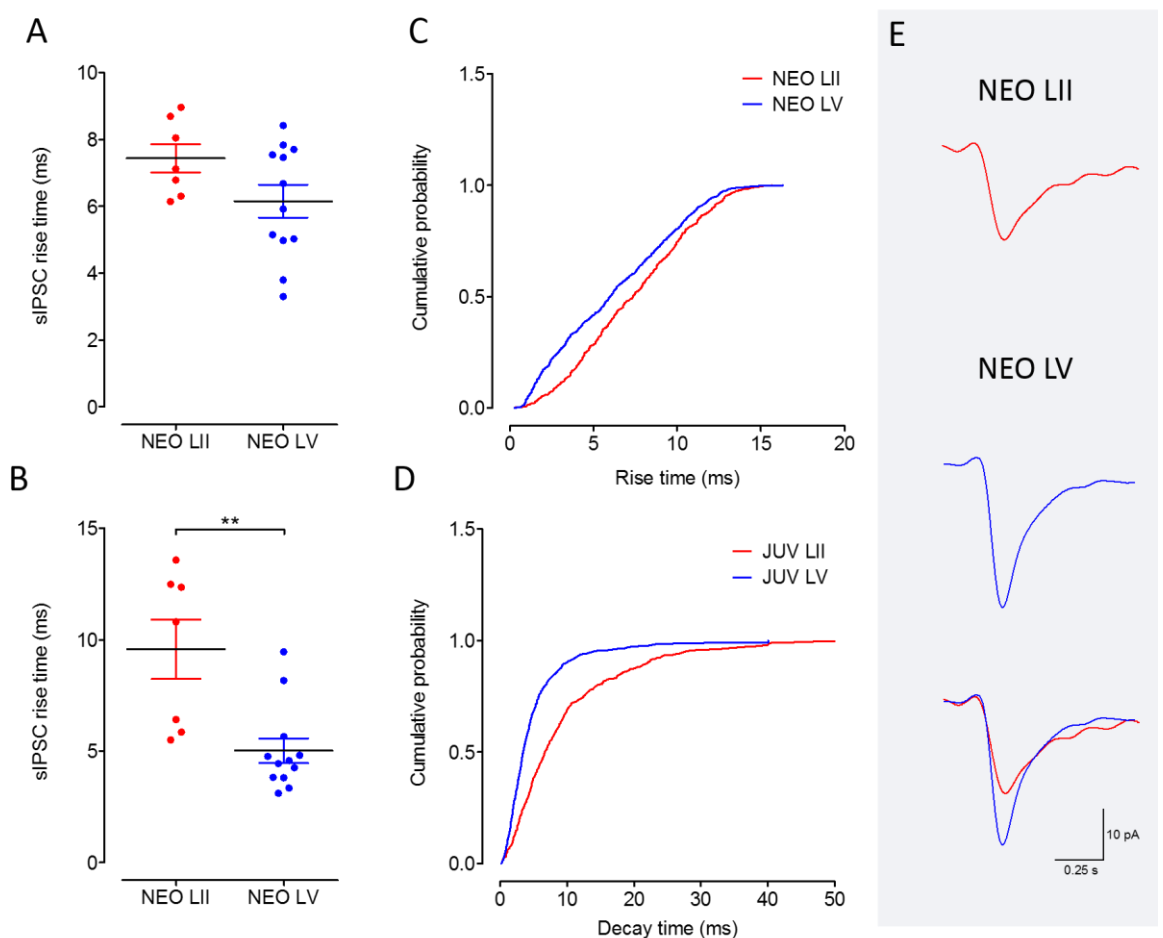
Figure 4.6: Comparison of sIPSC decay and rise time in LII and LV neurones of neonate rats. (A) Scatter plot of sIPSC rise time and **(B)** sIPSC decay time data from 7 LII (red) and 12 LV (blue) principal neurones. The average decay time of sIPSCs was significantly faster in LV neurones (P < 0.01; Mann Whitney test). **(C)** Cumulative probability distribution shown of the rise time and **(D)** decay time of events (>77) collected and pooled from each. Cumulative probability distributions show the faster rise and decay times in LV neurones (P < 0.0001; KS-test, both plots). **(E)** Averaged sIPSCs of a LII (top; red) and a LV (middle; blue) NEO neurone are shown (bottom: superimposed events).
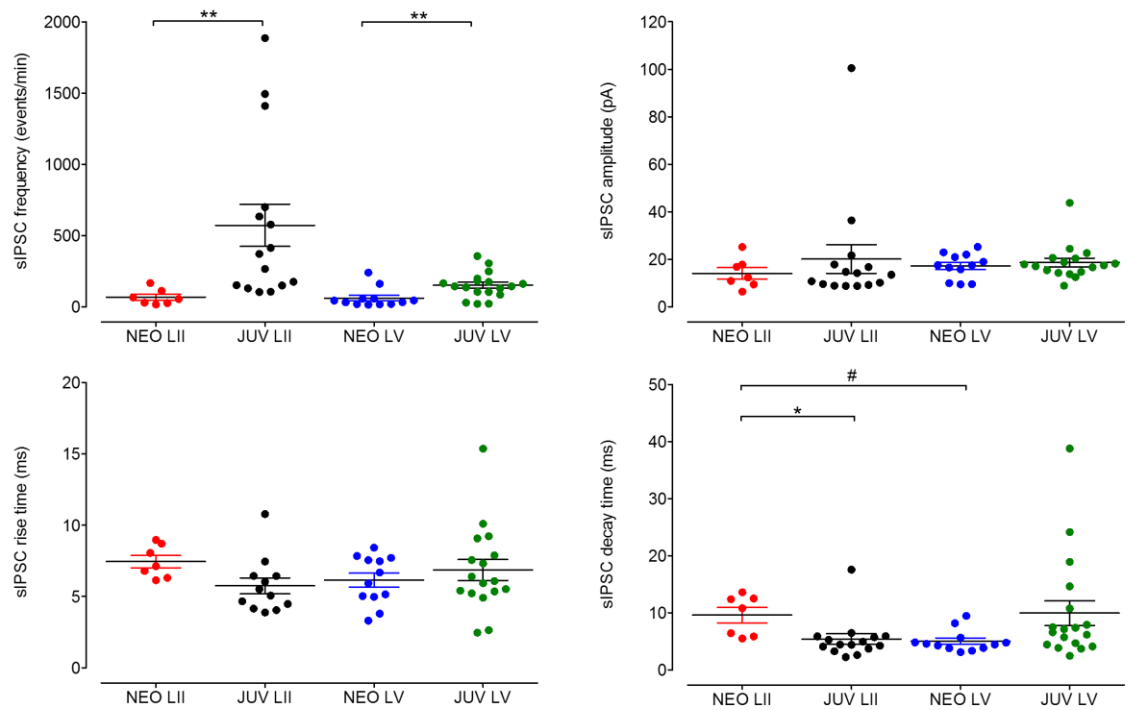
	Layer	N number	Frequency (events/min)	Amplitude (pA)	Rise time (ms)	Decay time (ms)
Neonate	**II**	**7**	**67.2 ± 20.7**	**14.1 ± 2.4**	**7.4 ± 0.4**	**9.6 ± 1.3**
Juvenile	II	15	571.0 ± 148.0	20.1 ± 6.0	5.7 ± 0.6	5.4 ± 0.9
Neonate	**V**	**12**	**61.5 ± 19.8**	**17.2 ± 1.5**	**6.2 ± 0.5**	**5.0 ± 0.6**
Juvenile	**V**	**18**	**150.7 ± 21.2**	**18.7 ± 1.8**	**6.9 ± 0.7**	**9.9 ± 2.2**

Table 4.1: Summary data of the baseline characteristics of sIPSCs in LII and LV MEC of neonate and juvenile neurones. *Scatter plots of sIPSC frequency, amplitude, rise times and decay times of sIPSCs in neurones from neonate LII MEC (red, n = 7)), juvenile LII MEC (black, n = 15), neonate LV MEC (blue, n = 12) and juvenile LV MEC (green, n = 18). * and # denote statistically significant developmental and laminar differences.*

4.3.3 Age Comparison

4.3.3.1 Frequency and amplitude

Whole cell recordings of sIPSCs were compared in 19 neonate (P8-14) and 33 juvenile (P20-28) neurones. At both ages and in both layers sIPSCs were abolished by bicuculline or gabazine, confirming their dependence on $GABA_A Rs$ activation (not shown).

In LII, the mean frequency of sIPSCs was considerably faster in juvenile (571.0 ± 148.0, or 9.5 Hz; n = 15) compared to neonatal (67.2 ± 20.7 events/min, or 1.1 Hz; n = 7) neurones (P = 0.004, Mann Whitney test). The developmental increase in sIPSC frequency (from 1.1 Hz to 9.5 Hz) in LII neurones was confirmed by cumulative distribution plots of IEI, showing a substantial leftward displacement of the distribution, reflecting the increased likelihood of GABA release within short intervals in the juvenile rats (P < 0.0001, KS-test).

The mean amplitude of sIPSCs slightly increased during development in LII neurones, from 14.1 ± 2.4 pA in neonatal to 20.1 ± 6.0 in juvenile neurones, but this was not statistically significant. The developmental changes in sIPSC frequency and amplitude of LII neurones are summarised in Fig. 4.7.

Developmental changes in frequency and amplitude in LV sIPSCs follow a similar pattern to that seen in LII. The mean frequency of sIPSCs was considerably faster in juvenile (150.7 ± 21.2, or 2.5 Hz; n = 18) compared to neonatal (61.5 ± 19.8 events/min, or 1.0 Hz; n = 12) neurones (P = 0.006, Mann Whitney test). It is clear that the frequency of sIPSCs in LV in neonatal neurones is very low indeed at this stage of development. The clear developmental increase in sIPSC frequency (from 1.0 Hz to 2.5 Hz) in LV neurones was reflected in the cumulative distribution plots of IEI (Fig. 4.8), showing a substantial leftward displacement of the juvenile sIPSC distribution, again, signifying the increased likelihood of GABA release at shorter intervals in the older rats (P < 0.0001, KS-test).

Again, as in LII, the mean amplitude of sIPSCs did not significantly change during development, from 17.2 ± 1.5 pA in neonatal to 18.7 ± 1.8 in juvenile neurones. The cumulative probability plots revealed similar distributions in amplitudes in sIPSCs in the

two age groups, except for a population of high amplitude (> 100 pA) events present 10-fold more in the pooled data from juvenile neurones (0.01% vs 0.001% in neonatal). The developmental increase in sIPSC frequency of LV neurones can be pictured in the raw traces in Fig. 4.8.
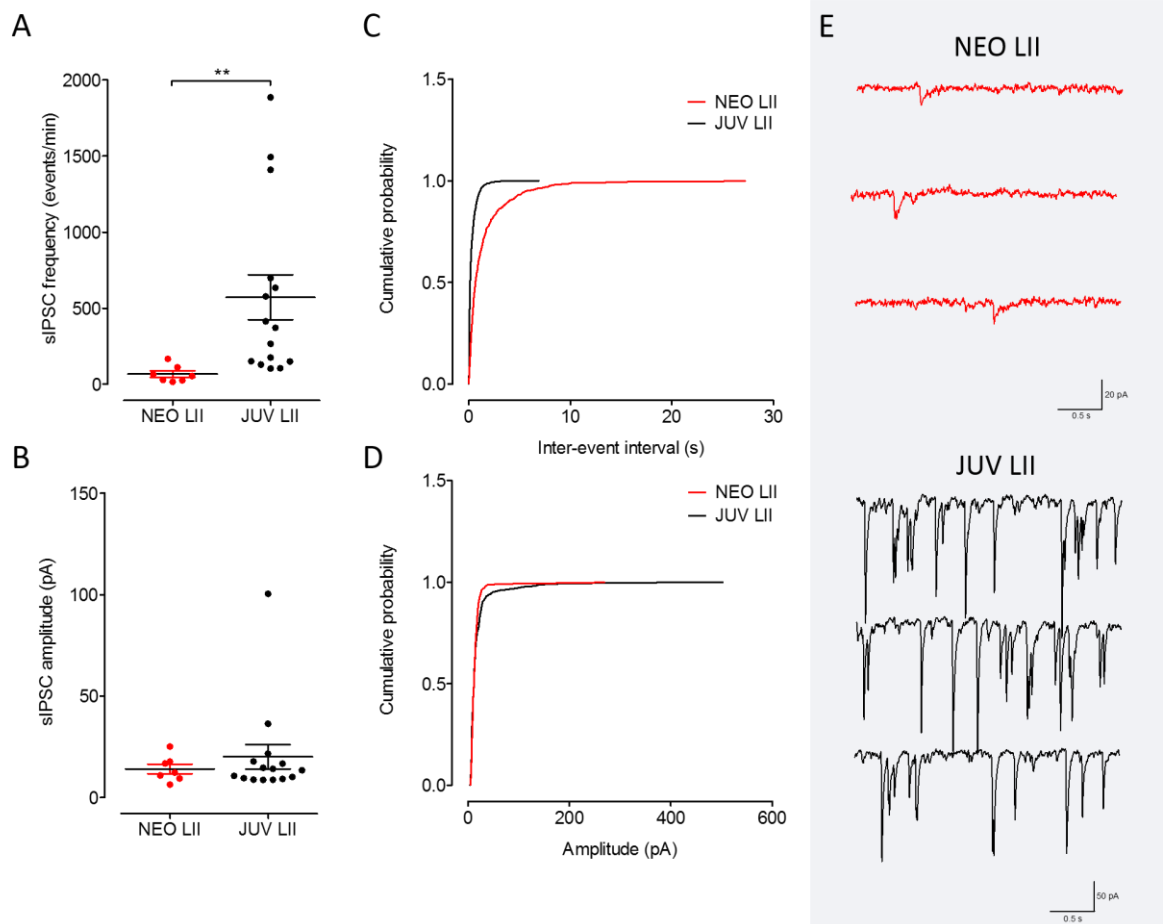
Figure 4.7: Comparison of sIPSC frequency and amplitude in neonate and juvenile neurones in LII. *(A) Scatter plots comparing the sIPSC frequency and (B) sIPSC amplitude data from 7 NEO (red) and 15 JUV (black) principal neurones. Note the significantly increased frequency of events in JUV rats (P = 0.002; Mann Whitney test) but no change in amplitude (C) Cumulative probability distribution shown of the IEI and (D) peak amplitude of events (> 60) collected and pooled from each neurone. Cumulative probability distribution plot shows the significantly shorter IEI JUV neurones (P < 0.0001; KS-test, both plots). (E) sIPSCs recorded in a LII NEO and a LII JUV principal neurone in the MEC. Three traces are consecutive recordings of spontaneous activity.*
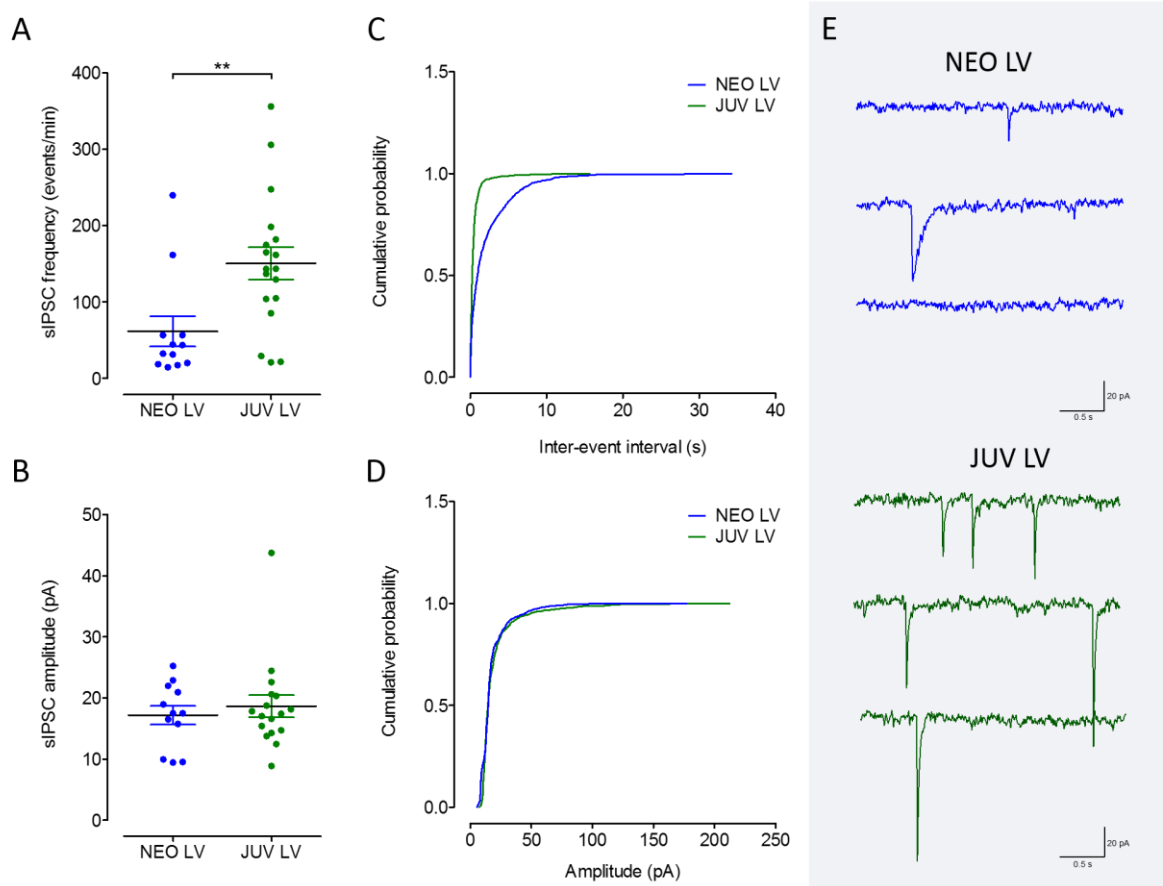
Figure 4.8: Comparison of sIPSC frequency and amplitude in neonate and juvenile neurones in LV. *(**A**) Scatter plot of sIPSC rise time and (**B**) sIPSC decay time data from 12 NEO (blue) and 18 JUV (green) principal neurones. The average frequency of sIPSCs in LV neurones significantly increases during development (P = 0.006; Mann Whitney test). (**C**) Cumulative probability distribution shown of the IEI and (**D**) peak amplitude of events (> 55) collected and pooled from each neurone. Note the clearly increased IEI (slower frequency) in NEO LV compared with JUV LV sIPSCs (P < 0.0001, KS-test). (**E**) sIPSCs recorded in a LV NEO and (**F**) sIPSCs recorded in a LV JUV principal neurone in the MEC.*

4.3.2.2 Kinetics

Examination of the properties of sIPSCs in both groups in both neuronal types at both ages showed a wide variation in both rise and decay times, and these may reflect separate populations of sIPSCs arising from different interneurones synapsing at specific locations on the postsynaptic principal neurones (cf Woodhall et al., 2005). We have not attempted to distinguish between such putative groupings in the analysis of the current data.

In neonatal neurones in LII (n = 7), the mean rise time (7.4 ± 0.4 ms) and decay time of (9.6 ± 1.3 ms) of sIPSCs were significantly slower compared with juveniles (rise 5.7 ± 0.6 ms; P < 0.05; decay 5.4 ± 0.9 ms; P < 0.01). Indeed, cumulative distribution analysis shows a clear leftward displacement of the pooled data from juvenile versus neonate sIPSC rise and decay times (P < 0.0001; KS-test, both plots). Changes to sIPSC kinetics could reflect the maturation or developmental changes to synaptic organisation of inputs from different sub-populations of interneurones (see discussion). Despite a general shift towards faster rise times in sIPSCs of juvenile neurones, there was also a population of much slower events in the juvenile sIPSCs, not present in neonatal neurones, such that the maximum rise time of sIPSCs in LII of juvenile neurones was 92.7 ms, compared with 15.7 ms in neonatal LII neurones.

sIPSCs in LV neurones followed a different pattern to LII, such that there were no significant changes to the mean rise times in neonate (6.2 ± 0.5 ms) compared to juvenile (6.9 ± 0.7 ms). However, similarly to in LII, a population of slower events were present in the juvenile neurones that was not apparent in neonate neurones, with a maximum rise time of 75.5 ms and 16.3 ms from the pooled data of each age group, respectively.

Interestingly, the average decay time was actually slower in the juvenile group of LV neurones (9.9 ± 2.2 ms) compared to neonatal sIPSCs (5.0 ± 0.6 ms), with a maximum decay time of 147.8 ms and 40.1 ms in the two groups, respectively. Cumulative analysis of decay times of sIPSCs of LV neurones show a clear rightward displacement of the distribution in the juvenile population, compared to neonatal, reflecting the presence of slower events. Clearly, a population of slower sIPSCs exist in the older rats, which were not apparent in

the neonatal neurones. The developmental changes to the kinetics of sIPSCs in LII and LV of the MEC are summarised in Fig. 4.9 and 4.10.
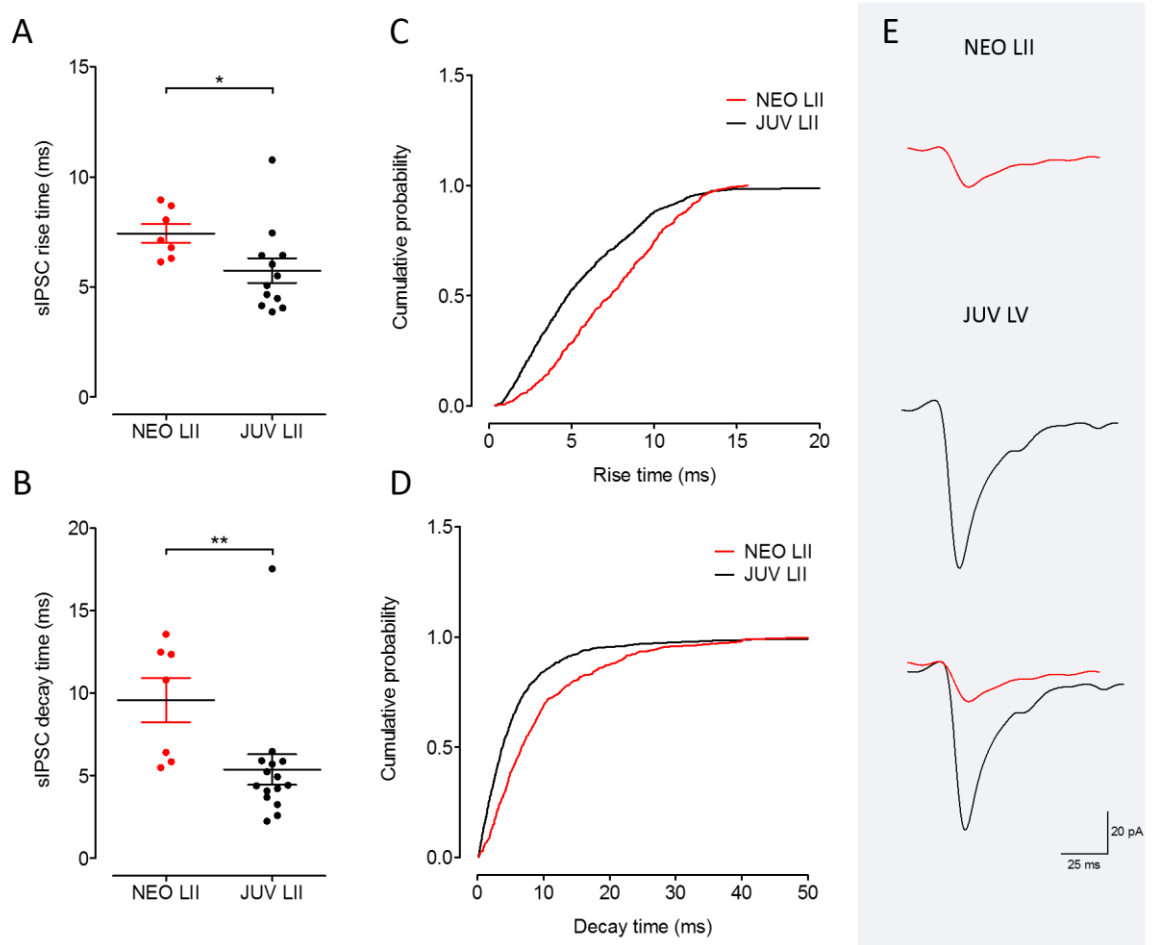
Figure 4.9: Comparison of sIPSC decay and rise time in neonate and 15 juvenile neurones in LII. *(**A**) Scatter plot of sIPSC rise time and (**B**) sIPSC decay time data from 7 NEO (red) and 15 JUV (black) principal neurones. Both rise and decay times are significantly faster in juvenile neurones compared with neonate neurones (**C**) Cumulative probability distribution shown of the rise time and (**D**) decay time of events (>54) collected and pooled from each neurone. Cumulative probability distributions show a skew towards faster rise and decay times in JUV neurones compared to NEO (P < 0.0001; KS-test). (**E**) Averaged sIPSCs of a NEO LII (top) and a JUV LII (middle) neurone(s) are shown (bottom: superimposed events).*
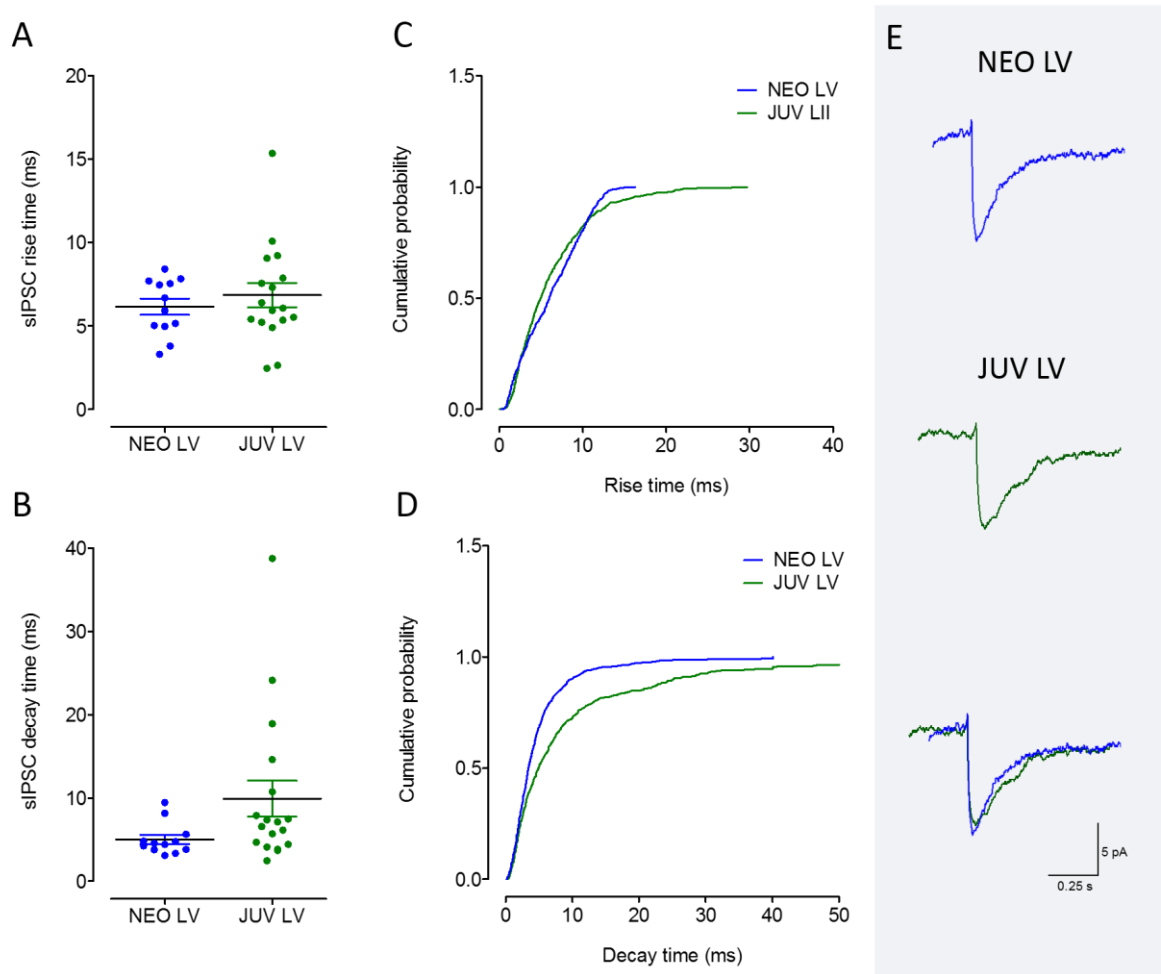
Figure 4.10: Comparison of sIPSC decay and rise time in neonate and juvenile neurones in LV. (**A**) Scatter plot of sIPSC rise time and (**B**) sIPSC decay time data from 12 NEO and 18 JUV principal neurones. (**C**) Cumulative probability distribution shown of the rise time and (**D**) decay time of events (>55) collected and pooled from each neurone. Cumulative probability distributions show the slower rise and decay times in JUV neurones compared to NEO (P < 0.0001 for both plots; KS-test). (**E**) Averaged sIPSCs of a NEO LV (top) and a JUV LV (middle) neurone(s) are shown (bottom: superimposed events).

Age group	Layer	Charge transfer (/min)	Charge transfer (/s)	Comparison	Ratio
Neonate	II	16108	268	**II:II** JUV v NEO	7.9:1
Juvenile	II	127396	2123	**V:V** JUV v NEO	4:1
Neonate	V	11847	198	**II:V** NEO	1.4:1
Juvenile	V	47344	789	**II:V** JUV	2.7:1

Table 4.2: Table showing charge transfer values and ratios inhibition in LII and LV MEC of neonate and juvenile neurones. Charge transfer values are indicative of the overall neuronal inhibition, and are calculated using the following equation: Rise time + decay time x amplitude x frequency. For /sec divide by 60. Note the substantial 7.9-fold increase in overall inhibition in LII during development.

Comparison	Ratio
I:E **NEO II**	1.5:1
I:E **JUV II**	9.2:1
I:E **NEO V**	3.7:1
I:E **JUV V**	6.5:1

Table 4.3: Table showing the ratio of overall inhibition and excitation in LII and LV MEC in juvenile and neonate neurones. Note the dominance of inhibition in juvenile neurones.

4.4 Discussion

4.4.1 Comparison of sIPSCs in juvenile compared to older animals

There have been previous lamina comparisons of sIPSC properties in the MEC of adult or older animals reported from this laboratory (Bailey et al., 2004; Woodhall et al., 2005; Greenhill et al., 2014). As with sEPSCs (Chapter 3) caution is needed required in assessing differences and similarities between these studies and the data in this thesis until equivalent studies have been conducted under the same conditions. Nevertheless there are parallels to be drawn between the two and which are worth pointing out. In adult animals the average frequency of sIPSCs in LII was around 11.5Hz (Woodhall et al., 2005) which compares well with the rate in juveniles of 9.5Hz seen here. sIPSC frequency in LV was the same in adult animals as in juveniles at 2.5Hz. Mean amplitudes were similar in both layers (~20 pA) in juvenile animals, and this was reflected in the adults (Woodhall et al., 2005). Further similarities were apparent when recording mIPSCs TTX application failed

to change amplitude or frequency of IPSCs in LII of juvenile rats, where as it induced a 60% decrease in frequency with no change in amplitude in LV. Almost identical results were reported for adult animals by Woodhall et al. (2005). The marked similarities between the results here compared to the older animals suggest that it is likely that inhibitory transmission in the juvenile animal group studied here was fully mature or close to it.

4.4.2 Developmental changes in sIPSCs

Directly equivalent examinations of sIPSCs in neonate and juvenile animals under identical conditions were conducted in the current experiments, so comparison of changes in properties of spontaneous inhibition should reflect genuine developmental maturation of GABA transmission of the period studied. As noted above, and summarised in table 4.1 there were a number of lamina specific differences within and across the two age groups.

Frequencies of sIPSCs were markedly low and equivalent in LII and LV in neonate animals suggesting minimal spontaneous activity of GABAergic interneurones at this stage in development. There are a multitude of reasons why this might be so, and in the absence of specific studies on interneurone development in the EC, it is only possible to speculate on these. For example, principal neurones may still be awaiting the formation of a full complement of mature synaptic contacts from interneurones, or these may exist but mechanisms for vesicular release of GABA might be undeveloped. Data in Chapter 3 show that excitatory transmission onto principal cells is also underdeveloped at this stage, and it could be also that excitatory drive onto interneurones is also weak or not fully morphologically developed, so the stimulus to GABA release may not yet be present.

We observed that the frequency of sIPSCs in the MEC increased substantially over the age range studied, but without a significant change in amplitude. Inhibitory circuitry in the MEC likely undergoes several transitions during post-natal development, directed by both gene expression and brain activity, which could influence sIPSC frequency. Such factors include changes to synaptic density, synaptogenesis and synaptic pruning, as well as changes to the expression of different receptor subunit compositions and interneurone excitability. No studies currently directly address these changes specifically in the MEC, but conclusions can be drawn with evidence from other brain regions. A developmental increase in synaptic

122

density or in the expression of VG-ion channels could cause an increased excitability of interneurones, and a concomitant increase in sIPSC frequency, as seen in the neocortex and hippocampus (Luhmann and Prince, 1991, Aoki and Baraban, 2000). Alternatively, instead of greater excitatory influences, developmental changes to membrane properties of GABAergic interneurones that contribute to the spontaneous activity could cause an increase in sIPSC frequency. The increased amplitude witnessed in both layers throughout development could reflect an increase in the strength of individual synapses, perhaps due to an increase in receptor density, or changes in receptor affinity or efficacy via expression of different receptor subunits.

The increase in sIPSC frequency effect was dramatic in LII where a ~10 fold increase was seen. It was also substantial in LV (~3-fold), but remained relatively low in the deep layer compared to the superficial. This increase in spontaneous synaptic inhibition reflects a remarkable maturation of the inhibitory system over a short period 1-2 weeks. Interestingly, similar changes in spontaneous inhibition have been noted in neocortex with low numbers of sIPSCs in the first week of life rising markedly in the second and third weeks (e.g. Luhmann and Prince, 1991). Interestingly, in visual cortex, immature interneurones and GAD activity are evident in the first week of life (Chronwall and Wolff, 1980, Miller, 1986, Wolff et al., 1984, McDonald et al., 1987) but increase dramatically during the next two weeks, increasing by about 5 fold between P8 and P20. Also, inhibitory axosomatic synapses only develop in large numbers from around P8 to P20 (Bahr and Wolff, 1985, Miller, 1986). It could be suggested, therefore, that the formation of functional synapses GABAergic at around this time is responsible for the big rise in spontaneous inhibition in both LV and LII in the EC.

Interestingly, the data in Chapter 3 show that the elevation of inhibition is coincident with a developmental increase in excitation in both layers, at least in principal neurones. If the same was also true for inputs to the interneurones, then an increase excitatory glutamatergic drive could also contribute to increased GABA release. However, this should be tempered by the observation that sIPSCs in LII were almost entirely action potential-independent mIPSCs. The same was not true in LV, and it may be pertinent that the developmental increase in excitation was relatively greater in LV than LII, so an increased

interneurone drive could be involved in directly in increased inhibition in the deep layer. An alternative possibility is that increased excitation of interneurones promotes synaptogenesis of inhibitory connections. These possibilities await further investigation

A recent study has looked at development of interneurones in entorhinal areas using immunohistochemistry (Ueno et al., 2017). Unfortunately, this was in mice, looked at LEC and not MEC, only studied animals at P14 and beyond (P21, 28, and 56), and did not look at lamina specific differences. Therefore, it is limited in use for comparison to the current findings. Large numbers of GAD positive cells were seen at P14 and this did not change dramatically throughout development (monitored at P21, 28 and 56). Studies of subtypes of interneurones showed differential development profiles. Parvalbumin positive cells were not present at P14, but had become visible by P21 and 28. A similar profile was seen with calretinin, although a few cells were present at P14. Substantial numbers of calbindin-positive neurones were present at P14 and this remained stable throughout. Somatostatin-positive cells were also present at high levels at P14, but this progressively decreased to a stable level at P21. The study does show that there are large numbers of GABA neurones present at P14 and these tend to increase with development, how this relates to the changes in GABA transmission we observe in rat MEC is a matter for conjecture.

4.4.3 Implications of changes in kinetics

There were developmental changes in sIPSC kinetics in both layers. PCs in CA1 of the hippocampus receive two kinetic classes of $GABA_A$Rs mediated inhibition: slow dendritic, and fast perisomatic, IPSCs, which are likely generated by two distinct groups of interneurones. Banks et al. (2002) found a differential developmental regulation of the firing properties of the fast and slow GABA events between the ages of P10 and P35. Specifically, slow kinetic IPSCs increased over 70-fold between these ages. In the MEC in adult animals (Woodhall et al., 2005) detailed analysis of sIPSC kinetics also permitted the conclusion that there were different populations of events that reflect release of GABA from different populations of interneurones. We have not made such an analysis here, but the changes in mean kinetics could suggest that there were different interneurones contributing to the spontaneous release in juvenile versus neonate animals. This would fit with the differential development of interneurone subtypes reported in mice (Ueno et al.,

2017). Alternatively, the change in kinetics could be associated with development of synapses at different morphological site on principal cells or as a result of changing postsynaptic neuronal morphology/electrotonic properties.

Whatever the reason, sIPSCs become much sharper and briefer in LII reflected by much faster kinetics. This would fit with an increased ability of neuronal networks to generate higher frequency synchronous firing patterns during development, which are dependent on faster kinetics of IPSCs (see Introduction and Chapter 7). sIPSCs in LV actually became broader and slower which would be due to the increased presence of a population of slower events, not evident in the younger rats, reflecting inputs from different subtypes of interneurones or inputs at different somatodendritic locations. Increased dendritic synaptic connections, further away from the cell soma, and an increase in electronic length of neurones during development could account for the presence of slower events.

4.4.5 Overall changes in inhibition

Assessment of arbitrary charge transfer values showed that inhibition was slightly more prominent in LII than LV in neonates, although the difference was not marked. However when animals reached the juvenile stage, the difference was huge with a profound dominance of inhibition in LII despite the decrease in both rise and decay times in this layer. This lamina related dominance of inhibition has been noted in previous studies in this laboratory (Jones and Buhl, 1993, Jones, 1994, Woodhall et al., 2005, Greenhill and Jones, 2010, Greenhill et al., 2014). Overall, this would fit with the susceptibility of the superficial layers to generation of oscillatory activity (Cunningham et al., 2003, Cunningham et al., 2004a, Cunningham et al., 2006b) which is largely driven by inhibitory interneurones. This is investigated in some detail in Chapter 7 of this thesis.

When looking at the overall changes in inhibition we must also take into account the developmental shift in GABAergic neurotransmission from depolarising to hyperpolarising responses (Cherubini et al., 1991). The switch occurs due to increased expression of the KCC2 co-transporter on neurones which alters the reversal potential of chloride ions, promoting fast hyperpolarising postsynaptic inhibition. In the rat hippocampus the expression levels of KCC2 are almost adult-like and exhibit a hyperpolarising action by the

age of P9 (Rivera et al., 1999). It is unknown what age the GABA shift occurs in the rat MEC, but it is likely that, at least in LII, the shift has also occurred by the age groups used in this study. As previously mentioned, however, LV MEC appears to have a slightly protracted development compared to both the hippocampus and superficial MEC, which may contribute to the reduced developmental increase in inhibition in the deeper layers (Donato et al., 2017). In addition, the baseline frequency of sIPSCs in neonate neurones of both layers was extremely low therefore we cannot rule out the depolarising action of GABAergic neurotransmission at this age.

Postnatal development of GABAergic neurotransmission is also associated with changes in the composition of GABAa receptors, namely the upregulation of $\alpha1$ and $\alpha4$ and down regulation of $\alpha3$ and $\alpha5$ subunits (Laurie et al., 1992). The change in GABA receptor subunits is usually paralleled by a decrease in the time decay of IPSCs which, again, may indicate a slower development of inhibition in the deep layers of the MEC, though this is rather speculative.

4.4.6 Wider picture

Similarly to the results regarding excitatory neurotransmission, here we show that the increase in synaptic inhibition during development is related to activity specifically at the synapse, due to the lack of change to amplitude. Increased synaptic noise is important in increasing synaptic strength and range, and ultimately support synchronised brain activity such as gamma oscillations (see Chapter 3, section 3.4.4) (Ermentrout et al., 2008). In addition, computational models of synaptic noise inversely correlated the amount of noise with the likelihood of a seizure in the MEC (Solanka et al., 2015). Interestingly, the developmental increase in synaptic noise was much less pronounced in LV compared to LII, which could contribute to the susceptibility of the deep layers to seizure generation.

A substantial difference observed between inhibitory events recorded in the deep and superficial layers of the MEC was their action potential dependence and independence, respectively. This likely reflects clear differences in the circuitry underlying inhibition in the two layers. For example, LV principle neurones may be subject to feedforward inhibition, whereby network activity is driving interneurones to fire, or an increase in recurrent

connectivity for which there is evidence for in the MEC (Finch et al., 1988). Activation of KARs are known to drive network excitability/inhibition, therefore the differences in lamina connectivity in LII and LV MEC are examined further in these conditions in the next two chapters.

Chapter 5

Functional role of kainate receptors at

glutamatergic synapses in LII and LV of

neonate and juvenile rats

5.1 Introduction

Recent papers from this laboratory have provided a comprehensive description of the properties of inhibitory (GABA) and excitatory (glutamate) transmission in LIII of the MEC, and the role of KAR in mediating and modulating transmission at both (Chamberlain et al., 2012; Greenhill et al., 2014; see previous chapters and below for details). In Chapters 3 and 4 of this thesis, I provided complementary descriptions of the characteristics of spontaneous excitation and inhibition in LII and LV, and examined changes associated with development from neonate to juvenile rats' state. In this chapter and the next I will detail the developing role of KAR in transmission in both layers and age groups.

KARs are ubiquitous in the central nervous system where they regulate excitatory neurotransmission at both sides of the synapse. At the postsynaptic membrane, KARs carry part of the synaptic charge, similarly to AMPARs and NMDARs. Indeed, in the hippocampus, the quantal release of glutamate can actually generate KAR-mediated EPSCs that contribute over half of the total excitatory current (Cossart et al., 2002). At the presynaptic level, KARs modulate transmitter release from both excitatory and inhibitory synapses, though this chapter will focus on the former. KAR mediated synaptic responses have been identified at various locations, including in the CA1 field of the hippocampus (Cossart et al., 1998), the cerebellum (Bureau et al., 2000), thalamocortical synapses (Kidd and Isaac, 1999), the basolateral amygdala (Li and Rogawski, 1998) and on principal cells in the superficial layers of the MEC (West et al., 2007). The postsynaptic responses in MEC are likely to be mediated by GluK2 KARs (West et al., 2007). From these studies, it has become apparent that KAR mediated synaptic transmission has characteristic kinetics that are different relative to those mediated by AMPARs, namely, excitatory responses are were smaller, with significantly slower decay time kinetics and were associated with tonic depolarising properties (Cossart et al., 2002).

There is also compelling evidence to suggest KARs are located presynaptically at both excitatory and inhibitory synapses, where they can modulate neurotransmitter release. Many studies have focused on mossy fibre synapses onto CA3 neurones. Here, presynaptic KARs act to modulate neurotransmission in a bidirectional fashion, such that low and high

concentrations of KA act to increase and decrease glutamate release, respectively. The exact mechanisms behind this two-way modulation are unknown, but may be related to KAR mediated depolarisation, whereby low levels increase transmitter release, and high levels inactivate sodium/calcium channels (Schmitz et al., 2001a, Schmitz et al., 2000). KARs function as presynaptic autoreceptors at these synapses, acting to boost glutamate release in a frequency-dependent manner, implicating these receptors in mediating some forms of short-term synaptic plasticity (frequency-dependent facilitation) (Delaney and Jahr, 2002). Previous work in this laboratory has identified a GluK1-containing autoreceptor in LIII of the MEC which acts to facilitate glutamate release onto principal neurones (Chamberlain et al., 2012).

KARs have also been implicated in long-term plasticity, e.g. LTP at mossy fibre-CA3 synapses. Specifically, LTP induction can be reversibly prevented after blockade of the GluK1-containing KAR, suggesting KARs can be an induction trigger for long-term changes in synaptic transmission (Bortolotto et al., 1999). The ability of KARs to modulate synaptic plasticity can have consequences for neuronal development. At thalamocortical synapses, postsynaptic KARs are involved in the induction and expression of synaptic plasticity in early development, because their slower kinetics increase synaptic integration from different inputs. During development, KAR expression is down-regulated at these synapses, decreasing the likelihood of summating an action potential (Kidd and Isaac, 1999). Studies from other brain regions, such as the sensory cortex, have reported GluK1-containing KARs undergo clear qualitative changes during neuronal development, thus suggesting roles for this receptor in developmental plasticity (Bahn et al., 1994). Other studies show changes to the editing of GluK1 and GluK2 KAR subunits at critical periods at late embryonic development and early postnatal stages in the rat brain (Bernard et al., 1999).

Lastly, KARs have been implicated in the manifestation of spontaneous, bursting network activity in the neonatal rat hippocampus, an inherent property of development in this structure (Lauri et al., 2005, Ben-Ari et al., 1989), which have also been described in the immature rat MEC (Jones and Heinemann, 1989). Clearly, KARs and their associated functional characteristics can modulate neuronal excitation at both the pre- and post-synaptic level, with the ability to influence synaptic plasticity and the development of

synapses in an activity-dependent manner. Much of this research has focused heavily on the hippocampus, but research from this lab has begun to unravel the location and functional roles of KARs in the MEC, specifically in LIII.

KARs have been implicated in many conditions with associated underlying pathology in the MEC, most prominently epilepsy (Epsztein et al., 2005, Tolner et al., 2007, Vincent and Mulle, 2009). In fact, KA is often used as a chemical model of epilepsy in rodents, due to its ability to closely resemble the physiological neuronal damage and seizure induction associated with the disorder (Ben-Ari, 1985, Ben-Ari and Cossart, 2000). Broadly speaking, epilepsy manifests as hyper-synchronous neuronal network activity as a result of an imbalance between excitation and inhibition within the brain. The KAR is therefore a major candidate for the involvement in the pathological mechanisms underlying epilepsy and for a new therapeutic target.

This chapter aims to elucidate the involvement of KARs, specifically containing the GluK1 subunit, in the modulation of spontaneous excitatory neurotransmission in LII and LV of the MEC. Unfortunately, time has not permitted examination of KAR contribution to evoked postsynaptic responses. I also aimed to determine developmental changes in the involvement of KAR modulation of excitatory neurotransmission. Knowledge on the contribution of various subunits to receptor function has been somewhat confounded by the lack of pharmacological specificity in the development of KAR agonists and antagonists. However, the recent development of UBP-310 and ATPA allow more selective antagonism and agonism of the GluK1 subunit, respectively, and have been used throughout this chapter, along with KA, to elucidate the roles of this subunit modulating excitatory transmission in LII and LV.

5.2 Methods

Recording methods were described fully in Chapter 2. All experiments in this chapter were conducted on combined slices of EC and hippocampus from neonatal (P8-11; 20-35 g) and juvenile (P20-28; 50-100 g) Wistar rats. Whole cell voltage clamp recordings of sEPSCs and mEPSCs were made from principal neurones in LII and LV MEC. Neurones were voltage

clamped at -60 mV. Cells were selected with good access resistance that remained stable for the duration of the recording. To investigate the contribution of KARs to excitatory neurotransmission the non-specific agonist, KA, the relatively selective GluK1-containing KAR agonist, ATPA, and GluK1 antagonist, UBP-310 were used.

Mean values for frequency, inter-event interval (IEI; inverse of frequency), amplitude, decay times and holding current were determined and compared between control and drug groups using either a paired t-test or a repeated measures ANOVA (rANOVA) for multiple comparison. Dunnett's post-test was used if all comparisons were made to the control group, whereas a Bonferroni's post-test was used when comparing selected pairs of columns when multiple drugs were added. The non-parametric Mann Whitney test was used when comparing different neuronal populations. Two-way ANOVA analysis was used when comparing groups which were influenced by two different independent variables (e.g. time and age).

Cumulative distribution analysis used pooled data from a sample of events during a continuous recording period for each neurone and statistical comparisons were made using a Kolmogorov-Smirnov (KS) test for average mean data and cumulative probability distributions, respectively. Statistical significance was defined when $P < 0.05$, except for KS-analysis, where significance was reached if $P < 0.01$ due to the sensitivity of the test.

Drug	Action	Target	EC50/IC50	Conc. used	Reference
Kainic acid	Agonist	All KARs	0.6-7.4 µM	0.2 µM	(Alt et al., 2004)
ATPA	Selective agonist	GluK1-containing KARs	0.33 ± 0.05 µM	0.1-0.5 µM	(Alt et al., 2004)
UBP-310	Selective antagonist	GluK1-containing KARs	23 ± 2 µM	20 µM	(Perrais et al., 2009)

Table 5.1: Table of KAR agonists and antagonists properties.

5.3 Results

5.3.1 Effects of KA on LII EPSCs

5.3.1.1 Effects of KA on Juvenile LII sEPSCs

A summary of the effects of KA on sEPSCs in juvenile LII neurones can be seen in Fig. 5.1A-E. The effects of non-selectively activating all KARs with KA on spontaneous glutamate release onto principal neurones in LII were determined. In the presence of 200 nM KA, the mean frequency of sEPSCs increased substantially from 113.9 ± 56.0 events/min (1.9 Hz) to 1070 ± 448.1 events/min (17.8 Hz) and 1049.0 ± 356.8 events/min (17.5 Hz) after 10 and 15 minutes, respectively ($P = 0.02$ for both, rANOVA, $n = 4$). The 9-fold increase in frequency was largely reversed by the subsequent application of UBP-310 (20 µM), which reduced the frequency of sEPSCs to 238.8 ± 88.5 events/min (4.0 Hz).

KA also slightly increased the amplitude of events from 10.1 ± 2.6 pA to 12.2 ± 2.6 pA and 13.0 ± 2.2 pA after 10 and 15 minutes application, which was reversed to 9.9 ± 1.5 pA after additional application of UBP-310. This suggests the increase in amplitude elicited by KA was due to activation of KARs containing the GluK1 subunit. It is unlikely that a change in amplitude distribution elicited by the agonist is mediated by a postsynaptic mechanism. It seems more likely that that an increase in network excitability and action potential generation in presynaptic axons causes increased synchronised transmitter release and larger amplitude events.

A noticeable effect of KA was to considerably depolarise neurones, evidenced by the significant increase in holding current applied to keep the neurone clamped at -60 mV. This effect occurred without change in series resistance, and therefore was not a result of jeopardised integrity of the cell or changes to the seal between the electrode and the cell membrane. Moreover, the significant KA-induced increase in holding current of 77%, from -271.8 ± 59.6 pA to -444.9 ± 55.0 pA, was reduced after application of UBP-310 to -319.0 ± 45.0 pA, indicating Gluk1-containing KARs maybe be responsible for positive inward current underlying the depolarisation. There was no change in the decay time of sEPSCs after the

133

application of KA. A summary of the effects of KA on sEPSCs in juvenile LII principal neurones in the MEC can be seen in Fig. 5.1A-E.
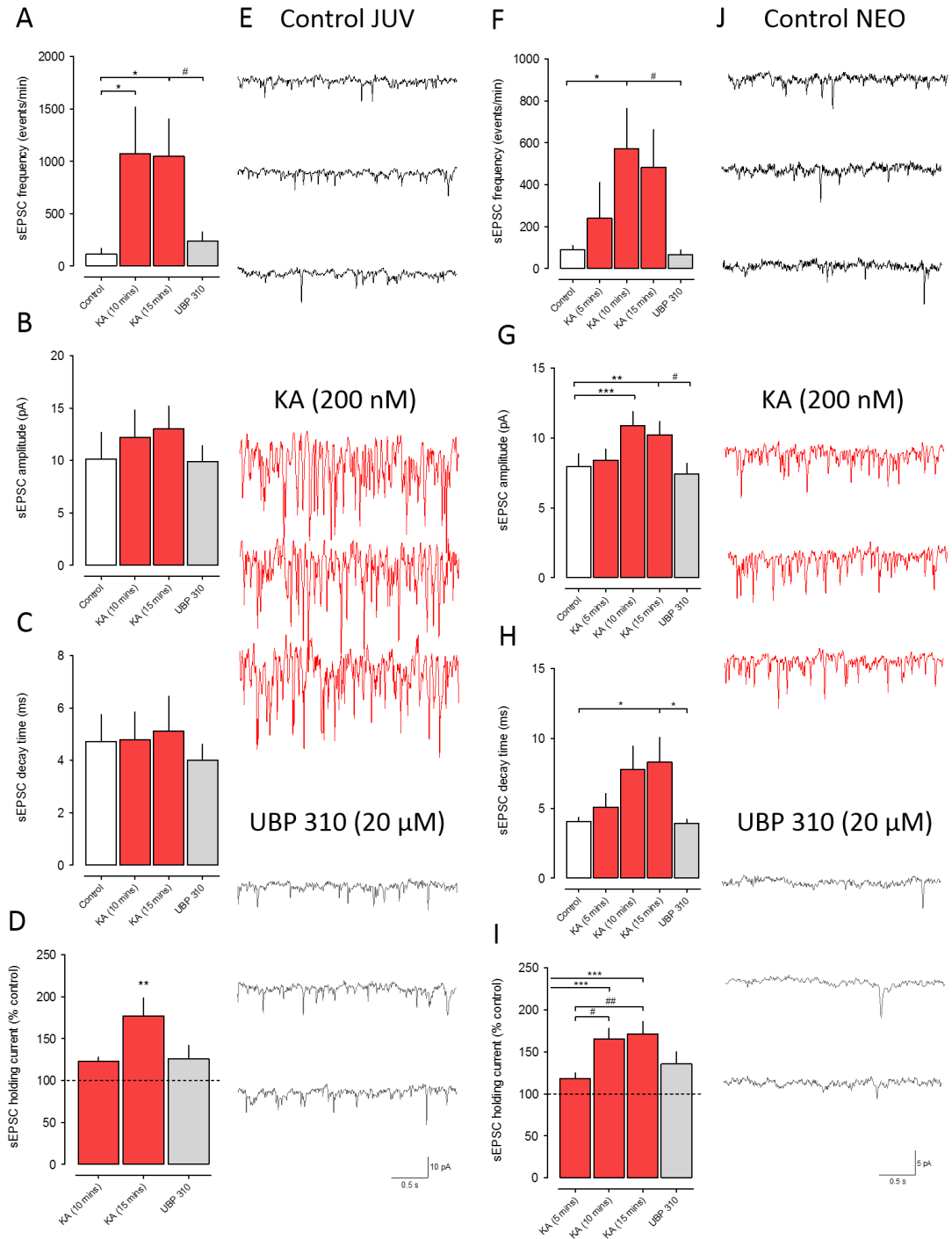
Figure 5.1. Effects of KA (200 nM) and UBP-310 (20 µM) on sEPSCs in 4 juvenile and 7 neonate LII neurones. (A/F) *Average sEPSC frequency,* ***(B/G)*** *amplitude,* ***(C/H)*** *decay time and* ***(D/I)*** *% change in holding current data from principal neurones. Control groups (white) represent sEPSCs before application of KA (red) and UBP-310 (grey). Average frequency and holding current was significantly increased in the presence of KA and reversed after addition of UBP-310. Traces show concurrent recordings of sEPSCs recorded in control conditions (black), in the presence of KA (red) and UBP-310 (grey) in a* ***(E)*** *juvenile and a* ***(J)*** *neonate principal neurone.*

5.3.1.2 Effect of KA on juvenile LII mEPSCs

The increased amplitude with KA might suggest activation of KAR receptors on excitatory neurones presynaptic to the recorded postsynaptic neurone was contributing to this effect by increasing excitatory drive. To examine this, the effect of KA on mEPSCs was determined. The effects of KA on mEPSCs are summarised in Fig. 5.2. Bath application of KA (200 nM) increased the mean frequency of mEPSCs from 136.6 ± 51.1 events/min (2.3 Hz) to 225.9 ± 77.5 events/min (3.8 Hz) after 15 minutes, an effect which was reversed by subsequent application of UBP-310, reducing the frequency of mEPSCs to 104.6 events/min (1.7 Hz). The increase in mEPSCs was dramatically less than that seen with sEPSCs, and, in fact, did not reach statistical significance.

Unlike with sEPSCs, there were no differences in the amplitude or decay times of mEPSCs after KA application. This does strongly suggest that the observed effects are due to enhanced glutamate release consequent on KAR activation on presynaptic excitatory neurones. Overall, the results support the suggestion that KARs that containing the GluK1 subunit are present on both presynaptic excitatory neurones, such that an increased excitatory drive elicited by KA facilitates glutamate release onto principal neurones. Moreover, the Gluk1-containing KARs may be present postsynaptically on the recorded neurone since the increase in holding current induced by KA was still present in TTX but still reversed by UBP-310. An alternative explanation for the postsynaptic depolarising effects of KA could be due to the sheer increase in active AMPARs on the postsynaptic membrane, reflecting the substantial increase in glutamate release and sEPSC frequency. However, the change in holding current was unaffected by TTX, and if anything was more marked, whereas the increase in sEPSC frequency was largely abolished, so a direct activation of postsynaptic GluK1 receptors seems more probable.

A likely explanation for these findings is that KA depolarises principal cells and activates recurrent excitatory connections in LII. However, it has been suggested that recurrent excitation between LII neurones is weak or non-existent in the EC (Dhillon and Jones, 2000, Couey et al., 2013, Pastoll et al., 2013a, Fuchs et al., 2016). This has been recently questioned by another study that found a connectivity of about 2.5% between stellate neurones in LII, but a much higher connectivity of LII PCs (12%) onto SCs in LII (Winterer et

al., 2017). Additionally, there was a substantial connectivity between LIII PCs (which themselves are highly interconnected; (Dhillon and Jones, 2000) and LII SCs (Winterer et al., 2017).Thus, the massive increase in sEPSC frequency with KA in the current data could be due to activation of KAR on both LII and LIII pyramids that provide feed-forward excitation to LII stellate neurones. Slightly at odds with this is the reduction of the effect with UBP-310, since it has been suggested that KAR receptors on LII and LIII neurones appeared to be more GluK2 than GluK1 containing (Beed et al., 2013, Chamberlain et al., 2012). However, the fact that UBP-310 only partially reversed the effect of KA on sEPSCs in LII might suggest that is a mixed population of receptors is being activated by KA.
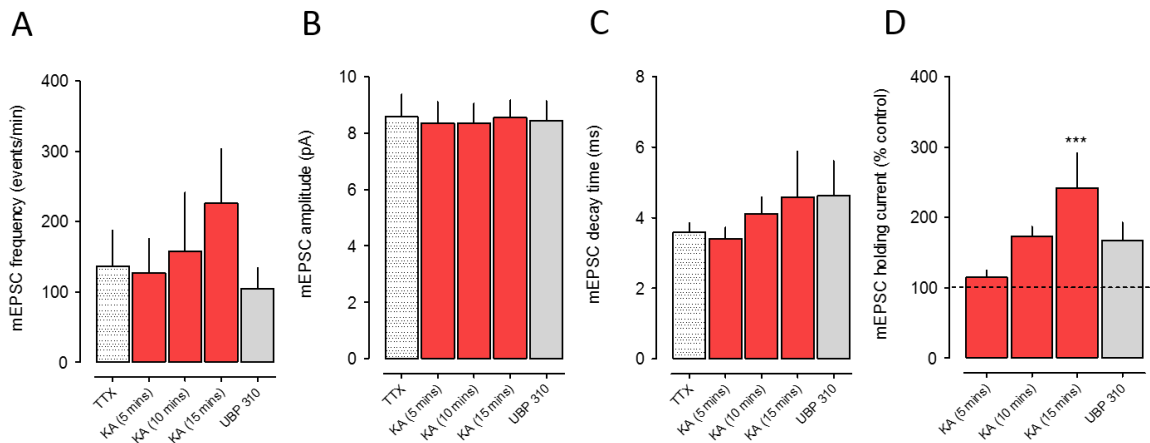
Figure 5.2. Effects of KA (200 nM) and UBP-310 (20 μM) on mEPSCs in juvenile LII neurones. (A) *Average sEPSC frequency,* ***(B)*** *amplitude,* ***(C)*** *decay time and* ***(D)*** *% change in holding current data from 4 principal neurones. Control groups (white) represent mEPSCs before application of KA (red) and UBP-310 (grey). Average frequency and holding current was significantly increased in the presence of KA and reversed after addition of UBP-310.*

5.3.1.3 Effects of KA on neonate LII sEPSCs

Unpublished immunohistochemical data made available by Professor Elek Molnar from the University of Bristol shows a progressive increase in expression of several KAR subtypes with development in the temporal lobe areas of the rat brain (see Fig. 1.6 in Chapter 1). Although the changes in the EC were not quantified, visual examination suggests a noticeable increase in GluK1 expression around P14 which appeared stable thereafter. GluK2 expression also appeared to increase but rose more progressively from around P10

upwards. It seems likely, therefore, that there may be alterations in KAR function in synaptic transmission with development.

The effects of KA on sEPSCs in LII neurones in neonate slices are also shown in Fig. 5.1 (F-J). In the presence of KA (200 nM), the mean frequency of sEPSCs increased substantially from 90.6 ± 19.8 events/min (1.5 Hz) to a maximum of 570.8 ± 194.2 events/min (9.5 Hz) after 15 minutes perfusion (P < 0.05, rANOVA; n = 7). This 6-fold increase in frequency was completely reversed to a level below control by the subsequent cumulative application of UBP-310 (20 µM), which reduced the frequency of sEPSCs to 67.4 ± 22.2 events/min (1.1 Hz; P < 0.05, rANOVA). KA also increased the amplitude of events from 7.9 ± 1.0 pA to 10.2 ± 1.0 pA after 15 minutes application (P < 0.01, rANOVA), an effect that was also reversed to 7.4 ± 0.8 pA by UBP 310 (P < 0.0001, rANOVA).

Surprisingly, the mean decay time of sEPSCs increased significantly from 4.1 ± 0.3 ms to 8.3 ± 1.8 ms after 15 minutes exposure to KA (P < 0.05, rANOVA; n = 7), again the effect was reversed to control levels (3.9 ± 0.3 ms) by UBP-310 (P < 0.05, rANOVA; n= 7).

As in LII neurones in juvenile slices (Fig. 5.1 A-E), KA appeared to have a substantial postsynaptic depolarising effect, reflected by an increase in holding current in the recorded cell. KA increased holding current by 71%, from -86.4 ± 22.6 pA to -137.5 ± 30.6 pA (P < 0.0004, rANOVA), and this was partially reduced by UBP-310 to -114 ± 29.4 pA.

By and large, the effects of KA and subsequent addition of UBP-310 in neonate neurones were qualitatively similar to that seen in juvenile neurones, although the magnitude of the frequency increase was somewhat less. The data supports the suggestion that KA is activating a GluK1 containing KAR on the soma/dendrites of other principal neurones in LII and LIII (cf Winterer et al., 2017) to increase glutamate release at recurrent inputs to the recorded neurone. One noticeable difference was the increase in decay time of events in KA. This could suggest that the population of neurones activated by KA do not contribute to sEPSCs at rest, and that when activated they generate a separate population of sEPSCs with a much longer decay time, thus resulting in an overall increase in the mean.

5.3.2 Effects of ATPA on LII EPSCs

5.3.2.1 Effect of ATPA on Juvenile LII sEPSCs

KA, at a concentration discriminatory between AMPAR and KAR but not between different KARs, led to an increase in sEPSC frequency that was as least partially reversed by blocking the GluK1-containing KAR. However, does this mean GluK1 KARs are initiating the change in frequency in the first place? To investigate this further, the effects of the selective GluK1 KAR agonist, ATPA, on sEPSC activity were determined.

The effects of ATPA on sEPSCs are summarised in Fig. 5.3. Unexpectedly, ATPA (100 nM) slightly but significantly decreased the mean frequency of sEPSCs in LII juvenile neurones, from 276.3 ± 71.4 events/min (4.6 Hz) to 188.3 ± 38.0 events/min (3.1 Hz) after 10 minutes ($P = 0.01$, rANOVA with Dunnett's post-test; n = 6), although the effect was small with only a partial recovery to 231.6 ± 52.4 events/min (3.9 Hz) after a wash-out, and ATPA had no effect on amplitude or decay time or on the holding current applied to maintain the neurone at -60 mV (although there was a trend towards an increase in it that actually reached significance during washout). These results are at odds with the experiments using KA, and would suggest the depolarisation observed with KA application was not due to activation of postsynaptic GluK1 KARs present on the recorded neurones. Likewise, it would also suggest that the increase in sEPSCs seen with KA is unlikely to be due to increased excitatory drive after activation of GluK1 receptors on recurrently connected neurones. However, what is most puzzling is that both effects of KA were substantially reversed by the GluK1 antagonist UBP-310. It is possible that the specificity of the drug is not as good as was previously thought. Indeed, previous studies have suggested that whilst UBP-310 has little affinity for GluK2, it may substantially block GluK3 receptors as well as GluK1 (Perrais et al., 2009, Atlason et al., 2010), so one possibility is that the effects of KA are mediated largely by the former and not the latter.
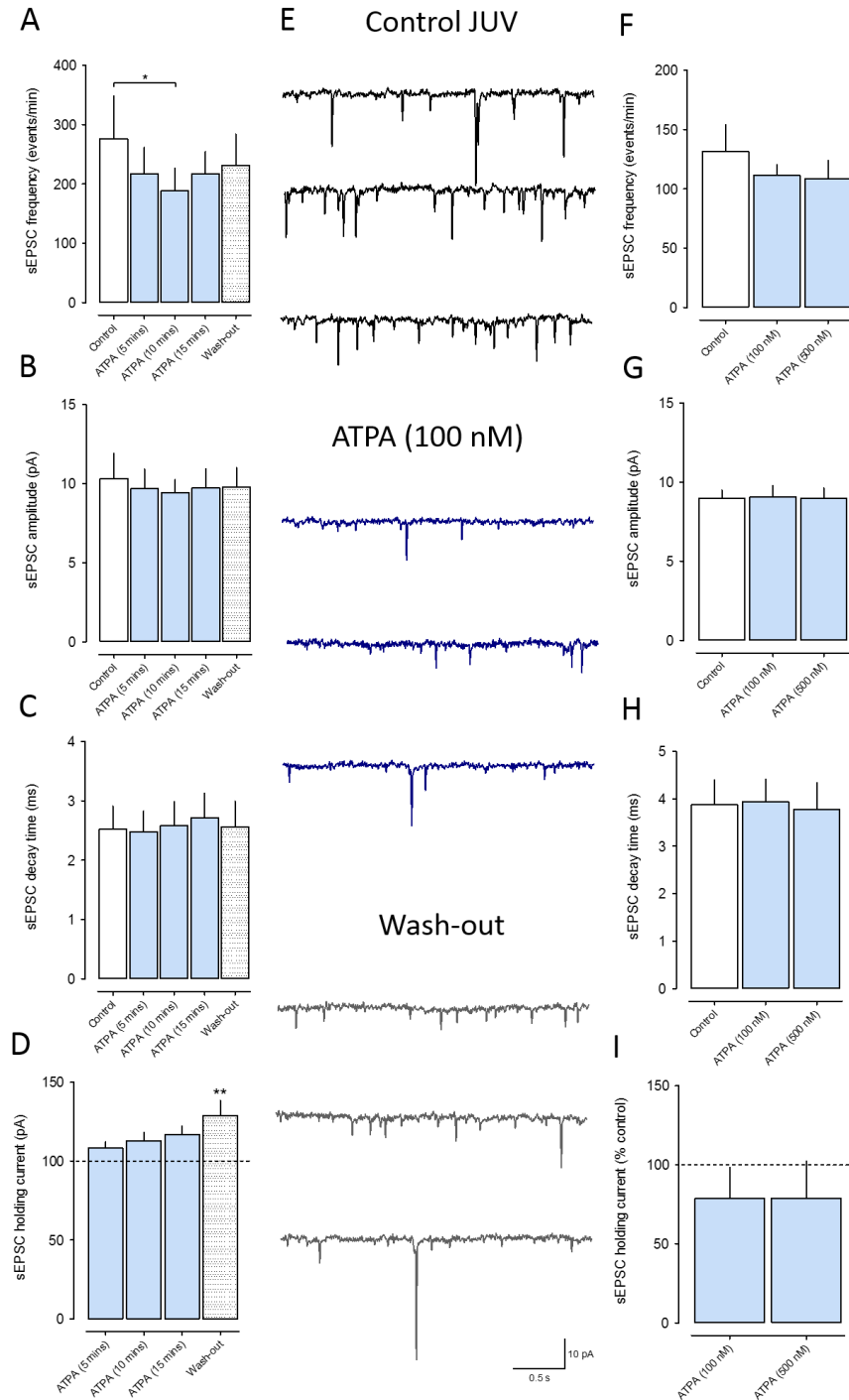
Figure 5.3 Effects of ATPA (100 & 500 nM) on sEPSCs in 4 juvenile and 3 neonate LII neurones. (A/F) *Average sEPSC frequency,* **(B/G)** *amplitude,* **(C/H)** *decay time and* **(D/I)** *% change in holding current data from principal neurones. Control groups (white) represent sEPSCs before application of ATPA (blue) and a wash-out (dotted). Average frequency of sEPSCs was significantly decreased in the presence of ATPA in juvenile (A) but not neonate slices (F).* **(E)** *Concurrent recordings of sEPSCs recorded from a juvenile neurone in control conditions (black), and in the presence of ATPA (blue) and after a wash-out (grey). NB: Due to the lack of an effect in neonate sEPSCs no traces are presented and the concentration of ATPA was increased to 500 nM.*

As noted, these results were unexpected, especially as we have previously shown that both KA and ATPA, induced a significant increase in sEPSC frequency in the adjacent LIII (Chamberlain et al., 2012). To check that the lack of an effect of ATPA was a true effect, I reconfirmed its effects on 3 principal neurones in LIII. Although not statistically significant due to the low n number, there was a clear increase in the average frequency of sEPSCs that was reversed upon wash-out of the drug (Fig. 5.4). However, it should be noted here that the effects of ATPA in LIII were unaffected by TTX, so were largely the result of activation of GluK1 receptors on excitatory synaptic terminals not somatic/dendritic receptors (Chamberlain et al., 2012).
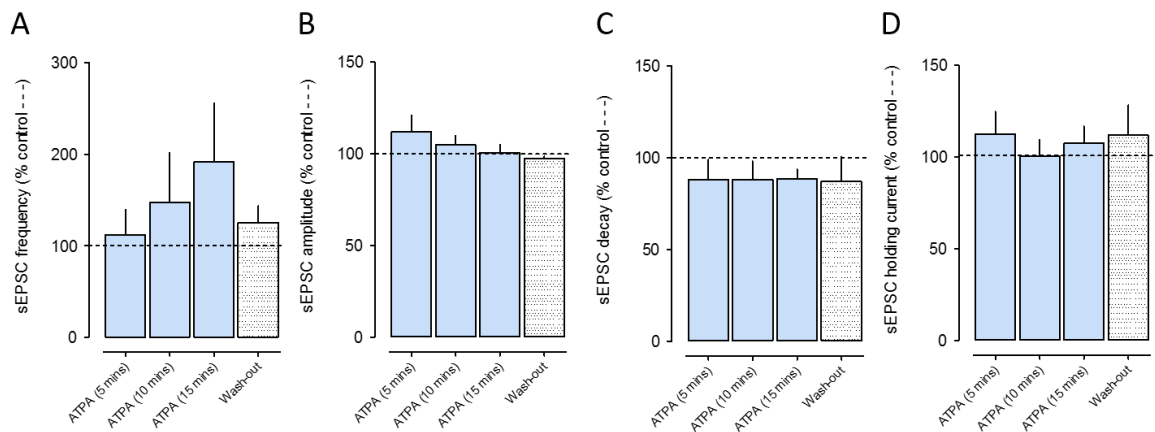
Figure 5.4: Effects of ATPA (100 nM) on sEPSCs in juvenile LIII neurones*. (A) Average % change in sEPSC frequency, **(B)** amplitude, **(C)** decay time and **(D)** holding current data from 3 principal neurones. Control (dashed line - - -) represents sEPSCs before application of ATPA (blue) and a wash-out (dotted). Note that in LIII neurones, ATPA increased sEPSC frequency.*

5.3.2.2 Effects of ATPA on juvenile LII mEPSCs

To determine whether the reduction of sEPSCs by ATPA in juvenile slices was due to activation of presynaptic GluK1-containing KARs on glutamate terminals, as opposed to GluK1 receptors on soma/dendrites, I tested the effects of ATPA on mEPSCs. ATPA (100 nM) had no effect on the frequency, amplitude or decay time kinetics of mEPSCs, as seen in Fig. 5.5 (n = 8).
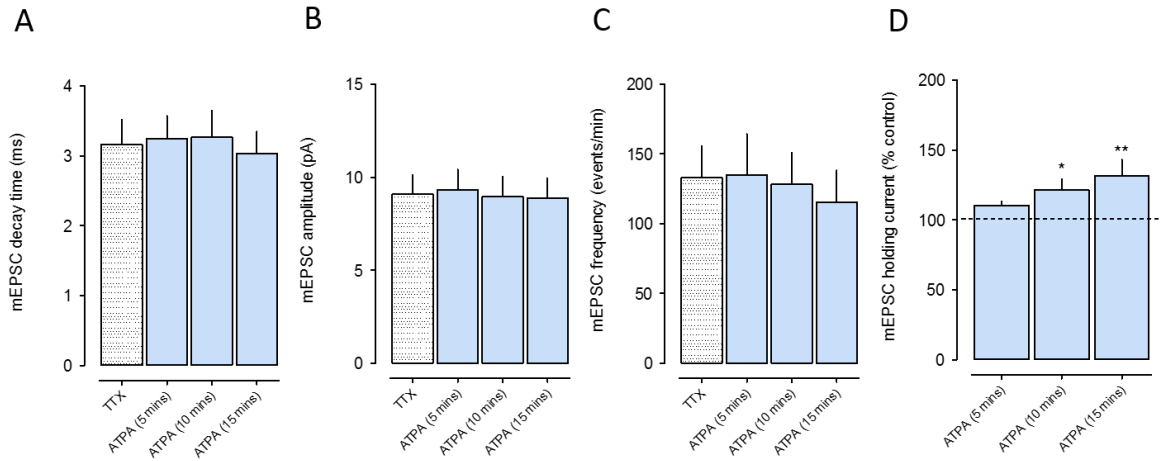
Figure 5.5: Effects of ATPA (100 nM) on mEPSCs in juvenile LII neurones in TTX (1 µM). (A) *Average mEPSC frequency,* **(B)** *amplitude,* **(C)** *decay time and* **(D)** *% change in holding current data from 8 principal neurones. Control groups (dotted) represent mEPSCs in the presence of TTX, before application of ATPA (blue). ATPA had no effect on the frequency of events.*

5.3.2.3 Effects of ATPA on neonate LII sEPSCs

Bath application of ATPA (100 nM), as in juvenile slices, appeared to slightly decrease the frequency of sEPSCs in neonate neurones, from 131.4 ± 22.8 events/min to 111.5 ± 8.9 events/min, but the change was not significant. Cumulative addition of ATPA to 500 nM had no additional effect (108.7 events/min). ATPA also had no effect on the mean amplitude of sEPSCs or mean decay time. Interestingly, unlike in juvenile slices, ATPA appeared to induce a slight, but non-significant, decrease in the average holding current in neonatal LII principal cells (from -101.5 ± 25.4 pA to -82.7 ± 32.8 and -84.8 ± 38.5 after 100 nM and 500 nM). Overall, the results generally reflect those seen with ATPA in juvenile slices and are summarised in Fig. 5.3 alongside the juvenile data.

Although the decrease in sEPSC frequency with ATPA was not marked, the absence of marked effects on mEPSCs could suggest that the decrease in sEPSC frequency was the result of a decrease in network excitation. Reasons for this could include: 1) receptor desensitisation due to excessive receptor activation, 2) the presence of GluK1-containing KARs on inhibitory interneurones acting to increase GABA release and a general decrease

in network activity, 3) GluK1 KAR activation with ATPA may have caused a depolarising block, a rate-limiting mechanism to protect neurones from excessive spiking. However, this is unlikely as the frequency of sEPSCs did not increase first, unless, however, the receptor is already very highly tonically active. Under high levels of tonic activity, sEPSC frequency could have decreased if ATPA had a lower efficacy or slower receptor binding kinetics than ambient glutamate, leading to a decrease in excitation relative to the tonic conditions. Tonic activation of GluK1-containing KARs was therefore investigated by testing the effect of UBP-310 alone.

5.3.3 Effects of UBP-310 on LII EPSCs

5.3.3.1 Effect of UBP-310 on Juvenile LII sEPSCs

The effects of UBP-310 on sEPSCs are summarised in Fig. 5.6. The mean frequency of sEPSCs was substantially decreased after 15 minutes application of 20 μM UBP-310 from 237.6 ± 70.9 events/min (4 Hz) to 96.1 ± 21.9 events/min (1.6 Hz) ($P = 0.02$, rANOVA with Bonferrini's post-test; n = 6), suggesting GluK1 KARs are highly tonically activated in LII and contribute substantially to spontaneous glutamate release. There was no effect on the mean amplitude of sEPSCs (control 7.1 ± 0.7 pA *vs* 6.8 ±1.1 pA after UBP-310). Additional application of 200 nM KA on top of UBP-310 had no effect on mean amplitude, frequency, decay time or holding current.

If we assume that UBP-310 may be blocking GluK1 receptors that are already tonically activated by ambient glutamate, this may indicate why ATPA had little effect on sEPSCs (Fig. 5.3), and it indeed could contribute to a reduction in the tonic effect by desensitisation of the GluK1 receptors. The fact that KA had virtually no effect in the presence of UBP-310 may be a further indication that the increase in sEPSCs and other effects seen with KA alone is due to non-GluK1 receptors in recurrent circuits that are also affected by UBP310 (e.g. GluK3; Perrais et al., 2009)
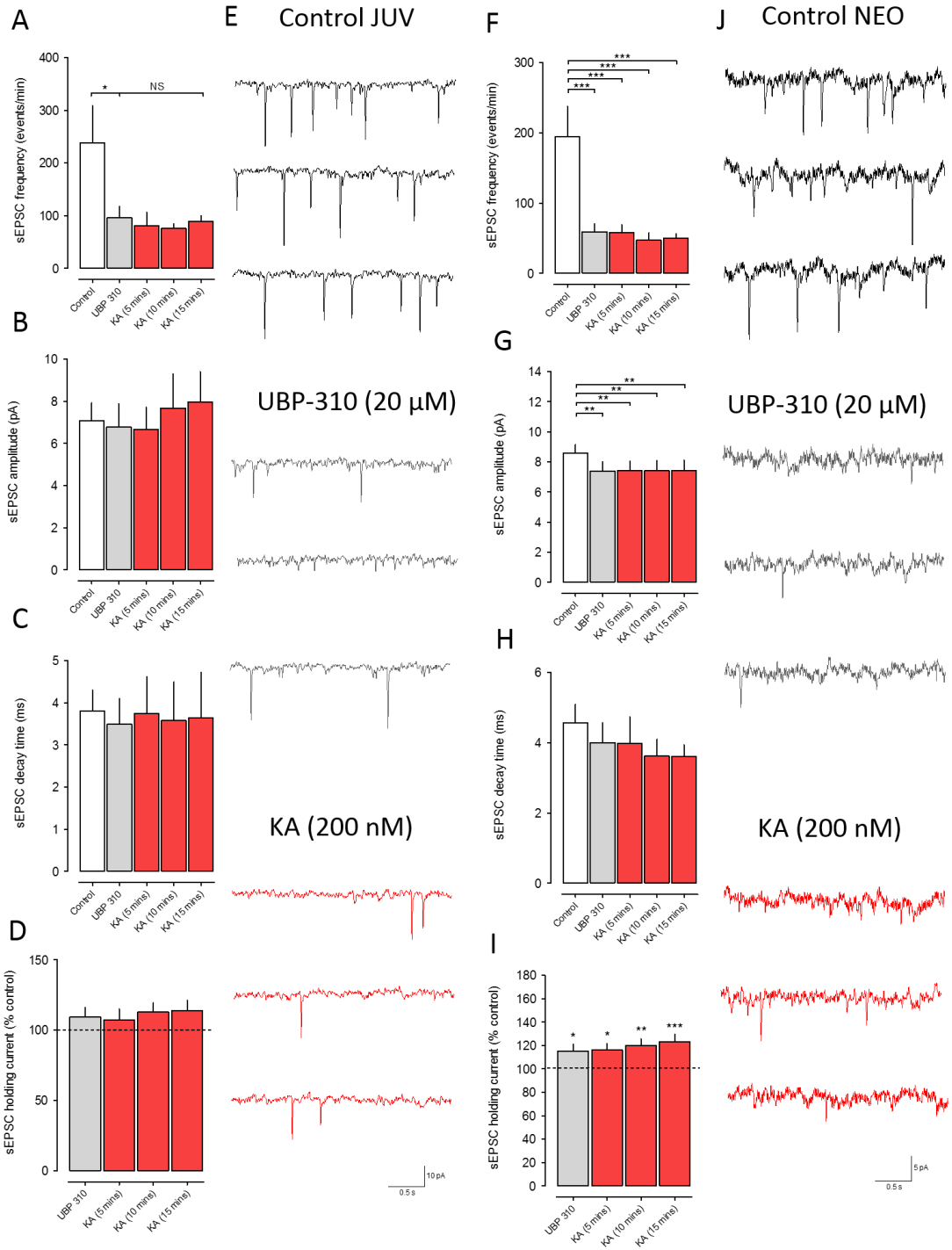
Figure 5.6: Effects of UBP-310 (20 μM) and KA (200 nM) on sEPSCs in 6 juvenile and 6 neonate LII neurones*. **(A/F)** Average sEPSC frequency, **(B/G)** amplitude, **(C/H)** decay time and **(D/I)** % change in holding current data from LII principal neurones. Control groups (white) represent sEPSCs before application of UBP-310 (grey) and KA (red). Average frequency was significantly decreased in the presence of UBP-310 and was not affected by the addition of KA. Concurrent recordings of sEPSCs recorded in control conditions (black), and in the presence of UBP-310 (grey) and KA (red) from a **(E)** juvenile and a **(J)** neonate neurone.*

5.3.3.2 Effects of UBP-310 on juvenile LII mEPSCs

To help determine the location of the tonically active GluK1-containing KAR, UBP-310 (20 µM) was tested on mEPSCs in the presence of TTX (1 µM). Interestingly, effects on sEPSCs were also seen with mEPSCs, the mean frequency being significantly decreased from 157.2 ± 45.0 events/min (2.6 Hz) to 89.2 ± 417 events/min (1.5 Hz) (P = 0.01, paired t-test; n = 4). There was no change in mean amplitude (9.3 ± 1.1 pA *vs* UBP-310: 8.3 ± 1.6 pA) or the mean decay time (3.3 ± 0.3 ms *vs* 2.6 ± 0.2 ms). The effects of UBP-310 on mEPSCs in juvenile slices are summarised in Fig. 5.6.

5.3.3.3 Effects of UBP-310 on neonate LII sEPSCs

UBP-310 was applied alone to determine if the tonic activation GluK1-containing KAR activation seen in LII in juvenile rats was also present in neonates. The effects are also summarised in Fig. 5.6, alongside the effects on juvenile slices. In the presence of the antagonist, the mean frequency of sEPSCs was substantially and significantly decreased from a control of 194.6 ± 45.6 events/min (3.2 Hz) to 59.2 ± 11.5 events/min (1.0 Hz) after UBP-310 (P < 0.0001, rANOVA, n = 6). Cumulative application of KA had no further effect in the presence of UBP-310. The substantial decrease in frequency suggests tonic activation of GluK1 autoreceptors on synaptic terminals by ambient glutamate, which accounts for about 50-60% of spontaneous release.

UBP-310 appeared to induce very small, but significant decrease in the average amplitude of sEPSCs, from a control of 8.6 ± 0.6 pA to 7.4 ± 0.6 pA (P = 0.0006, rANOVA; n = 6). UBP-310 did not change the mean decay time of sEPSCs (4.6 ± 0.5 ms to 4.0 ± 0.6 ms). Addition of UBP-310 also appeared to induce a very small but significant increase in the amount of holding current which was applied to maintain the neurone at -60 mV, from a control of -164.7 ± 49.1 pA to 195.4 ± 67.8 pA. Thus, again, the effect of UBP-310 on sEPSCs in LII of neonates reflects that seen in juveniles.

The results thus far have identified that KARs have major roles in the regulation of glutamatergic transmission in LII. Specifically, generalised KAR activation substantially increases glutamate release onto principal neurones, and it seems likely that this is due to

activation of soma/dendritic KAR in neurones that provide inter- and intra-lamina recurrent excitatory inputs to the recorded neurone. This is supported by depolarising effects of KA in the latter, and the fact that TTX largely abolished the response. This effect was partially reversed by UBP-310, which initially suggests that the receptor involved is GluK1-containing. However, a GluK1 agonist did not increase the frequency sEPSCs, in fact, ATPA led to a small decrease in frequency. One interpretation of these results is that UBP-310 is not in fact specific for GluK1 receptors, and that KA is activating another receptor, possibly GluK3 (Perrais, 2009). Surprisingly, however, UBP-310 alone substantially reduced sEPSC and mEPSC frequency suggesting that GluK1-containing KARs are tonically active autoreceptors on glutamate terminals in LII and are activated by ambient glutamate, helping to maintain a high level of release. This leads to the possibility that the component of sEPSCs and mEPSCs reduced by UBP-310 after addition of KA is actually the tonic presynaptic component and that the remainder is recurrently driven release by non-GluK1 receptors on principal cells.
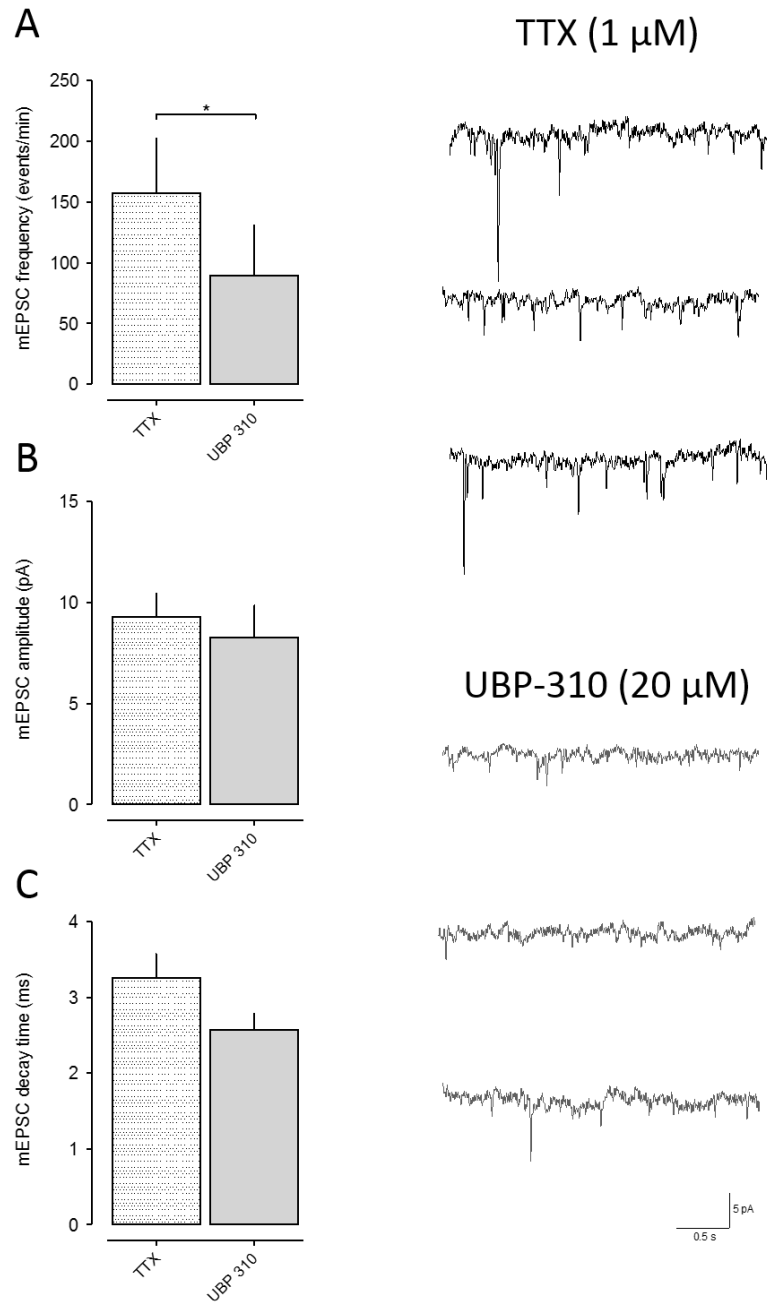
Figure 5.7: Effects of UBP-310 (20 μM) on mEPSCs in juvenile LII neurones. *(A) Average sEPSC frequency, (B) amplitude and (C) decay time of sEPSCs from 4 principal neurones. Control groups in the presence of TTX (dotted) represent mEPSCs before application of UBP-310 (grey). Average frequency was significantly decreased in the presence of UBP-310. Traces show concurrent recordings of mEPSCs recorded in control conditions (black), and in the presence of UBP-310 (grey).*

5.3.4 Effects of KA on LV EPSCs

5.3.4.1 Effect of KA on Juvenile LV sEPSCs

The effects of KA on sEPSCs are summarised in Fig. 5.8. Generalised activation of KARs using KA caused a gradual and significant increase in sEPSC frequency from 167.8 ± 49.1 events/min (2.8 Hz) to a maximum of 356.9 ± 49.1 events/min (5.9 Hz) after 15 minutes ($P = 0.0002$, rANOVA; n = 5). This effect was substantially less (~2 fold) than that seen in LII (~9 fold). Subsequent cumulative application of UBP-310 (20 µM) reversed the increase in frequency to 122.9 ± 38.5 events/mins, or 1.9 Hz ($P < 0.001$, rANOVA) and this actually fell slightly below control levels, perhaps indicating tonic activation of GluK1 KARs in LV. The increase also appeared slower in onset than in LII (cf Fig. 5.1).

Unlike in LII, KA had no effect on the amplitude of sEPSCs in LV (control: 8.5 ± 0.4 pA vs KA: 8.2 ± 0.2 pA), perhaps suggesting the increase in frequency did not have a large network driven component. KA also had no effect on sEPSC decay time (3.0 ± 0.3 ms v 3.1 ± 0.4 ms). KA did induce a significant increase in holding current from 148 ± 33.3 pA to -218.3 ± 29.9 pA after 15 minutes in KA, which was similar to that seen in LII. However, this was not affected by UBP-310.

Overall these results show that KAR activation can increase glutamate release in LV, but this effect is more restrained than that seen in LII. The lack of a change in amplitude could indicate that KA is having its effects directly on the presynaptic terminals rather than activating other principal neurones that provide recurrent input to the recorded neurone. If we accept that UBP-310 is fairly specific for GluK1, its effects suggest that KA is largely activating GluK1 receptors but that overall release levels may involve a tonic activation of the receptor by ambient glutamate.
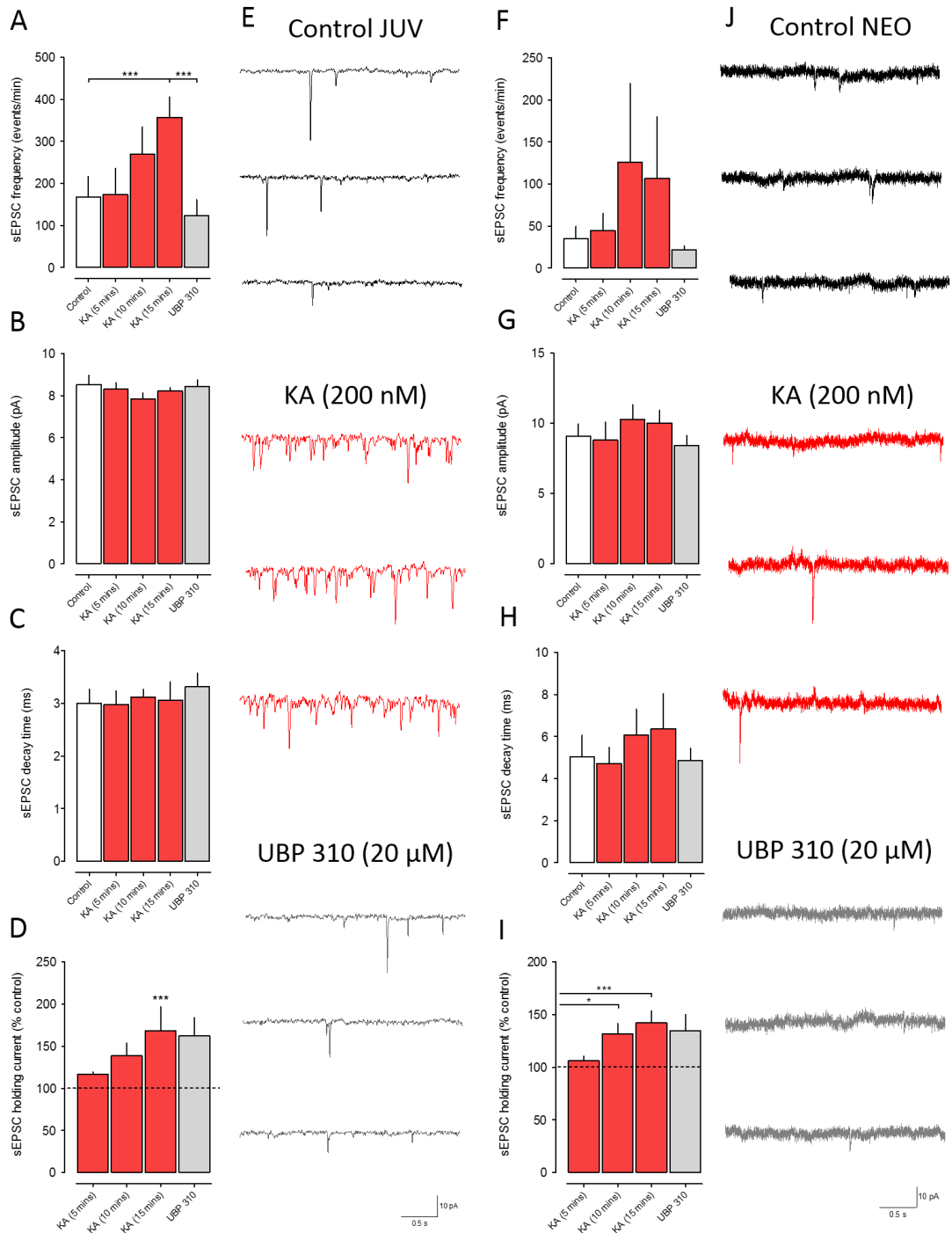
Figure 5.8: Effects of KA (200 nM) and UBP-310 (20 µM) on sEPSCs in 5 juvenile and 8 neonate LV neurones. (A/F) *Average sEPSC frequency,* **(B/G)** *amplitude,* **(C/H)** *decay time and* **(D/I)** *% change in holding current data from LV principal neurones. Control groups (white) represent sEPSCs before application of KA (red) and UBP-310 (grey). Average frequency and holding current was significantly increased in the presence of KA and reversed after addition of UBP-310. Concurrent recordings of sEPSCs recorded in control conditions (black), in the presence of KA (red) and UBP-310 (grey) in a juvenile* **(E)** *and a* **(J)** *neonate LV principal neurone. Note the substantial increase and decrease in sEPSC frequency and amplitude after exposure to KA and subsequent UBP-310, respectively.*

5.3.4.2 Effects of KA on LV mEPSCs

Bath application of KA (200 nM) did not significantly alter the average frequency of mEPSCs in 6 LV principal neurones from an average control of 87.5 ± 24.8 events/min (1.5 Hz) to 79.3 ± 17.5 events/min (1.3 Hz) and 71.9 ± 25.1 events/min (1.2 Hz) after 5 and 10 minutes KA, respectively (Fig. 5.9). A slight increase in the frequency of mEPSCs does appear after 15 minutes KA, however, on closer analysis this reflects a large increase in frequency in one cell. KA had no effect on the amplitude of mEPSCs, from an average of 7.6 ± 0.3 pA to 7.6 ± 0.3 pA and 7.3 ± 0.4 pA after 10 and 15 minutes, respectively. No changes were detected in mean decay time of mEPSCs. However, the holding current was significantly increased after 15 minutes exposure to KA, suggesting the presence of post-synaptic KARs on the recording neurone.
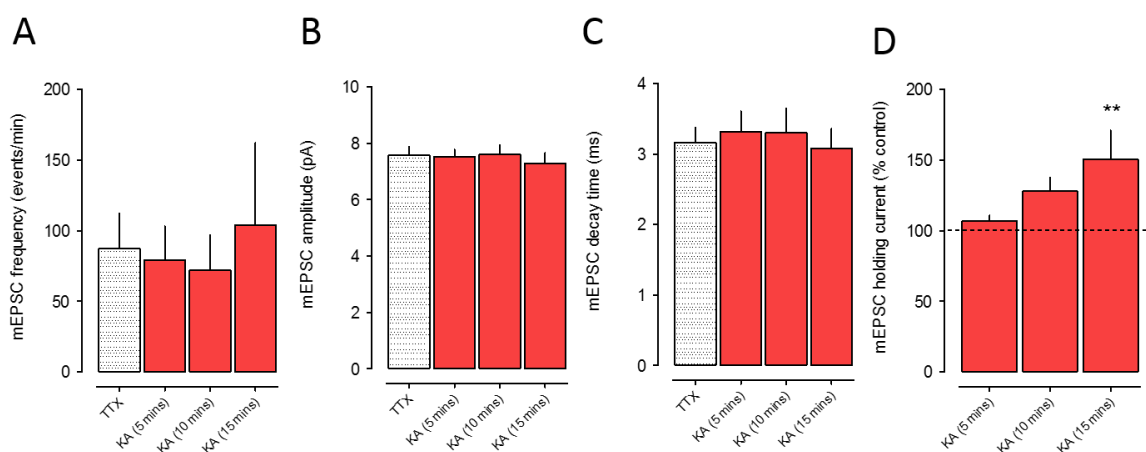
Figure 5.9: Effects of 200 nM KA on mEPSCs in juvenile LV neurones in TTX (1 μM). (A) *Average sEPSC frequency, **(B)** amplitude, **(C)** decay time and **(D)** % change in holding current data from 6 LV principal neurones. Control groups (white) represent mEPSCs before application of KA (red). There were no significant changes in the presence of KA except an increase in holding current.*

Thus, the lack of effect on mEPSCs suggests that most of the increased release induced by KA in LV is again largely due to activation of KAR on local input neurones recurrently innervating the recorded neurone. This would be supported by the similarity in direct depolarizing effects of KA on neurones regardless of whether TTX is present or not. The similarity in amplitude of sEPSCs and mEPSCs and lack of any change in amplitude of sEPSCs with KA, indicates that the input neurones are likely to be releasing glutamate at quantal levels. This would be supported by previous studies which have shown a relatively high degree of recurrent connectivity between neurones in LV, but very small amplitude single axon EPSPs in dual cell recordings (Dhillon and Jones, 2000).

5.3.4.3 Effects of KA on neonate LV sEPSCs

The effects of non-selectively activating KAR on sEPSCs are shown in Fig. 5.8F-J. In the presence of KA (200 nM), the mean frequency of sEPSCs moderately increased from 35.0 ± 14.6 events/min (0.6 Hz) to 126.2 ± 93.3 events/min (2.1 Hz) and 106.7 ± 73.4 events/min (1.8 Hz) after 10 and 15 minutes KA, respectively (n = 8). However, the high degree of variability between individual neurones meant that this did not reach statistical significance. On closer analysis it became apparent there were two separate responses to KA in LV neonatal neurones: 1) Neurones that showed no increase in frequency of sEPSCs in the presence of KA, deemed 'non-responsive' (n = 4) and 2) neurones that increased the frequency of sEPSCs in response to KA (n = 4). In the non-responsive group, KA had no apparent effect on the frequency, amplitude or decay time of sEPSCs.

The other 4 neonatal LV neurones examined neurones tested responded to KA. The amino acid increased the frequency of sEPSCs from a control of 48.7 ± 29.3 events/min (0.8 Hz) to 228.9 ± 183.3 events/min (3.8 Hz) and 193.1 ± 142.0 events/min (3.2 Hz) after 10 and 15 minutes KA, respectively. This effect was reversed to below control levels (23.2 ± 8.9 events/min - 0.4 Hz) after addition of 20 µM UBP-310. Despite this, the increase in average frequency did not reach statistical significance in this KA responsive group mostly due to the large variation between neurones (n = 4). In the responsive group, the average amplitude was significantly increased by KA to 10.1 ± 2.0 pA after 10 minutes KA, from a control of 7.7 ± 1.1 pA (P = 0.01, rANOVA; n = 4), but just dropped blow significance after 15 min. The increase in amplitude was returned to control levels on addition of UBP-310

(to 7.7 ± 1.2 pA). As in the neurones in LII of neonate animals, KA appeared to increase the mean decay time in the LV responsive group (3.6 ± 0.4 ms to 7.7 ± 3.3 ms after 15 min KA), again this was non-significant, but the change did appear to be reversed (4.7 ± 0.8 ms) by UBP-310. In the neurones that responded to KA, holding current increased from -56.4 ± 18.4 pA to 87.1 ± 26.5 pA after 15 minutes in KA (P = 0.02, rANOVA; n = 4), partially reversed to -77.1 ± 28.7 pA by UBP-310, again. These effects are summarised in Fig. 5.10.
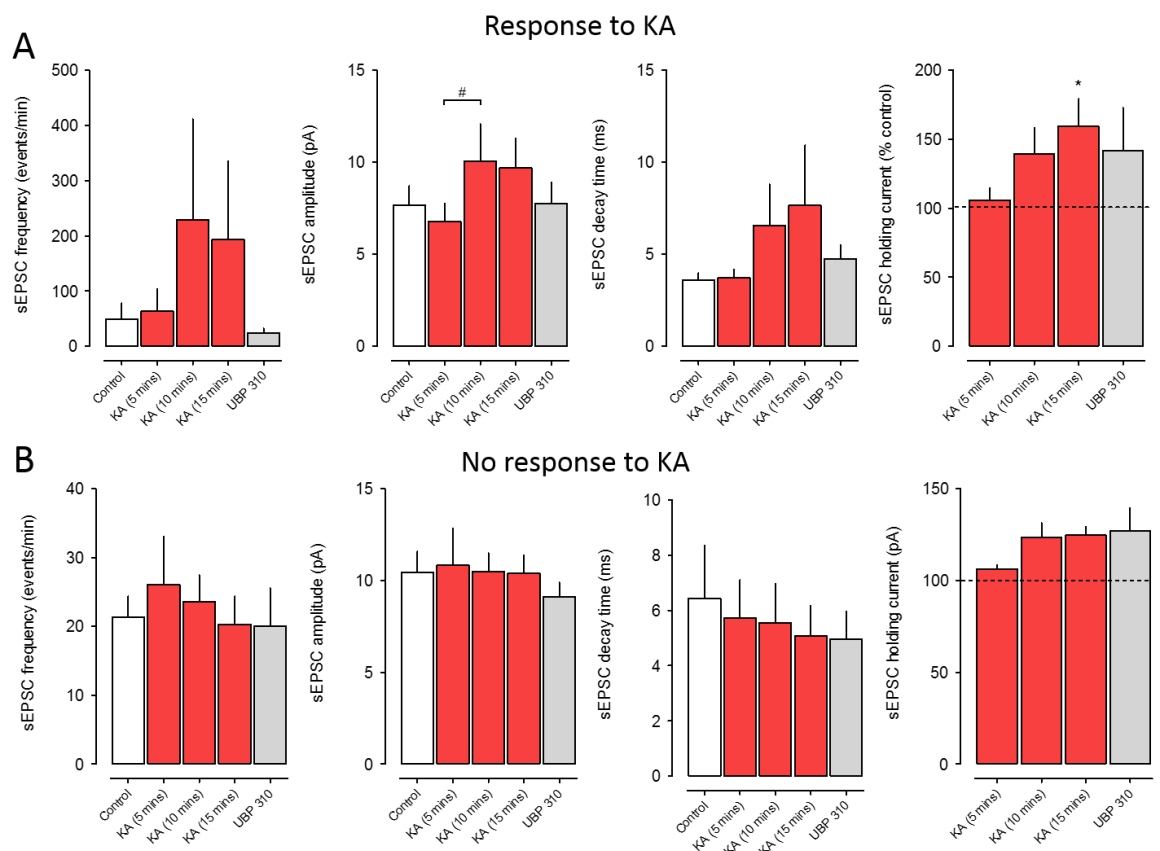
Figure 5.10: Effects of KA and UBP-310 on sEPSCs in neonatal LV neurones. (A) *Overall average sEPSC frequency, amplitude, decay time and % change in holding current data from 8 principal neurones.* **(B)** *The average sEPSC frequency, amplitude, decay time and % change in holding current data from a subset of 4 principal neurones that responded to KA.* **(C)** *The average sEPSC frequency, amplitude, decay time and % change in holding current data from a subset of 4 principal neurones that did not respond to KA. Note the responsive neurones* **(B)** *increased all parameters in the presence of KA, which was reversed with UBP-310.*

5.3.5 Effects of ATPA on LV EPSCs

5.3.5.1 Effect of ATPA on Juvenile LV sEPSCs

To determine if activation of GluK1-containing KARs alone was sufficient to cause the increased frequency of sEPSCs, the effect of ATPA, was determined. A summary of the effects of ATPA on sEPSCs in principal neurones in LV MEC summarised in Fig. 5.11.

As seen in LII, bath application of ATPA (100 nM) again appeared to weakly decrease the average frequency of sEPSCs in LV MEC principal neurones, from 155.5 ± 78.6 events/min (2.6 Hz) to a maximum decrease to 110.7 ± 37.6 events/min (1.8 Hz) after 5 minutes application, although the difference did not reach significance (n = 8) and continued application of ATPA actually saw a return to close to baseline levels.

ATPA also had no effect on the amplitude or decay time of sEPSCs. The holding current weakly increased from an average of -50.7 ± 12.3 pA to -72.5 ± 19.5 pA after 15 minutes ATPA. This could suggests that GluK1 KARs are present on the membrane of the recorded neurones, but it was a weak effect and may be simply gradual drift in the recording conditions, especially as it did not reverse with washout of ATPA.

Overall these results indicate that as in LII the effects of KA on sEPSCs are likely to be mediated by a receptor other that GluK1, or that the receptors may be occupied close to saturation by ambient glutamate.
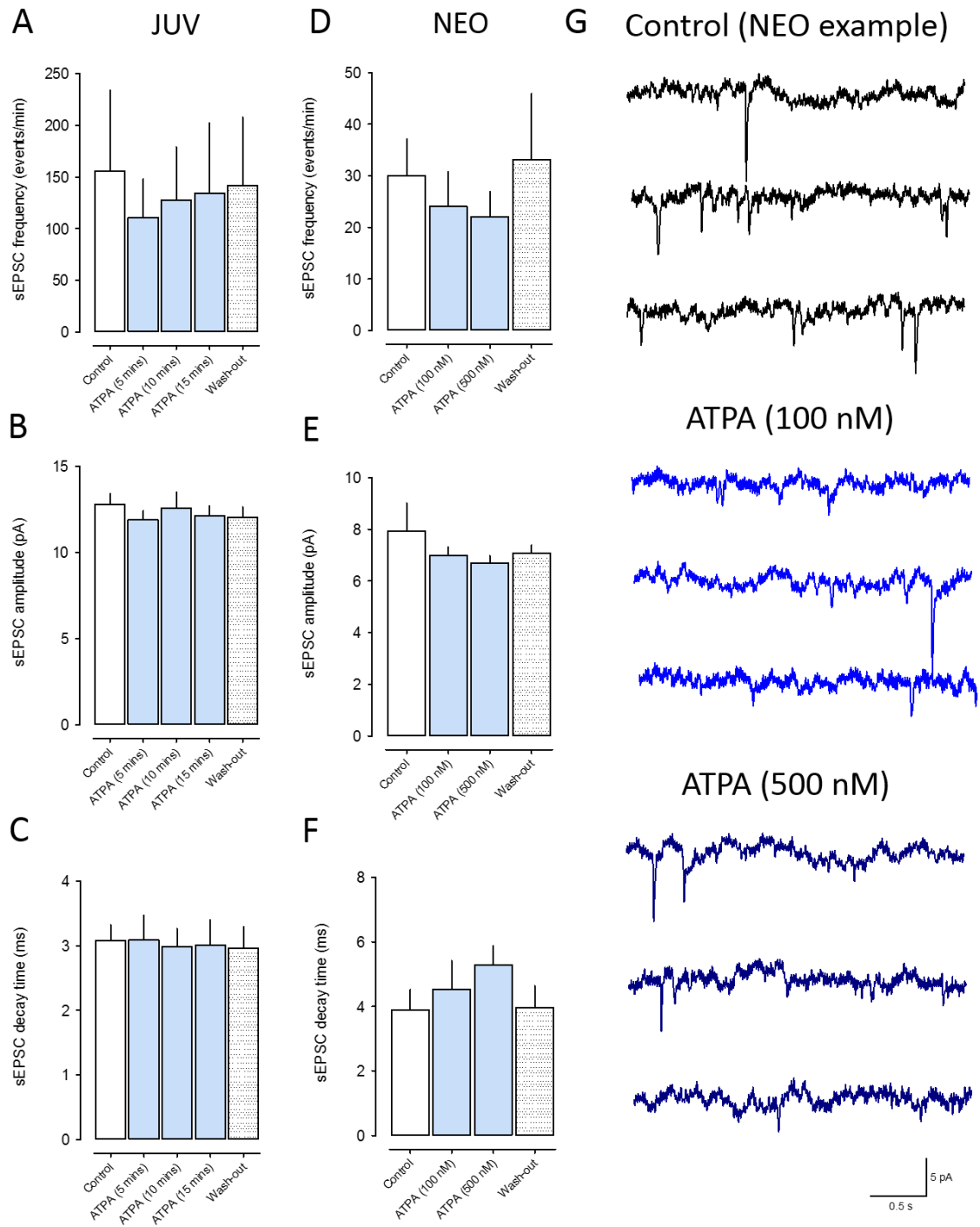
Figure 5.11: Effects of ATPA (100 & 500 nM) on sEPSCs in 8 juvenile and 4 neonate LV neurones. (A/D) *Average sEPSC frequency,* **(B/E)** *amplitude and* **(C/F)** *decay time of sEPSCs from LV principal neurones from juvenile (left) and neonate (middle) slices. Control groups (white) represent sEPSCs before application of ATPA (blue) and a wash-out (dotted). ATPA had no effect on sEPSCs.* **(G)** *Concurrent recordings of sEPSCs recorded from a neonate neurone in control conditions (black), in the presence of 100 nM ATPA (blue) and 500 nM ATPA (dark blue). NB: ATPA had no effect on sEPSCs of neonate or juvenile neurones.*

.

5.3.5.2 Effects of ATPA on LV juvenile mEPSCs

Next, the effect of ATPA was determined in the presence of TTX (1 μM) to see if a presynaptic mechanism was the cause of the slight decrease in frequency of sEPSCs. A summary of the effects of ATPA can be observed in table 5.2 and in Fig. 5.11. As with sEPSCs, ATPA had only very weak and non-significant effect mEPSCs in LV neurones.
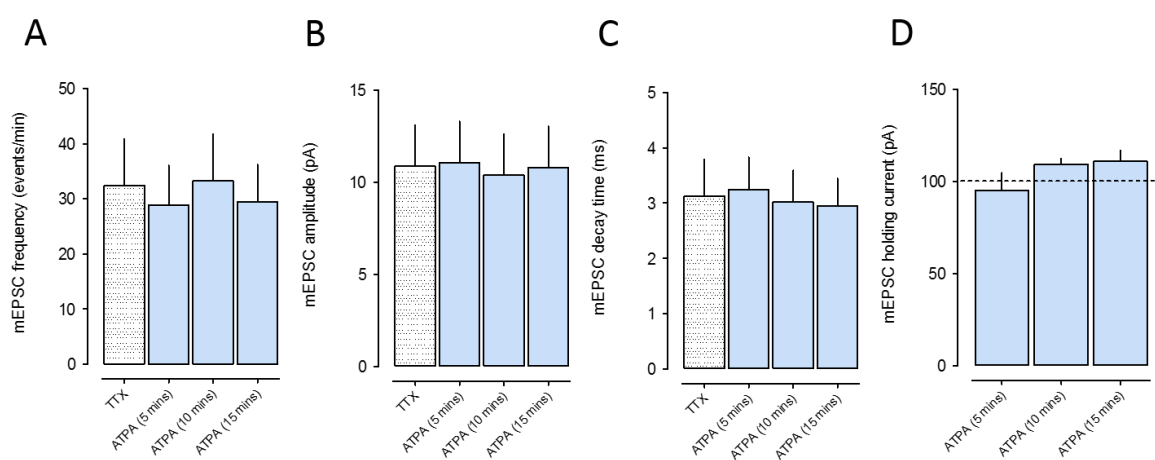
Figure 5.12: Effects of ATPA on mEPSCs in juvenile LV neurones. (A) *Average sEPSC frequency,* ***(B)*** *amplitude,* ***(C)*** *decay time and* ***(D)*** *% change in holding current data from 8 principal neurones. Control groups in TTX (dotted) represent sEPSCs before application of ATPA (blue).*

5.3.5.3 Effects of ATPA on LV neonate sEPSCs

ATPA, as in all the previous cell groups detailed in this chapter, elicited a slight and non-significant decrease in sEPSC frequency in neonate sEPSCs from a low baseline frequency of 30.0 ± 7.2 events/min (0.5 Hz) to 25.1 ± 6.8 events/min (0.4 Hz) after 100 nM, with no further change (22.1 ± 4.8 events/min (0.4 Hz) with 500 nM. Although the decrease in frequency was small, it did appear to reverse (33.2 ± 12.8 events/min) after wash-out, suggesting it was an effect of the drug. There were no significant changes in amplitude and although the mean decay time appeared to increase slightly (from 3.9 ± 0.6 ms to 4.5 ± 1.7 ms (100 nM) and 5.3 ± 0.6 ms (500 nM), again effects were not significant. However the

change was reversed (3.9 ± 0.7 ms) on wash-out so the effect could have been induced by the drug. ATPA did not affect holding current at either concentration. The effects of ATPA on LV neonate sEPSCs are summarised in Fig. 5.11.

5.3.6 Effects of UBP-310 on LV EPSCs

5.3.6.1 Effect of UBP-310 on Juvenile LV sEPSCs

To determine if GluK1-containing KAR were tonically activated in LV, UBP-310, was applied during recording of sEPSCs. The results are summarised in Fig. 5.13. The mean frequency of sEPSCs was noticeably and significantly decreased from 112.3 ± 4.7 events/min (1.9 Hz) to 46.7 ± 12.5 events/min (0.8 Hz) in the presence UBP-310 ($P = 0.0002$, rANOVA; n = 4). Thus, as in LII, GluK1 KARs appear to be tonically activated by ambient glutamate in LV, which then helps to maintain on-going spontaneous glutamate release. This could indicate that a failure of ATPA to affect release could be because the GluK1 receptors on the terminals are already saturated by glutamate, and that the small decrease induced by the agonist could reflect a level of desensitisation of the receptors. Addition of KA cumulatively with UBP-310 had no further effect on the average frequency (45.7 ± 11.1 events/min (0.8 Hz). Application of UBP-310 alone had no effect on the amplitude of sEPSCs (control 7.1 ± 0.2 pA vs 6.7 ± 0.4 pA after UBP-310) and further application of KA also had no effect on the average amplitude (6.6 ± 0.5 pA).

The decay time of sEPSCs was unaffected by the addition of UBP-310 (from 1.7 ± 0.1 ms to 2.7 ± 0.1 ms). Strangely, decay time appeared to increase when KA was cumulatively applied, but this is likely to be a spurious result as further cumulative probability analysis showed very little shift in distributions (not shown). No statistically significant changes were observed in the average holding current after the application of UBP-310 and KA.
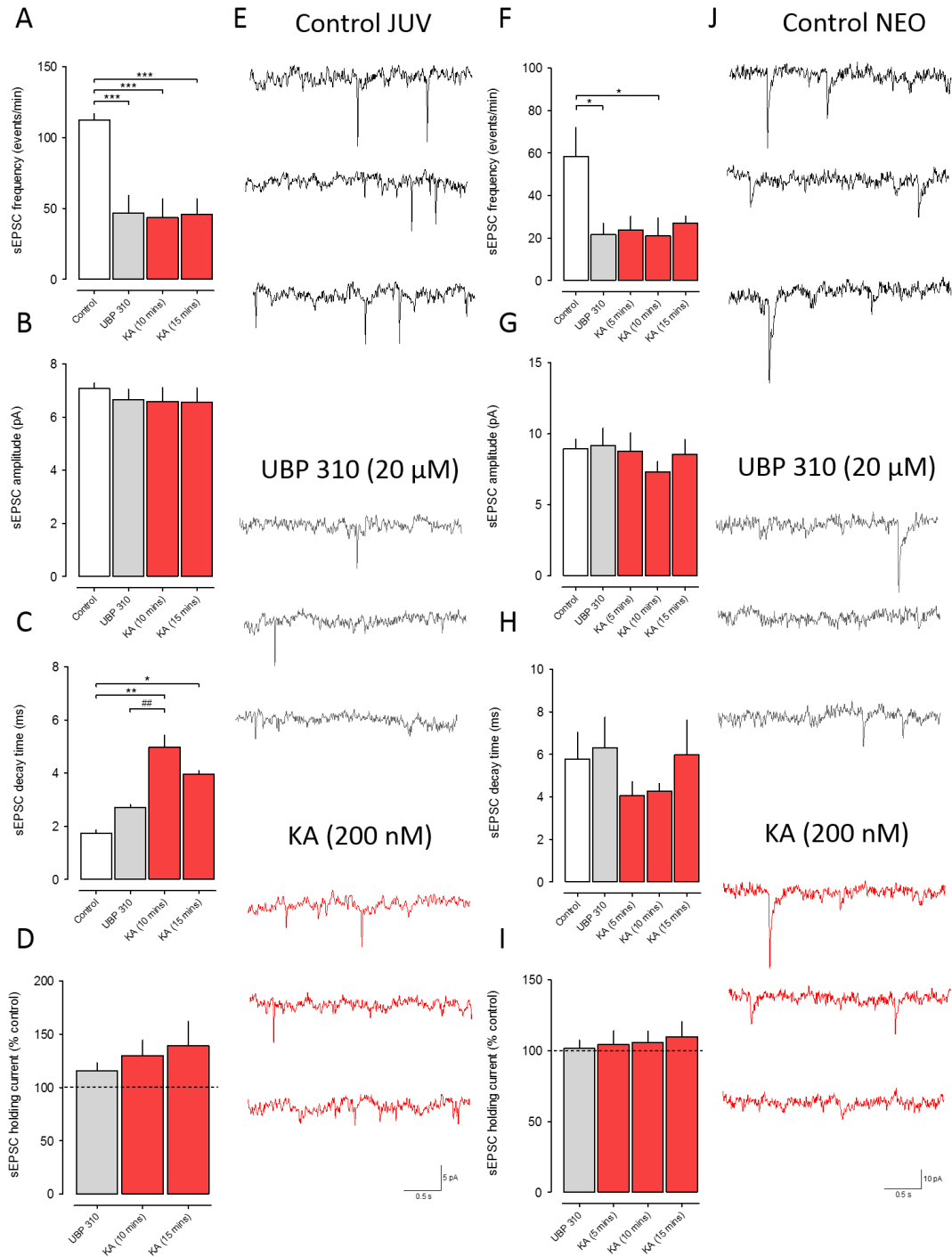
Figure 5.13: Effects of UBP-310 (20 μM) and KA (200 nM) on sEPSCs in 4 juvenile and 4 neonate LV neurones. *(A/F) Average sEPSC frequency, (B/G) amplitude, (C/H) decay time and (D/I) % change in holding current data from LII principal neurones. Control groups (white) represent sEPSCs before application of UBP-310 (grey) and KA (red). Average frequency was significantly decreased in the presence of UBP-310 and was not affected by the addition of KA. Concurrent recordings of sEPSCs recorded in control conditions (black), and in the presence of UBP-310 (grey) and KA (red) from a (E) juvenile and a (J) neonate neurone.*

5.3.6.2 Effects of UBP-310 on juvenile mEPSCs

To help determine the location of the tonically active GluK1-containing KAR, UBP-310 (20 µM) was applied to mEPSCs in the presence of TTX (1 µM). Interestingly, the mean frequency of mEPSCs was still significantly decreased from 129.9 ± 27.0 events/min (2.2 Hz) to 63.5 ± 11.0 events/min (1.1 Hz) in the presence of UBP-310 ($P < 0.05$, t-test; n = 4). As with sEPSCs, UBP-310 did not significantly change the amplitude of mEPSCs (TTX: 6.9 ± 0.7 pA vs UBP-310: 6.6 ± 0.2 pA).

UBP-310 had no effect on the average decay time of mEPSCs (from 2.1 ± 0.2 ms to 2.1 ± 0.1 ms), or on the mean holding current. Results are summarised in Fig. 5.14.

Accepting the potential limitations on specificity of UBP-310, these results largely confirm that GluK1-containing KAR reside on the presynaptic terminals of inputs to LV neurones and are tonically activated by ambient glutamate to maintain its on-going release.

Thus, overall, the results suggest that KARs modulate glutamate transmission in LV, but their role may be more limited than in LII. Generalised KAR activation did increase glutamate release onto principal neurones by activating neurones with recurrent inputs to the recorded neurone but this is likely to be due to a receptor other than GluK1. The overall level of release was reversed by UBP-310, but a large component of this effect may be due to blockade of tonic effect of ambient glutamate at GluK1 autoreceptors on synaptic terminals.
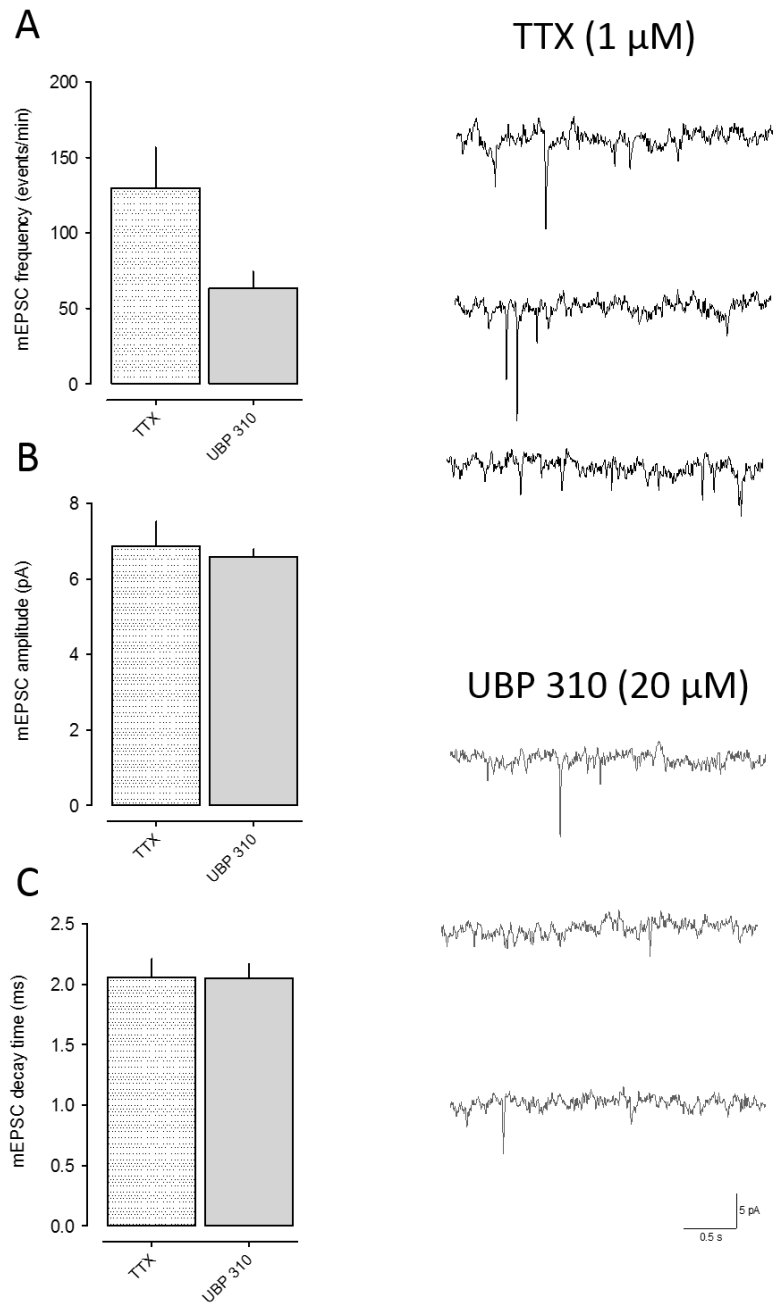
Figure 5.14: Effects of 20 µM UBP-310 on mEPSCs in juvenile LV neurones. *(A) Average sEPSC frequency, (B) amplitude and (C) decay time of sEPSCs from 4 principal neurones. Control groups in the presence of TTX (dotted) represent mEPSCs before application of UBP-310 (grey). Average frequency was significantly decreased in the presence of UBP-310. Traces show concurrent recordings of mEPSCs recorded in control conditions (black), and in the presence of UBP-310 (grey).*

5.3.6.3 Effects of UBP-310 on neonate sEPSCs

Potential tonic activation of GluK1-containing KAR was assessed in LV neonate neurones by application of UBP-310 alone. sEPSCs frequency was significantly decreased from 58.4 ± 13.7 events/min (1.0 Hz) to 21.6 ± 13.7 (0.4 Hz) events/min by UBP-310 (P = 0.03, rANOVA; n = 4). Subsequent application of KA had no effect on the frequency of sEPSCs. Likewise, neither UBP-310 nor KA had any substantial effect on sEPSC amplitude, decay time or holding current. The results are summarised in Fig. 5.13(F-J).

It should be noted that as with the effects of KA on the LV neonatal neurones, UBP-310 differentially affected a subset of cells. In 4/6 cells, UBP-310 decreased the frequency of events but in 2/6 cells, it clearly had no effect. This could suggest that the function or expression of the GluK1-containing KAR is still very low in LV at this stage in development or perhaps that ambient levels or glutamate are lower at this stage of development, and therefore the receptor is either not tonically activated by low levels of glutamate, or even expressed at levels that are functionally activated. The cells that had no response to UBP-310 had a very low baseline frequency, which may be suggestive of a low ambient glutamate level. It was thought to be a worthwhile exercise to compare the baseline properties of the cells that did respond to either KA or UBP-310 application and those that did not.
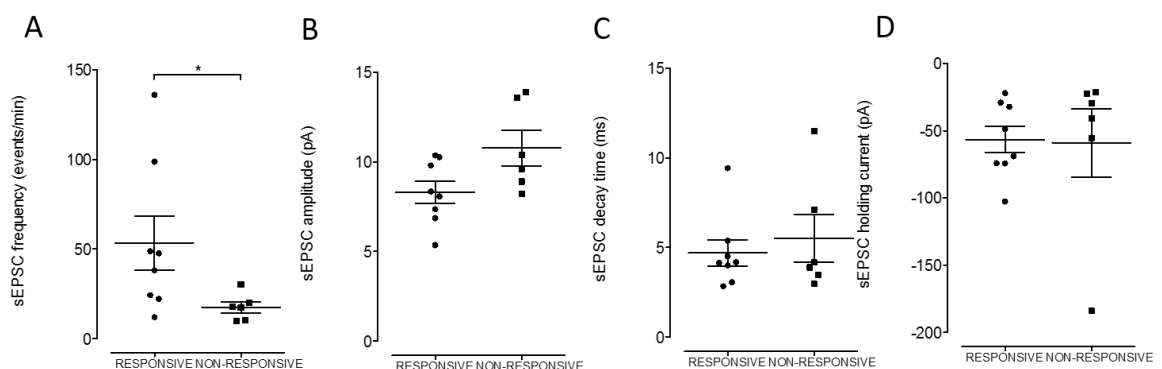
Figure 5.15: Comparing the baseline characteristics of UBP-310 and KA responsive neurones vs non-responsive neurones. *(**A**) Average sEPSC frequency, (**B**) amplitude, (**C**) decay time and (**D**) holding current data from 8 LV responsive (circles) and 6 LV non-responsive (squares) principal neurones. Average frequency of sEPSCs was significantly*

increased in the subset of neurones that were responsive to KA and UBP-310 (P < 0.01, Mann Whitney test).

Fig. 5.15 summarises the results. Mean frequency of sEPSCs was significantly lower in the non-responsive group, at 17.6 ± 3.1 events/min, or 0.3 Hz (n = 6), compared to the responsive group at 53.5 ± 15.1 events/min, or 0.9 Hz (n = 8) (P = 0.02, Mann Whitney test). However, the amplitude, although slightly larger in the non-responsive group (10.8 ± 1.0 pA v 8.3 ± 0.6 pA) was not significantly different (P = 0.08). There were no differences observed in the average decay times or holding current between the two groups. Whether the lower frequency in the non-responsive group reflects a reduced ambient level of glutamate or whether the ambient level is low due to low expression of tonically active KAR is a matter for conjecture.

	JUV LII sEPSCs		JUV LV sEPSCs	
	Frequency (Events/min)	Amplitude (pA)	Frequency (Events/min)	Amplitude (pA)
Control	113.9 ± 56.0	10.1 ± 2.6	167.8 ± 49.1	8.5 ± 0.4
+ KA (200 nM, 10m)	1070 ± 448.1*	12.2 ± 2.6	268.9 ± 65.4	7.8 ± 0.3
+ KA (200 nM, 15m)	1049.0 ± 356.8*	13.0 ± 2.2	356.9 ± 49.1***	8.2 ± 0.2
+ UBP-310 (20 µM)	238.8 ± 88.5#	9.9 ± 1.5	122.9 ± 38.5###	8.5 ± 0.3
	(n = 4)	(n = 4)	(n = 5)	(n = 5)
Control	276.3 ± 71.4	10.3 ± 1.6	155.5 ± 78.6	12.8 ± 0.6
+ ATPA (100 nM, 5m)	216.8 ± 45.3	9.7 ± 1.2	110.7 ± 37.6	11.9 ± 0.5
+ ATPA (100 nM, 10m)	188.3 ± 38.0*	8.4 ± 0.9	127.4 ± 51.8	12.5 ± 1.0
+ ATPA (100 nM, 15m)	217.3 ± 37.7	9.7 ± 1.2	131.4 ± 67.9	12.1 ± 0.6
Wash-out	231.6 ± 52.6	9.8 ± 1.2	141.7 ± 66.1	12.0 ± 0.6
	(n = 4)	(n = 4)	(n = 8)	(n = 8)
Control	237.8 ± 70.9	7.1 ± 0.9	112.3 ± 4.7	7.1 ± 0.2
+ UBP-310 (20 µM)	96.1 ± 21.9*	6.8 ± 1.1	46.7 ± 12.5***	6.7 ± 0.4
+ KA (200 nM, 10m)	75.7 ± 8.8*	7.7 ± 1.6	43.5 ± 13.2***	6.6 ± 0.5
+ KA (200 nM, 15m)	88.7 ± 11.5*	8.0 ± 1.4	45.7 ± 11.1***	6.6 ± 0.5
	(n = 6)	(n = 4)	(n = 4)	(n = 4)

Table 5.2: Summary of the effects of KAR agonists and antagonists on juvenile sEPSCs. *Data shows the average amplitude and frequency of sEPSCs before (control) and after the application of KA (pink), ATPA (blue) and UBP-310 (grey). * denotes statistically significant changes from control (*: P < 0.05, **: P < 0.01, ***P < 0.001). # denotes statistically significant changes from the previous drug condition. (#: P < 0.05, ##: P < 0.01, ###P < 0.001).*

	JUV LII mEPSCs		JUV LV mEPSCs	
	Frequency (Events/min)	Amplitude (pA)	Frequency (Events/min)	Amplitude (pA)
Control (+ 1 TTX µM)	136.3 ± 51.1	8.6 ± 0.8	87.5 ± 24.8	7.6 ± 0.3
+ KA (200 nM, 10m)	157.7 ± 83.3	8.4 ± 0.7	71.9 ± 25.1	7.6 ± 0.3
+ KA (200 nM, 15m)	225.9 ± 77.5	8.6 ± 0.6	104.1 ± 58.4	7.3 ± 0.4
+ UBP-310 (20 µM)	104.6 ± 29.9	8.4 ± 0.6	-	-
	(n = 5)	(n = 5)	(n = 6)	(n = 6)
Control (+ 1 TTX µM)	133.0 ± 22.6	9.1 ± 1.0	32.4 ± 8.4	10.9 ± 2.2
+ ATPA (100 nM, 5m)	135.1 ± 29.5	9.3 ± 1.1	28.8 ± 7.2	11.1 ± 2.2
+ ATPA (100 nM, 10m)	128.3 ± 22.8	9.0 ± 1.1	33.3 ± 8.5	10.4 ± 2.2
+ ATPA (100 nM, 15m)	115.2 ± 23.1	8.9 ± 10	29.5 ± 6.7	10.8 ± 2.3
	(n = 8)	(n = 8)	(n = 4)	(n = 4)
Control (+ 1 TTX µM)	157.2 ± 45.0	9.3 ± 1.1	129.9 ± 27.0	6.9 ± 0.7
+ UBP-310 (20 µM)	89.2 ± 41.7*	8.3 ± 1.6	63.5 ± 11.0	6.6 ± 0.3
+ KA (200 nM, 10m)	38.2 ± 9.1	8.1 ± 1.2	74.3 ± 21.4	6.5 ± 0.1
+ KA (200 nM, 15m)	77.0 ± 37.6	7.9 ± 1.0	63.3 ± 14.2	6.1 ± 0.3
	(n = 4)	(n = 4)	(n = 4)	(n = 4)

Table 5.3: Summary of the effects of KAR agonists and antagonists on juvenile mEPSCs. *Data shows the average amplitude and frequency of sEPSCs before (control) and after the application of KA (pink), ATPA (blue) and UBP-310 (grey). * denotes statistically significant changes from control (*: P < 0.05, **: P < 0.01, ***P < 0.001). # denotes statistically significant changes from the previous drug condition. (#: P < 0.05, ##: P < 0.01, ###P < 0.001).*

	NEO LII sEPSCs		NEO LV sEPSCs	
	Frequency (Events/min)	Amplitude (pA)	Frequency (Events/min)	Amplitude (pA)
Control	90.6 ± 19.8	7.9 ± 1.0	35.0 ± 14.6	9.1 ± 0.9
+ KA (200 nM, 10m)	570.8 ± 194.2*	10.9 ± 1.0***	126.2 ± 93.3	10.3 ± 1.0
+ KA (200 nM, 15m)	483.0 ± 179.2	10.2 ± 1.0**	106.7 ± 73.4	10.0 ± 0.9
+ UBP-310 (20 µM)	67.4 ± 22.2#	7.4 ± 0.8#	21.6 ± 4.9	8.4 ± 0.7
	(n = 7)	(n = 7)	(n = 7)	(n = 8)
Control	131.4 ± 22.8	9.0 ± 0.6	30.0 ± 7.2	7.9 ± 1.1
+ ATPA (100 nM)	111.5 ± 8.9	9.1 ± 0.7	24.1 ± 6.8	7.0 ± 0.3
+ ATPA (500 nM)	108.7 ± 15.5	9.0 ± 0.7	22.1 ± 4.8	6.7 ± 0.3
Wash-out	-	-	33.2 ± 12.8	7.1 ± 0.3
	(n = 3)	(n = 3)	(n = 4)	(n = 4)
Control	194.6 ± 46.6	8.6 ± 0.6	58.4 ± 13.7	8.9 ± 0.7
+ UBP-310 (20 µM)	59.2 ± 11.5***	7.4 ± 0.6**	23.8 ± 6.5*	9.2 ± 1.2
+ KA (200 nM, 10m)	47.2 ± 10.4 ***	7.4 ± 0.7**	21.1 ± 8.4*	7.3 ± 0.7
+ KA (200 nM, 15m)	49.8 ± 6.8***	7.4 ± 0.7**	27.0 ± 3.4	8.6 ± 1.0
	(n = 6)	(n = 6)	(n = 4)	(n = 4)

Table 5.4: Summary of the effects of KAR agonists and antagonists on neonate sEPSCs. Data shows the average amplitude and frequency of sEPSCs before (control) and after the application of KA (pink), ATPA (blue) and UBP-310 (grey). * denotes statistically significant changes from control (*: P < 0.05, **: P < 0.01, ***P < 0.001). # denotes statistically significant changes from the previous drug condition. (#: P < 0.05, ##: P < 0.01, ###P < 0.001).

5.3.7 Age-comparison

The sections above detail the actual experimental findings in two different neuronal populations at two stages of development. There is a considerable amount of data, but by and large the patterns of responsiveness to KAR activation and blockade are qualitatively similar in the 4 groups. Despite this, there are certain clear differences both qualitative and quantitative. This section will now directly compare across location and age to emphasise where the principal differences lie.

5.3.7.1 Developmental differences in the effects of KA

Fig. 5.16 (A-C) compares the percentage change in the effects of KA on sEPSCs in neonatal versus juvenile neurones in LII. Although both age groups show a large increase in frequency, juvenile neurones showed a massively greater change (~200 fold) compared to neonatal neurones (~4 fold). It should be noted that there was a huge variability associated with increase in the juvenile neurones. In this group there was sometimes indications that KA may be induced a degree of synchronised oscillatory activity, which could elevate the frequency and amplitude of sEPSCs in some slices.

Another clear difference between neonatal and juvenile sEPSCs was the effect on decay time. KA doubled the decay time of sEPSCs in neonatal neurones but had no apparent effect in juvenile neurones.

Mean amplitudes of sEPSCs were increased by KA and the percentage increase (around 40%) was almost identical in the two groups. Likewise an increase in holding current (by ~50%) induced by KA was similar in both age groups.

The ability of UBP-310 to reverse the effects of KA also showed one difference. In neonate neurones, the increase in frequency was reversed to a level lower than control, whereas the massive increase seen in juveniles was reduced but remained above control. All other parameters were largely restored to control.
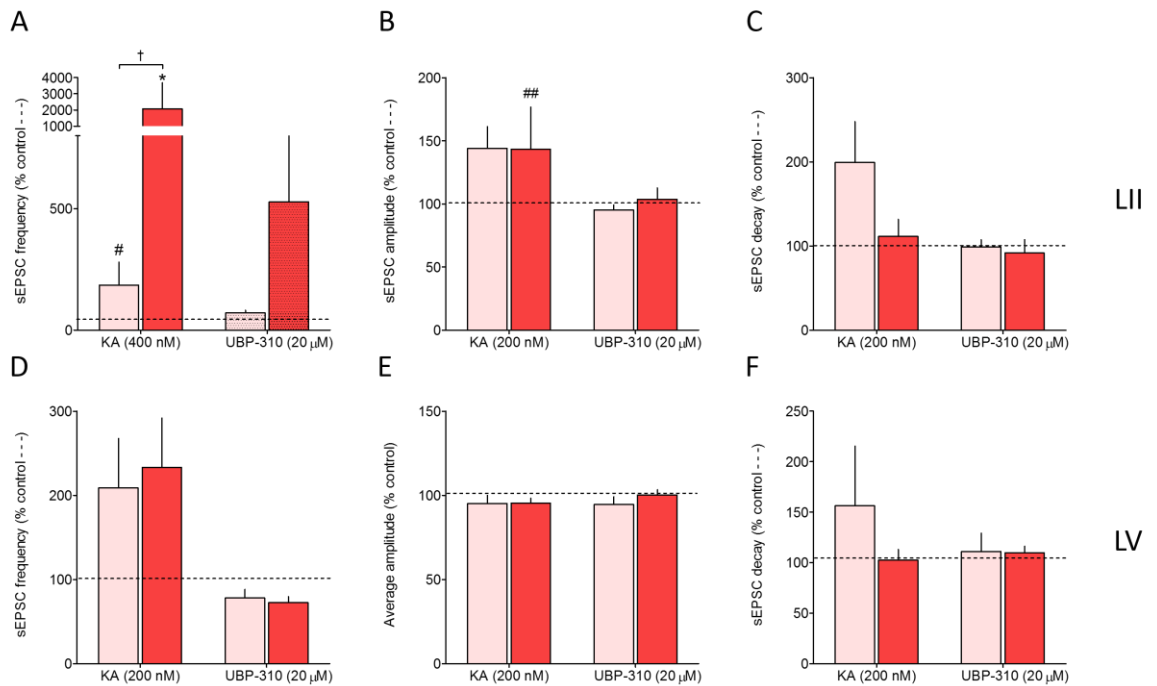
Figure 5.16: Percentage change in sEPSC activity with KA (200 nM) and UBP-310 (20 µM) in neonate and juvenile neurones. (A) *Average sEPSC percentage change in frequency,* **(B)** *decay time and* **(C)** *amplitude data from 7 neonate (pink) and 4 juvenile (red) LII principal neurones. KA increased the frequency of sEPSCs more in juvenile compared to neonatal neurones, and increased the decay time in neonate, and not juvenile, neurones. Average sEPSC percentage change in frequency* **(D)**, *decay time* **(E)** *and amplitude* **(F)** *data from 4 neonate (pink) and 5 juvenile (red) LV principal neurones.*, # and † denote significant differences between: * juvenile % change vs control (100 %, dashed line), # neonatal % change vs control (100 %, dashed line), † juvenile % change vs neonatal % change.*

Comparisons in LV (Fig. 5.16 D-F), are a little more complex as some neonatal neurones were clearly responsive to KA and others not. These neurones were subsequently subdivided into two groups: responsive and non-responsive. In contrast, all juvenile LV neurones responded to KA. There is little to be gained from comparing responsive neurones in juveniles to non-responsive neurones in neonates so the comparison has been restricted to responsive neurones in each group . The comparison is summarised in Fig. 5.16 (D-F). Like LII, KA induced an increase in frequency of sEPSCs neurones in both neonates and juveniles. The % changes in sEPSC frequency after KA were similar in the two age groups (~250-300%) . The changes were less marked than seen in either age group in LII, and dramatically less than that in the juvenile LII (Fig. 5.16).

In neonate LV neurones KA application resulted in an increase in mean amplitude of around 25% in neonatal sEPSCs but left it paractically unaltered in juvenile neurones. Concurrently, as in LII, there was doubling in decay time in neonate neurones with no change in the juvenile LV neurones.

UBP-310 reversed the frquency changes in both age groups, although in contrast to LII this was reduced below control levels in both age groups, an effect only seen in neonates in LII. The changes in amplitude in both groups and in and decay time in neonates were restored to control levels by UBP-310.

5.3.7.2 Developmental differences in the effects of ATPA

A comparison of the effects of ATPA in neonatal and juvenile neurones is summarised in Fig. 5.17. The only consistent effect of note was a slight decrease in the frequency of sEPSCs in both layers in both age groups, with perhaps a more prominent effect in the older rats. The effect was small, but the fact that it consistently disappeared with washout of the agonist does indicate that it was a genuinely drug induced.
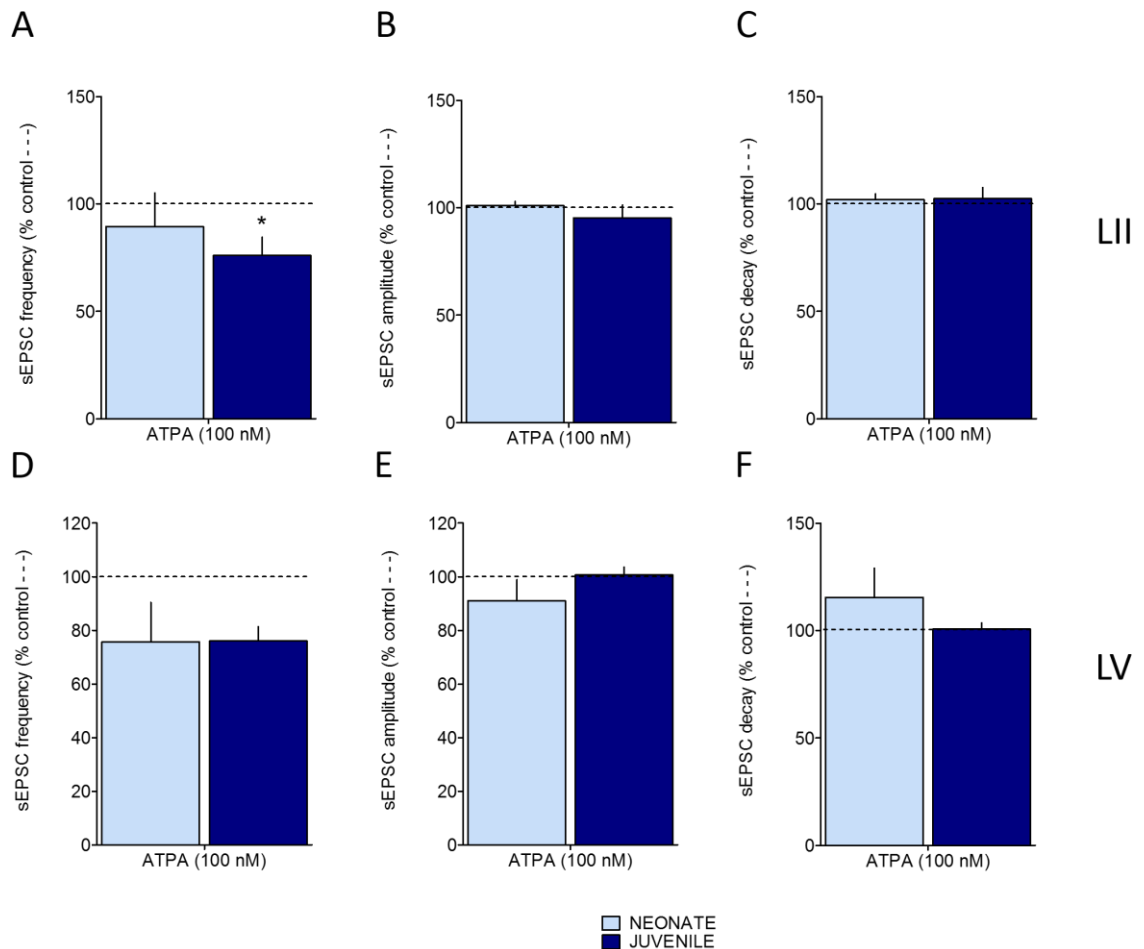
Figure 5.17: Percentage change in sEPSC activity in the presence of ATPA (100 & 500 nM) in neonate and juvenile neurones. (A) *Average sEPSC percentage change in frequency,* ***(B)*** *amplitude,* ***(C)*** *decay time from 3 neonatal (light blue) compared to 6 juvenile (dark blue) principal neurones.* ***(D)*** *Average sEPSC percentage change in frequency,* ***(E)*** *amplitude, and* ***(F)*** *decay time data from 4 neonate (light blue) compared to 7 juvenile (dark blue) principal neurones.* *, *# and † denote significant differences between: * juvenile % change vs control (100 %, dashed line), # neonatal % change vs control (100 %, dashed line), and † juvenile % change vs neonatal % change. There were no significant differences in % change in response to ATPA between the two age groups.*

5.3.7.3 Developmental differences in the effects of UBP-310

UBP-310 applied alone was remarkably consistent in its effects in both layers and age groups (Fig. 5.18). Unlike ATPA the effect was quite marked in all groups. Thus, the antagonist reduced the frequency of sEPSCs in neonate LII neurones by around 60%, and a comparable decrease (~50%) was recorded in juvenile LII cells. In LV the reduction in neonates was again about 60% but that in neonates was marginally stronger (~70%). There

168

were no changes of note in any other parameters in any groups, other than occasional indications of a slight (~10-20%) decrease in amplitude. The effects of UBP-310 are strongly indicative that KARs containing the GluK-1 subunit are tonically activated by ambient glutamate release and contribute significantly to maintaining sEPSC frequency at both ages in both layers.
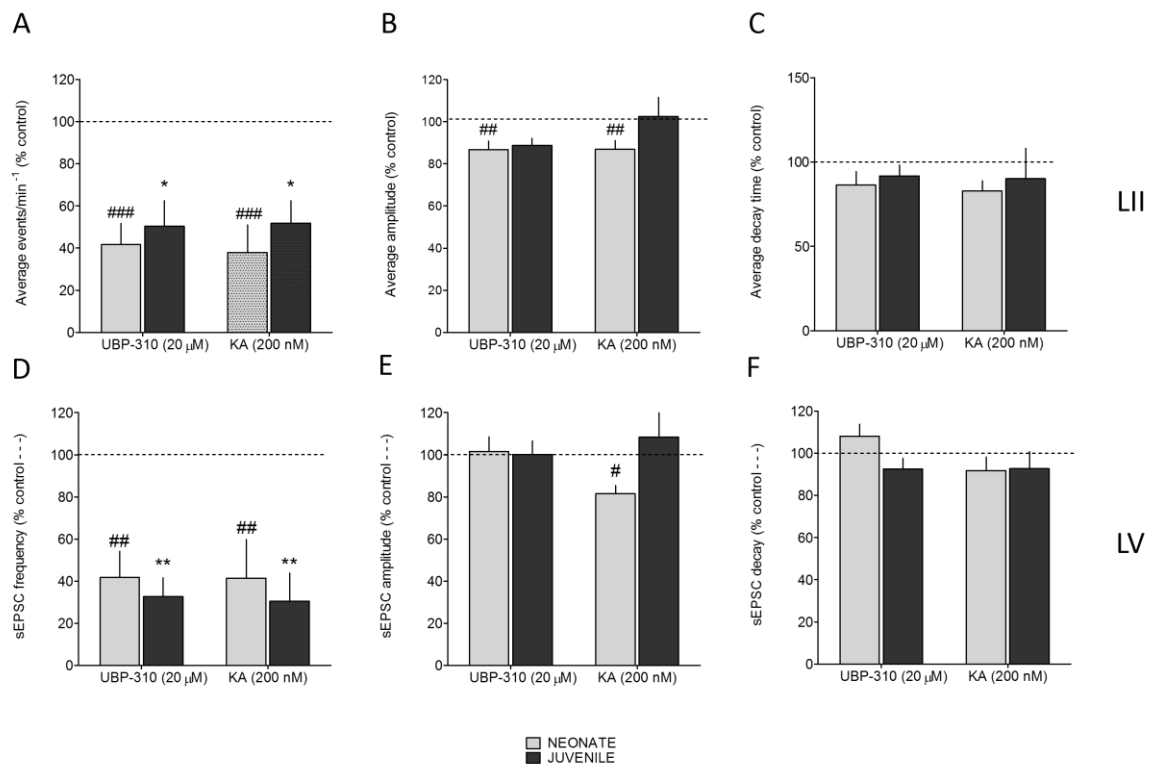
Figure 5.18: Percentage change in sEPSC activity with UBP-310 (20 μM) and KA (200 nM) in neonate and juvenile neurones. *Average sEPSC percentage change in frequency **(A)**, decay time **(B)** and amplitude **(C)** data from 5 neonate (grey) and 5 juvenile (black) principal LII neurones. Average sEPSC percentage change in frequency **(D)**, amplitude **(E)** and decay time **(F)** data from 5 neonatal (grey) and 4 juvenile (black) principal LV neurones. UBP-310 significantly decreased the frequency of sEPSCs equally in both age groups, but UBP-310 decreased sEPSC amplitude in neonatal neurones only. *, # and † denote significant differences between: * juvenile % change vs control (100 %, dashed line), # neonatal % change vs control (100 %, dashed line), † juvenile % change vs neonatal % change. There were no significant differences in % change in response to UBP-310 between the two age groups.*

5.4 Summary

The suggested locations of KARs mediating excitatory neurotransmission in the MEC are summarised in Fig. 5.19.

1) A presynaptic GluK1-containing KAR, which is tonically active in was demonstrated LII and LV in juvenile and neonate neurones (although TTX studies are needed to confirm a presynaptic location in neonate, though similarities in the effects of UBP-310 on sEPSCs would be in favour of a similar mechanism in both ages.)

2) A postsynaptic non GluK1-containing KAR is likely mediating the effects of KA, and the reversal in activity with addition of UBP-310 may be due to a reduction in tonic glutamate release.

3) ATPA had no effect/slightly decreased glutamate release, which may be due to GluK1-containing KARs having already being tonically activated. Further receptor activation has no effect or may lead to desensitisation, which could account for the small decrease in activity.

Layer II

K⁺

Tonically active presynaptic GluK1-containing KAR.

GluK1-containing KAR
Non GluK1-containing KAR
AMPAR
Glutamate

Evidence for KAR driven recurrent excitation in LII neonate and juvenile neurones.

Principal neurone

Pyramidal neurone

Layer V

Tonically active presynaptic GluK1-containing KAR.

GluK1-containing KAR
Non GluK1-containing KAR
AMPAR
Glutamate

No evidence of KAR driven recurrent excitation in neonate or juvenile LV neurones.

Principal neurone

Pyramidal neurone

Figure 5.19: Summary of the suspected location of KARs at excitatory synapses in LII and LV MEC. *KARs appeared to be present at similar locations in both layers and in both neonate and juvenile neurones, however, a significant increase in sEPSC amplitude in LII neurones only suggests the presence of KAR mediated recurrent excitation. Recurrent connectivity has previously been shown to be present in the superficial layers of the MEC (Winterer et al., 2017).*

171

5.5 Discussion

5.5.1 Pre- and post-synaptic KARs facilitate glutamate release at excitatory synapses in LII and LV MEC of juvenile MEC

The working hypothesis to interpret these results would suggest the presence of KARs both pre- and postsynaptically at excitatory synapses. More specifically, experiments with UBP-310 in the presence of TTX have confirmed a GluK1-containing KAR is present at glutamatergic terminals, where they are tonically active and maintain a high level of spontaneous background excitation onto principal neurones.

The fact that ATPA alone generally had no effect on sEPSCs may be due to the high tonic activity of this receptor, such that addition of nanomolar concentrations of ATPA cannot further increase the activation of an already saturated receptor. Moreover, this may even explain the small decrease in frequency of sEPSCs witnessed in the presence of ATPA (Fig. 5.3), as excessive activation could then lead to receptor desensitisation, which is commonly associated with KARs (Fisher and Mott, 2011, Mott et al., 2010) thus reducing the tonic facilitatory effect. In addition, some studies suggest that KAR subunits can be individually activated within a heteromeric complex and serve dramatically different functions, whereby the high affinity subunits control channel gating, and low affinity subunits have strong desensitising properties (Fisher and Mott, 2011). In this scenario, additional activation of the GluK1 subunit, in conditions of high tonic activity, could encourage desensitisation of the complex, and account for the slight decrease/no effect of ATPA in these conditions. The results from this chapter were in stark contrast to previous work within this lab, in the adjacent LIII MEC, which showed significant increases in sEPSC frequency in response to ATPA, however, there was no tonic activation of GluK1-containing KARs in LIII, despite their existence, which may well account for the differences observed in LII and LV (Chamberlain, 2009, Chamberlain et al., 2012). Alternatively, in the face of such high GluK1-containing KAR tonic activity, a higher concentration of ATPA may be require to elicit a noticeable effect. Alternatively, if ATPA has a lower efficacy at the GluK1 subunit than ambient glutamate, then sEPSC frequency may decrease relative to the high tonic activity. Either way, it is clear that KAR function in LII and LV MEC are very different to LIII,

and these differences are probably related to tonic activity of GluK1-containing KARs located at presynaptic terminals.

Lastly, experiments with KA greatly facilitated glutamate release at excitatory synapses, as expected. The addition of UBP-310 appeared to reverse the actions of KA, giving the impression the GluK1-containing KAR was responsible for the increase in frequency. However, this suggestion is confounded by the lack of an effect of ATPA on its own. Therefore, a more likely scenario is that a KARs that do not contain the GluK1 subunit are responsible for the KA-induced increase in sEPSC frequency, and it seems likely that they are located at the soma/dendrites of neurones that provide inter- and intra-lamina recurrent excitatory inputs to the recorded neurone. This is supported by depolarising effects of KA, and the fact that TTX largely abolished the response. In this scenario, the reversal by UBP-310 would be due to blockade of the tonic effect of ambient glutamate at GluK1 autoreceptors on synaptic terminals, as we have shown this to contribute ~60% of ongoing spontaneous glutamate release. This would then appear as a reversal of the effect of KA.

To summarise, the results from this chapter suggest the presence of a tonically active presynaptic GluK1-containing KAR facilitating on-going glutamate release onto principal cells, and a non-GluK1 containing KAR located postsynaptically at the soma/dendrites of neurones providing recurrent excitatory inputs to the recorded cell, in the juvenile rats.

5.5.2 Developmental differences in KAR function at glutamatergic synapses

The effects of KAR modulation on sEPSCs were fairly similar within the two age groups studied, though there were some subtle effects to note. As in juvenile neurones, there was a strong tonic facilitation of on-going glutamate release by KARs containing the GluK1 subunit in neonate neurones, though further experiments in TTX are required to confirm a presynaptic location. Likewise, experiments with ATPA had no effect, or imposed a slight decrease of glutamate release onto principal neurones in both layers and ages. However, developmental and lamina differences were noted in the effects of KA on sEPSCs.

In LII, although the frequency was increased in both age groups, and qualitative changes should be viewed with caution due to the variability between experiments, the extent of the increase was substantially more pronounced in the juveniles (~200 fold increase) versus neonates (~4 fold increase). The difference in response to KA may be due to the levels of KAR expression themselves, or due to the stage of maturation of the MEC circuitry at this point in post-natal development, such as the number of excitatory synapses onto principal neurones. KA increased the amplitude of excitatory events in both age groups in LII, which may be indicative of roles of KARs in driving multi-quantal glutamate release. Another subtle difference was that KA increased the decay time in neonate, but not juvenile, neurones. This may suggest KA activates synapses that were not initially tonically releasing glutamate onto the recorded cell, but that KA activated a population of otherwise silent input interneurones, the slow decay time possibly reflecting release at more distal locations on the soma.

Subtle lamina differences were also apparent. Whilst neurones in LII showed a clear developmental increase in the excitatory effects of KA, in LV, the effects of KA were the same in neonate and juvenile (+ 250-300 %) neurones. Moreover, there were no KA-induced increases in amplitude, suggesting a lack of multi-quantal glutamate release onto principal neurones, unlike in LII. In accordance with LII, however, there was also an increase in decay time in the younger age group, which, as mentioned, may reflect the activation of silent neurones making synapses onto the recorded neurone at more distally located sites.

5.5.2.1 A subset of LV neonatal neurones were insensitive to KA and UBP-310

Upon analysis of the effects of KAR manipulation in LV neonatal principal neurones, it became apparent that a subset of cells (n = 6 of 14 cells) were insensitive to KA and UBP-310. There is no experimental evidence to show the KA insensitive neurones were also insensitive to UBP-310, but we can perhaps assume they belong to the same population. What was particularly noticeable about the non-responsive population of cells was their extremely low baseline frequency compared with the neurones that did respond to KA and UBP-310. From this we can, perhaps, infer that these neurones do not have functional KARs or AMPARs, or that synapses onto these principal neurones are silent.

One theory is that these neurones are being selected against through a synaptic pruning developmental process. During development, synapses are constantly generated, and newly formed glutamatergic synapses lack functional AMPA or KAR mediated transmission, known as silent synapses (Isaac et al., 1995). Many of these silent synapses are developmentally eliminated, though some are said to be selected for AMPAR unsilencing, which requires synchronised activity of pre- and post- synaptic activity. The KA-insensitive neurones had an extremely low baseline frequency of sEPSCs compared to sensitive neurones, and could reflect a population of neurones which are in the process of unsilencing, or conversely, they could represent immature neurones that are being selected against.

A previous study showed that presynaptic KARs are upregulated at immature CA3-CA1 synapses in an activity-dependent fashion (Clarke et al., 2014). In the KA responsive neurones in this study, a large proportion of the sEPSCs were dependent on the action of KARs containing the GluK1 subunit, which, in the juvenile neurones, was shown to be located presynaptically. In the non-responsive neurones, no such presynaptic GluK1 KAR is present. Considering that all juvenile neurones tested were responsive to both KA and UBP-310, the presence of KARs at immature synapses could be critical in determining neuronal fate in developing circuitry. KARs have powerful roles in the synchronisation of neuronal network activity, especially in the MEC, which drives Hebbian strengthening of naïve synapses via a process known as STDP. Asynchronous neuronal activity, perhaps associated with neurones lacking KARs, may lead to a functional weakening and ultimately morphological elimination (Clarke et al., 2014). Moreover, the depolarisation and slow decay properties of synaptic KARs are thought to bring the cell closer to spike threshold and therefore can exaggerate the effect of a single input. In this manner, KARs can bring unique integrative properties to the neurones upon which they reside, which, again, could have implications for synaptic pruning during development.

Overall, these results suggest that the function of KARs does not change dramatically between the two age groups studied (P8-11 and P20-27), though there are subtler differences in response to KA ,which likely reflect the ability of the MEC circuitry to drive network activity at each stage of development. We have identified a presynaptic GluK1-

containing KAR in juvenile and neonate rats. Lastly, the effects of KA appear to be driven by a non GluK1-containing KAR that activates neurones via recurrent excitatory inputs that may lead to the synchronisation of neuronal activity.

Chapter 6

Functional role of kainate receptors in

GABAergic transmission in LII and LV in

neonate and juvenile rats

6.1 Introduction

In the previous chapter I identified functional effects of KARs located both pre- and post-synaptically that act to facilitate glutamate release at excitatory synapses. KARs are also known to exist at inhibitory synapses throughout the CNS (Cossart et al., 1998, Min et al., 1999, Aroniadou-Anderjaska et al., 2007), where they can both facilitate or depress GABA release. Previous work in this laboratory has made a detailed analysis of KAR function in both excitatory and inhibitory transmission in LIII of the MEC (Chamberlain et al., 2012). In GABAergic transmission this study uncovered the presence of a GluK1-containing KAR driving excitation at glutamatergic synapses onto interneurones. In addition, it suggested that a putative non-GluK1 containing KAR (possibly GluK2) may act as a presynaptic heteroreceptor, facilitating GABA release at inhibitory terminals onto principal neurones

As with the previous chapter, this thesis is concerned with the function of KARs during development as they show patterned and dynamic changes in expression during maturation. For example, gene expression studies identified peak levels of the GluK1-containing KAR at birth in the sensory cortex, CA1 hippocampal interneurones, stratum oriens, septum and thalamus which were thought to be down-regulated thereafter (Bahn et al., 1994, Bahn and Wisden, 1997). Functional electrophysiology studies have identified a decreased contribution of KAR mediated synaptic transmission at critical periods of development related to experience dependent synaptic plasticity at thalamocortical synapses (Kidd and Isaac, 1999). In the hippocampus, tonic activation of presynaptic kainate receptors that facilitates glutamate release is developmentally down-regulated, which, again, occurs during a period of activity-dependent maturation of the circuitry (Lauri et al., 2005). Moreover, developmental downregulation of the presynaptic effects of KARs have also been identified at inhibitory synapses in the hippocampus (Maingret et al., 2005).

Studies addressing specifically the developmental changes of KARs in the MEC are limited. Preliminary data from the lab of Professor Elek Molnar, which was in support of this project (Figure 1.6; Chapter 1), conducted a developmental profile of KAR subtype expression in hippocampal areas of the rat brain. The expression of GluK1-containing KARs in the EC appeared to increase from about 7 days old and peaked around 14 days old, before

expression declined into adulthood (Molnar et al. unpublished). Only one other study has addressed the developmental changes of KAR expression in the EC, amongst other brain regions, and showed a similar increase in the expression of the GluK1 subunit at ~12 days old (Bahn et al., 1994). The temporal increase in KAR expression may implicate the GluK1-containing KAR in a functional role in the development of synaptic connectivity in the MEC. Of course, immunohistochemical studies such as these can make no assumptions as to the location of the expressed receptors. Thus, any developmental changes could reside with receptors on interneurones and inhibitory synapses with equal probability to those on principal neurones and excitatory synapses. Having determined functional roles in excitatory transmission in Chapter 5, in this chapter I turned my attention to KAR in inhibitory transmission in LII and LV of the MEC, and possible changes in these roles during development.

Understanding changes to KAR functioning during development is of particular importance with regards to their roles in the generation of synchronised neuronal network activity, especially in the MEC (Cunningham et al., 2003, Cunningham et al., 2004a, Stanger et al., 2008). Furthermore, the MEC has been strongly linked to many disorders associated with aberrant or pathological synchrony, such as epilepsy and schizophrenia (Cunningham et al., 2006a, Uhlhaas and Singer, 2010). Existing data strongly supports a role for KARs in pathological network activity, largely with the use of KA to model epileptiform activity (Rogawski et al., 2001), however, it is important to also understand the physiological roles of KARs in modulating neurotransmission, and the synaptic mechanisms underlying them. Thus, this chapter aims to clarify the role of KARs in modulating GABAergic neurotransmission. Moreover, I aim to identify changes to KAR function during development. Together, these experiments will aid understanding of the physiological roles of KARs in mediating inhibitory neurotransmission throughout development, which can help inform understanding of the development of many neurodevelopmental disorders.

6.2 Methods

Recording methods were described fully in chapter 2. All experiments in this chapter were conducted on combined slices of EC and hippocampus, described in the methods section, from neonatal (P8-11; 20-35 g) and juvenile (P20-28; 50-100 g) Wistar rats. Whole cell voltage clamp recordings of sIPSCs and mIPSCs were recorded from principal neurones in LII and LV MEC. Neurones were voltage clamped at -60 mV. Cells were selected with good access resistance that remained stable for the duration of the recording. In all recordings DL-AP5 and SYM-2206 were included in the bath to block NMDARs and AMPARs, respectively. To investigate the contribution of KARs to inhibitory neurotransmission I used the general agonist, KA, a relatively selective GluK1-containing KAR agonist, ATPA, and antagonist, UBP-310.

Mean values for frequency, inter-event interval (IEI; inverse of frequency), amplitude, decay times and holding current were determined and compared between control and drug groups using either a paired t-test or a repeated measures ANOVA (rANOVA) for multiple comparison. Dunnett's post-test was used if all comparisons were made to the control group, and a Bonferroni's post-test was used when comparing selected pairs of columns when multiple drugs were added. The non-parametric Mann Whitney test was used when comparing different neuronal populations. Two-way ANOVA analysis was used when comparing groups that were influenced by two different independent variables (e.g. time and age).

Cumulative distribution analysis used pooled data from a sample of events during a continuous recording period for each neurone and statistical comparisons were made using a Kolmogorov-Smirnov (KS) test for mean data and cumulative probability distributions, respectively. Statistical significance was defined when $P < 0.05$, except for KS-analysis, where significance was reached if $P < 0.01$ due to the sensitivity of the test.

Drug	Action	Target	EC50/IC50	Conc. used	Reference
Kainic acid	Agonist	All KARs	0.6-7.4 µM	0.2 µM (submaximal)	(Alt et al., 2004)
ATPA	Selective agonist	GluK1-containing KARs	0.33 ± 0.05 µM	0.1-0.5 µM (selective)	(Alt et al., 2004)
UBP-310	Selective antagonist	GluK1-containing KARs	23 ± 2 µM	20 µM (selective)	(Perrais et al., 2009)
DL-AP5	Selective antagonist	NMDAR	0.28-1.6 µM	40 µM (supramaximal)	(Ambert et al., 2010)
SYM-2206	Selective non-competitive antagonist	AMPAR	2.8 µM	10 µM (supramaximal)	(Grisanti, 2010)

Table 6.1: Table of pharmacological agents.

6.3 Results

6.3.1 Effects of KA on LII IPSCs

6.3.1.1 Effects of KA on juvenile LII sIPSCs

In the first set of experiments I determined the effects of non-selective activation of KARs with KA, on GABA release onto principal neurones in LII in juvenile rats. sIPSCs were recorded in the presence of SYM 2206 (10 µM) and DL-AP5 (40 µM) to block AMPAR and NMDAR, respectively. The results are summarised in Fig. 6.1. KA (200 nM) increased the mean frequency of sIPSCs ~3-4 fold, from 246.7 ± 111.2 events/min (4.1 Hz) to 917.7 ± 150.8 events/min (15.3 Hz) and 727.1 ± 191.2 events/min (12.1 Hz) after 10 and 15 minutes, respectively ($P < 0.05$ and $P < 0.01$, rANOVA; n = 4). Subsequent addition of UBP-310 (20 µM) decreased the frequency back to control levels (267.4 ± 68.5 events/min; 4.5 Hz) after 15 minutes ($P < 0.05$; rANOVA), indicating the involvement of GluK1-containing KARs in eliciting the high frequency of GABA release onto principal neurones after KA application.

The increase in frequency was concurrent with an increase in amplitude which almost doubled from 18.25 ± 6.2 pA to a maximum of 35.9 ± 6.3 pA after 10 minutes KA ($P < 0.05$, rANOVA), again the effect was largely reversed close to control levels (23.3 ± 10.4 pA) after

cumulative application of UBP-310. Changes in amplitude suggest that neurones presynaptic to the recorded neurone are likely to be driven to fire by activation of postsynaptic receptors on their cell bodies, and the effects of UBP-310 would suggest a KARs containing the GluK1 subunit is mediating this effect.

The mean decay time of sIPSCs was also doubled (from 5.3 ± 0.3 ms to a maximum of 10.6 ± 2.2 ms) by KA and, again, reversed to 5.9 ± 1.5 ms by UBP-310. This probably indicates that the presynaptic neurones that were activated by KA were giving rise to IPSCs of slower time course and longer duration, and could be a separate population of neurones that were not spontaneously active in baseline conditions. A population of large amplitude slow time course events is readily visible in KA in the traces shown in Fig. 6.1.

Lastly, the mean holding current increased by $+ 45.3 \pm 21.2$ % after 15 minutes KA ($P < 0.05$, rANOVA) with a partial recovery after UBP-310 (-22.3 ± 13.9 %). This is similar to the effect seen when recording sEPSCs, but since we were recording principal cells in both cases it would be expected. The results can be interpreted in a number of ways: 1) activation of GluK1-containing KARs postsynaptic to glutamate terminals are driving GABA release by exciting interneurones and increasing the summation of sIPSCs occurring at high frequency, 2) GluK1-containing KARs are located pre- or postsynaptically on interneurones, acting to directly influence GABA release onto principal neurones, or 3) due to the depolarisation induced by activation of KARs on the recording neurone. This would mean the depolarisation is not caused by an outward current of chloride ions through GABA receptors, but an inward current via KARs on the postsynaptic membrane. Further experiments using a GABAR antagonist should be able to discriminate between these possibilities

6.3.1.2 Effects of KA on neonate LII sIPSCs

Having documented the role of KA in inhibitory transmission in juvenile rats, we next decided to determine the effect of KA on inhibitory neurotransmission in neonate slices. It is important to note that the baseline frequencies of sIPSCs in neonate neurones was very low prior to the addition of drugs.

In the presence of KA, the mean frequency of sIPSCs weakly increased from 23.8 ± 3.6 events/min (0.4 Hz) to 32.4 ± 11.4 event/min (0.5 Hz), but this was not statistically significant with rANOVA analysis. The data are illustrated in Fig. 6.1. There were no concurrent effects on the mean amplitude of events, or their decay time. These results contrast markedly with those in juvenile animals where sIPSC frequency was markedly elevated by KA by over 300% compared to control whilst the small increase seen here amounted to only ~35%. The absence of an effect on amplitude in neonates also contrast sharply with the 100% increase seen in juveniles

Despite the relatively minimal increase in frequency with KA a decreased frequency of sIPSCs occurred with cumulative application of UBP-310, and frequency actually fell to below control levels (11.9 ± 5.3 events/min, or 0.2 Hz), although again, this did not reach statistical significance. Due to the very low baseline frequency of events, only a small sample could be pooled from each cell in the cumulative analysis. Nevertheless, cumulative probability analysis of IEIs confirmed the non-significant increase with KA on the frequency of sIPSCs, but showed that the effect of UBP-310 did reach significance ($P < 0.0001$, KS-test, n = 3, not shown). Thus, despite such a low baseline frequency of sIPSCs, the GluK1-containing KAR may be tonically active and may be modulating GABA release.

Interestingly, also unlike in juvenile neurones, KA had no effect on the holding current, and by implication did not depolarise neonate neurones. A larger sample size is needed to clarify these effects.

Overall, these results suggest that KAR control of spontaneous GABAergic inhibition is not well developed in neonates at P8-11. This could be for several reasons. It may simply be that KAR receptors are poorly expressed or have a reduced intrinsic function at this age. Certainly the immunohistochemical data that we have been given access to by Professor Elek Molnar (Fig. 1.6, introduction) suggest that there is substantially increased expression around P14. Therefore it may be that the GABA neurones themselves are poorly functional at this age. The low baseline frequency of sIPSCs would indicate that GABAergic synaptogenesis is not fully developed, that interneurones are not spontaneously active or driven, or that there are low levels of GABA$_A$R on the principal cells.
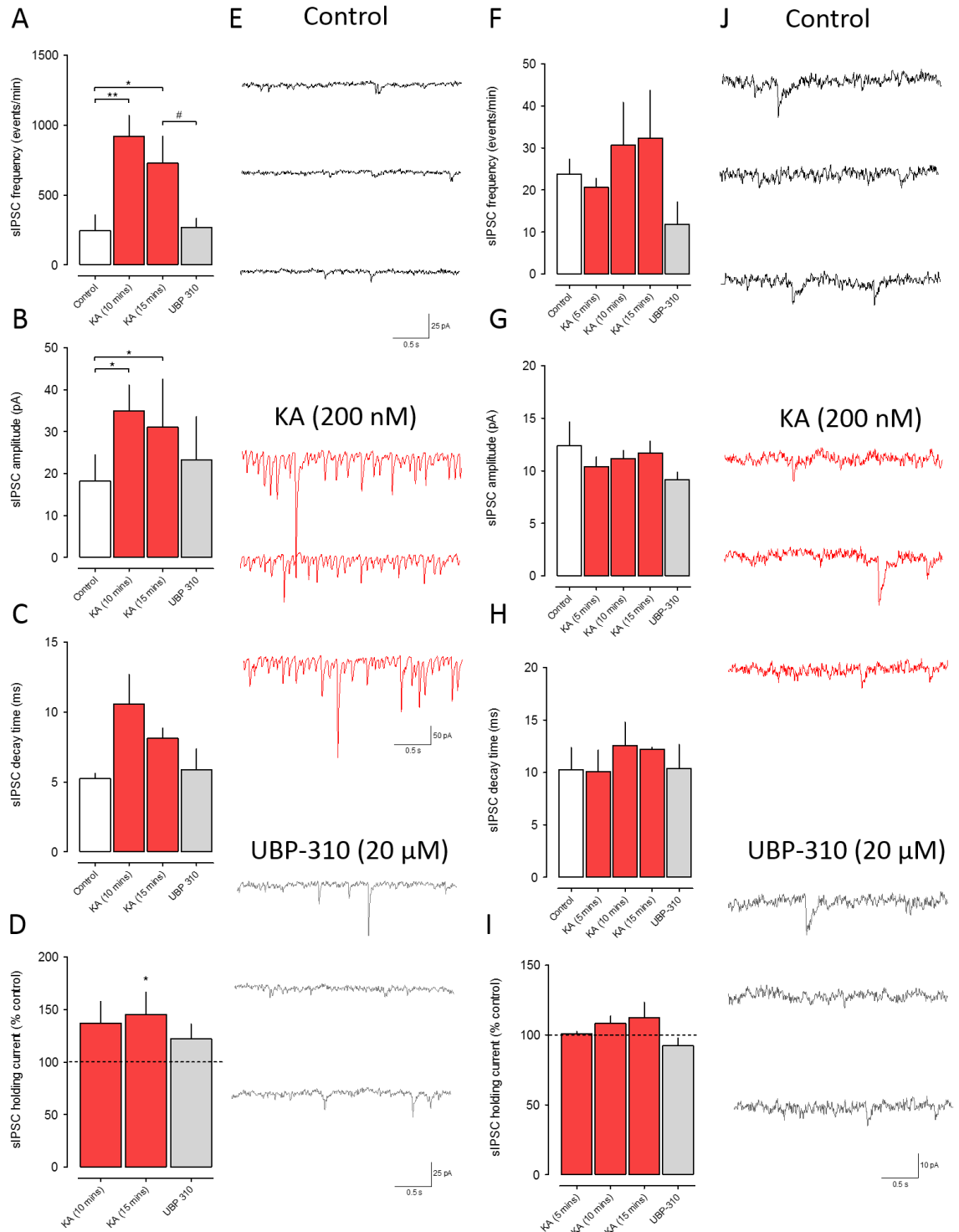
Figure 6.1: Effects of KA (200 nM) and UBP-310 (20 μM) on sIPSCs in 4 juvenile and 3 neonate LII neurones. (A/F) *Average sIPSC frequency, **(B/G)** amplitude, **(C/H)** decay time and **(D/I)** % change in holding current data from LII principal neurones. Control groups (white) represent sEPSCs before application of KA (red) and UBP-310 (grey). Average frequency, amplitude and holding current were significantly increased in the presence of KA and reversed after addition of UBP-310. **(E)** Concurrent recordings of sEPSCs recorded in control conditions (black), in the presence of KA (red) and UBP-310 (grey) in a juvenile and a **(J)** neonate principal neurone.*

6.3.2 Effects of ATPA on LII IPSCs

6.3.2.1 Effects of KA on juvenile LII sIPSCs

In contrast to KA, ATPA at either 100 or 500 nM had no detectable effect on the mean frequency, amplitude, decay time or holding current of sIPSCs in LII juvenile neurones. Data are summarised in Fig. 6.2 (A-E).

This was a surprising result given the powerful effect of KA and it's reversal by UBP-310. As noted in the previous chapter, it may call into question the specificity of the antagonist for GluK1 receptors (Perrais et al., 2009, Atlason et al., 2010). It also contrasts markedly with the strong increase in sIPSC frequency seen with ATPA in previous studies from this laboratory in LIII (Chamberlain et al., 2012).

6.3.2.2 Effects of ATPA on neonate LII sIPSCs

The effects of ATPA (100 nM and 500 nM) were assessed on 3 neurones in LII and the results are illustrated in Fig. 6.2 (F-J). Whilst ATPA (100 nM) had little effect on the mean frequency (it actually fell non-significantly from 95.7 ± 35.9 events/min to 69.8 ± 46.6 events/min), cumulative addition to 500 nM substantially increased the frequency to 415.1 ± 135.5 events/min, although this did not reach significance due to the low sample size. Percentage-wise, this was a similar change (~400%) to that seen with KA in the juvenile animals, although the absolute increase was less.

Similarly, the mean amplitude was unaffected by 100 nM ATPA (14.6 ± 5.6 pA *vs* 14.5 ± 5.1 pA), but with 500 nM it increased to 21.8 ± 6.7 pA. The increase did not reach significance with rANOVA analysis, but KS-analysis confirmed a clear and significant rightward displacement in the amplitude distribution, reflecting the increase in amplitude (P < 0.0001, KS-test, not shown). The mean decay time was also increased, almost doubling from 7.9 ± 2.2 ms to 14.9 ± 3.5 ms in the presence of ATPA.

One interpretation of these results is that activation of the GluK1-containing KAR may increase synchronised multi-quantal release of GABA from the interneurone terminals that are already releasing GABA at quantal levels. Alternatively, the agonist may be exciting an

entirely separate population of interneurones that are innervating the recorded cell, but are not driven to fire and release GABA until excited by ATPA acting at receptors on their soma/dendrites. The much longer mean decay times of the sIPSCs seen in ATPA could support this possibility. However, such a scenario is very difficult to reconcile with the lack of effect of KA in the neonate neurones and the lack of effect of ATPA on the frequency of sIPSCs in juvenile LII neurones. It is possible that the receptor subunit composition/variant present at P8-11 has a high affinity for ATPA but a low affinity for KA, and with development this switches to an isoform with the reverse affinities. Nevertheless, the results are exciting because they are quite different in the different age groups and implicate the GluK1-containing KAR as having a developmental role in the regulation of GABA release. Amongst other scenarios, this could reflect the dominance of a sub-type of interneurone that is modulated by the GluK1-containing KAR in neonatal neurones relative to juvenile, and will be discussed later.
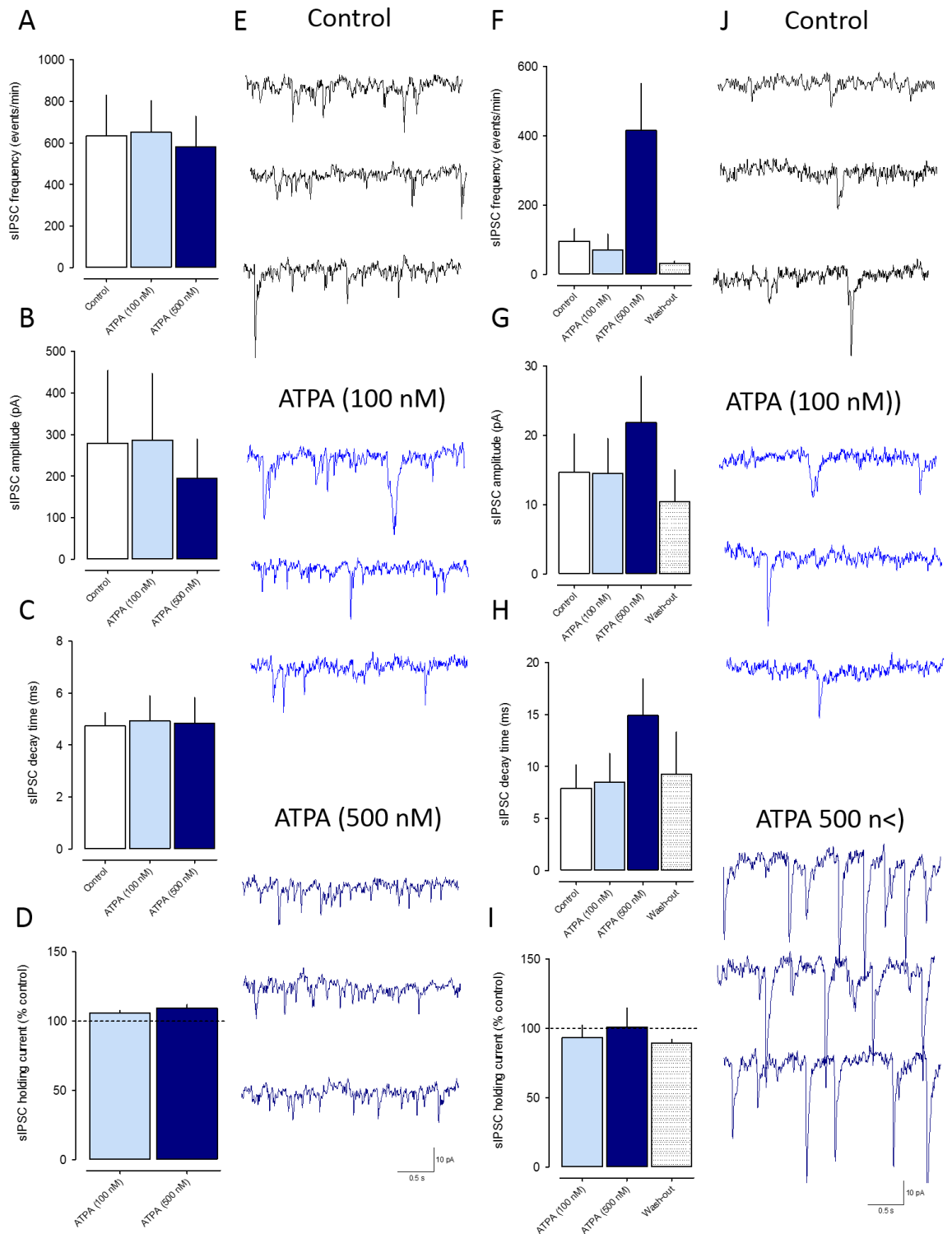
Figure 6.2: Effects of ATPA (100 nM and 500 nM) on sIPSCs in 4 juvenile and 3 neonate LII neurones. (A/F) *Average sIPSC frequency,* ***(B/G)*** *amplitude,* ***(C/H)*** *decay time and* ***(D/I)*** *% change in holding current data from LII principal neurones. Control groups (white) represent sEPSCs before application of 100 nM ATPA (light blue) and 500 nM ATPA (dark blue). Average frequency, amplitude and decay time were increased in the presence of ATPA in neonate, but not juvenile, LV neurones. Traces show concurrent recordings of sEPSCs recorded in control conditions (black), in the presence of 100 nM ATPA (light blue) and 500 nM ATPA (dark blue) in a* ***(E)*** *juvenile and a* ***(J)*** *neonate principal neurone.*

6.3.3 Effects of UBP-310 on LII IPSCs

6.3.3.1 Effects of UBP-310 on juvenile LII IPSCs

The lack of effect of ATPA in these experiments surprising given previous studies in LIII (Chamberlain et al., 2012), but is, nevertheless, similar to its relative lack of effect on sEPSCs in the previous chapter. The results suggest that GluK1 receptors are not directly modulating transmitter release at either glutamate of GABA synapses in juvenile neurones. However, as noted in the previous chapter, addition of UBP-310, the putative GluK1-containing KAR antagonist, demonstrated that these receptors are likely to be tonically activated at glutamate synapses, and may be saturated by ambient glutamate.

I determined the effect of UBP-310 alone on sIPSCs in LII juvenile neurones and the data are summarised in Fig. 6.3. UBP-310 had no significant effect on the mean frequency, amplitude or decay time of sIPSCs in these neurones although there was trend towards a decrease in both frequency and amplitude (~15-20% in each case). This was reflected also in cumulative probability analysis, which did identify a small increase in IEIs of sIPSCs with UBP-310 ($P < 0.0001$, KS-test; $n = 4$, not shown) and a leftward displacement in the cumulative distribution of amplitudes ($P = 0.003$; KS-test).

The decrease in frequency could reflect a small degree of tonic facilitation of GABA release by GluK1 receptors. A change in amplitude would normally be suggestive of a postsynaptic mechanism but it is difficult to see how this would happen.

Perhaps a more probable explanation is that GluK1-containing KARs are tonically active on GABAergic terminals and activated by spillover from glutamate synapses, a scenario that has backing from studies in other areas (Jiang et al., 2001, Binns et al., 2003). This tonic effect may result in synchronised multi-quantal GABA release onto the principal neurones. When the heteroreceptors are blocked, there is decrease in multi-quantal, spontaneous GABA release, but the more frequent mono-quantal release is unaffected, and so the overall amplitude and frequency of inhibitory events is decreased. An alternative is that the GluK1 receptors may be restricted to specific GABA inputs that give rise to large amplitude

sEPSCs on the recorded neurone, and not present on others that give rise to smaller mono-quantal events. The end result of blocking the heteroreceptor would be the same.

What is also interesting is that addition of KA cumulatively with UBP-310 resulted in a partial restoration of sIPSC frequency and amplitude. Whilst this could simply reflect competition between agonist and antagonist, it may also result from activation of non-GluK1 receptors on the soma/dendrites of other interneurones providing input to the recorded neurone. Such a scenario actually presupposes that the large events that disappear in UBP-310 are probably not from the same source as those that are evident when KA is added. These possibilities should be investigated in future experiments.
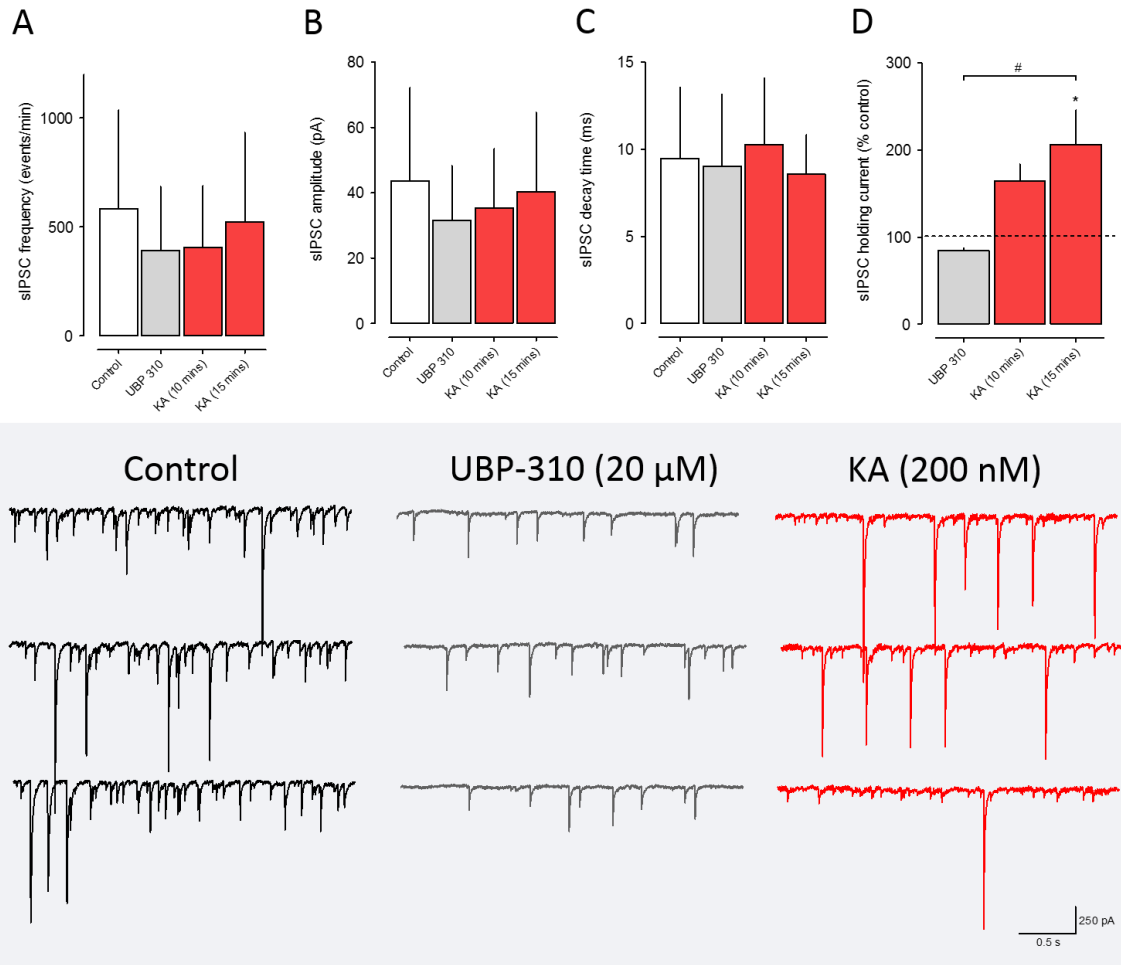
Figure 6.3: Effects of UBP-310 (20 μM) and KA (200 nM) on sIPSCs in juvenile LII neurones. *(A) Mean sIPSC frequency, (B) amplitude, (C) decay time and (D) % change in holding current of sIPSCs from 4 principal neurones. Control groups (white) represent sIPSCs before application of UBP-310 (grey) and KA (red). (E) Traces show concurrent recordings of sIPSCs recorded in control conditions (black), in the presence of UBP-310 (grey) and KA (red). Note the decrease in sIPSC amplitude after exposure to UBP-310.*

6.3.4 Effects of KA on LV IPSCs

6.3.4.1 Effects of KA on juvenile LV sIPSCs

The effect of non-selectively activating KARs with KA on sIPSCs in juvenile LV neurones are shown in Fig. 6.4. The agonist significantly increased the mean frequency of sIPSCs to around 300% of control levels (from 166.5 ± 45.3 events/min (2.8 Hz) to 553.2 ± 158.8 events/min (9.2 Hz) after 10 minutes; $P < 0.01$, rANOVA; $n = 7$). Again, this increase appears to be partially reversed by the addition of UBP-310, suggesting KAR containing the GluK1 subunit were responsible for the increase. As in LII neurones in juvenile rats the mean

amplitude and decay times of sIPSCs were was significantly increased by KA and partially reversed by UBP-310 (Fig. 6.1). Changes in holding current followed a similar pattern.

Thus, KA induced the appearance of much larger amplitude sIPSCs with a slower decay time. This is suggestive that the agonist was activating receptors directly on the soma/dendrites of GABAergic interneurones to increase action potential driven release resulting in synchronised multi-quantal sIPSCs. I next looked at the effects of KA on mIPSCs to investigate this further
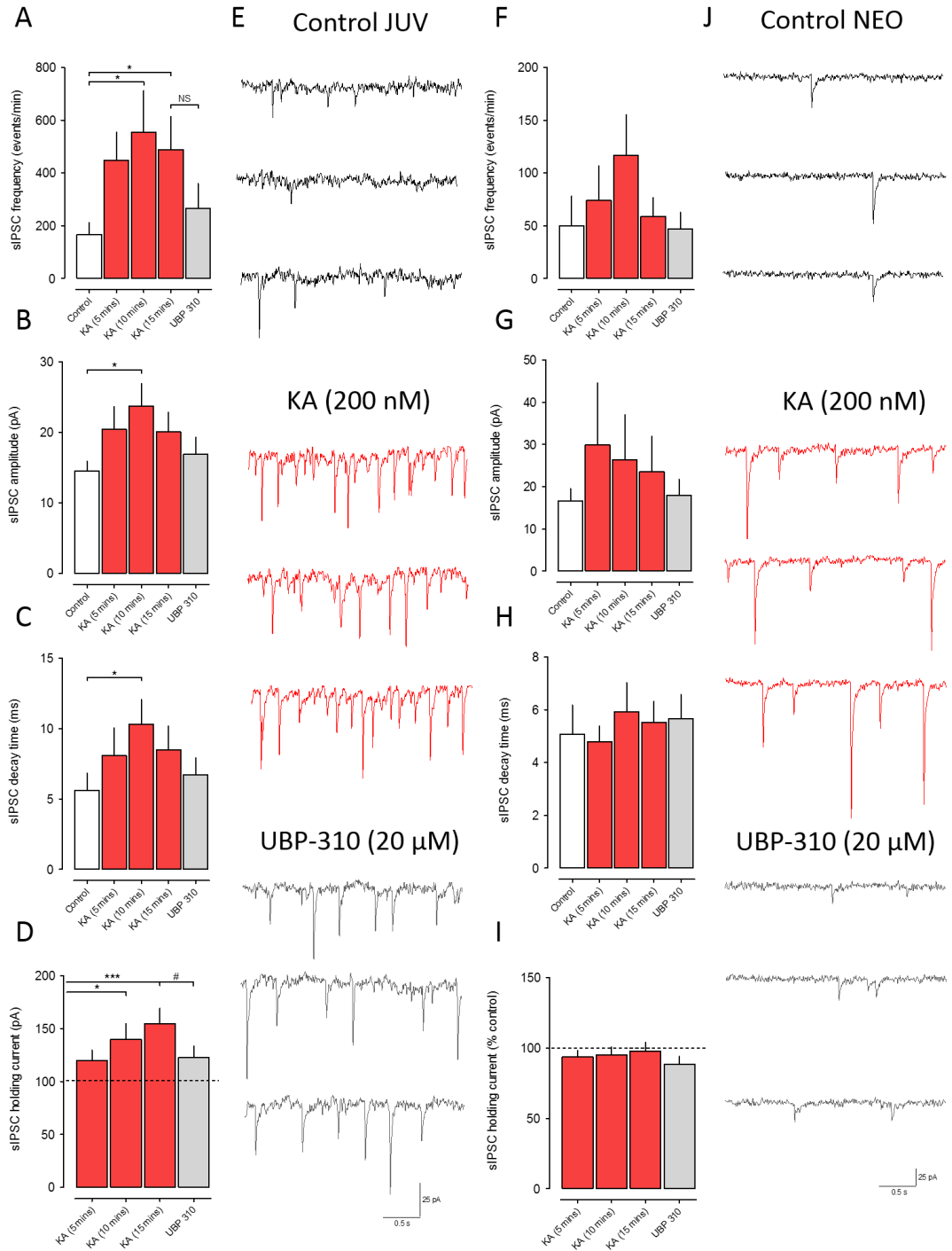
Figure 6.4: Effects of KA (200 nM) and UBP-310 (20 μM) on sIPSCs in 7 juvenile and 4 neonate LV neurones. (A/F) *Average sIPSC frequency,* **(B/G)** *amplitude,* **(C/H)** *decay time and* **(D/I)** *% change in holding current data from LV principal neurones. Control groups (white) represent sEPSCs before application of KA (red) and UBP-310 (grey). Average frequency, amplitude and holding current were significantly increased in the presence of KA. Traces show concurrent recordings of sEPSCs recorded in control conditions (black), in the presence of KA (red) and UBP-310 (grey) in a* **(E)** *juvenile and a* **(J)** *neonate principal neurone.*

6.3.4.2 Effects of KA on juvenile LV mIPSCs

To help clarify the origin of KA-induced increase in sIPSC frequency and amplitude, the experiments were repeated in the presence of TTX (1 µM), to remove the action potential dependent network driven effects. KA induced a small, but significant, increase in the mean frequency of mIPSCs, from a control of 42.7 ± 13.4 events/min (0.7 Hz) to 60.1 ± 20.0 events/min (1.0 Hz) after 15 minutes (P < 0.05, rANOVA; n = 4). It has to be stressed that this effect was very small compared to sIPSCs (~40% v 300). In essence, apart from the marginal increase in frequency, the effects of KA on sIPSCs were abolished by recording in TTX.
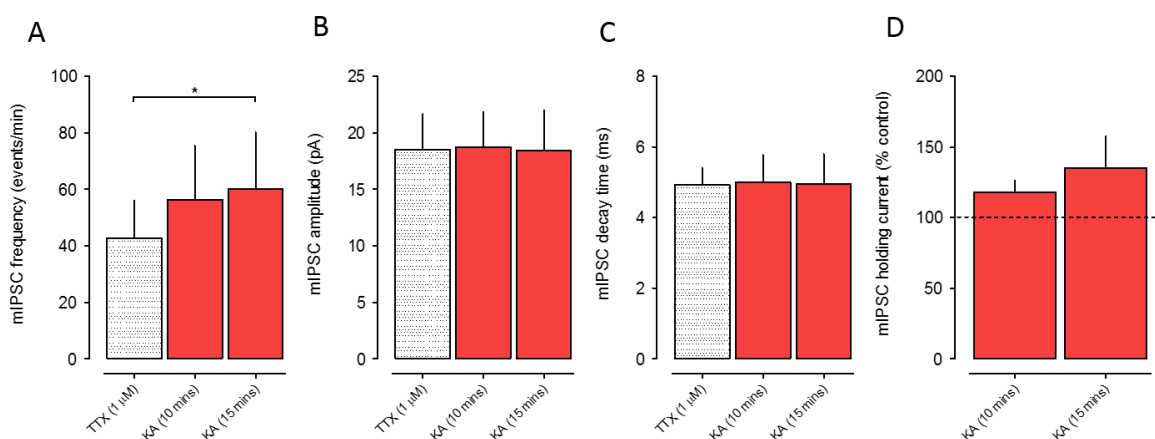
Figure 6.5: Effects of KA on mIPSCs in juvenile LV neurones (A) *Mean sIPSC frequency, **(B)** amplitude, **(C)** decay time and **(D)** % change in holding current data from 4 principal neurones. Control groups (dotted) represent mEPSCs in the presence of TTX, before application of KA (red). TTX largely abolished the effects of KA.*

6.3.4.3 Effects of KA on neonate LV sIPSCs

The effects of KA and UBP-310 were assessed on neonate neurones in LV. The results are illustrated and summarised in Fig. 6.4. KA (200 nM; n=5) increased the mean frequency of sIPSCs from 50.1 ± 28 events/min (0.8 Hz) to a maximum of 117.0 ± 38.4 events/min (2.0 Hz) after 10 minutes, however, this increase was not sustained and decreased back to 58.8 ± 17.8 events/min (1.0 Hz) after 15 minutes. Addition of UPB-310 had no effect on the frequency of sIPSCs (46.9 ± 15.8 events/min, or 0.8 Hz). The 80% increase in frequency was considerably less than the 300% seen in juvenile LV neurones and was not significant with rANOVA.

KA modulated the amplitude of sIPSCs in a similar pattern to the frequency, such that the mean amplitude was increased after the initial exposure to KA, from a control of 16.7 ± 2.9 pA to a maximum of 29.9 ± 14.7 pA after 5 minutes KA. After 15 minutes in the continued presence of KA, sIPSC amplitude decreased to 23.5 ± 8.4. This pattern of an initial peak followed by a decline in frequency was not unusual in MEC principal neurones and seen with sEPSCs, sIPSCs, in both layers and age groups. It was also seen previously with ATPA in LIII (Chamberlain S.E.L. and Jones R.S.G., unpublished findings). The effect was almost always marginal and in many cases not seen at all, but in the case of the neonate LV neurones it was particularly pronounced, and sIPSC frequency was almost restored to control levels after 15 min. The mean frequency was 17.9 ± 3.8 pA after additional application of UBP-310, though it is difficult to say if this slight decrease is due to UBP-310 or a late continued decline with KA.

Mean amplitude of sIPSCs increased with initial application of KA but also fell back towards control with continued application. The amplitude increase appeared to be due largely to the appearance of a population of large amplitude events that appeared initially in KA and then progressively disappeared. They were eliminated after addition of UBP-310, but again it's not possible to say whether this was an effect of the drug. Neither KA nor UBP-310 had any noticeable effect on the decay time.

Overall, the results do tend to show a small increase in GABA release with KA. This was considerably less pronounced than its effect in juvenile animals, and of the same order of the effect of KA in LII in neonates. The most interesting aspect was the lack of sustained effect of KA during continued application, with sIPSCs returning essentially to baseline levels after 15 minutes. This made it impossible to tell if UBP-310 had any effect, and so the initial increase cannot be ascribed to GluK1 receptors at this stage. Whatever the receptor involved, the rapid decline of the response suggests that in the neonate animals, it becomes inactivated or desensitised in the continued presence of the agonist. The increase appeared to reside largely with the transient appearance of a population of large amplitude events and this could possibly be due to facilitation of multi-quantal release from already active inhibitory terminals, or activation of a population of interneurones that are silent under baseline conditions.

6.3.5 Effects of ATPA on LV IPSCs

6.3.5.1 Effects of ATPA on juvenile LV sIPSCs

KA substantially increased the frequency of sIPSCs in juvenile neurones, an effect partially reversed by UBP-310. I investigated the role of GluK1 receptors further by examining the effect of ATPA. The agonist had no effect on the mean frequency, amplitude, decay time or holding current of sIPSCs in principal neurones tested (Fig. 6.6; n=7). However, in one additional cell ATPA did appear to induce a substantial increase in the frequency of sIPSCs, from a control of 247.8 events/min (4.13 Hz) to 561.9 events/min (9.4 Hz) and 660.4 events/min (11.0 Hz) after 100 nM and 500 nM ATPA, respectively. Amplitude was unaffected but decay time was increased (not shown). This neurone had a much higher baseline frequency before the application of ATPA, which could suggest that it was a subtype of principal neurone or perhaps an interneurone. In any case it was left out of the group analysis. I also investigated the effects of ATPA in the presence of TTX (n=5), and as expected, it failed to alter any parameters of the mIPSCs. Combined group data from sIPSCs and mIPSCs clearly illustrated the overall lack of effect (Fig. 6.6, A-E).
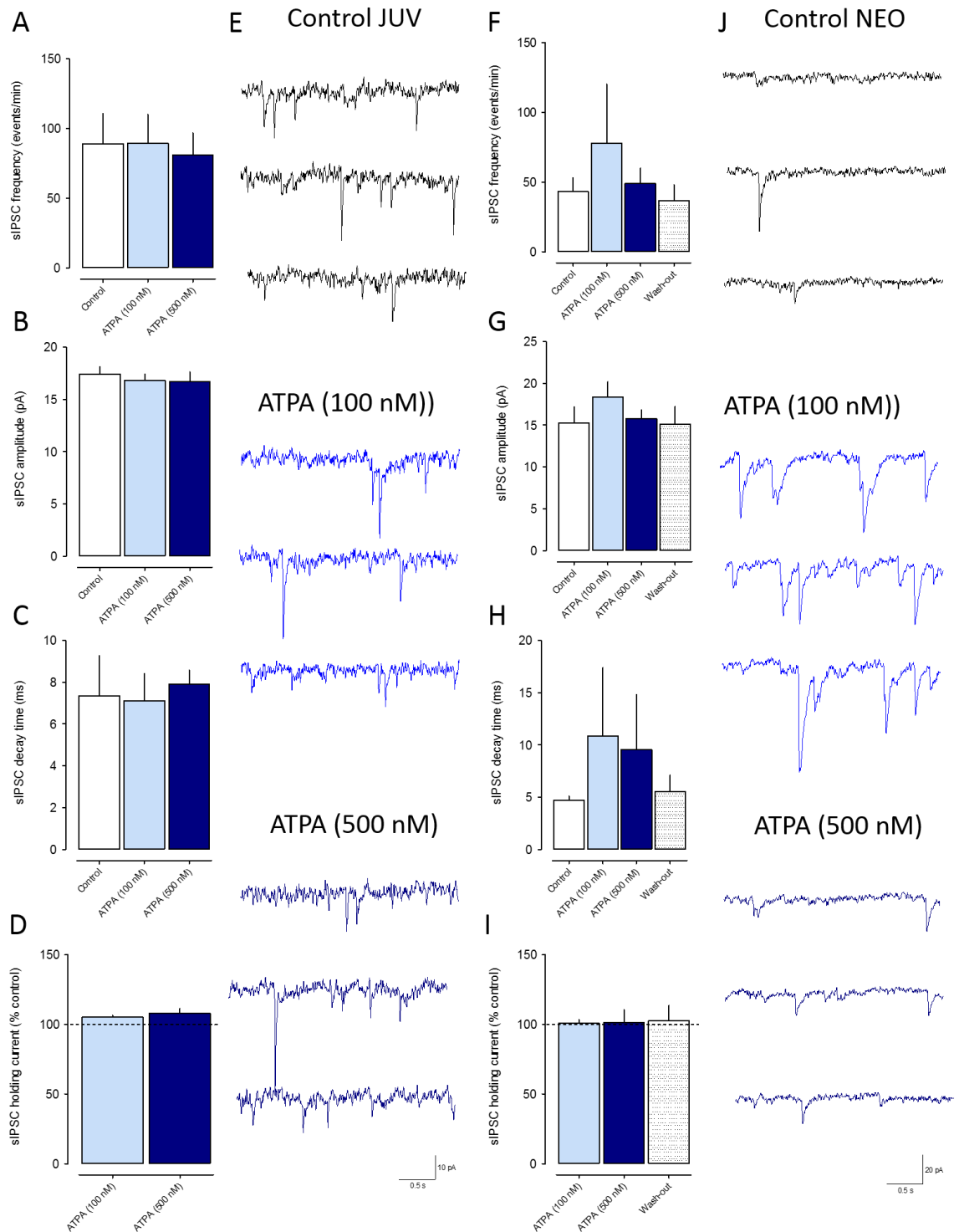
Figure 6.6: Effects of ATPA (100 nM and 500 nM) on sIPSCs in 7 juvenile and 4 neonate LV neurones. (A/F) *Average sIPSC frequency,* **(B/G)** *amplitude,* **(C/H)** *decay time and* **(D/I)** *% change in holding current data from LV principal neurones. Control groups (white) represent sEPSCs before application of 100 nM ATPA (light blue) and 500 nM ATPA (dark blue). Average frequency, amplitude and decay time were increased in the presence of ATPA in neonate, but not juvenile, LV neurones. Traces show concurrent recordings of sEPSCs recorded in control conditions (black), in the presence of 100 nM ATPA (light blue) and 500 nM ATPA (dark blue) in a* **(E)** *juvenile and a* **(J)** *neonate principal neurone.*

6.3.5.2 Effects of ATPA on neonate LV sIPSCs

To try to clarify a role of potential role for GluK1 receptors in the transient increase in sIPSCs produced by KA, the effects of ATPA were determined on LV neonatal neurones (Fig. 6.6 F-J). Addition of 100 nM ATPA induced a small increase in mean frequency from 43.2 ± 9.9 events/min (0.7 Hz) to 78.0 ± 42.3 events/min (1.3 Hz). With the cumulative addition of ATPA to 500 nM the frequency of sIPSCs fell back to control levels (48.8 ± 11.1 events/min, or 0.8 Hz).

Amplitude increased slightly from a control level of 15.3 ± 1.9 pA to 18.4 ± 1.8 pA with 100 nM ATPA, but again, even this small effect was not sustained with 500 nM ATPA (15.8 ± 1.0 pA). The mean decay time doubled in the presence of 100 nM and although it again declined with 500 nM it remained well above control. Decay time did return close to control levels after wash-out of the drug, but it is difficult to say if this is due to the wash per se or the result of a time dependent decline due to ATPA.

These results could suggest that, unlike in juvenile neurones in LV, KARs containing the GluK1 subunit can facilitate GABA release onto neonatal principal neurones, and this could also underlie the transient increase in sIPSCs induced by KA. It may even be possible to equate the time-dependent decline with KA with the concentration dependent decline seen with ATPA. In this regard the appearance of large amplitude sIPSCs with 100 nM, which then essentially disappeared with 500 nM, could reflect the activation of a population of interneurones that were initially silent under baseline conditions. The substantial change in decay kinetics would support this, and again the transient nature of this effect could be an indication that the receptor involved was rapidly desensitising in the presence of the agonist.

6.3.5 Effects of UBP-310 on LV IPSCs

6.3.5.1 Effects of UBP-310 on juvenile LV sIPSCs

I have shown that GluK1-containing KARs act as tonically active facilitatory autoreceptors on glutamate terminals in both LII and LV, and play a similar though less marked role as

heteroreceptors at GABA terminals in LII (above). To determine if a similar function pertains in LV, the effects of UBP-310 on sIPSCs were studied. The antagonist had no effect on the mean frequency of sIPSCs (120.4 ± 27.9 events/min vs 118.2 ± 40.0 events/min; see Fig. 6.7), suggesting that GluK1 KARs may not tonically modulate GABA release onto juvenile neurones in LV. UBP-310 decreased the mean amplitude (from 25.3 ± 1.8 pA to 20.3 ± 1.6 pA; Fig 6.7B) and this change is also evident from the cumulative probability analysis (P < 0.0001, KS-test, not shown). Examination of the records in Fig. 6.7 shows a similar phenomenon to that seen in LII i.e. UBP-310 appeared to remove a population of large but infrequent events, and this has influenced the population mean, without markedly affecting its frequency. Subsequent application of KA in the presence of UBP-310 increased the mean frequency of sIPSCs to 173.2 ± 31.6 event/min, although this did not reach statistical significance (rANOVA) analysis of the IEIs on the cumulative probability plot did suggest it was a real effect (P < 0.0001, KS-test; n = 5, not shown). Similar explanations to those proposed for LII could be advanced to account for the effect of UBP-310 and KA in LV. To avoid the repetition of these proposals here, the reader is referred back to section 6.3.3.1 above (Effects of UBP-310 on juvenile LII sIPSCs).

Taken together with previous results, a decrease in the amplitude of sIPSCs in the presence of UBP-310 could suggest the GluK1-containing KAR has roles in the synchronisation of GABA release onto principal neurones, and its blockade decreases the likelihood of multi-quantal release. The decay time is not affected by UBP-310 (from 12.6 ± 3.8 ms to 13.6 ± 5.2 ms), but subsequent application of KA did tend to decrease the mean decay time (not significant with rANOVA). This could support the proposal (Section 6.3.3.1) that the large sIPSCs that become evident when KA is added in the presence of UBP-310 are from a different interneurone source than those that disappear when UBP-310 is added. Careful comparison of event kinetics and subsequent experiments in the presence of TTX could help confirm these possibilities.

6.3.5.2 Effects of UBP-310 on neonate LV sIPSCs

The studies above suggest that there may be a role for GluK1 receptors in early development, although the transient nature of the effects seen with KA and ATPA are not conclusive. To determine if GluK1-containing KARs are tonically modulating GABA release

onto LV neonatal neurones the, UBP-310, was bath applied. UBP-310 slightly and non-significantly decreased the mean frequency of sIPSCs, from 105 ± 67.5 events/min to 74.9 ± 35.7 events/min. With subsequent addition of KA mean frequency of sIPSCs full slightly further but it was not really possible to determine the basis of this effect. Mean amplitude was largely unaltered (20.7 ± 2.7 pA to 18.9 ± 1.6 pA) in the presence of UBP-310 although there did appear to be an elimination of some higher amplitude events. In the pooled data from the control group, 6.2 % of event amplitudes exceeded 50 pA compared to 0.01 % in the presence of UBP-310. These results are summarised in Fig. 6.7.

Overall the effects of UBP-310 in these studies are weak and the numbers of cells tested is low, so it may be dangerous to place any emphasis on the results. The only real effect of note is the apparent loss of some of the larger events when UBP was applied. This is reminiscent of the time dependent decline with KA and the concentration-dependent decline with ATPA noted above, which could be a result of receptor desensitisation. This could be equivalent to blocking the receptor with UBP-310. Interestingly, the baseline frequency of sIPSCs in the small sample tested here was double that in the studies with KA and ATPA. One possibility is that 'silent" interneurones that become activated by the agonists, are now already active in the current studies, and UBP-310 by blocking somatic GluK1 receptors is now switching them off. This is highly speculative and much further work is necessary to clarify the picture.
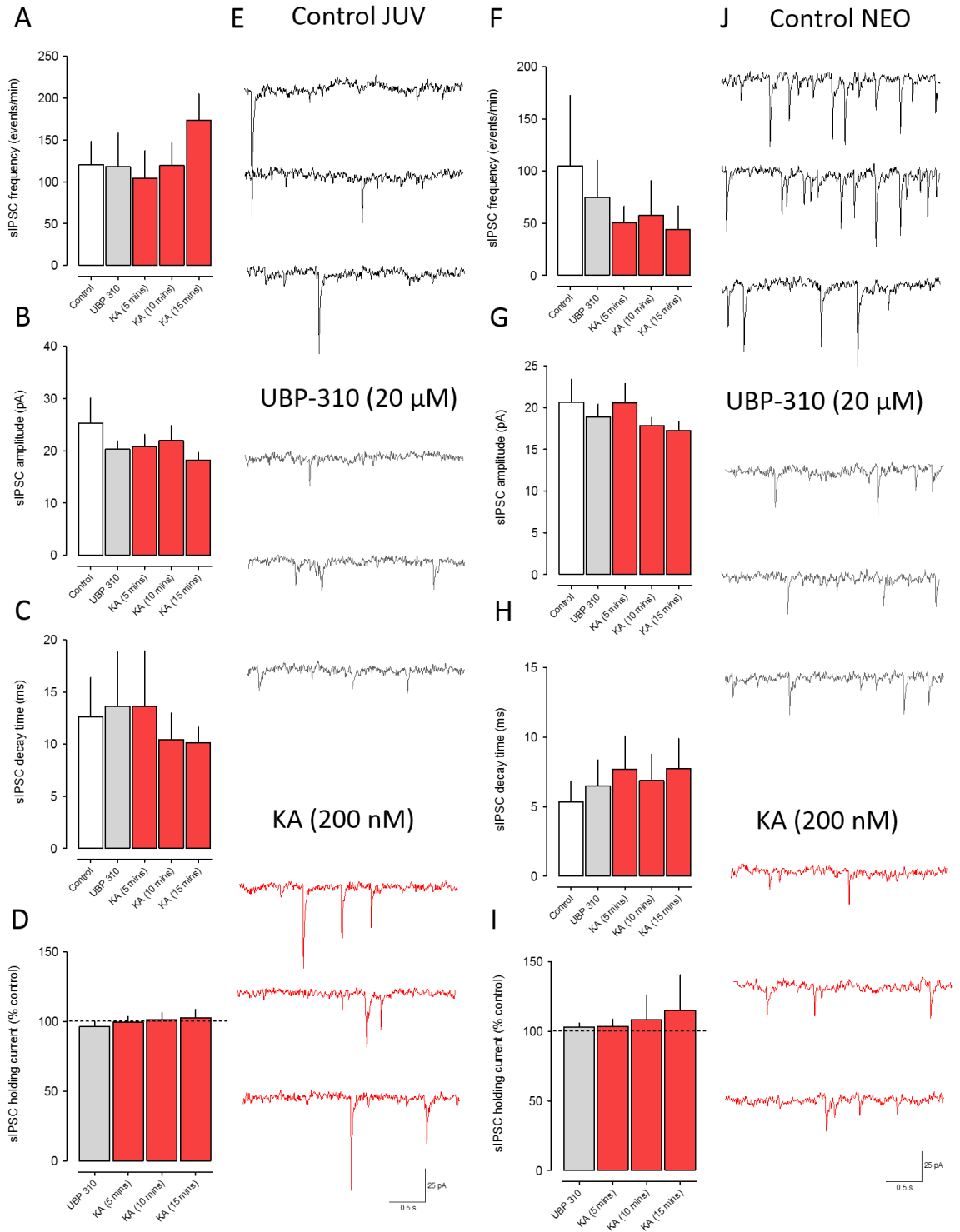
Figure 6.7: Effects of UBP-310 (20 µM) and KA (200 nM) on sIPSCs in 5 juvenile and 3 neonate LV neurones. *(A/F) Average sEPSC frequency, **(B/G)** amplitude, **(C/H)** decay time and **(D/I)** % change in holding current data from LV principal neurones. Control groups (white) represent sEPSCs before application of UBP-310 (grey) and KA (red). Traces show concurrent recordings of sIPSCs recorded in control conditions (black), and in the presence of UBP-310 (grey) and KA (red) from a **(E)** juvenile and a **(J)** neonate neurone. UBP-310 and KA did not significantly affect sIPSCs, though there was a trend of a decrease in amplitude.*

	JUV LII sIPSCs		JUV LV sIPSCs	
	Frequency (Events/min)	Amplitude (pA)	Frequency (Events/min)	Amplitude (pA)
Control	246.7 ± 111.2	18.3 ± 6.2	166.5 ± 45.3	14.6 ± 1.4
+ KA (200 nM, 10m)	917.7 ± 150.8**	34.9 ± 6.3*	553.2 ± 158.8*	23.7 ± 3.2*
+ KA (200 nM, 15m)	727.1 ± 191.2*	31.1 ± 11.4*	488.4 ± 124.5*	20.1 ± 2.8
+ UBP-310 (20 µM)	267.4 ± 68.5#	23.3 ± 10.4	265.0 ± 95.2	16.9 ± 2.4
	(n = 4)	(n = 4)	(n = 7)	(n = 7)
Control	633.7 ± 194.6	278.8 ± 175.2	89.1 ± 21.5	17.4 ± 0.7
+ ATPA (100 nM)	650.8 ± 152.2	286.6 ± 156.8	89.3 ± 20.7	16.8 ± 0.6
+ ATPA (500 nM)	582.1 ± 145.7	195.5 ± 94.2	81.1 ± 15.7	16.7 ± 0.9
	(n = 7)	(n = 7)	(n = 8)	(n = 8)
Control	595.7 ± 322.4	35.4 ± 21.9	120.4 ± 37.9	25.3 ± 4.8
+ UBP-310 (20 µM)	337.8 ± 214.0	26.4 ± 12.9	118.2 ± 40.0	20.3 ± 1.6
+ KA (200 nM, 10m)	353.7 ± 205.8	29.0 ± 14.3	119.3 ± 27.2	22.0 ± 2.8
+ KA (200 nM, 15m)	446.2 ± 330.2	33.2 ± 18.5	173.2 ± 31.6	18.2 ± 1.5
	(n = 4)	(n = 4)	(n = 5)	(n = 5)

Table 6.2: Summary table of the effects of KAR modulation on sIPSCs of juvenile neurones.

	NEO LII sIPSCs		NEO LV sIPSCs	
	Frequency (Events/min)	Amplitude (pA)	Frequency (Events/min)	Amplitude (pA)
Control	23.8 ± 3.6	12.4 ± 2.2	50.1 ± 28	16.7 ± 2.9
+ KA (200 nM, 10m)	30.6 ± 10.2	11.2 ± 0.8	117.0 ± 38.4	26.4 ± 10.7
+ KA (200 nM, 15m)	32.4 ± 11.4	11.7 ± 1.2	58.8 ± 17.8	23.5 ± 8.4
+ UBP-310 (20 µM)	11.9 ± 5.3	9.2 ± 0.7	46.9 ± 15.8	17.9 ± 3.8
	(n = 3)	(n = 3)	(n = 5)	(n = 5)
Control	95.7 ± 35.9	14.6 ± 5.6	43.2 ± 9.9	15.3 ± 1.9
+ ATPA (100 nM)	69.8 ± 46.6	14.5 ± 5.1	78.0 ± 42.3	18.4 ±1.8
+ ATPA (500 nM)	415.1 ± 135.5	21.8 ± 6.7	48.8 ± 11.1	15.8 ± 1.0
	(n = 3)	(n = 3)	(n = 4)	(n = 4)
Control	-	-	105.0 ± 67.5	20.7 ± 2.7
+ UBP-310 (20 µM)	-	-	74.9 ± 35.7	18.9 ± 1.6
+ KA (200 nM, 10m)	-	-	57.7 ± 33.1	17.8 ± 1.1
+ KA (200 nM, 15m)	-	-	43.9 ± 22.7	17.3 ± 1.1
			(n = 3)	(n = 3)

Table 6.3: Summary table of the effects of KAR modulation on sIPSCs of neonate neurones.

6.3.5 Age-comparison

In this section the effects of the changes in sIPSCs will be directly compared between neonate and juvenile neurones, to identify KAR dependent developmental changes in inhibitory neurotransmission in LII and LV. Effects of KAR modulation on sIPSC activity are compared in the two age groups in terms of percentage change from control

6.3.5.1 Developmental differences in the effects of KA on sIPSCs

Fig. 6.8 shows the percentage change in sIPSC frequency, amplitude and decay time with KA in neonatal and juvenile rats in LII. There are clear and marked differences between the groups. KA induced a large change in frequency to +479.2 ± 223.5 % in juvenile animals compared to a very weak increase in neonatal neurones (+51.1 ± 76.0 %). The effect in both age groups was reversed by UBP-310 although, in juveniles, frequency remained at +68.3

± 71.8 % above control levels in neonates it fell below the control levels (-53.3 ± 15.7 %). The mean percentage change in sIPSC frequency in the presence of KA is not significantly different between the two age groups due to the huge variability in responses.

Interestingly, there was also a very clear-cut difference the effect of KA on sIPSC amplitude in neonatal versus juvenile rats. KA increased the amplitude of events by +126% over control in juveniles compared to a complete lack of effect in neonates (mean remaining at 100% of control). When UBP-310 was added in juvenile slices the amplitude fell to just +18.5 % above control. Interestingly, mean amplitude in neonates actual fell slightly at this point although the effect was very small (-15%) but was concurrent with the fall in frequency noted above.

A similar pattern was evident in decay time as in the other parameters. Thus, the increased frequency and amplitude in juveniles with KA saw a concurrent increase in decay to nearly twice that (+96.5) % in control. This increase in decay time was again reversed by UBP-310. Neonate neurones showed no change in decay time throughout.

These results suggest that, in juvenile LII neurones activation of KARs leads to a strong increase in sIPSCs with a large amplitude and slow decay compared to control events. This could indicate that the receptors responsible may be located on active presynaptic GABAergic terminals and act to provoke a high level of synchronised multi-quantal release. Alternatively, the receptors may reside on the soma/dendrites of interneurones that are presynaptic to the recorded neurone, and that these neurones are driven to fire only when KA is present. The shift in and amplitude distribution decay time may support the latter proposal and may also suggest that the population of interneurones activated may differ from those responsible for sIPSCs at baseline. Clearly, a combination of these effects is also possible and further experiments in the presence of TTX are needed to confirm this. The ability of UBP310 to reverse the increases suggests, at least at this stage, that the receptor is likely to contain the GluK1 subunit.

In neonates, the frequency of sIPSCs was low and only a minimal increase was observed with KA and there was no increase in amplitude or decay. This strongly suggests that KAR

receptors are weakly expressed at this stage, or that GABA interneurones are poorly developed, connected or functional.
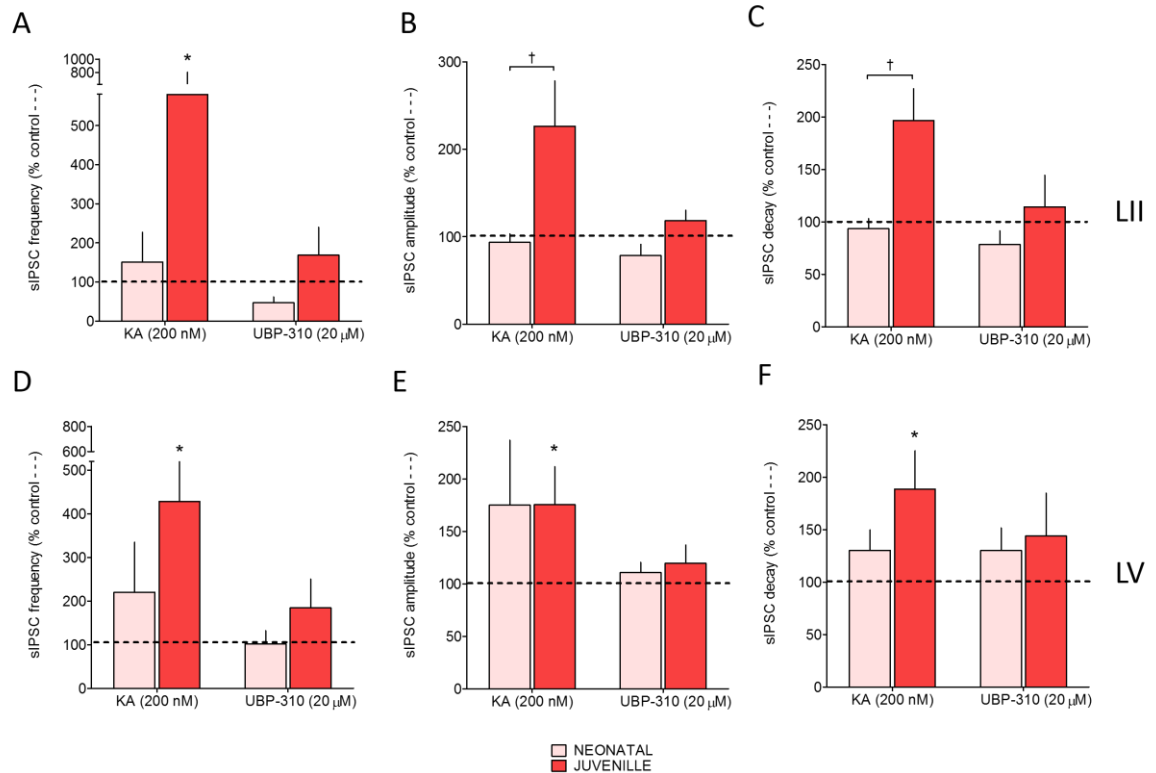
Figure 6.8: Comparative change in sIPSCs with KA (200 nM) and UBP-310 (20 μM) in neonate and juvenile neurones. (A&D) *Mean sIPSC percentage change in frequency, **(B&E)** amplitude, **(C&F)** decay time data from 3 neonate (pink) and 4 juvenile (red) principal neurones from LII (top) MEC, and from 3 neonate (pink) and 7 juvenile (red) principal neurones from LV (bottom) MEC. *, # and ϯ denote significant differences between: * juvenile % change vs control (100 %, dashed line), # neonatal % change vs control (100 %, dashed line), and ϯ juvenile % change vs neonatal % change.*

In some respects the age comparison In LV (also shown in Fig. 6.8) was qualitatively similar to LII although the quantitative differences between the age groups was not. Thus, KA maximally increased the frequency of events by ~+350% over control in juveniles, which was rather less than that seen in LII. In neonate LV, however, KA elicited a maximal +120% increase, which was greater than the effect in LII. Thus, the overall difference in increase was more exaggerated in LII compared to LV.

It should be noted that increased frequency in juveniles was sustained throughout exposure to KA in juvenile neurones, but that in juvenile neurones it started to fall markedly after about 10 min and was actually ~5% below control by 15 min. This may suggest that KARs at this stage of development in LV are more susceptible to desensitisation compared to the older animals. Repeating the experiment in the presence of concanavalin a, a ligand which prevents desensitisation of glutamate receptors, could clarify this possibility.

Interestingly, KA induced an increase in the amplitude of sIPSCs in LV, and percentage wise, the change was similar in neonatal (+74.9%) and juvenile (+75.3%). Likewise, the decay time of sIPSCs was increased in neonatal LV (+ 30%) juvenile (+88.6%) neurones but to a much greater extent in the latter. These effects contrast with complete lack of change in either parameter in LII neonates.

In neonate LV UBP-310 substantially reversed the increased amplitude seen with KA, abolished the increase in amplitude but only weakly affected decay time. Similar effects were seen in the neonates with amplitude and decay, but because of decline in frequency back to baseline it was not possible to assess the effect of UBP on this parameter.

6.3.5.2 Developmental differences in the effects of ATPA

Comparison of changes to sIPSCs induce by ATPA in neonatal and juvenile LII neurones is summarised in Fig. 6.9. ATPA (100 nM) had no effect on sIPSCs in either age group. At 500 nM it also failed to alter any parameter of sIPSCs in the juvenile animals but, in complete contrast, greatly increased the frequency in neonatal neurones by over +480 % of control. An increase in the amplitude (+57 %) of sIPSCs in neonatal neurones accompanied the increased frequency. Additionally, the mean decay time of sIPSCs increased by +95 % in neonatal neurones
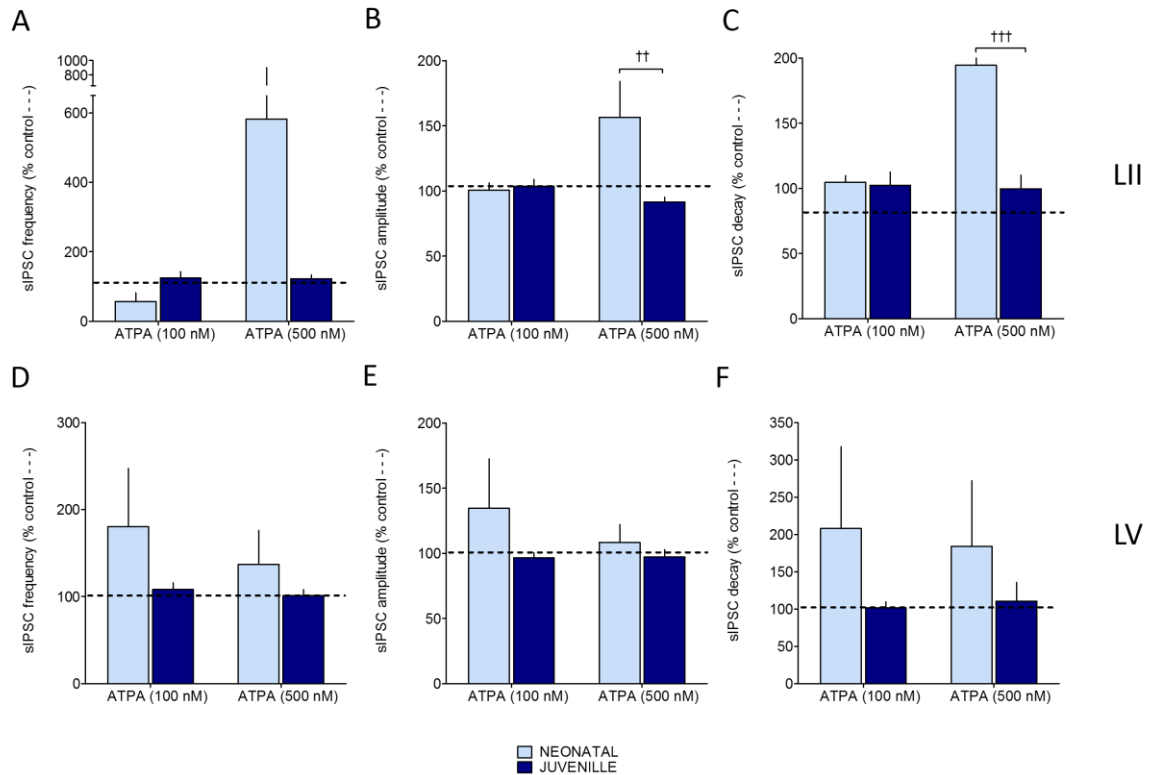
Figure 6.9: Comparative change in sIPSCs with ATPA (100 &500 nM) in neonate and juvenile neurones. (A&D) *Mean sIPSC percentage change in frequency,* ***(B&E)*** *amplitude and* ***(C&F)*** *decay time data from 3 neonate and 4 juvenile principal neurones from LII, and 4 neonate and 8 juvenile principal neurones from LV, MEC. Note the different effects of ATPA in neonatal versus juvenile sIPSCs. *, # and † denote significant differences between: * juvenile % change vs control (100 %, dashed line), # neonatal % change vs control (100 %, dashed line), and † juvenile % change vs neonatal % change.*

These results suggest a developmental difference in the ability of ATPA to modulate GABA release in LII MEC. This could reflect a developmental downregulation of interneurones expressing KARs containing the GluK1 subunit, or of the excitatory drive onto interneurones, perhaps via receptor internalisation, differential expression of interneurone subtypes or alterations in the synaptic connectivity via pruning mechanisms. The results also suggest that it is possible for GluK1 receptors to activate GABA release in the neonates, possibly by exciting interneurones that are normally silent, but it is difficult to match this with the lack of effect of KA. One speculative possibility that the receptor subunit composition or variant present at P8-11 has a high affinity for ATPA but a low affinity for KA, and with development to the juvenile stage this switches to an isoform with the reverse affinities.

Fig. 6.9 also presents the comparison of the changes to sIPSC activity in neurones in LV. sIPSCs in juvenile animals showed no change in any parameter with ATPA at either 100 or 500 nM. However, in neonatal neurones a +80% increase in frequency was seen with 100 nM although this declined to +37%. This contrasts slightly with LII where in the same age group 100 nM was ineffective but 500 nM evoked a large response. Nevertheless, it does show that GluK1 receptors may be involved in modulating GABA transmission in both layers, albeit weakly, at an early age.

ATPA also changed the amplitude of sIPSCs in neonatal neurones, increasing it by ~35% at 100 nM. Like the frequency, this was not sustained with the higher concentration where it returned to control levels. A similar pattern was evident with decay time, with an increase of +108% at 100 nM and a smaller but still substantial increase at 500 nM +84%. The decline in effect of ATPA at high concentrations again could indicate that the receptor responsible, whilst likely to contain the GluK1 subunit, undergoes substantial desensitisation. This could be verified by additional experiments using concavanalin a.

6.3.5.3 Developmental differences in the effects of UBP-310

Unfortunately, due to time restaints, experiments on the effects of UBP-310 on inhibitory transmission in neonatal LII were not completed, so I can only compare changes in LV. These are summarised in Fig. 6.10. UBP-310 had no effect on the frequency, amplitude, or decay time in either age group, suggesting that GluK1 receptors are not involved in maintaining tonic GABA release in juveniles or adults.

The responses to the additional application of KA in the presence of UBP were intriguing. KA actually decreased the frequency of sIPSCs in neonatal neurones by - 48.3 ± 11.2 % of control in the neonatal group and this was accompanied by a decline in decay time (-48.25 ± 11.2 %) but not amplitude. In complete contrast, in juvenile neurones, KA plus UBP-310 induced a clear increase in frequency (+107.5 ± 78.7 %) with an elevation of decay time (+73.2 ± 31.6), but again no amplitude change. These results could suggest that a non-GluK1 containing KAR may be acting to depress GABA release onto neonatal neurones and facilitate release onto juvenile principal neurones. This intriguing and exciting finding awaits further detailed examination, and comparison with other layers of the MEC.
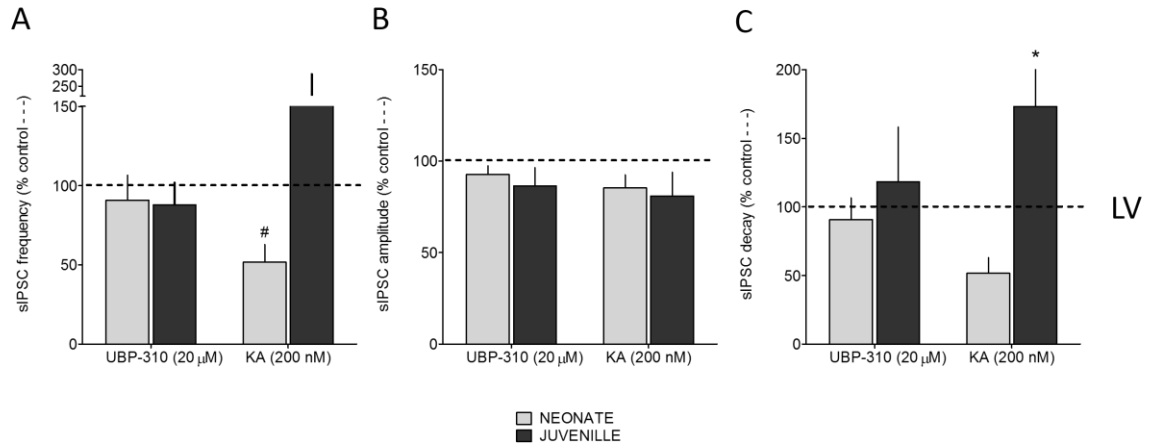
Figure 6.10: Comparative change in sIPSC activity with UBP-310 (20 μM) and KA (200 nM) in neonate and juvenile neurones. (A) Mean sIPSC percentage change in frequency, *(B)* amplitude, *(C)* decay time and *(D)* holding current of sIPSCs recorded from 4 neonate and 4 juvenile principal neurones from LII MEC (top), and from 3 neonate and 5 juvenile principal neurones from LV MEC (bottom). UBP-310 had no effect on sIPSCs in both age groups, but addition of KA induced opposite effects. *, # and † denote significant differences between: * juvenile % change vs control (100 %, dashed line), # neonatal % change vs control (100 %, dashed line), † juvenile % change vs neonatal % change.
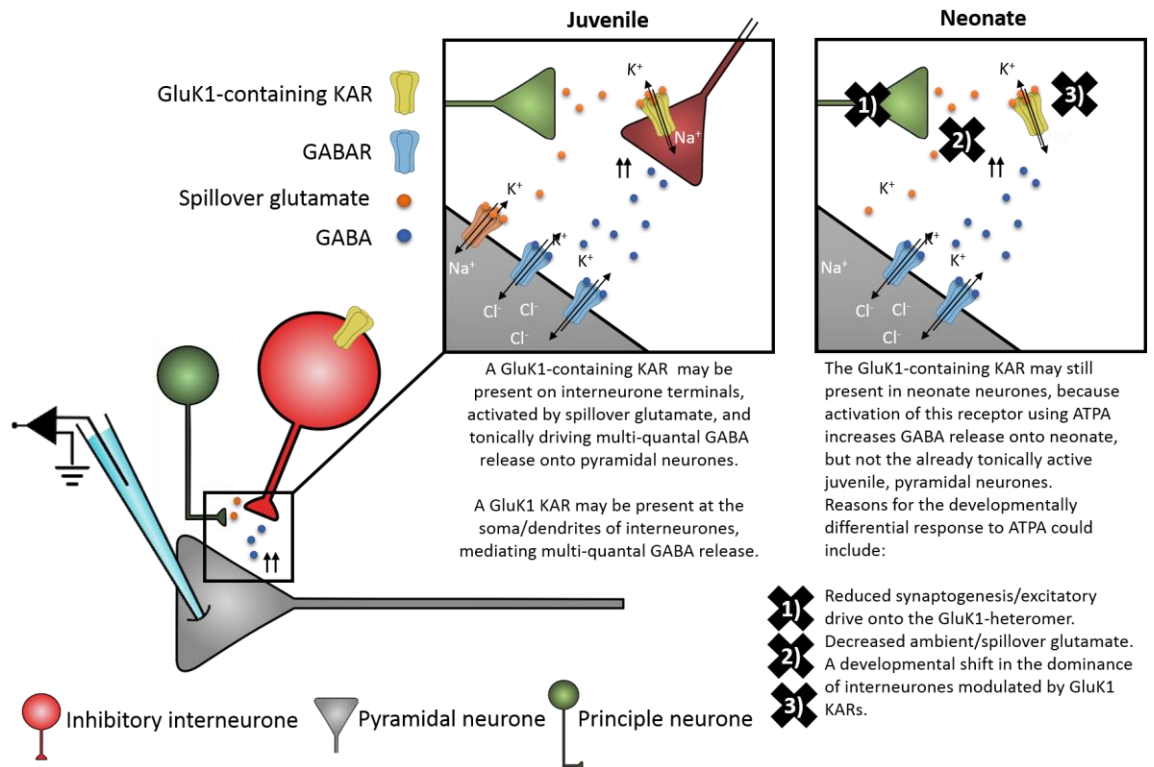
Figure 6.11: Summary of the suspected location of KARs at inhibitory synapses in LII and LV MEC. *A clear difference in GABA release in response to ATPA was noted between neonate and juvenile sIPSCs. ATPA increased the frequency of sIPSCs in neonate, but had no effect on juvenile, sIPSCs. This would suggest a population of interneurones driven by the GluK1 KAR are being activated in the neonate which may already be tonically active in the juvenile neurones. In addition, the effects of KA on sIPSCs in juvenile neurones would support the presence of a GluK1-containing KAR on the soma/dendrites (Frerking et al., 1999) or even the axon of interneurones (Semyanov and Kullmann, 2001), like in the hippocampus.*

6.4.3 Summary of findings

The suggested locations of KARs mediating inhibitory neurotransmission in the MEC are summarised in Fig. 6.11.

1) A presynaptic GluK1-containing KAR may be present on interneurones, acting to tonically facilitate GABA release onto principal neurones by activation by spillover of glutamate.

2) A KAR is likely located at the soma/dendrites of interneurones, mediating multi-quantal release of GABA onto principal neurones

3) The interplay between KARs located on both principal cells and interneurones allow the generation of synchronised neuronal activity.

6.4 Discussion

The aim of this Chapter was to determine the roles of KARs in mediating inhibitory neurotransmission in LII and LV MEC, and to identify any developmental differences in this activity in neonate (P8-11) and juvenile (P20-27) neurones.

As in the previous Chapter, interpretation of results are made more difficult considering the plethora of KARs located pre- and postsynaptically where they can both facilitate and depress excitatory and inhibitory neurotransmission (Cossart et al., 2001, Contractor et al., 2001, Semyanov and Kullmann, 2001). Moreover, the current lack of pharmacological specificity of agonists and antagonists confounds scrutiny between KAR subunits. Together with data from Chapter 5 I will discuss the findings and identify potential scenarios accounting for KAR modulation of inhibitory neurotransmission, firstly in the juvenile MEC, followed by an explanation of the clear developmental differences in KAR function at GABAergic synapses.

6.4.1 Presynaptic GluK1-containing KARs facilitate GABA release via spillover mechanisms

From the results in Chapter 5 I suggested that a GluK1-containing KAR was present pre-synaptically at glutamatergic synapses onto principal neurones, which had a very high level of tonic activity contributing to ~50% of spontaneous glutamate release. Here, when this receptor is blocked, there appeared to be a consistent decrease in the amplitude of sIPSCs across both layers and in both age groups. This may suggest that GluK1-containing KARs are also tonically active on GABAergic terminals and activated by spillover from glutamate synapses, which has been shown to occur in other brain regions (Jiang et al., 2001, Binns et al., 2003). This tonic effect may result in synchronised multi-quantal GABA release onto the principal neurones. When the heteroreceptors are blocked, there is decrease in multi-

quantal, spontaneous GABA release, but the more frequent mono-quantal release is unaffected, and so the overall amplitude and frequency of inhibitory events is only decreased slightly.

Next, KA induced a significant increase in the frequency and amplitude of sIPSCs recorded in LII and LV juvenile neurones, though to a much larger extent in LII, which may reflect the increased inhibitory tone in the superficial relative to the layers as shown in chapter 4 and in previous studies (Greenhill et al., 2014, Jones and Woodhall, 2005, Woodhall et al., 2005). In Chapter 5, we suggested the presence of a postsynaptic non-GluK1 containing KAR mediating the effects of KA, therefore the large increase in sIPSCs may be driven by excitatory connections onto interneurones, which increase summation of sIPSCs. Once again, further addition of UBP-310 appears to somewhat reduce the effects of KA. The small reduction in frequency and amplitude may reflect a reduction in on-going facilitation of GABA release mediated by spillover glutamate to nearby inhibitory synapses. On the other hand, it is possible that KAR containing the GluK1 subunit are located directly on the soma/dendrites of interneurones, driving GABA release.

Lastly, in juvenile neurones, ATPA had no effect on GABA release onto principal neurones, except for one neurone. As previously mentioned, this neurone had much higher baseline frequency to the other neurones in the data set, so may reflect a different type of principal neurone. Nevertheless, this may shine light on the developmental differences in response to ATPA discussed in the next section.

Taken together, these results suggest there may be a GluK1-containing KAR facilitating GABA release at interneurone terminals, which can be tonically activated by spillover of glutamate from nearby excitatory synapses. It is probable that KARs are also located on the soma/dendrites of interneurones, as in other brain regions (Mulle et al., 2000, Cossart et al., 1998, Cossart et al., 2001), including the adjacent LIII MEC (Chamberlain, 2009, Chamberlain et al., 2012), however further experiments will need to be done to establish their location.

6.4.2 Developmental differences in KAR function at GABAergic synapses

In LII, the effects of KA in neonate neurones was virtually non-existent (+51.1 ± 76.0%) compared to in juvenile neurones (+479.2 ± 223.5%). In juveniles, the huge increase in frequency was accompanied by increases in both amplitude and decay time, suggesting the increase in GABA release may be a network driven action potential dependent effect. The lack of such changes in the neonate neurones strongly suggests that excitatory synapses onto interneurones are underdeveloped, not connected or non-functional. Alternatively, this could reflect a reduced expression of KARs at this stage of development, though KA still caused a small, increase in glutamate release at excitatory synapses at the same age, indicating their presence, at least at excitatory synapses.

There were also clear lamina differences in response to KA, with LV exhibiting a greater response to KA (+120%) compared to LII (+51%) in neonate neurones, which was accompanied by an increase in amplitude. This may suggest that, unlike in LII, excitatory to inhibitory connectivity is more established, and can provide the excitatory drive mediating synchronised GABA release from interneurones.

By far the most compelling developmental difference in KAR function between the two age groups was the effects of ATPA, which induced a substantial increase in the frequency of GABA release onto principal neurones in both layers of neonatal MEC, but had no effect on the frequency of sIPSCs in juvenile neurones. The fact that ATPA had no effect on, or slightly decreased, glutamate release in the previous chapter strongly suggests the GluK1-containing KAR mediating the increase in GABA release are located directly on interneurones. Indeed, KARs have been previously shown to be located on interneurones in the hippocampus, located at directly on the axons (Semyanov and Kullmann, 2001), at the terminals and the soma/dendrites (Cossart et al., 2001, Daw et al., 2010).

These results suggest a developmental difference in the ability of ATPA to modulate GABA release the superficial and deep layers of the MEC. This could reflect a developmental downregulation of interneurones expressing KARs containing the GluK1 subunit, or in the excitatory drive onto interneurones, perhaps via receptor internalisation, differential expression of interneurone subtypes or alterations in the synaptic connectivity via pruning

mechanisms. The results suggest that it is possible for GluK1 receptors to activate GABA release in the neonates, possibly by exciting interneurones that are normally silent, but these results are confounded by the reduced effect of KA in neonates. One possibility is that the receptor subunit composition or variant present at P8-11 has a high affinity for ATPA but a low affinity for KA, and with development to the juvenile stage this switches to an isoform with the reverse affinities. Or, perhaps, the intense effects of KA lead to receptor desensitisation, which appears to be happening at least in LV. Moreover, previous work in this laboratory has observed similar desensitising effects of KA in juvenile neurones using a higher concentration of KA (unpublished findings). A study by Maingret et al. (2005) looked at the role of KARs expressed in neonatal hippocampal interneurones, and found they modulated GABAergic neurotransmission using two distinct and opposing mechanisms, which were mediated by different populations of neurones. A presynaptic KAR at GABAergic terminals, acted to decrease release probability, and a somatodentric and axonal population of KARs powerfully up-regulated action-potential dependent sIPSCs (Maingret et al., 2005). A similar somatodentric/axonally located GluK1-containing KAR may be mediating the effects of ATPA in neonate neurones here, especially considering the large increases in frequency, amplitude and decay time, which may reflect the activation of a population of interneurones that were previously silent.

Either way, it is clear there are developmental differences in the GluK1-containing KAR function between the two age groups. As previously mentioned, preliminary work in Professor Elek Molnar's lab showed changes in GluK1-containing KAR expression during development, and it appeared there was a peak in expression in the MEC at ~P14. Perhaps one way to account for these results is that there is a transient increase in the expression of GluK1-containing KARs, around the age of the neonate group (P8-11). The expression of these KARs on interneurones may still exist in juvenile neurones, but to a lesser degree, and may also have a degree of tonic activity so that ATPA has a reduced effect (1/7 cells responded to ATPA in juvenile). Perhaps KARs located on interneurones require a larger stimulus, considering that only 500, and not 100 nM, was effective. Indeed, KARs in other brain regions have a frequency dependence, such that the response of the receptor depends on the frequency of stimulation (Kidd and Isaac, 1999, Kidd et al., 2002).

The mechanisms underlying the differences in GluK1-containing KAR activity are still up for debate, but the idea there may be a transient increase in expression of KARs located directly on interneurones gives potential for a developmental period in which KARs can mediate intense synchronised activity within the MEC. This patterned and synchronised activity may be critical for plasticity, and could implicate KARs in activity-dependent fine-tuning and maturation of synapses, during which some synapses are strengthened and others eliminated (Clarke et al., 2014, Lauri and Taira, 2012, Lauri et al., 2003, Lauri et al., 2006).

Chapter 7

Developmental profile of kainic acid-induced oscillatory activity in the MEC

7.1 Introduction

In the previous chapters of this thesis I have detailed the characteristics of glutamatergic excitatory and GABAergic inhibitory transmission in the MEC using spontaneous synaptic currents as a model for transmission, and compared the deep and superficial layers. I have examined how KAR may be involved in modulating transmission in both layers and determined changes in baseline activity and KAR modulation with development. In this chapter I want to explore the contribution of excitatory and inhibitory transmission to synchronised oscillatory activity, focussing on the role of KAR in initiating such activity during early development.

Synchronised neuronal oscillations in the gamma frequency band (30-80 Hz) are fundamental for many higher order cognitive processes, and can be seen throughout the cortex (Singer and Gray, 1995, Fries, 2005, Whittington et al., 2011, Buzsáki and Wang, 2012). It is thought that such activity has the ability to link the activity of single neurones that fire synchronously in an assembly to the nature of a sensory stimulus. The synchronised response to sensory input allows communication between both spatially distributed and regional populations of neurones, which is thought to underlie aspects of cognition specific to the brain region in which they reside. The MEC is critically important in both spatial and memory processes (Coutureau and Di Scala, 2009, Schultz et al., 2015), and early cortical changes in GFO have been identified in neurological disorders, such as AD, where deficits in these aspects of cognition is an early and severe consequence of the disorder (Klein et al., 2016, Verghese et al., 2017, Allison et al., 2016, Vlček, 2011, Vlcek and Laczo, 2014).

Much evidence implicates inhibitory mechanisms in the generation of GFO, specifically through the action of fast-spiking perisomatic parvalbumin-containing basket interneurones (Buhl et al., 1998, Fisahn et al., 1998, Whittington et al., 2011). Basket interneurones provide a temporal structure that can entrain firing patterns and generate synchronous IPSPs in neighbouring neurones (Whittington et al., 1995, Traub et al., 1996a, Wang and Buzsaki, 1996). GFO have been described in many brain regions *in vivo*, including the neocortex (Gray et al., 1989, Sirota et al., 2008), hippocampus (Buzsaki et al., 1983,

Bragin et al., 1995), striatum (Berke et al., 2004), amongst other areas, but most importantly, the MEC (Chrobak and Buzsaki, 1998). Common to all of these areas is the presence of dense inhibitory innervation and its associated GABA$_A$R-mediated synaptic transmission.

Previous work has indicated that GFO arise by two main mechanisms, although these are necessarily interrelated (for more detail, see Chapter 1). Interneurone network gamma, or ING relies solely on the excitation of inhibitory neurones. In this model, GFO are mediated by GABA$_A$Rs and gap junctions (Traub et al., 2001) between interneurones, which are pharmacologically disconnected from principal neurones by blockade of ionotropic glutamate receptors (Whittington et al., 1995). Pyramidal-interneurone network gamma, or PING, as its name suggests, involves a network containing populations of excitatory, as well as inhibitory, neurones, which are reciprocally connected to each other (Wilson and Cowan, 1972, Whittington et al., 2000).

GFO can also be reliably induced in *in vitro* slice preparations either transiently, via electrical stimulation (Traub et al., 1996a, Whittington et al., 1997a), or persistently, via chemical activation of muscarinic receptors (Whittington et al., 1995), the cholinergic pathway (Traub et al., 2000, Van Der Linden et al., 1999) or KARs (Buhl et al., 1998, Cunningham et al., 2003), the latter being the focus of this chapter. These models generate synchronised gamma activity with underlying properties that are mechanistically different and specific to the brain region in which they are induced, but crucially, all induction protocols for GFO require intact inhibitory neurotransmission. The time-course of the IPSPs is key to setting the frequency of GFOs (Whittington et al., 1995, Traub et al., 1996a), and blocking GABA$_A$Rs abolishes rhythmic activity (Buhl et al., 1998, Fisahn et al., 1998).

GFO can be generated in the MEC *in vitro* by KA (Cunningham et al., 2003). Computational and experimental studies using knock-out mice suggest that KA is able to generate oscillatory activity due to the interplay of KARs containing the GluK1 subunit directly on the axons of interneurones (Semyanov and Kullmann, 2001), and KARs containing the GluK2-subunit, likely located in the somatodendritic region of both interneurones and pyramidal neurones in the hippocampus (Fisahn et al., 2004). Mechanisms underlying the ability of

KA to induce KA-O are less understood in the MEC, but the GluK1-containing KAR appears to be critically important for GFO generation and maintenance (Stanger et al., 2008). This observation was not replicated in the hippocampus (Brown et al., 2006), emphasising the mechanisms underlying KA-O are likely influenced by the regional specific neuronal architecture supporting the rhythm.

The balance between inhibitory and excitatory transmission differs across layers of the EC (Jones, 1993; Berretta and Jones, 1996; Woodhall et al., 2005; Woodhall and Jones, 2006; Greenhill et al., 2014). The data in this thesis have considerably extended this distinction and shown that there developmental changes to this balance and differential effects of KAR in modulating this balance, which also change with development. It is also the case that there is a lamina specific susceptibility to generation of GFO in the MEC (Cunningham et al., 2003) and other forms of oscillations (Cunningham et al., 2006b) with superficial layers (LII and LIII) being more likely to generate oscillatory activity than the deeper layers.

In this chapter, I have used examined the characteristics of KA-O in LII and LV and used these oscillations to follow changes in the contribution of KAR activity to network synchrony during development in the MEC. Unpublished work from Professor Elek Molnar's laboratory at the University of Bristol (see Fig. 1.6 in Chapter 1) has shown changes in KAR expression during development, particularly a distinct increase in the expression of KARs containing the GluK-1 containing subunit at around P14. It seems likely that changes in KAR expression during development will influence the ability of the network to engage in or generate synchronised activity.

As mentioned, KA-O are dependent on inhibitory neurotransmission which undergoes significant changes during development, as addressed in Chapter 4. In LII, the overall inhibitory tone increases 8-fold between the neonatal (P 8-11) and juvenile (P 20-27) age groups, compared to a 5-fold increase in LV. In addition, in Chapter 6 I showed that KAR activation had a reduced effect on the modulation of inhibitory neurotransmission in neonate versus juvenile MEC. Therefore the balance between inhibition and excitation (Chapters 3 and 4), age-related changes in EPSCs and IPSPs (determined in Chapters 5 and

6), and the differences in the expression of KARs observed during development (Molnar et al. unpublished), may inform the interpretation of the developmental changes in KA-O.

What is interesting about using KA to induce GFO is that it mimics both physiological and pathological manifestations of neuronal activity, such that small concentrations of KA can induce GFO, but high concentrations can induce epileptogenic activity. This poses a potential role for KARs in the generation of synchronised oscillatory activity and in the development of epilepsy and other disorders of synchrony. It is of great interest to understand the development of both GFO and the contribution of KARs to this activity.

Therefore, the main aims of this chapter were to:

1) Determine a developmental profile of KA-O in LII and LV, which would act as a reporter of KAR involvement in synchronised neuronal network activity.
2) Identify developmental changes in the contribution of GABAergic and glutamatergic neurotransmission to KA-O in LII and LV.
3) Draw conclusions about the changes in inhibitory neurotransmission in previous chapters and changes to KA-O during development.

7.2 Methods

All experiments described in this chapter were conducted using MEC-hippocampal slices (400 µM) obtained from male or female Wistar rats aged P8-27. Slices were maintained in an interface chamber as described in Chapter 2. Dual extracellular LFP recordings were made from LII and LV MEC of the same slice. Drugs were recirculated via a reservoir system. Numbers of observations (n) in these studies reflect the number of slices. Mean values for frequency and amplitude were determined and compared between different age groups using the non-parametric Mann Whitney test as data are not normally distributed. Two-way ANOVA analysis was used when comparing groups that were influenced by two different independent variables (e.g. time and age). When comparing before and after effects of a drug on oscillatory activity, a paired t-test or a repeated measures ANOVA (rANOVA) was used. When comparing oscillatory activity within LII and LV MEC of the same

slice, a non-parametric, paired Wilcoxon signed rank test was used. Statistical significance was reached if P < 0.05.

Control recordings of baseline activity were made for at least 20 min prior to the addition of any pharmacological agents to ensure the oscillatory activity was a result KAR activation, and not spontaneous network activity. Oscillatory activity was induced by perfusion with KA (400 nM) bath applied via the circulating reservoir of ACSF. One-minute epochs of activity were recorded at 15 min intervals during the establishment and maintenance of oscillatory activity, and analysed immediately for amplitude and frequency. Drug treatments were only applied when the oscillatory activity had stabilised i.e. the amplitude and frequency was within 15 % variability in 3 consecutive recordings.

7.3 Results

7.3.1 Generation of GFO in the juvenile rat MEC

Cunningham et al. (2003) first demonstrated that that GFO could be induced by KAR activation in the MEC. They showed that the power of GFO peaked in LII/LIII and was considerably less in LV/VI. In superficial layers there was a medial *vs* lateral gradient with power falling of abruptly at the MEC-LEC border. GFO in the MEC persisted independently of the hippocampus (Cunningham et al., 2003). We used LFP recordings from LII and LV to confirm that GFO could be reliably induced in the MEC of juvenile (P24-27) rats under our preparation and recording conditions.

LFP recordings were made simultaneously from LII and LV in the same slice. Bath perfusion of KA (400 nM) reliably generated rhythmic field activity in LII and LV in all slices studied in the P24-27 age group (n = 23). Activity in LII had a mean frequency of 31.7 ± 0.6 Hz and this was identical in LV (31.9 ± 0.6 Hz) However, the mean peak amplitude of activity in LII ($0.4 \pm 0.06 \ \mu V^2 /$ Hz) was about 10-fold that seen in LV ($0.05 \pm 0.01 \ \mu V^2 /$ Hz). In all slices, the amplitude of the GFO was greater in LII ($P < 0.0001$, Mann-Whitney test; n = 23), but there was no difference in the mean frequencies. Once initiated, KA-induced synchronised neuronal network activity persisted for 4-5 hours.
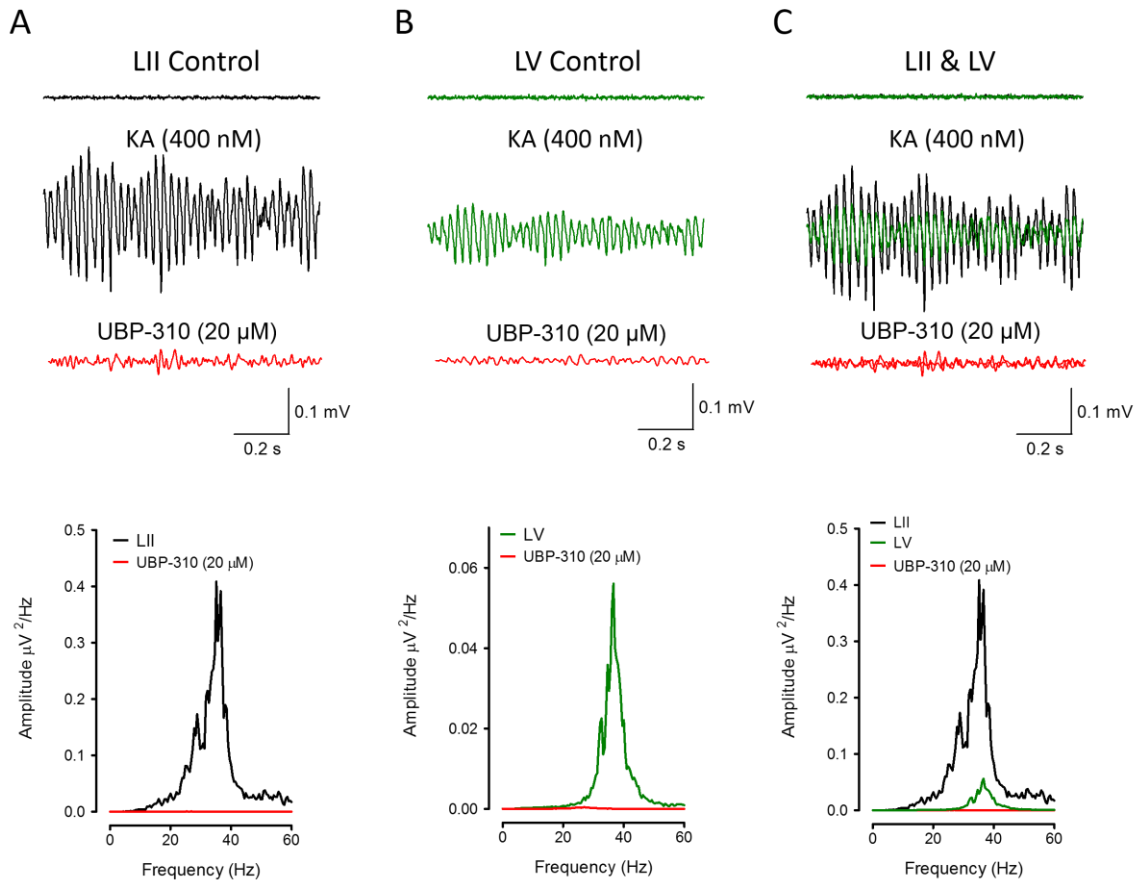
Figure 7.1: KA induced GFO in LII and LV of juvenile rats. 1 second example traces of extracellular activity (top) and example power spectra from 60 second epochs of raw data (bottom) before and after the application of KA (400 nM) in LII (**A:** black) and LV (**B:** green) of the same slice, and in the presence of 20 µM UBP-310 (red). **(C)** Overlay of activity in LII and LV. Gamma activity had a significantly larger amplitude in LII compared to LV, but the frequency of activity was the same activity was abolished in the presence of UBP-310.

7.3.2 Involvement of GluK1-containing KARs in KA-O

UBP-310, inhibited KA-O in both layers and at all ages (P8-27). KA-O were abolished in all slices tested, and there were no discernible differences at any age, therefore the data from all ages was grouped together. The results are shown in Fig. 7.1. UBP-310 (20 µM) decreased the mean amplitude of KA-Os by -94.5 % in LII. (P < 0.0001, rANOVA, n = 12). Likewise, in LV in the same slices, mean amplitude was decreased by 96.2 % in the presence of UBP-310, (P < 0.0001, rANOVA, n = 12). Although the mean frequency appears to decrease, this is mainly due to the abolition of a detectable peak.

Stanger et al. (2008) identified a role for the GluK1-containing KAR in KA-O in the MEC. They used another GluK1 antagonist (UBP-302) and the effect of this was less pronounced compared to the current experiments withUBP-310 (40 % reduction *vs* ~95 %). This may be related to the specificity of the antagonists used (UBP-302 *vs* UBP-310), or due to the age of the rats (adult >150g compared with neonatal and juvenile 10-100g). Unpublished immunohistochemical studies (Molnar, E, personal communication; see Fig. 1.6) showed a developmental decrease in the expression of the GluK1-containing KAR as animals progressed from juvenile state to adulthood. This may account for the increased sensitivity to blockade of this receptor in the younger rats. It should also be noted that Stanger et al., (2008) conducted their studies in LIII, so lamina differences in the function and expression of GluK1 (Greenhill et al., 2014, Chapters 5 and 6 in this thesis) could also contribute to differences between the results. In patch clamp studies I identified a tonic activation of the GluK1-containing KAR in LII and LV, which was not apparent in LIII (Chamberlain et al., 2012). This may have implications for the generation of GFO between layers.

7.3.3 Laminar comparison of KA-O during development

Having established that KA-O can be reliably generated in the juvenile MEC, and that they are dependent on the GluK1-containing KAR, a developmental profile was conducted. Rats' aged postnatal day 8 to 27 were separated into 5 age groups: P 8-11, P12-15, P16-19, P20-23 and P24-27. In total, data on KA-O in LII and LV was gathered from 236 slices from 118 P8-27 rats

7.3.3.1 Age P8-11

A summary of the results is shown in Fig. 7.2. Application of 400 nM KA induced KA-O in LII and LV of all slices tested (n = 39). Power spectra analysis showed KA-O in the P 8-11 group were characterised by mean peak frequencies in the beta range in both LII (17.8 ± 0.3 Hz) and LV (18.1 ± 0.4 Hz) MEC. At this stage, unlike in the juvenile P24-27 age group, the mean amplitude in LV (0.05 ± 0.01 μV^2 / Hz) was significantly higher than in LII (0.03 ± 0.001 μV^2 / Hz). The amplitude in LV exceeded that in LII in 82 % of slices tested (P = 0.003, Wilcoxon signed rank test; n = 39).
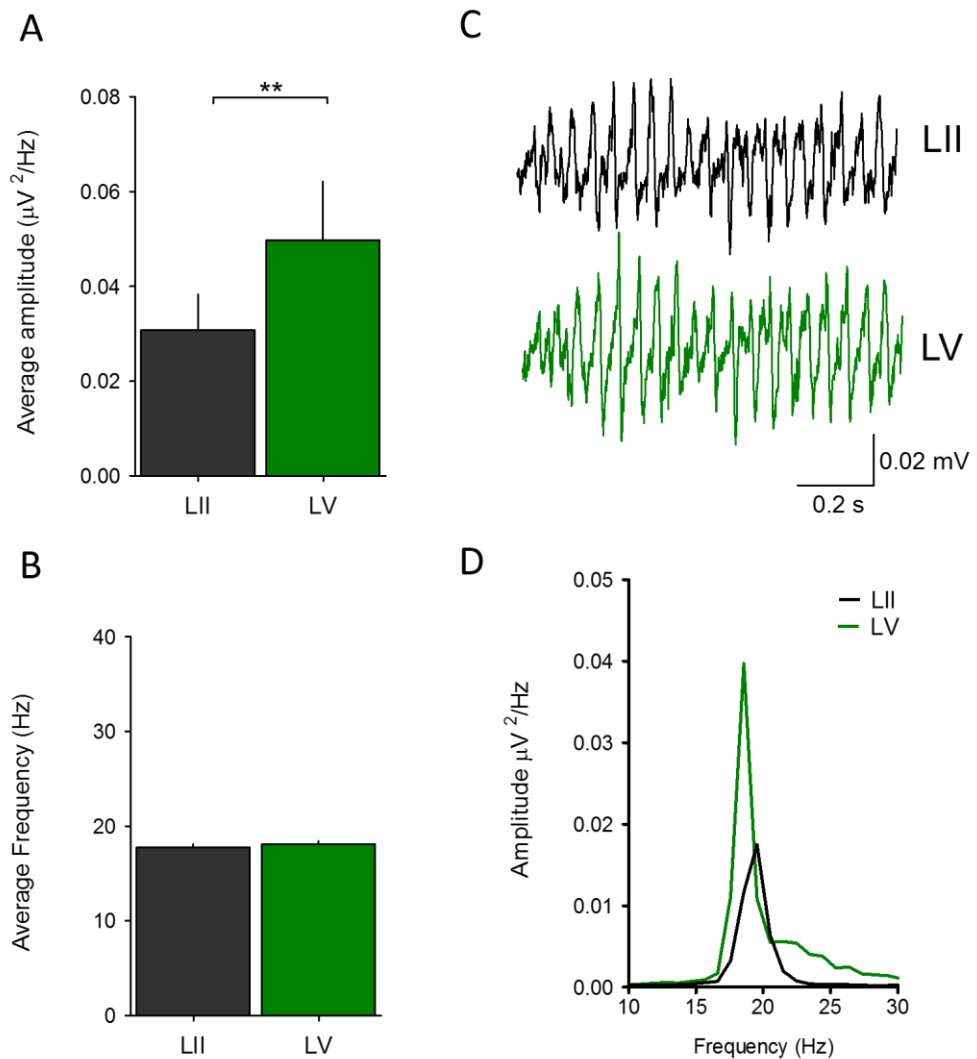
Figure 7.2: Lamina comparison of KA-O at P8-11. *Mean amplitude **(A)** and frequency **(B)** of KA-O induced by 400 nM KA in LII (black) and LV (green) of the same slice (n = 39). **(C)** 1 second example traces of LFP recordings in LII (black) and LV (green) in the presence of 400 nM KA. **(D)** Example power spectra produced from 60 second epochs of extracellular data showing KA-O induced in LII (black) and LV (green) of the same slice. The mean amplitude of KA-O was significantly larger in LV vs LII (P = 0.003, Wilcoxon signed rank test), but there was no difference in the mean frequency of KA-O between layers.*

7.3.3.2 Age P12-15

At P12-15, there was no significant difference in amplitude and LV had a slightly lower mean amplitude compared to LII. The mean amplitude of KA-Os in LII was 0.11 ± 0.03 μV^2 / Hz compared to 0.08 ± 0.01 μV^2 / Hz in LV. Despite this slight increase in the mean amplitude in LII compared to LV, the amplitude in LV still exceeded that of LII in 61 % of slices. Frequencies in both layers had increased slightly compared to P8-11, but there were still no statistically significant differences between them (LII 21.3 ± 0.7 Hz and LV 21.2 ± 0.7 Hz). The comparison of KA-O in P12-15 rats is summarised in figure 7.3.
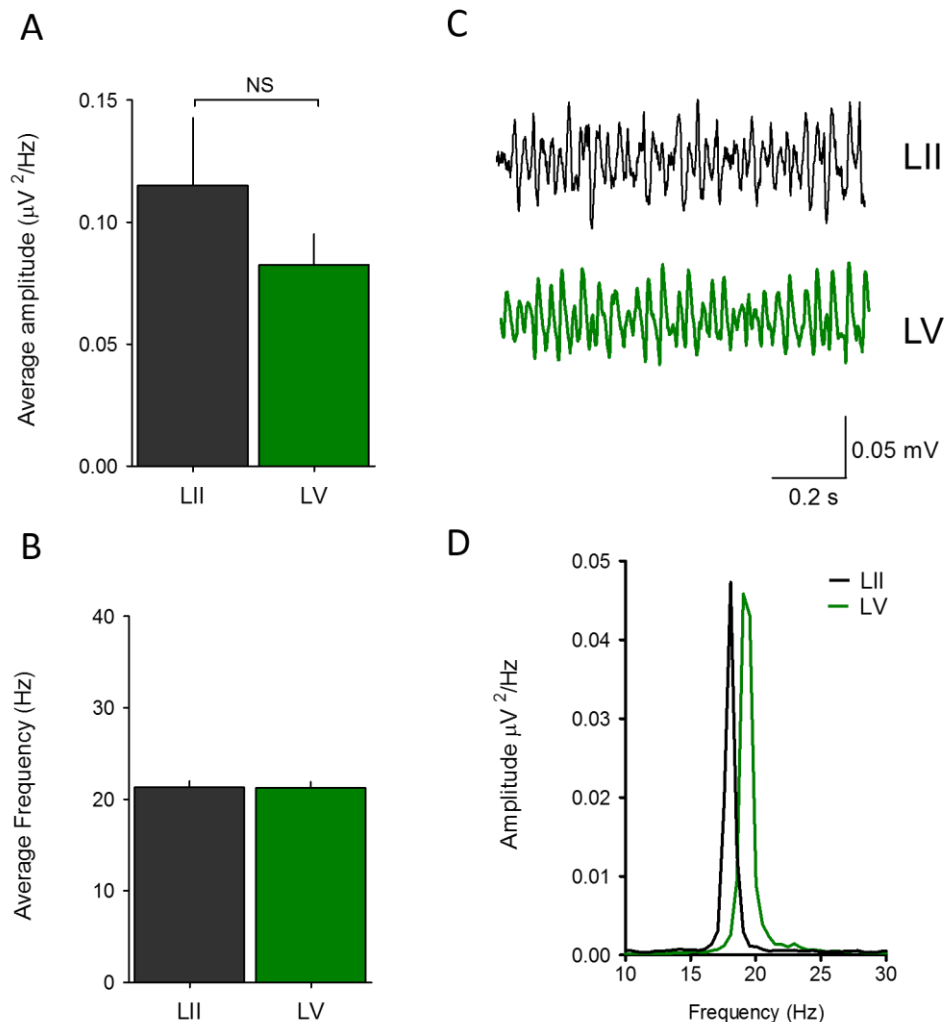
Figure 7.3: Lamina comparison of KA-O at P12-15. *Mean amplitude **(A)** and frequency **(B)** of KA-O induced by 400 nM KA in LII (black) and LV (green) of the same slice (n = 18). **(C)** 1 second example traces of LFP recordings in LII (black) and LV (green) in the presence of 400 nM KA. **(D)** Example power spectra produced from 60 second epochs of extracellular data showing KA-O induced in LII (black) and LV (green) of the same slice. There were no significant differences in the amplitude or frequency of KA-O at this stage of development.*

7.3.3.3 Age P16-19

Although, again, there were no lamina differences in the mean frequencies in LII (29.4 ± 0.7 Hz) and LV (29.2 ± 0.7 Hz) in P16-19 rats, there was a noticeable increase in mean frequency relative to the adjacent younger age group (P12-15). What was also now very clear was that the mean amplitude of KA-O was substantially and significantly higher in LII (0.19 ± 0.05 μV^2 / Hz) compared to in LV (0.03 ± 0.00 μV^2 / Hz) 23 slices (P < 0.0001, Wilcoxon signed rank test; n=23). This was reinforced by the fact that the amplitude in LII was larger than that in LV in 96 % (22/23) of slices. The difference between layers largely occurred through a substantial rise in amplitude in LII, whereas LV remained around the same level as the preceding age groups, regardless of the increase in frequency. The comparison of KA-O in rats aged P16-19 is summarised in figure 7.4.
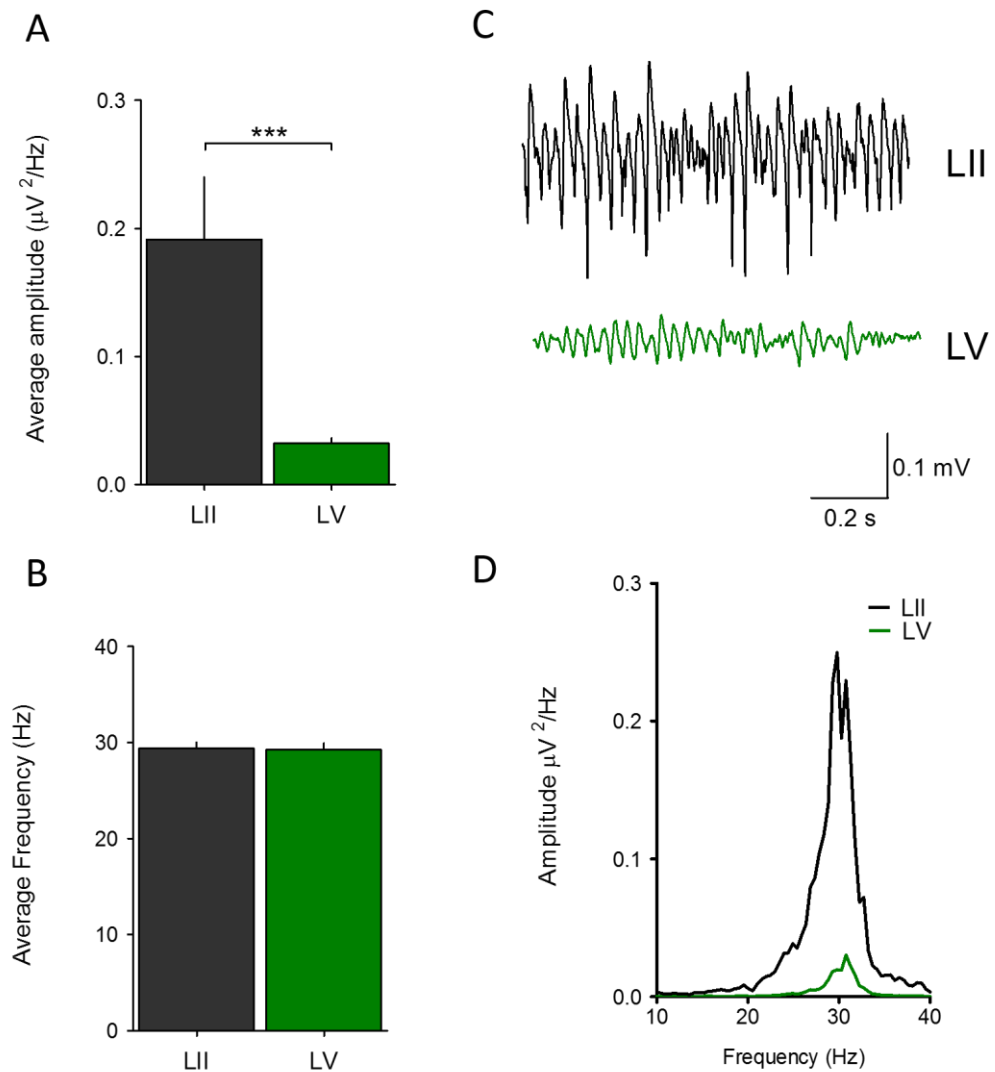
Figure 7.4: Lamina comparison of KA-O at P16-19. *Mean amplitude (A) and frequency (B) of KA-O induced by 400 nM KA in LII (black) and LV (green) of the same slice (n = 23). (C) 1 second example traces of LFP recordings in LII (black) and LV (green) in the presence of 400 nM KA. (D) Example power spectra produced from 60 second epochs of extracellular data showing KA-O induced in LII (black) and LV (green) of the same slice. The mean amplitude of KA-O was significantly larger in LII vs LII (P < 0.001, Wilcoxon signed rank test), but there was no difference in the mean frequency of KA-O between layers.*

7.3.3.4 Age P20-23

At 20-23 days old, the mean amplitude was again significantly and substantially larger in LII than LV. The difference was made more marked still by a further incremental increase in LII ($0.28 \pm 0.05 \ \mu V^2 / Hz$) compared to LV ($0.04 \pm 0.01 \ \mu V^2 / Hz$), the latter remaining largely

unchanged from the mean amplitude in younger age groups. The amplitude in LII was now larger than in LV in all slices tested (n = 14). Despite this, there were again no differences in the mean frequencies of KA-O in LII (30.9 ± 0.7 Hz) and LV (31.6 ± 0.8 Hz). The characteristics of KA-O in rats aged P20-23 is summarised in figure 7.5.
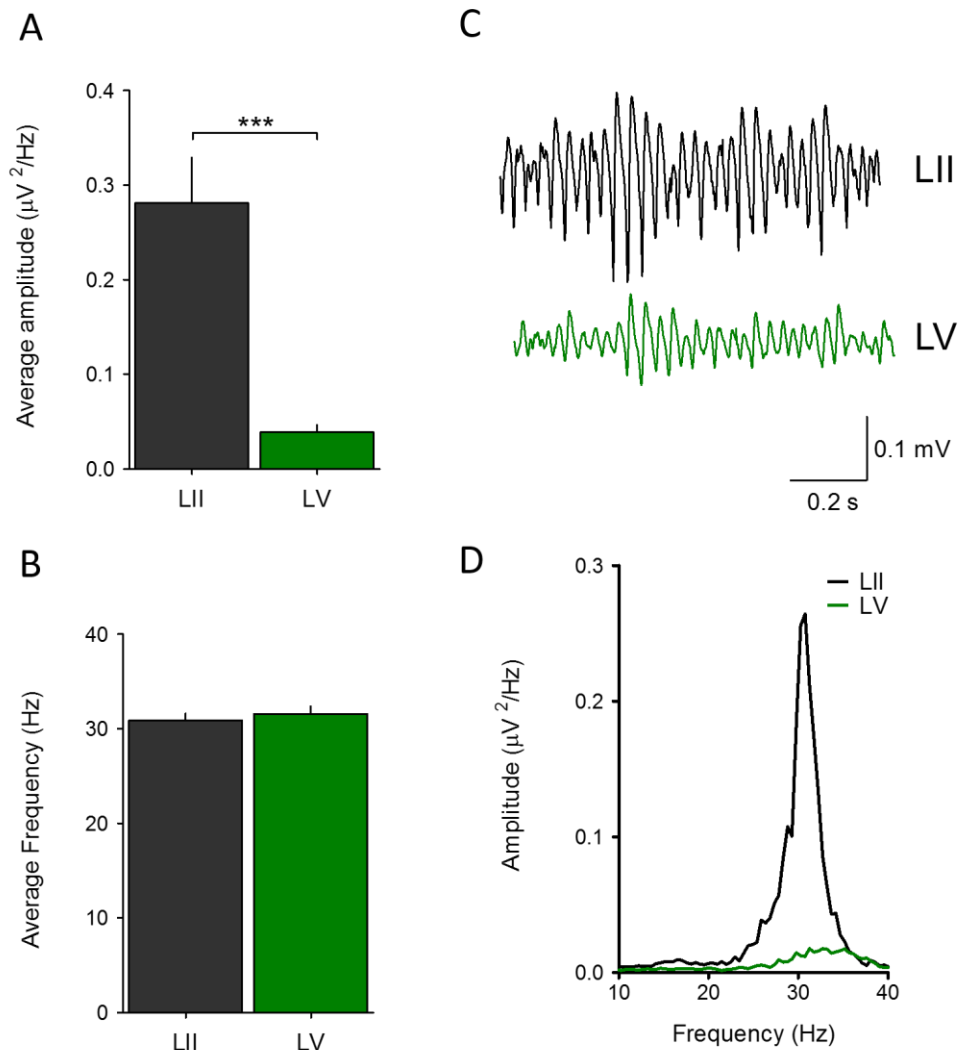
Figure 7.5: Lamina comparison of KA-O at P20-23. *Mean amplitude **(A)** and frequency **(B)** of KA-O induced by 400 nM KA in LII (black) and LV (green) of the same slice (n = 14). **(C)** 1 second example traces of LFP recordings in LII (black) and LV (green) in the presence of 400 nM KA. **(D)** Example power spectra produced from 60 second epochs of extracellular data showing KA-O induced in LII (black) and LV (green) of the same slice. The mean amplitude of KA-O was significantly larger in LII vs LII (P < 0.001, Wilcoxon signed rank test), but there was no difference in the mean frequency of KA-O between layers.*

7.3.3.5 Age P24-27

A comparison of KA-O in rats aged P24-27 is summarised in figure 7.6. In the oldest animals tested (n = 24), the mean amplitude continued to increase in LII with a slight increment in LV, and amplitude remained significantly larger in LII (0.4 ± 0.06 μV^2 / Hz) compared to LV (0.05 ± 0.01 μV^2 / Hz). As with previous findings, despite a clear age-dependent difference in amplitude, there were no statistically significant differences in the mean frequency of KA-O in LII (31.7 ± 0.6 Hz) and LV (31.9 ± 0.6 Hz) MEC.
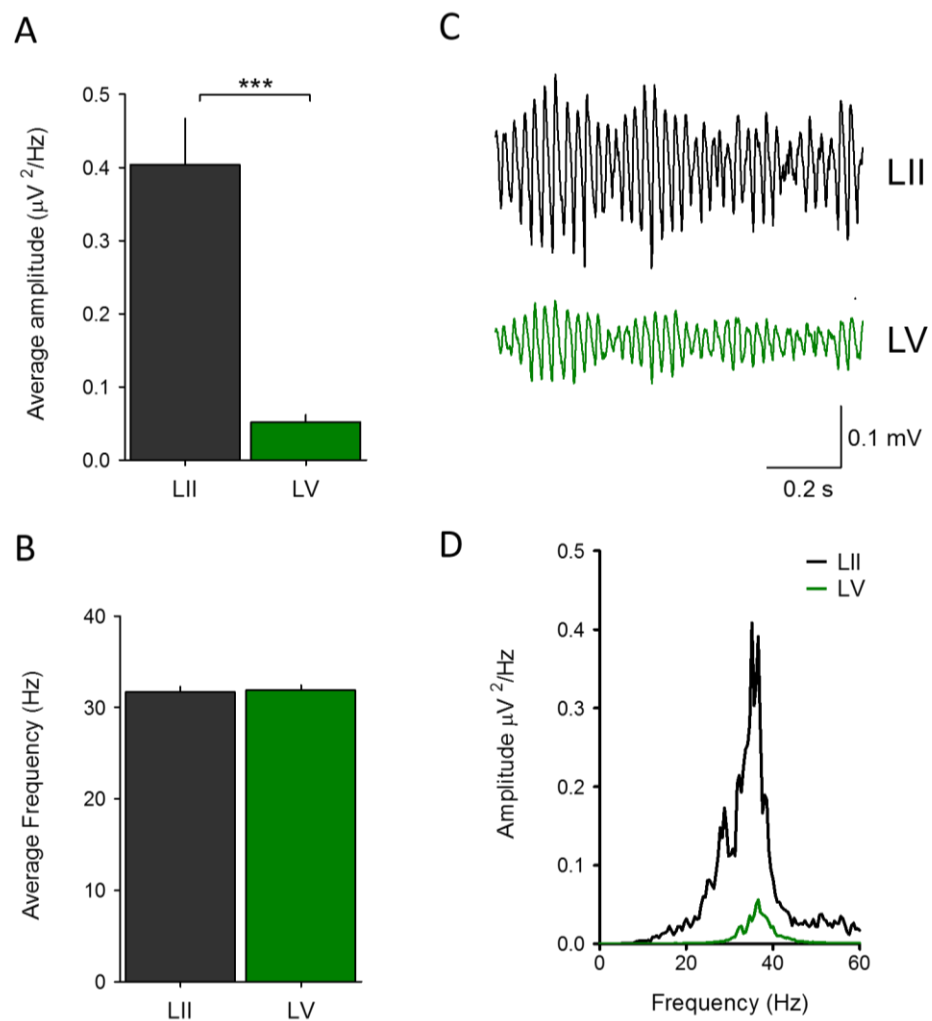
Figure 7.6: Lamina comparison of KA-O at P24-27. *Mean amplitude **(A)** and frequency **(B)** of KA-O induced by 400 nM KA in LII (black) and LV (green) of the same slice (n = 23). **(C)** 1 second example traces of LFP recordings in LII (black) and LV (green) in the presence of 400 nM KA. **(D)** Example power spectra produced from 60 second epochs of extracellular data showing KA-O induced in LII (black) and LV (green) of the same slice. The mean amplitude of KA-O was significantly larger in LII vs LII (P < 0.001, Wilcoxon signed rank test), but there was no difference in the mean frequency of KA-O between layers.*

7.3.4 Developmental profile of KA-O

The full comparison of the developmental changes in amplitude and frequency of KA-Os can be seen in figures 7.7 and 7.8.

When assessing the lamina differences with development it is obvious that there was a progressive and incremental age-dependent increase in the amplitude of KA-O generated in LII. This was just as clearly not seen in LV recorded in the same slices. LV followed a different developmental pattern. There was a small, but significant increase in the amplitude of KA-Os from P8-11 to P12-15 (P < 0.0001, Kruskal-Wallis test). However, this surge in the amplitude of KA-O in LV was a temporary change, and was reversed in the P16-19 group and actually decreased to a slightly smaller mean amplitude than in the P8-11 rats. It rose again marginally over the course of further development, but always remained at or slightly below the amplitude recorded at P8-11. It should be stressed that the amplitude in LV was relatively low throughout.

Despite the marked differences in amplitude, there were no lamina differences in the mean frequencies of KA-O in each age group, and a parallel age-dependent change in the frequency of KA-O was apparent in both layers. However, this was not a progressive incremental change, but rather a clear step increase was apparent between P12-15 and P16-19 age groups in both layers (P < 0.05, Kruskal-Wallis test). At this point, the KA-O in both layers switched from beta frequency to low gamma. Thereafter, frequency continued to increment marginally in both layers, but the changes were not dramatic.

These results show that there are clear developmental changes in KA-O in the MEC *in vitro.* An age-dependent step increase in frequency of KA-O occurs in both layers, but in LII this is accompanied by an incremental increase in KA-O amplitude which is not seen in LV, such that GFO in the MEC become dominated by activity in the superficial layer as development progresses.
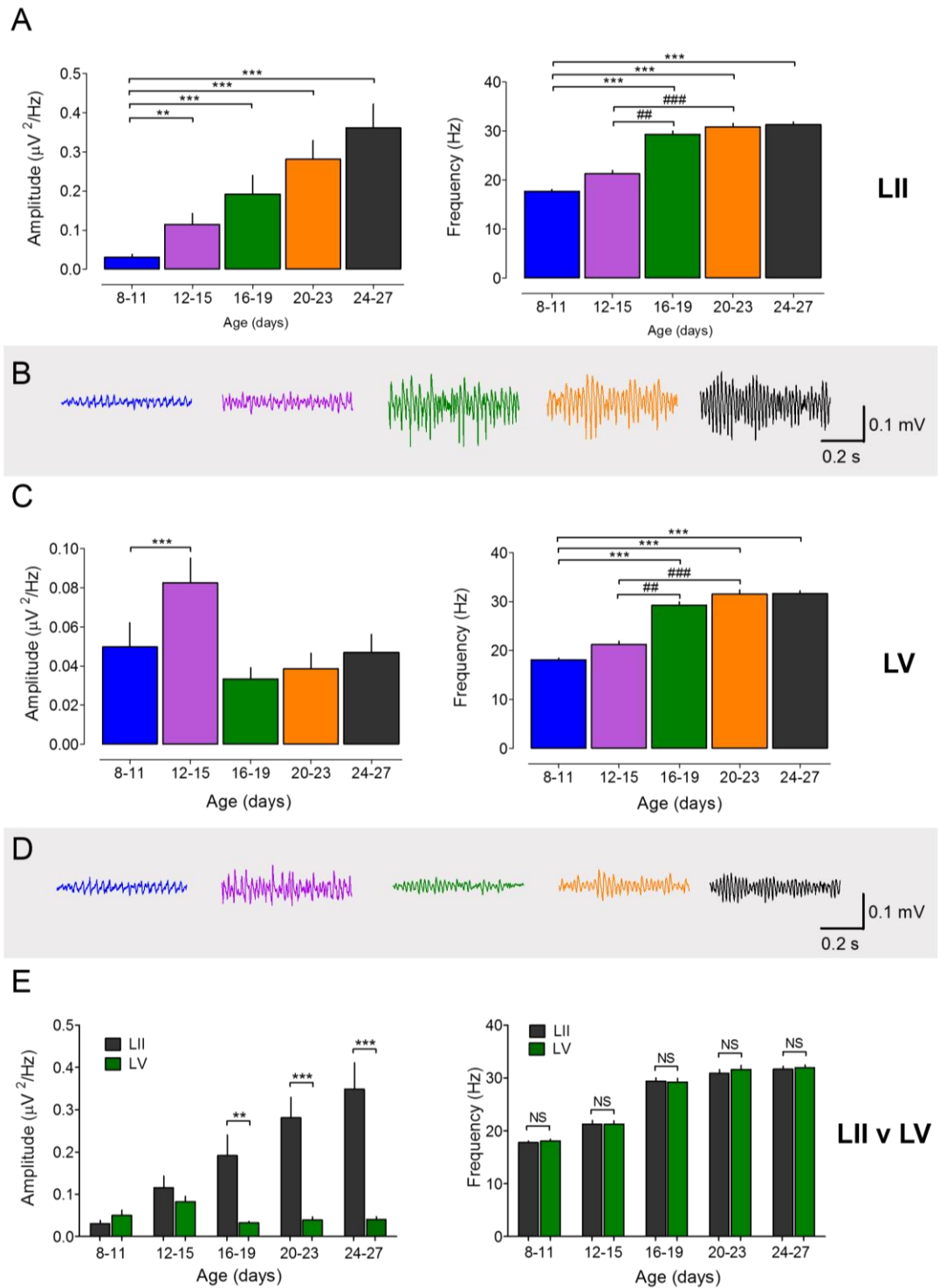
Figure 7.7: Developmental profile of KA-O in LII and LV at P8-27. *Bar charts showing the mean amplitude (left) and frequency (right) of KA-O in LII* ***(A)*** *and LV* ***(C)*** *from rats split into 5 age groups. KA-O show a gradual developmental increase in amplitude in LII but not in LV, and a stepwise increase in frequency from between P12-15 and P16-19 in both layers. **(B)** 1 second example traces of LFP recordings in LII and **(D)** LV, in the presence of 400 nM KA, from 5 age groups. **(E)** Laminar comparison of KA-O amplitude (left) and frequency (right) during postnatal development (P8-27).*
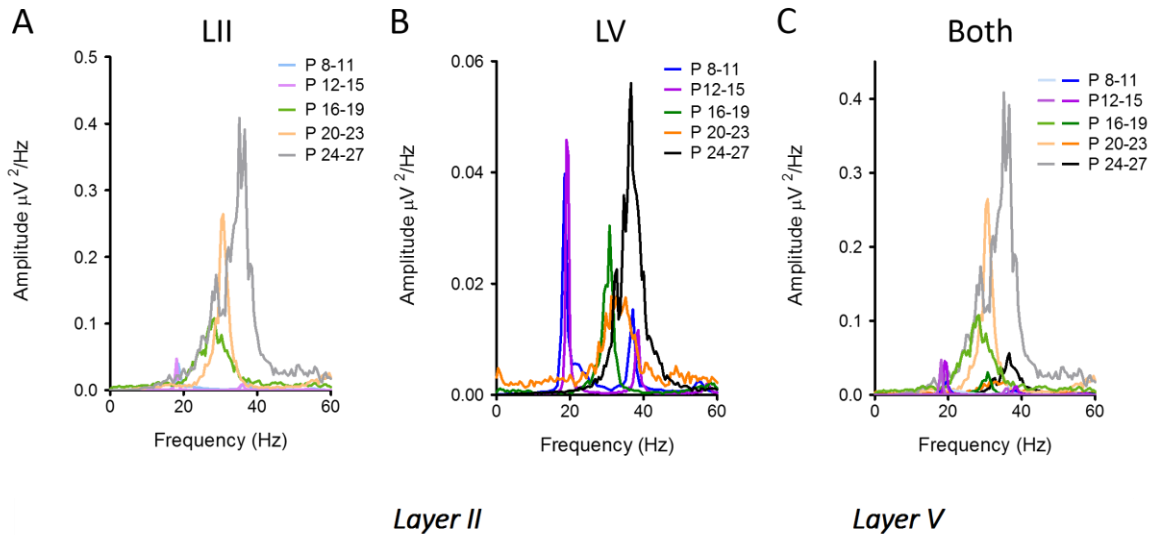
Age (days)	Layer II		Layer V	
	Amplitude (μV^2 / Hz)	Frequency (Hz)	Amplitude (μV^2 / Hz)	Frequency (Hz)
8-11 (n = 39)	0.03 ± 0.00	17.8 ± 0.3	0.05 ± 0.01	18.1 ± 0.4
12-15 (n = 18)	0.10 ± 0.03	21.3 ± 0.7	0.08 ± 0.01	21.2 ± 0.7
16-19 (n = 23)	0.19 ± 0.05	29.4 ± 0.7	0.03 ± 0.00	29.2 ± 0.7
20-23 (n = 14)	0.28 ± 0.05	30.9 ± 0.7	0.04 ± 0.01	31.6 ± 0.8
24-27 (n = 24)	0.40 ± 0.06	31.7 ± 0.6	0.05 ± 0.01	31.9 ± 0.6

*Figure 7.8: Summary of the development of KA-O. Top: Example power spectra from 60 second epochs of raw data from each age group in LII **(A)** and LV **(B)**. **(C)** Overlay of example power spectra from both layers. Note the larger amplitude in LII compared to in LV from P16 onwards. Bottom: Summary table of the mean amplitudes and frequencies of KA-O in LII and LV in all 5 age groups.*

7.3.5 Developmental changes to KA-O amplitude coincide with eye opening in LII

Looking at the developmental changes in KA-O above, it is clear that the major changes are occurring between the P12-15 and P16-19 age groups. A major life event that occurs during the former period is eye-opening, so I have conducted further detailed developmental analysis to examine the relationship between KA-O and eye opening.

As eye opening occurs around P13-14, initial further analysis was conducted on the P12-15 age group to identify a correlation between eye opening and increased KA-O. The data

231

were subdivided into groups according to whether the rat had 1) both eyes closed, 2) one eye open, or 3) both eyes open at the point of brain removal.

In LII, the mean amplitude of KA-O in the eyes closed group was 0.07 ± 0.02 μV^2/ Hz (n = 6) and this was not significantly different to the one eye open group (0.08 ± 0.02 μV^2/ Hz; n = 4). However, the mean amplitude rose to 0.18 ± 0.06 μV^2/ Hz (n = 7) when both eyes were open, although this did not reach statistical significance with two-way ANOVA analysis. In LV, the mean amplitudes of KA-O in the same slices with eyes closed, one eye open and both eyes open were 1.0 ± 0.03 μV^2/ Hz (n = 6), 0.08 ± 0.03 μV^2/ Hz (n = 4) and 0.07 ± 0.02 μV^2/ Hz (n = 7), respectively. The data are summarised in Fig. 7.9. Although there were no significant differences between groups there was a slight decline in amplitude that contrasted with the increase seen in LII. Thus, the amplitude of KA-O does tend to increase in LII after eye opening, a phenomena not seen in LV.

Developmental changes in the frequency of KA-Os also appeared to coincide with the onset of eye opening. KA-O activity flips abruptly from beta to gamma frequency between the P12-15 to P16-19 age groups, with little significant change before or after this point. In the P12-15 group the mean frequency of KA-O in LII in rats with their eyes closed was 19.2 ± 0.6 Hz and virtually the same with one eye open (19.5 ± 0.4 Hz). However, when both eyes were open mean frequency rose to 23.8 ± 1.5 Hz (P < 0.05, 2-way ANOVA). Unlike the developmental changes in amplitude, the frequency of KA-O in LV MEC followed the same pattern as in LII. The mean frequencies of KA-O with eyes closed and one eye open and both eyes open were 20.2 ± 1.3 Hz (n = 6), 19.5 ± 0.4 μV^2/ Hz (n = 4), and 23.5 ± 1.3 Hz (n = 7), respectively (P < 0.05, 2-way ANOVA). Results are summarised in Fig. 7.10.

These results show there is a developmental shift in the power of oscillatory activity from LV to LII of the MEC at the onset of eye opening, along with a marked increase in the frequency of synchronised activity from a beta to a gamma band in both layers. These data are the first to make a potential association between the development of GFO and visual sensory input in the MEC, which could have major implications for the development of the spatial representation system and grid cell firing patterns (see discussion).
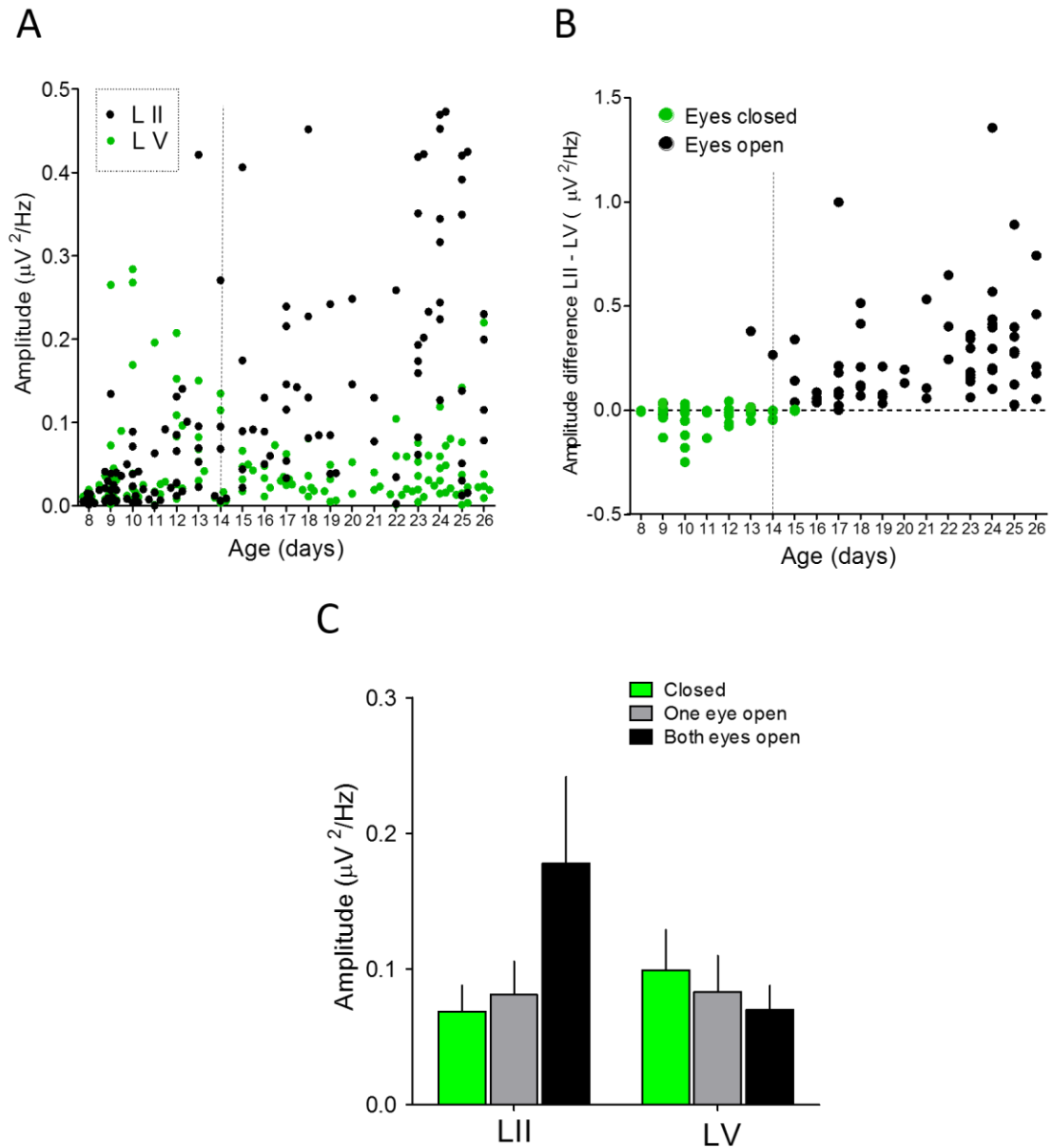
Figure 7.9: Change in KA-O amplitude before and after eye opening. (A) *Individual amplitudes of KA-O recorded in 143 MEC slices, in LII (black) and LV (green) of the same slice. Note the developmental increase in amplitudes in LII and decrease in amplitudes in LV.* ***(B)*** *Paired amplitudes from LII and LV in (A) are subtracted to determine a dominating layer. Positive values represent a larger amplitude of KA-O in LII relative to LV of the same slice, and vice versa. There appears to be a switch from a larger amplitude in LV relative to LII at the onset of eye-opening.* ***(C)*** *Mean amplitude of KA-O in rats aged P12-15 only, split into 3 groups according to whether the rat had 1) eyes closed (green, n = 6), 2) one eye open (grey, n = 4), or 3) both eyes open (black, n = 7) at the point of brain removal. Mean amplitude of KA-O was appears to increase when both eyes were open, in both LII and LV. Vertical dotted line represents approximate day of eye opening.*
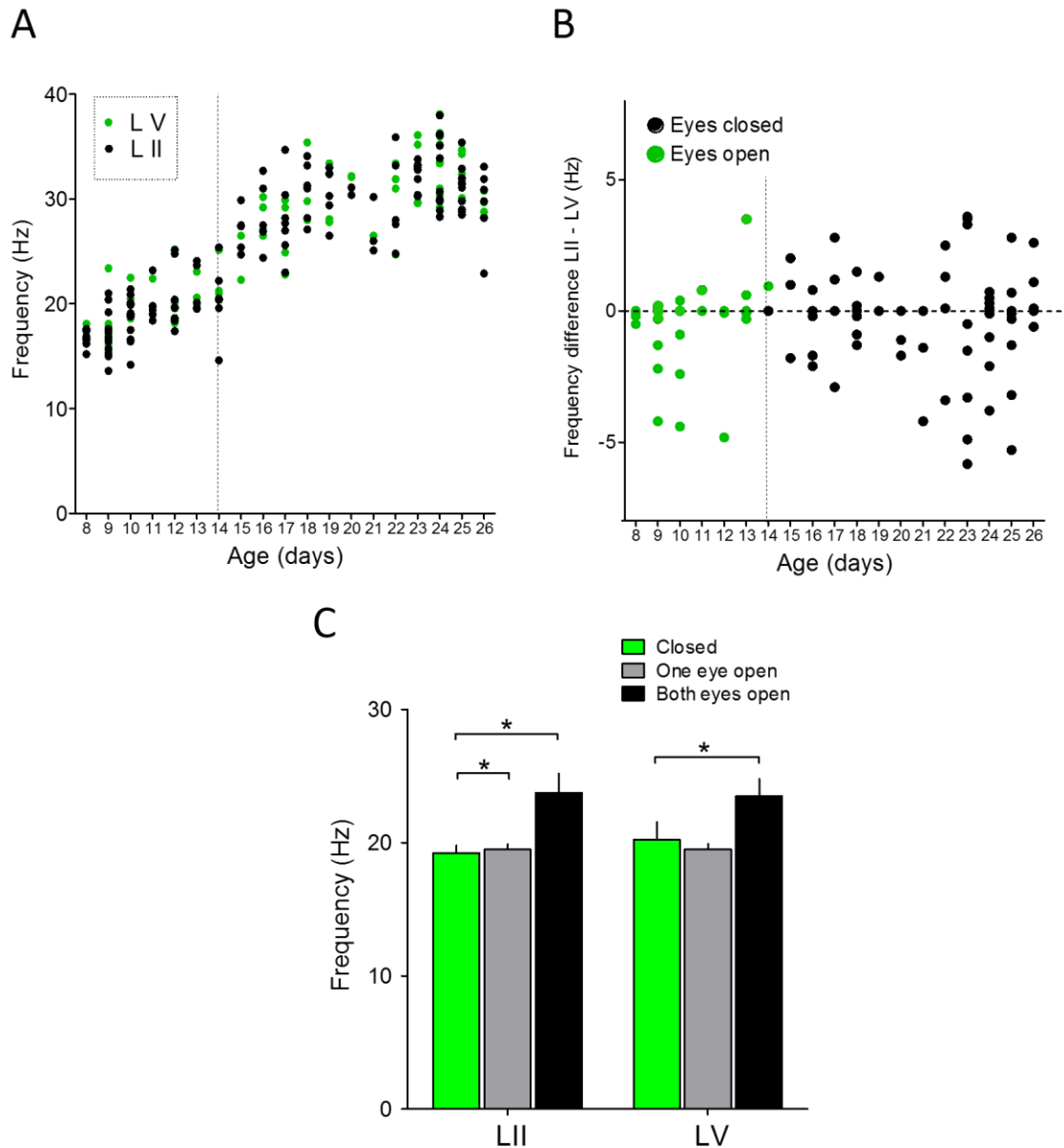
***Figure 7.10: Change in KA-O frequency before and after eye opening. (A)** Individual frequencies of KA-O recorded in 143 MEC slices, in LII (black) and LV (green) of the same slice. Note the developmental increase in frequency in both layers. **(B)** Paired frequencies from LII and LV in (A) are subtracted to determine a dominating layer. Positive values represent a larger frequency of KA-O in LII relative to LV of the same slice, and vice versa. Unlike with amplitude, there was no changes in activity between the two layers. **(C)** Mean frequency of KA-O in rats aged P12-15 only, split into 3 groups according to whether the rat had 1) eyes closed (green, n = 6), 2) one eye open (grey, n = 4), or 3) both eyes open (black, n = 7) at the point of brain removal. Mean frequency of KA-O was significantly increased when both eyes were open, in both LII and LV (P < 0.05, 2-way ANOVA). Vertical dotted line represents approximate day of eye opening.*

7.3.6 Detailed time course of changes in KA-O in relationship to eye-opening

To look at the changing relationships between KA-O frequency and amplitude in the two layers around the point of eye opening I now examine the time course of changes in more detail by plotting data from individual slices against developmental age. The results of this analysis are shown in Figs 7.9 and 7.10.

In the analysis of the P12-15 group above it was clear that there was little change in amplitude in LV but LII increased with eye opening. To examine this relative change in amplitude between the two layers further, I plotted amplitudes for the two layers at all ages over the entire data set. In addition, amplitudes in LII and LV of the same slice were subtracted from each other (LII – LV) and plotted against age. In this case, a positive value will denote a larger amplitude of KA-O in LII relative to LV of the same slice, and vice versa. The data are shown in fig 7.9. In LV, there appears to be a slightly higher amplitude in the 2-3 days before eye opening, but thereafter it slowly declined. In contrast, eye opening coincided with a dramatic rise in amplitude in LII in many slices

When eyes were shut at the point of brain removal, the amplitude of KA-O exceeded LII 84.4 % (38/45 slices), whereas LII exceeded the amplitude in LV in 95.5 % of slices prepared from rats with eyes open at the point of removal. Figure 7.9 illustrates the changes in amplitude in the two layers before and after eye opening. This is emphasised in the subtraction data where many slices fall below the zero line when eyes were closed and a switch to predominantly positive values is marked precisely by eye opening.

Changes in frequency are plotted against age for the whole dataset in Fig. 7.10. Whilst it is clear that frequencies are similar across layers at all ages, eye opening is marked by the abrupt shift from beta to gamma frequency. The similarity in frequency across layers at all ages is emphasised by subtracting LII from LV, shown in Fig 7.10B. Most slices lie around the zero line regardless of whether eyes are open or not. Interestingly the relative frequencies in the two layers showed an element of divergence somewhat in favour of higher values before and following eye opening, but around the time of the event, is when divergence is least.

7.3.7 Pharmacological studies

As noted above, GFO induced by KA were highly sensitive to blockade of KAR by UBP-310 in the adult rat MEC (Stanger et al., 2008), which was also confirmed in this thesis (Fig. 7.1), suggesting a strong involvement of GluK1 receptors. Studies have also confirmed KA-O in the adult rat were also reduced by bicuculline and could be virtually abolished if the concentration was high enough, showing a strong dependence on inhibitory transmission mediated via $GABA_A$R activation. GFO were also sensitive to AMPAR blockade and partially reduced by blocking NMDAR (Cunningham et al., 2003, Middleton et al., 2008a).

In the following studies, the contribution of GABAergic and glutamatergic transmission to KA-O was examined in more detail to compare neonate (P 8-11) and juvenile (P 20-27) rats and to identify developmental changes in the pharmacology, which could reflect developmental changes in amplitude and frequency observed in the previous section. Bicuculline (2-6 μM), GYKI52466 (10-20 μM) and DL-AP5 (40 μM) were used to determine the contribution of $GABA_A$Rs, AMPARs and NMDARs to KA-O, respectively.

Table 7.2 summarises these pharmacological studies.

7.3.7.1 Involvement of $GABA_A$ receptors in KA-O

The $GABA_A$R antagonist, bicuculline, was cumulatively bath applied at concentrations of 2, 4 and 6 μM in slices from neonate (P8-15) and juvenile (P20-27) rats. The results of these studies are shown in Fig 7.11

In LII, bicuculline substantially decreased the amplitude of KA-O in both age groups. In the neonates (P8-15), the mean amplitude of KA-O in LII MEC was significantly and concentration dependently decreased by bicuculline from 139.6 ± 74.2 nV^2 / Hz to a maximal reduction with 6 μM (12.5 ± 6.0 nV^2 / Hz; P < 0.01, rANOVA; n = 5). In juvenile slices (n = 7) application of bicuculline again significantly decreased the amplitude of KA-O essentially abolishing them at 6 μM (136.6 ± 55.4 nV^2 / Hz to 2.1 ± 1.1 nV^2 / Hz; P < 0.001, rANOVA).

In LV, bicuculline also significantly decreased the amplitude of KA-O in both age groups. In the younger neonate group, KA-O amplitude was significantly decreased from 102.5 ± 49.4 nV^2 / Hz to a maximum of ~65-70% with 6μM bicuculline (36.3 ± 22.0 nV^2 / Hz). In juvenile slices, bicuculline also concentration-dependently reduced KA-O, essentially abolishing them at 6 μM (control 26.4 ± 7.9 nV^2 / Hz to 1.2 ± 0.7 nV^2 / Hz).

When KA-O were still present in the presence of the drug, bicuculline had no significant effect on the frequency in either age group or layer.

Whilst bicuculline reduced amplitude in both layers in each age group, it was a more prominent effect in juvenile slices. The maximal reduction in LII neonate slices (with 6 μM), was -78.1 ± 16.1%, compared to -96.9 ± 1.4% in juvenile slices. Likewise, in LV, bicuculline reduced the amplitude by -59.6 ± 16.7% in neonate *vs* -95.5 ± 1.6% in juvenile slices.

These results suggest that fast inhibition neurotransmission mediated by the GABA$_A$R is critical for the maintenance of KA-O in both neonate and juvenile rats, however, the contribution and dependence of GABA$_A$R activity may increase with age, inferred by the larger percentage decrease in activity in the older animals.
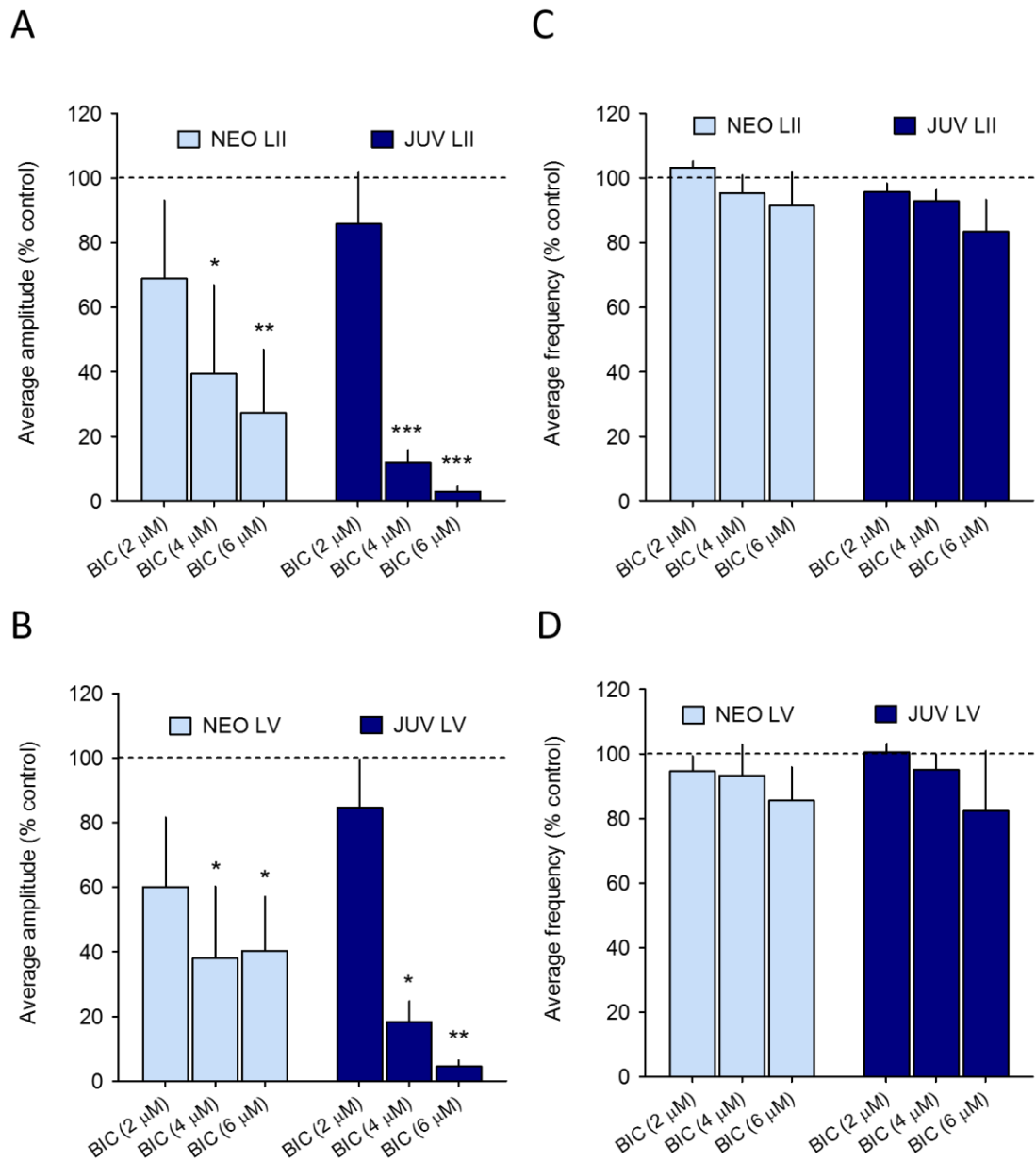
Figure 7.11: Effects of bicuculline on KA-O. *Bars represent the percentage of control (- - -) of (A) amplitude LII (B) amplitude LV, (C) frequency LII and (D) frequency LV in neonate (light blue) and juvenile (dark blue) MEC. Dotted line represent control (100%). * = P < 0.05, ** = P < 0.01, *** P < 0.001. Statistical comparisons made using rANOVA analysis and represent statistically significant changes from control (dashed line).*

7.3.7.2 Involvement of AMPA receptors in KA-O

Fast phasic excitation onto interneurones has been shown to be important in the generation of GFO in the hippocampus and LIII MEC. To investigate the involvement AMPAR in KA-O in LII and LV, GYKI-52466 (10 and 20 μM), a non-competitive AMPAR antagonist, was tested. The results are illustrated in Fig 7.12.

In LII, the mean amplitude of KA-O in neonate slices (n = 10) was decreased from 36.6 ± 8.1 nV^2/Hz 14.7 ± 4.4 nV^2/Hz by 20 μM with a smaller effect seen at the lower concentration (10 μM). Neither change reached statistical significance. However, in juvenile slices (n = 6), the reduction in amplitude was much greater, with the mean amplitude significantly decreased from a control of 133 ± 36.2 nV^2/Hz to 53.3 ± 36.3 nV^2/Hz with 10 μM GYKI-52466, and a cumulative reduction to 35.7 ± 17.4 nV^2/Hz at 20 μM ($P < 0.01$ for both, rANOVA).

Results were similar in LV. The mean amplitude of KA-O in neonate slices (n = 10) was decreased, from 40.4 ± 11.4 nV^2/Hz in control to maximal reduction to 16.8 ± 7.6 nV^2/Hz with 20 μM of GYKI52466 (not significant). On the other hand, GYKI52466 significantly decreased the amplitude of KA-O in juvenile slices, from 15.8 ± 5.3 nV^2/Hz to 2.2 ± 1.0 nV^2/Hz at 20 μM.

The frequency of KA-O was significantly decreased in juvenile slices (in both layers), but not neonate, slices. In LII of neonate slices, the mean frequency of KA-O was 17.9 ± 0.9 Hz and this decreased slightly to 15.7 ± 1.7 Hz with GYKI52466 (20 μM). In LII of juveniles, mean frequency of KA-O was significantly decreased from 31.0 ± 0.3 Hz to 20.5 ± 2.7 Hz ($P < 0.05$, rANOVA) after addition of 20 μM. Percentage-wise there was not a huge difference between the age groups, but the change was only significant in the juveniles.

GYKI52466 clearly had no effects on the frequency of KA-O in LV in neonate slices (control: 18.1 ± 0.6 Hz vs 18.2 ± 0.8 Hz at 20 μM) whereas in juvenile slices a significant decrease from 31.0 ± 0.3 Hz to 20.3 ± 3.1 Hz was seen with 20 μM GYKI52466.

These results suggest that KA-O may become increasingly dependent on the contribution of AMPARs during development. The lower frequency seen in juvenile KA-Os after AMPAR blockade may be due to a decreased excitatory drive onto interneurones which are setting the pace of the synchronised activity. In the younger rats, GYKI54266 may have had less of an effect on KA-O because there are fewer AMPARs are available, or fewer synapses onto interneurones driving the KA-O activity.
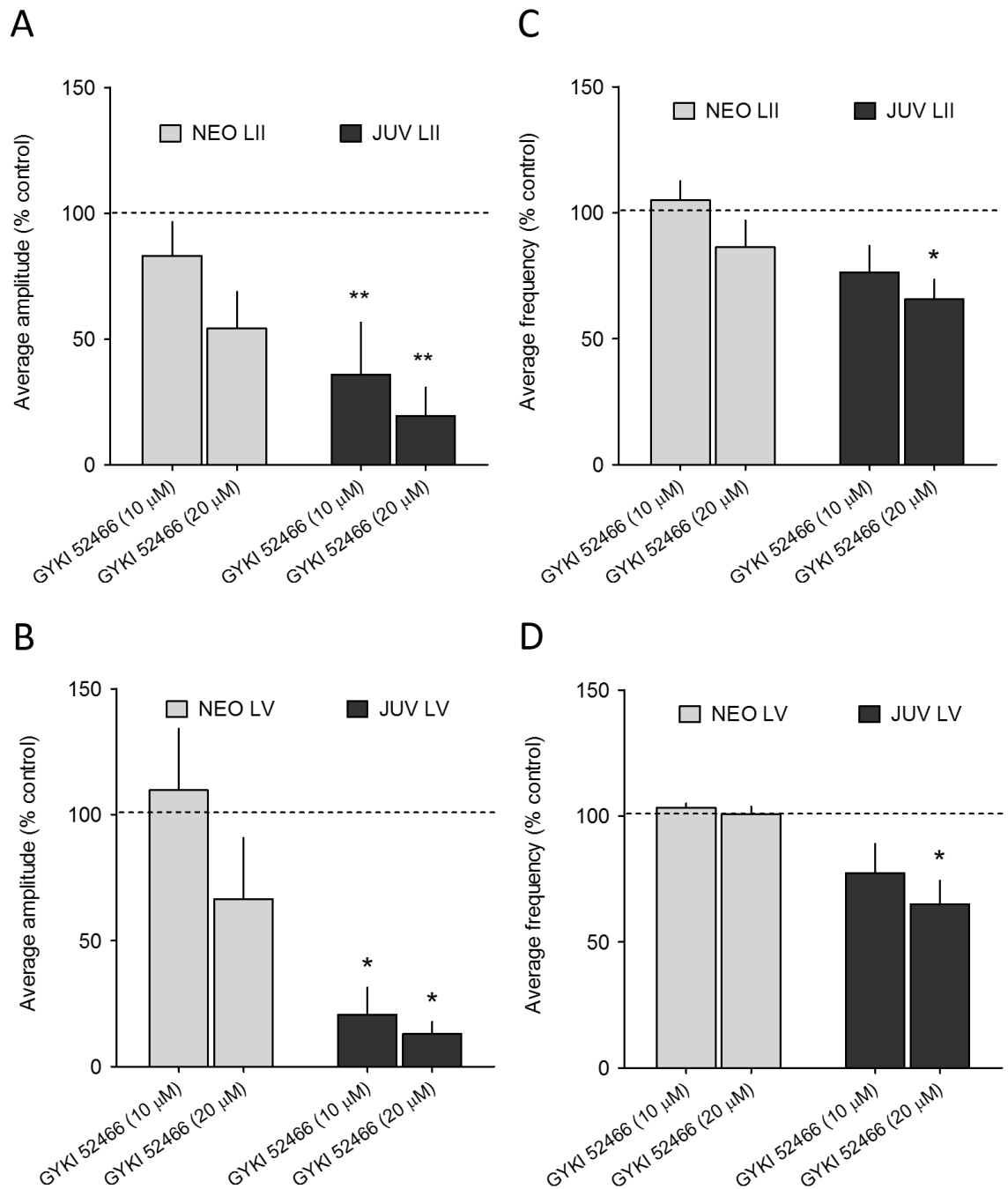
Figure 7.12: Effects of GYKI 52466 on KA-O. *Bars represent the percentage of control (- - -) of (A) amplitude LII (B) amplitude LV, (C) frequency LII and (D) frequency LV in neonate (light blue) and juvenile (dark blue) MEC. Dotted line represent control (100%). * = P < 0.05, ** = P < 0.01, *** P < 0.001. Statistical comparisons made using rANOVA analysis and represent statistically significant changes from control (dashed line). Note KA-O have an increased dependence on AMPAR in juvenile rats.*

7.3.7.3 Involvement of NMDA receptors in KA-O

Previous studies have shown that GFOs are modulated by NMDARs in the superficial layers of the MEC in adult rats, due to the involvement of GABAergic basket cells in this layer, which are highly sensitive to excitation driven by NMDARs (Middleton et al., 2008a). However, blocking NMDARs certainly does not abolish GFO in the MEC, but reveals a second gamma rhythm of a lower frequency, driven by a different type of interneurone (goblet cell; (Middleton et al., 2008a, Cunningham et al., 2003). This provides evidence for the existence of both a NMDAR-dependent and a NMDAR-independent gamma rhythm in the superficial layers of the MEC, which can switch, dependent on the subtype of interneurone recruited into the rhythm (Middleton et al., 2008a).

Here, we determined the contribution of NMDAR activity using the competitive NMDAR antagonist, DL-AP5. The results are summarised in Fig 7.13.

In LII in neonate slices (n = 14), blocking NMDARs significantly decreased the mean amplitude of KA-O, but had no effect on frequency. Amplitude decreased from 36.1 ± 9.3 nV^2 / Hz to 11.1 ± 3.8 at 40 µM DL-AP5 ($P < 0.05$, rANOVA). Concurrently, the frequency was unaltered. In LII of juvenile slices (n = 12), DL-AP5 also decreased the amplitude of KA-O, but despite the effect being almost identical to that seen in neonate slices it failed to reach significance (see table 7.1 for raw data). In contrast to neonates, however, the frequency of KA-O was significantly lowered albeit only marginally, from a control of 31.5 ± 0.6 Hz to 27.8 ± 1.0 Hz (with 40 µM DL-AP5; $P < 0.001$)

Very similar results were observed in LV. DL-AP5 decreased the mean amplitude of KA-O in neonate slices (n = 14) from 52.0 ± 13.1 nV^2 / Hz 16.1 ± 6.6 nV^2 / Hz (40 µM, $P < 0.01$, rANOVA). It also decreased the amplitude of KA-O in LV in juvenile slices (n = 12), from 42.2 ± 10.7 nV^2 / Hz to 11.0 ± 2.8 nV^2 / Hz ($P < 0.001$) in the presence 40 µM DL-AP5. Unlike in LII the change in juveniles was significant. Concurrent changes in frequency were also similar to LII, with no effect of NMDAR blockade in neonates, but a very small, but significant reduction occurring in juveniles. See table 7.1.
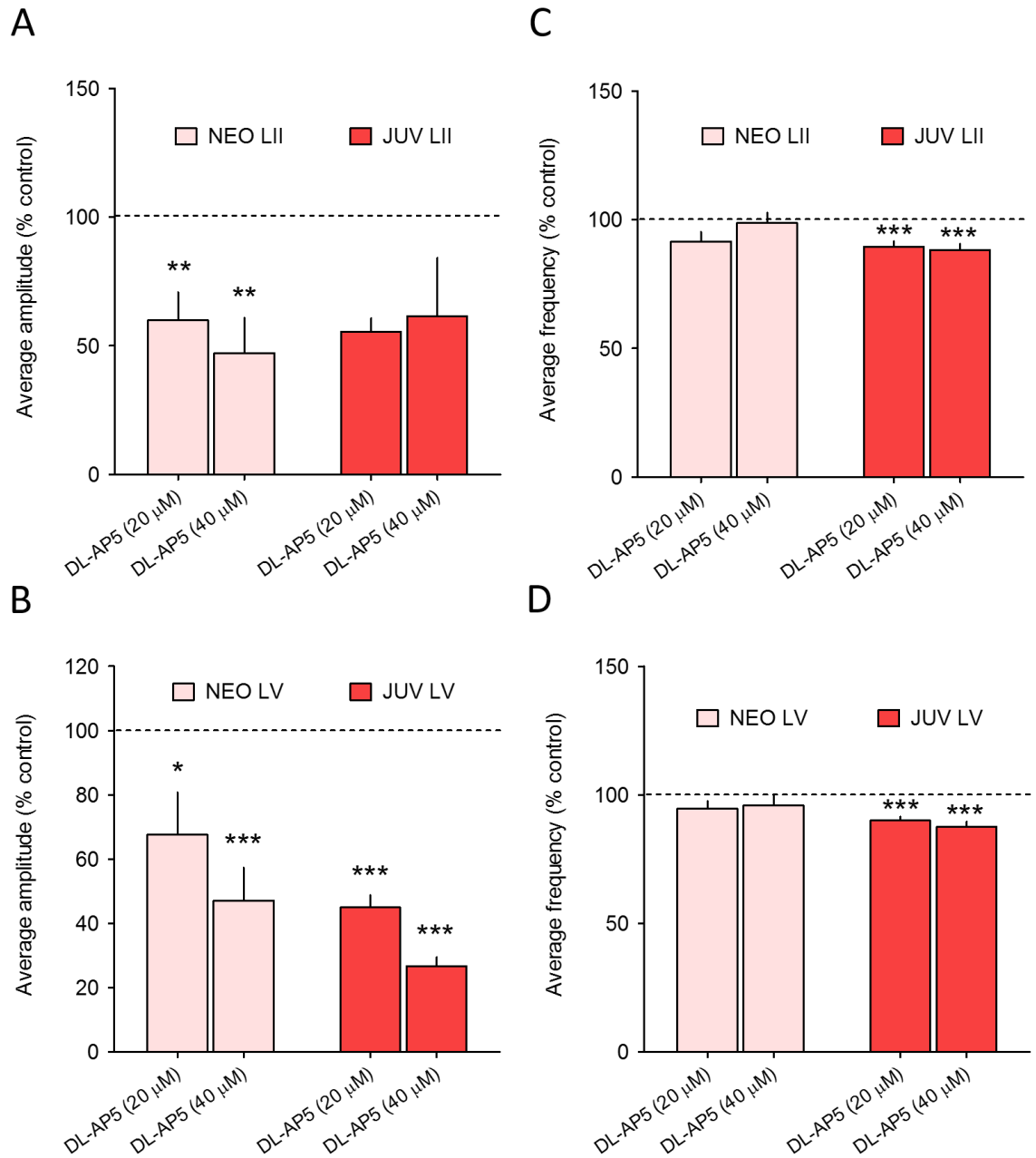
Figure 7.13: Effects of DL-AP5 on KA-O. *Bars represent the percentage of control (- - -) of (A) amplitude LII (B) amplitude LV, (C) frequency LII and (D) frequency LV in neonate (light blue) and juvenile (dark blue) MEC. Dotted line represent control (100%). * = P < 0.05, ** = P < 0.01, *** P < 0.001. Statistical comparisons made using rANOVA analysis and represent statistically significant changes from control (dashed line).*

		Layer II		Layer V	
		Amplitude (nV^2 / Hz)	Frequency (Hz)	Amplitude (nV^2 / Hz)	Frequency (Hz)
NEO (n = 5)	Control	139.6 ± 74.2	18.7 ± 1.6	102.5 ± 49.4	19.0 ± 1.9
	+ BIC (2 µM)	111.3 ± 88.6	19.8 ± 1.9	42.9 ± 28.7	17.8 ± 1.5
	+ BIC (4 µM)	14.3 ± 9.1*	18.2 ± 1.7	25.4 ± 14.2*	17.6 ± 2.0
	+ BIC (6 µM)	12.5 ± 6.0**	17.4 ± 2.4	36.3 ± 22.0*	16.6 ± 2.6
	Wash-out	47.0 ± 26.1*	19.2 ± 2.7	22.3 ± 12.7*	14.8 ± 2.5
JUV (n = 7)	Control	136.6 ± 55.4	30.5 ± 0.8	26.4 ± 7.9	31.2 ± 0.9
	+ BIC (2 µM)	126.0 ± 50.5	29.2 ± 1.3	24.6 ± 8.6	30.3 ± 1.1
	+ BIC (4 µM)	11.0 ± 3.7***	28.5 ± 1.3	5.5 ± 2.9*	28.7 ± 1.1
	+ BIC (6 µM)	2.1 ± 1.1***	25.9 ± 3.0	1.2 ± 0.7**	26.0 ± 6.0
	Wash-out	12.6 ± 6.2***	24.3 ± 1.9	4.3 ± 1.9	24.0 ± 3.6
NEO (n = 10)	Control	36.6 ± 8.1	17.9 ± 0.9	40.4 ± 11.4	18.1 ± 0.6
	+ GYKI 52466 (10 µM)	28.6 ± 9.0	18.5 ± 1.1	35.1 ± 10.9	18.5 ± 0.7
	+ GYKI 52466 (20 µM)	14.7 ± 4.4	15.7 ± 1.7	16.8 ± 7.6	18.2 ± 0.8
	Wash-out	23.9 ± 9.4	13.8 ± 1.8	11.9 ± 4.4	16.8 ± 1.0
JUV (n = 6)	Control	133.3 ± 36.2	31.0 ± 0.3	15.8 ± 5.3	31.0 ± 0.3
	+ GYKI 52466 (10 µM)	53.3 ± 36.3**	23.8 ± 3.5	2.6 ± 1.2*	24.1 ± 3.8
	+ GYKI 52466 (20 µM)	35.7 ± 17.4**	20.5 ± 2.7*	2.2 ± 1.0*	20.3 ± 3.1*
	Wash-out	65.5 ± 30.0*	24.6 ± 3.7	3.7 ± 1.1	25.3 ± 3.2
NEO (n = 14)	Control	36.1 ± 9.3	20.2 ± 0.8	52.0 ± 13.1	20.3 ± 0.8
	+ DL-AP5 (20 µM)	16.5 ± 4.4**	18.3 ± 0.8	27.7 ± 8.4***	19.2 ± 0.9***
	+ DL-AP5 (40 µM)	11.1 ± 3.8**	19.8 ± 0.9	16.1 ± 6.6***	19.2 ± 0.8***
	Wash-out	14.1 ± 5.8***	22.2 ± 1.2	23.0 ± 11.1	20.9 ± 1.0*
JUV (n = 12)	Control	224.7 ± 40.1	31.5 ± 0.6	42.2 ± 10.7	32.1 ± 0.8
	+ DL-AP5 (20 µM)	121.5 ± 26.3	28.1 ± 0.7***	17.6 ± 4.3***	28.8 ± 0.7***
	+ DL-AP5 (40 µM)	100.6 ± 26.6	27.8 ± 1.0***	11.0 ± 2.8***	28.0 ± 1.0***
	Wash-out	284.3 ± 131.5	29.5 ± 0.5*	30.3 ± 6.3	30.5 ± 0.6
NEO (n = 9)	Control	35.7 ± 13.6	20.5 ± 0.9	57.4 ± 23.1	20.5 ± 0.9
	+ UBP-310 (20 µM)	0.10 ± 0.05**	3.0 ± 3.0***	0.3 ± 0.2*	3.0 ± 2.9***
	Wash-out	18.5 ± 6.3	20.9 ± 2.1	29.7 ± 18.8	22.0 ± 1.0
JUV (n = 4)	Control	173.6 ± 126	27.1 ± 1.6	16.9 ± 4.3	26.9 ± 2.4
	+ UBP-310 (20 µM)	0.9 ± 0.7*	8.3 ± 5.1*	0.5 ± 0.2*	19.1 ± 6.4
	Wash-out	87.5 ± 65.3	26.4 ± 1.6	10.7 ± 3.2	27.0 ± 1.2

Table 7.1: Summary table of the effects of 2-6 µM bicuculline (BIC), 10 µM GYKI 52466, 20-40 µM DL-AP5 and 20 µM UBP-310 on KA-O in LII and LV MEC of neonate and juvenile rats. * = P < 0.05, ** = P < 0.01, *** P < 0.001. *Statistical comparisons made using rANOVA analysis and represent statistically significant changes from control.*

7.3.8 Summary of findings

1) An age-dependent increase in KA-O amplitude was seen in the superficial, but not deep, layers of the MEC.

2) A developmental flip in the frequency of KA-O from a beta to a gamma band occurs shortly after eye opening.

3) KA-O are more pronounced in the deep layers of neonate (P8-11) but become progressively more pronounced in the superficial layers of juvenile rats (20-27) with, the switch in dominance occurring at the onset of eye opening.

4) KA-O in the MEC are dependent on fast GABA$_A$R mediated neurotransmission, and are partially driven by NMDAR and AMPAR mediated excitatory drive, which appears to be more dominant in KA-O of older rats.

7.4 Discussion

7.4.1 Developmental changes in KA-O

This chapter set out to determine how oscillatory activity, induced by KAR activation, arises and develops in networks of the MEC. The results of this study identified that KA-O were induced at all ages studied, therefore future experiments should be done to clarify exactly when KA-O arise. KA-Os were present in the form of beta oscillations in the youngest age groups (P8-11 and P12-15), in both layers. A gamma frequency was attained in a step-wise manner between the P12-15 to P16-19 age groups. KA-O are known to be critically dependent on large compound phasic excitatory inputs onto interneurones and their ensuing inhibitory synaptic outputs (Cunningham et al., 2004b, Gillies et al., 2002, Cunningham et al., 2003). The development of synchronised activity within a network of neurones will therefore be intrinsically linked to the development of the inhibitory machinery supporting the rhythm. A recent study has addressed postnatal development of GABAergic interneurones in the temporal cortex sub-regions, including in the MEC, and revealed an increase in the density of PV-interneurones between P14 and P21 (Ueno et al., 2017). PV-interneurones are fast spiking basket cells thought to enable the generation of

GFO due to several distinctive features, including their ability to fire rapidly without fatigue (Buzsaki et al., 1983, Kawaguchi and Kubota, 1997, Traub et al., 1996a). Another study performed a more region specific analysis of PV-expression in single neurones, as a marker of interneurone maturity, in areas of the MEC-hippocampal network (Donato et al., 2017). They showed that LII of the MEC was the first area to upregulate PV-expression at approximately P17, compared with P26 in LV, suggesting inhibitory neurotransmission matures earlier in the superficial layers relative to the deep. It is important to note that the above studies (Ueno et al. 2017, Donato et al. 2017) were conducted in mice, therefore caution should be taken when drawing parallels with the data from this thesis, though a similar developmental timeline is likely in the rat temporal cortex.

The patch clamp data from Chapter 4 nicely complements these results, showing that, between neonate (P8-13) and juvenile neurones (P20-27), there was a substantial surge (8-fold increase) in inhibitory activity in LII. This also ties in well with results from the current chapter, showing a large, age-dependent increase in the amplitude of KA-O in LII, which was not apparent in LV. Within the same time-frame, patch studies in Chapter 4 showed that inhibition in LV also increased (4 fold), but the overall inhibition was much stronger in the superficial layers comparatively, and likely accounts for the greater tendency of the superficial layers to generate GFO in this study and others (Cunningham et al., 2003, Cunningham et al., 2004a, Middleton et al., 2008a). In addition, in Chapter 4 we showed that IPSP kinetics were faster in juvenile rats (P20-27) versus neonate (P8-13) in LII, but not LV, which could reflect the maturation or activation of a sub-population of fast spiking inhibitory interneurones. The reasons for lamina differences in KA-O likely include the delayed maturation of inhibitory circuits in LV versus LII (Donato et al., 2017), as well as the underlying neuronal architecture in each layer. For example, principal neurones are thought to be mainly interconnected via inhibitory interneurones in the superficial layers of the MEC (Couey et al., 2013, Fuchs et al., 2016), though this is a working hypothesis that has been recently challenged (Winterer et al., 2017). Other factors that may influence the development of GFO are the formation of electrical synapses between basket cells, increases in glutamatergic inputs onto basket cells, general increases in basket cell to basket cell and basket cell to PC connectivity, or the presence of gap junctions (Du et al.,

1996, Taketo and Yoshioka, 2000, Chattopadhyaya et al., 2004, Le Magueresse and Monyer, 2013, Traub et al., 2001, Schmitz et al., 2001b, Traub et al., 2000).

Either way, it is clear from the results of this study, and other studies from this lab (Greenhill et al., 2014, Greenhill and Jones, 2010, Jones and Woodhall, 2005, Jones and Bühl, 1993), there is a developmental surge in the level of inhibition in the superficial layers of the MEC which may support the ability of the microcircuitry in this layer to generate and maintain oscillatory activity.

7.4.2 GABAergic and glutamatergic pharmacology of KA-O in the neonate and juvenile rat MEC

Cunningham et al. (2003) were the first to induce KA-O in the MEC of adult rats, and a full pharmacological profile was conducted (Cunningham et al., 2003). In agreement with these studies, KA-O were significantly decreased in LII and LV MEC in the presence of bicuculline, reinforcing that gamma rhythms generated by local neuronal circuits have a dependence on fast inhibitory neurotransmission.

Cunningham et al. (2003) also determined that KA-O in the adult rat MEC required AMPARs and gap junctions, suggestive of a PING mechanism underlying the oscillation (see Introduction for explanation), however, the frequency of EPSPs invading fast spiking interneurones was actually lower than the frequency of these cells, implying a degree of tonic excitation of interneurones, a prominent feature of an ING mechanism. Therefore, the mechanisms underlying KA-O in the adult MEC would appear to contain components of both a tonic and phasic excitatory drive (Cunningham et al., 2003). In this chapter, the relative contribution of AMPARs to KA-O was determined in the two age groups: neonate (P8-13) and juvenile (P20-27). Interestingly, the results in the juvenile group were comparable to those of Cunningham et al. (2003), showing a clear decrease in the amplitude of KA-O when AMPARs are blocked, in both layers. This is accompanied by a slight decrease in the frequency of KA-O, again in both layers, which is likely the result of reduced excitatory drive onto interneurones, which are pacing the rhythm. This does not appear to be the case in the younger age group. Although there appears to be a decrease

in amplitude, it was not statistically significant, and the effect is clearly not as prominent as in the juvenile group.

This could mean the excitatory connections onto interneurones driving the rhythm are less dependent on AMPAR activation, or have not fully developed yet. Perhaps in the neonate MEC, the slower, beta oscillation may be predominantly generated by a different (slower) subtype of interneurone, considering that, as mentioned earlier, maturation of fast spiking PV-containing interneurones likely occurs after the age of the young rats (PV interneurones mature ~P17 in temporal cortex of mice). Indeed, Middleton et al. identified two rhythms within the MEC, with different frequencies (Middleton et al., 2008a), which were sustained by different populations of interneurones. Therefore, it is entirely possible that there is a shift in the dominance, or ability, of certain interneuronal subtypes to generate rhythmic activity at different stages of development. Middleton et al. (2008a) revealed the slower rhythm within the superficial layers of the MEC after blocking NMDARs with ketamine, implying that the output frequency of neurones in the MEC is controlled by the extent of NMDAR activation.

In this chapter, a different antagonist, DL-AP5, was used to block NMDARs, and decreased the amplitude of KA-O in both layers and both ages. However, it is important to note that whilst drugs were only applied when oscillatory activity was deemed 'stable', after 2 consecutive recordings of +/-20 % variability in KA-O amplitude, control data for stability within LV MEC was variable, therefore caution should be taken when looking at more subtle drug effects, especially if there was no recovery in the wash-out (see Appendix for build-up of KA-O in both layers and all age groups). Frequency, on the other hand, was extremely stable after 1 hour application of KA, in both layers and all age groups. It is entirely possible that the lack of stability within LV MEC is directly related to the delayed maturation of inhibitory neurotransmission in this layer (Donato et al., 2017). Recovery in KA-O amplitude after a wash-out period only occurred in the juvenile group, so we can assume that, at least in the older animals, NMDARs do contribute to the maintenance of KA-O in LII and LV. Moreover, there was a small (only 3.5 Hz), but very significant, decrease in the frequency of KA-O in the juvenile group only, which may reflect a decrease in NMDAR driven fast spiking basket cell output, as previously described (Middleton et al., 2008a, Cunningham et

al., 2003). The fact DL-AP5 decreased the frequency of KA-O in juvenile, but not neonates, may be indicative of a protracted development of some interneuronal subtypes which are driven by NMDAR activation.

7.4.3 KA-O as a reporter of KAR activity during development

From this chapter and the patch clamp studies in chapter 6, it is clear that there are major differences in the action of KA in neonate (P8-11) versus juvenile (P20-27) rats. Whilst it is likely this reflects the maturation of neuronal connectivity as a whole, these studies also shed light on the role of KARs in neuronal synchrony during development. An interesting observation from this chapter was that, in the youngest age group, KA-O were more powerful in LV relative to LII. Moreover, there was a small, but significant, surge in the amplitude of KA-O in LV between the first two age groups, which was not maintained in the older animals. From the patch clamp data, although KA had minimal effects on sIPSC frequency in the neonate age groups, the mean increase was much more prominent in LV relative to LII (+25% LII vs +150% LV). In juvenile rats, KA increased the frequency of sIPSCs to a similar degree in LII (+273%) and LV (+230%), however, the baseline frequency in LV started much lower, therefore LII sIPSCs had a much higher frequency after KA compared to LV (15.3 Hz vs 9.2 Hz).

The frequency of GABA release onto principal neurones in response to KA may certainly account for the lamina differences in KA-O observed in LII and LV during development, which may be a reflection on the development of synaptic contacts from interneurones, or the expression of KARs. Unpublished immunohistochemistry studies from the lab of Professor Elek Molnar showed that expression of the GluK1-containing KAR peaks at ~P14, followed by a steady decline into adulthood (Molnar et al. unpublished data, figure 1.6). Other studies have suggested a similar developmental pattern of expression of this receptor (Bahn et al., 1994). Interestingly, we found a significant increase in the amplitude of KA-O around this same stage of development (P12-15 age group) in the deep layers of the MEC, which decreased in older animals. Having shown that KA-O are heavily dependent on the GluK1 subunit (Fig.7.1), it is possible that the temporal surge in amplitude in the deep layers is related to the increased expression of GluK1-containing KARs at this point in development. Moreover, patch clamp studies (Chapter 6) showed an increase in sIPSC

frequency in response to activation of KARs containing the GluK1 subunit only in the neonate (P8-11) group, which, again, may be related to a temporal developmental increase in the expression of this receptor in the deep layers of the MEC.

7.4.4 Oscillations, eye opening and wider implications

A particularly interesting observation in this chapter was that the increased amplitude of KA-O in LII MEC appeared to occur at the onset of eye opening. The increase in amplitude of KA-O is undoubtedly linked to the maturation of the neuronal architecture underpinning the synchronised activity, but it is not unwarranted to suggest visual sensory input may influence, or indeed kick-start, this maturation process, especially given the roles of the MEC, and adjacent hippocampus, in spatial navigation processing (Hafting et al., 2005, Moser et al., 2008, Sargolini et al., 2006, O'Keefe and Dostrovsky, 1971, O'Keefe, 1976). Cortical plasticity is influenced by sensory input during development in other areas of the brain, such as the visual cortex (Espinosa and Stryker, 2012, Song and Abbott, 2001). In a series of ground-breaking experiments on developmental plasticity, Wiesel and Hubel showed that visual deprivation during development imposed life-long changes in the strength and organisation of inputs from the eyes to cortical cells, in kittens (Wiesel and Hubel, 1963b, Hubel and Wiesel, 1963, Wiesel and Hubel, 1963a). Moreover, a recent study looking at the early development of network oscillations in the ferret visual cortex concluded there was an increase in the power of gamma oscillations after eye opening which may influence cortical maturation (Li et al., 2017).

Whilst the MEC does not receive direct visual sensory input, other adjacent regions, such as the retrosplenial cortex, do and provide a strong afferent input to the MEC (Kerr et al., 2007, Burwell and Amaral, 1998b). Moreover, the retrosplenial cortex has fundamental roles in forming associations between environmental stimuli and in spatial navigation (Oess et al., 2017, Clark, 2017, Mao et al., 2017, Epstein, 2008). It is possible that the development of MEC microcircuitry is influenced by input from nearby structures receiving direct visual sensory information.

As previously mentioned, maturation of the MEC has recently been suggested to occur in a linear and hierarchical fashion, beginning with an excitatory and activity-dependent

instructive signal in SCs in LII, which spreads directionally to LII PCs, and cells of the CA3, CA1, dentate gyrus, subiculum, LV MEC and lastly LII LEC, throughout the first month of post-natal life (Donato et al., 2017). Although this study was in mice, they propose LII SCs become fully mature at approximately P14, which is also around eye opening (in rats and mice).

The nature of this instructive signal from LII SCs is currently unknown, but I propose that a surge in gamma activity, consequent on eye opening, may provide the source of excitation, which may kick-start the development of the MEC. Indeed, it is becoming increasingly apparent that rhythmic brain activity has critical roles in structuring the development of cortical networks (Lowel and Singer, 1992, Singer, 1995, Uhlhaas et al., 2009). Specifically, neuronal oscillations allow the precise temporal coordination of pre- and postsynaptic neuronal activity which leads to the modification of synapses, or STDP, which has major roles in shaping the maturation of the cortex (Song and Abbott, 2001). As mentioned in the Introduction to this thesis, one of the defining features of the MEC is the presence of grid cells. These cells have grid-like firing patterns which map out the environment, acting as a metric and reflecting the structure of local space (Hafting et al., 2005). Of yet, the mechanisms underlying the development of grid cell firing patterns is unknown, but some models theorise the involvement of synchronised brain activity, particularly theta nested gamma-oscillations (Pastoll et al., 2013a, Solanka et al., 2012, Solanka, 2015). Moreover, current available experimental evidence places the emergence of grid cell firing at around ~P19 (Wills et al., 2012).

This has led me to the hypothesis that the onset of gamma oscillatory activity in layer II (~P16) is linked to increased sensory input consequent on eye-opening (~P14), which I propose may also be linked to the development of synaptic organisation leading to grid cell activity. In support of this hypothesis, the literature strongly suggests there is a dorsal to ventral maturation of the MEC accompanied by an inhibitory gradient intrinsically linked to the power of GFO along this axis (Beed et al., 2013, Ray and Brecht, 2016, Stensola et al., 2012). Interestingly, a progressive change in the size of spatial scales represented by grid cells is also apparent along this axis, whereby larger spacing between the grid cell firing

patterns are noted in the ventral MEC, which are present at the onset of exploratory behaviour/eye opening (Brun et al., 2008).

This hypothesis could be investigated using visual deprivation (reared in darkness) experiments to determine if the increased GFO in LII is a result of visual sensory input. Moreover, it would be interesting to determine if disrupting GFO during development affects the synaptic organisation and connectivity of grid cells, and determine if GFO are important for the development of grid cell firing patterns.

Another interesting phenomena was the disappearance of a beta oscillation upon eye opening in the deep layers of the MEC. Indeed, beta oscillations have been identified in deep layers of other cortical areas, such as the somatosensory cortex, also via KAR activation (Roopun et al., 2006). Beta oscillations have distinct pharmacological properties, for example they are dependent on gap junctions and have a lower sensitivity to GABAaR blockade compared with gamma rhythmogenesis, of which they can exist independently from. Neuronal activity involving gap junctions has been associated with the immature developing nervous system, therefore its possible beta oscillations may have a temporal role in maturation of the deep MEC prior to eye opening (Dupont et al., 2006). Further experiments to block gap junctions and GABAaR (at a lower concentration) will help classify the rhythm observed in the deep MEC at ~P12-15.

Chapter 8

General discussion

8.1 Overall developmental changes to excitation and inhibition

Chapters 3 and 4 from this thesis aimed to directly compare changes in the properties of spontaneous excitation and inhibition during post-natal development in the rat MEC. Moreover, to identify lamina specific differences in sEPSC and sIPSC activity in the age groups studied (P8-11 and P20-27). Changes to background excitation and inhibition are summarised in Fig. 8.1 below.
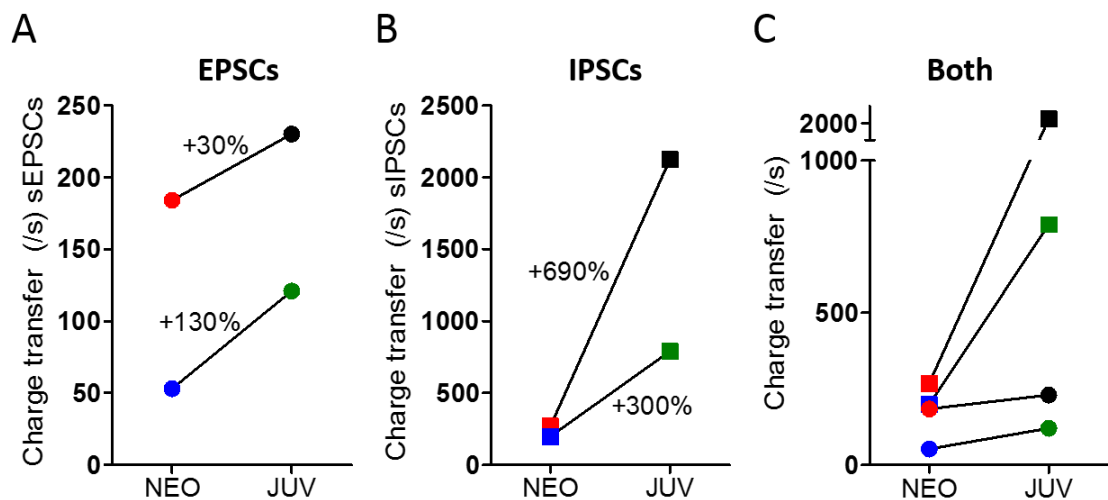
Figure 8.1: Changes to overall excitation and inhibition in neonate and juvenile neurones. (A) Charge transfer values of sEPSCs in neonate (NEO: LII=red, LV=blue) and juvenile (JUV: LII=black, LV=green) neurones. (B) Charge transfer values of sIPSCs in neonate (NEO: LII=red, LV=blue) and juvenile (JUV: LII=black, LV=green) neurones. (C) Charge transfer values from both EPSCs and IPSCs of all groups.

We concluded that background excitation levels were higher in LII *v* LV at both stages of development (Fig. 8.1A). The lamina ratios of excitation in LV:LII were 1:3.5 in neonate and 1:1.9 in juvenile neurones. Previous work from this lab comparing background excitation in adult rats also found higher levels in LII *v* LV, but only marginally (LV:LII; 1:1.2), indicating the levels of excitation may continue to equalise into adulthood. In agreement, Donato et al. identified a delayed maturation of both excitatory and inhibitory neurotransmission in

LV MEC, compared to in LII, therefore the difference in activity may well become less prominent with in older, adult rats (Donato et al., 2017).

Despite this, the relative change in excitation during development was much more pronounced in LV (+130%) compared to in LII (+30%).

The developmental increase in background inhibition was much more substantial in LII (+690%), but there was also a marked increase in LV (+300%). The level of inhibition in neonates was similar in both layers, but dominated the superficial layers of juvenile neurones, in agreement with previous studies in this lab (Jones and Woodhall, 2005, Woodhall et al., 2005, Greenhill et al., 2014). The significant increase in the frequency of IPSCs during this developmental time period correlates with a recent study showing expression of PV-containing interneurones occurred at around P21 (Ueno et al., 2017).

Noticeable developmental changes were also observed in the kinetics of both inhibitory and excitatory events, summarised in Fig. 8.2 and discussed fully in section 3.4. Generally, in LII MEC, rise and decay time were much faster in the older age group, in both EPSPs and IPSPs, which, coupled to the heightened inhibitory tone, may predispose this layer to the generation of synchronised neuronal network activity in the juvenile MEC, and indeed, this is exactly what we saw in chapter 7 (Fig. 7.6). In LV, a similar pattern was observed regarding excitatory events, however, the kinetics of IPSPs were actually slower in the older juvenile groups, which, among other reasons previously discussed, may reflect inputs from different subtypes or somatodendritic locations of interneurones or different $GABA_AR$ subunit compositions.
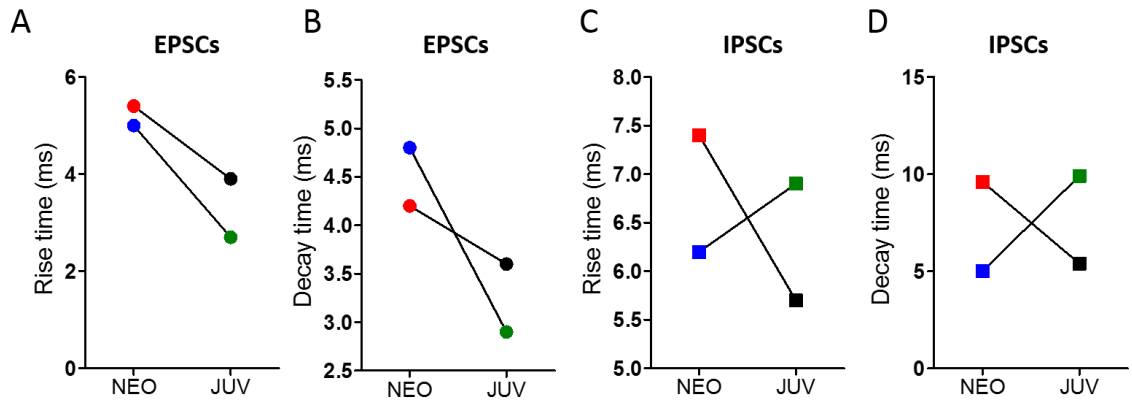
Figure 8.2: Developmental changes to EPSC and IPSC kinetics. (A) *Average rise times and* ***(B)*** *decay times of sEPSCs in neonate (NEO: LII=red, LV=blue) and juvenile (JUV: LII=black, LV=green) neurones.* ***(C)*** *Average rise times and* ***(D)*** *decay times of sIPSCs in neonate (NEO: LII=red, LV=blue) and juvenile (JUV: LII=black, LV=green) neurones.*

Decay time kinetics are significantly influenced by the composition and cellular distribution of $GABA_A$Rs, which changes during the course of neuronal maturation (Wisden et al., 1992). Generally, IPSPs get faster during post-natal development due to the upregulation of α1 and α4 subunits, and down-regulation of α3 and α5 $GABA_A$R subunits, shown in other areas of the cortex (Bosman et al., 2002, Dunning et al., 1999, Hutcheon et al., 2000) and hippocampus (Cohen et al., 2000). It is therefore unusual that the kinetics of inhibitory events in LV MEC became much slower during development, contrary to changes observed in other cortical regions, including LII MEC shown in this thesis (Fig. 8.2). There are no other comparative developmental studies on IPSC kinetics in the MEC laminas, though studies in the adult MEC do show slower decay times in LV IPSCs relative to in LII (Woodhall et al., 2005). In addition, other lamina comparisons of EPSC kinetics from this lab showed LV neurones had faster EPSPs compared to LII, in accordance with this thesis, showing these characteristics are remarkably similar, even across studies.

It is not unreasonable to suggest that the prolonged inhibition (due to slower kinetics) in the deep layers is a means to counteract the substantial quickening of excitation observed in the same layer during post-natal development. Especially considering the high prevalence of recurrent excitatory connections between LV neurones (Jones and Woodhall,

2005, Jones and Heinemann, 1988), compared to in LII (Dhillon and Jones, 2000). As such, the deep layers of the MEC have been previously demonstrated to have a pronounced susceptibility to epileptogenesis (Jones and Lambert, 1990, Jones, 1993, Avoli et al., 1996). The exact mechanisms underlying the development of epilepsy are still unknown, but broadly involve an imbalance between excitation and inhibition within neuronal networks, and the EC has been heavily implicated (Spencer and Spencer, 1994, Lothman et al., 1990). Altered $GABA_A$R function, as a result of aberrant subunit expression, has been identified in both human patients and animal models of TLE (Brooks-Kayal et al., 1998, Gibbs et al., 1997). In theory, such alterations in LV MEC could affect the physiological increase in decay time throughout development, which coincident with the clear developmental quickening of excitatory neurotransmission, could lead to a reduced inhibitory tone and predisposition to hyper-excitable and pathologically synchronous network activity. Indeed, many current anti-epileptic drugs, such as benzodiazepines, target $GABA_A$Rs, act to increase the amplitude and decay time of IPSCs (Macdonald and Barker, 1978). Prolonging IPSC decay time enables summation of multiple synaptic inputs, increasing the overall inhibitory "tone" of GABAergic synapses, and decreasing the likelihood of hypersynchronous neuronal activity underlying seizures (Otis and Mody, 1992, Edwards et al., 1990).

Thus, the developmental changes to the properties of excitatory and inhibitory neurotransmission determined in chapters 3 and 4 of thesis may have important implications for the generation of both physiological and pathological synchrony in LII and LV MEC.

8.2 Overall developmental changes to KAR function at glutamatergic synapses

Chapter 5 provided evidence of the presence of two types of KAR involved in glutamatergic neurotransmission in LII and LV MEC. Firstly, experiments with UBP-310 on sEPSCs and mEPSCs identified a KAR containing the GluK1 subunit, which was highly tonically active, located at presynaptic terminals. The lack of an effect of the GluK1-containing KAR, ATPA, was surprising, especially considering its ability to significantly increase spontaneous excitation in the adjacent LIII MEC. However, unlike in both LII and LV, there was no tonic

activity of GluK1-containing KARs in LIII MEC, therefore it is entirely possible that the lack of an effect is because this receptor was already tonically activated by ambient glutamate. In addition, there was often a small decrease in the frequency of sEPSCs associated with ATPA, which may reflect receptor desensitisation as a result of excessive activation. Whilst this theory makes sense, it was confounded by the fact that UBP-310 reversed the substantial increase in excitation in response to KA, implying the GluK1-containing KAR was responsible for this activity in the first place. However, taken together with the lack of effect of ATPA on its own, and the considerable tonic facilitation of glutamate by presynaptic GluK1-containing KARs, it may be more likely that KA was acting at KAR that did not contain the GluK1 subunit, and the decrease in sEPSC frequency after UBP-310 is due to the substantial (~50-60%) reduction in tonic glutamate release at the terminals. Alternatively, as previously mentioned in chapter 5, the discrepancy of these results may also be explained by calling into question the specificity of UBP-310, as reports have identified antagonism at GluK3 KAR subunits (Perrais et al., 2009).

Either way, it would seem that KA acts at KARs on principal cells which may activate recurrent excitatory connections in LII MEC, however, recurrent excitation between LII neurones is weak or non-existent in the EC (Dhillon and Jones, 2000, Couey et al., 2013, Pastoll et al., 2013a, Fuchs et al., 2016), though this is being questioned by a study showing connectivity of pyramidal (12%) cells onto stellate neurones in LII, and pyramidal cells in LIII (Winterer et al., 2017). Unfortunately, elucidation of the exact subunits of postsynaptic KARs mediating KA induced recurrent excitation awaits the development of more selective subunit antagonists.

Pinpointing the location of KARs that modulate GABAergic neurotransmission was tricky because experiments looking at mIPSCs in the presence of TTX await completion. However, we identified interesting developmental differences in inhibitory neurotransmission in response to activation of the GluK1-containing KAR with ATPA. Specifically, ATPA had no effect on spontaneous GABA release in juvenile rats, but significantly increased the frequency, amplitude and decay time of sIPSCs in neonate neurones. It is particularly interesting that the response to ATPA in neonate neurones parallels an observed increase in the expression of the GluK1 subunit, observed in preliminary studies from the lab of Elek

Molnar (unpublished data, Fig. 1.6). This transient peak in expression, coupled with a clear functional difference at this age, may lead us to speculate a role for the GluK1-containing KAR in activity dependent maturation of the MEC, as seen in other regions (Lauri et al., 2005, Lauri et al., 2003).

Overall, the results from Chapter 6 point towards the presence of a presynaptic KAR enhancing inhibitory transmission in neonate and juvenile neurones. Moreover, it seems likely there is a KAR located at the soma/dendrites of interneurones, as has previously been reported in the hippocampus, but direct interneuronal recordings must be achieved to confirm this.

Overall, we show that KARs can directly mediate postsynaptic excitation at glutamatergic synapses, and likely do not contain the GluK1 subunit. Secondly, we show that KARs containing the GluK1 subunit are located presynaptically, where they are highly tonically active and contribute substantially to ongoing spontaneous glutamate release. Third, we suggest the presence of a presynaptic GluK1-containing KAR located at GABAergic terminals, and lastly, we suggest the presence of a GluK1-containing KAR located at the soma/dendrites of interneurones, mediating powerful synchronised network activity which appears to be developmentally regulated.

We are only beginning to understand the physiological functions of KARs in both mature and immature networks. Work is still confounded by the lack of pharmacological specificity of current drugs, and the plethora of functions in the modulation of both excitatory and inhibitory neurotransmission which appear to differ during development.

8.3 KARs in synchronised neuronal activity during development

Synchronised neuronal activity in the gamma frequency (30-80Hz; GFO) can be generated across all laminas of the adult MEC via activation of KARs (KA-O). KA-O are dependent on KARs containing the GluK1 subunit and fast $GABA_A R$ mediated inhibitory neurotransmission driven by NMDAR phasic excitation (Cunningham et al., 2003, Middleton et al., 2008a, Cunningham et al., 2004b). In Chapter 7, we used KA-O as a reporter of KAR involvement

in synchronised network activity during development. In combination with patch clamp data in Chapter 5 and 6, we aimed to determine the roles of KARs at both a synaptic and network level.

In the juvenile rat MEC, KARs were clearly very powerfully involved in the generation and maintenance of GFO, with activity dominating the superficial layers. On the other hand, synchronised activity in the neonate MEC was much slower, at a beta frequency, and was more powerful in the deep layers. This correlates nicely with the stronger response of sIPSCs to KA in the deep layers of neonate neurones, and vice versa in juvenile neurones. As discussed in Chapter 7, the mechanisms underlying these differences may relate to KAR expression or functioning, or the level of maturation of neurotransmitter systems supporting the rhythm. However, given that LV MEC apparently matures much later than LII (Donato et al., 2017), it may be suggested that the increased response to KA in LV is not due to a more advanced maturation of the microcircuitry underlying the activity, but perhaps a reflection on KAR functioning in LV at this stage of development. Unpublished data from Molnar et al. pointed to altered expression of KARs during post-natal development, leading to the assumption that KARs may have important roles in the development of cortical networks. Moreover, developmentally down-regulated expression of KARs that occur in parallel with maturation of the circuitry have also been reported in other brain regions. For example, presynaptic KARs are down-regulated in the hippocampus (Lauri et al., 2005, Sallert et al., 2007), and at thalamocortical synapses in the barrel cortex (Kidd and Isaac, 1999, Kidd et al., 2002), whereas postsynaptic KARs are developmentally downregulated in the nociceptive pathways in the spinal cord (Stegenga and Kalb, 2001).

Functionally, the dynamic actions of KARs at both inhibitory and excitatory synapses enable the generation of patterned and synchronised activity, as shown in this thesis, which is critical for plasticity, and an emerging idea is that KARs have roles during synapse maturation. In the hippocampus, a tonically active KAR that facilitates glutamate release, as well as interneurones excitability, is gradually lost in a manner that parallels circuit maturation during the first 2 postnatal weeks of life of the rat (Lauri et al., 2005, Lauri et al., 2006, Maingret et al., 2005). Whether KARs are internalised, modified, or if there is

another mechanism to account for the downregulation of KARs is currently up for debate. Nonetheless, temporally correlated neuronal activity is crucial in wiring developing networks (Katz, 1993, Palva et al., 2000), therefore the clear roles of KARs in network synchrony (Chapter 7), their ability to modulate both excitatory (Chapter 5) and inhibitory (Chapter 6) neurotransmission, and the indication of altered expression patterns during development (Molnar et al. unpublished data; Fig. 1.6), would strongly implicate these receptors as having roles in shaping the development of the MEC circuitry.

Recurrent bursts of synchronised network activity are a general feature of developing cortical networks, or indeed the developing CNS in vertebrates as a whole (O'Donovan, 1999), and have been identified in the hippocampus (Palva et al., 2000) and MEC (Jones and Heinemann, 1989, Cunningham et al., 2006b). In the superficial layers of the MEC, Jones et al. reported pronounced spontaneous bursting activity in neonate rats aged P9-13. Interesting, similar bursts of activity were also observed in extracellular recording related to this thesis (Fig. 9.7, appendix), and in accordance with Jones et al., the spontaneous bursting activity was dependent on NMDARs. In addition, application of UBP-310 in a separate set of experiments also abolished the bursts (Fig. 9.7). The prevalence of these spontaneous bursts appeared to decrease with age (data not shown, example P18: 17events/hour vs P13: 243 events/hour). Moreover, in Chapter 6 we showed that the ability of ATPA to induce synchronised GABA release onto principal cells appears to be developmentally downregulated, providing further evidence of temporal roles of KARs in post-natal development. By virtue of this, it may be suggested that KARs could act as a functional enhancement of synaptic activity in immature neurones, which could influence and shape the formation of synaptic circuitry.

Lastly, this work has opened up new avenues linking the development of rhythmic brain activity in the superficial layers of the MEC with increased sensory input consequent on eye opening, which, hypothetically, may be linked to the development of synaptic organisation leading to grid-cell activity and the spatial navigation system.

8.4 KARs, pathological synchrony and neurodevelopmental disorders

KARs mediate postsynaptic depolarisation, modulate synaptic release of neurotransmitters and have been shown to have roles in the maturation of neural circuits during development in the hippocampus (Lauri and Taira, 2012, Lauri et al., 2005, Maingret et al., 2005, Lauri et al., 2006). Previous work from this lab (Chamberlain, 2009, Chamberlain et al., 2012) and work in this thesis has identified KARs located pre- and post-synaptically at excitatory and inhibitory synapses, where they are ideally located to mediate synchronised neuronal network activity in the developing and mature cortex (Chapter. 7). In addition, we have identified altered GluK1-cotnaining KAR functioning during post-natal development, which may pose consequences for maturation of the MEC. With the wide ranging actions in both the immature and mature MEC, it is not surprising that aberrant KAR functioning is associated with many neurological disorders, particularly associated with neurodevelopment, including autism (Jamain et al., 2002, Shuang et al., 2004), schizophrenia (Beneyto et al., 2007, Shaltiel et al., 2008, Shibata et al., 2006) Alzheimer's disease (Palop and Mucke, 2016) and epilepsy (Li and Rogawski, 1998, Li et al., 2010, Lucarini et al., 2007), which are all separately associated with the EC (Salmond et al., 2005, Baiano et al., 2008, Salmenperä et al., 2000, Vismer et al., 2015, Fuhrer et al., 2017) and abnormal network synchrony (see (Uhlhaas and Singer, 2010)). Cognitive deficits are a major symptom of many neurological disorders, which are often paralleled by abnormalities in neuronal synchronisation, including GFO. For example, EEG recordings show abnormal GFO in patients with schizophrenia (Uhlhaas and Singer, 2010, Sun et al., 2011, Williams and Boksa, 2010). A question to ask is whether the dysfunction in the co-ordination of neural activity in such disorders is the result of disconnection, or is it due deficits in synchronised neural responses needed for the propagation of signals. Besides, network disconnectivity may actually be a result of aberrant synchrony during development, which is essential for the maturation of neural circuitry and connectivity, and indeed, the KAR is heavily implicated in this process.

Whatever the reason, the clear roles of KARs in network synchrony during development would implicate this receptor in both the underlying pathophysiology, and as a therapeutic

target, in many disorders of abnormal neuronal synchrony, including schizophrenia and epilepsy.

8.5 Therapeutic targeting of KARs

The original aims of this thesis set out to establish the normal physiological roles of KARs in during development, with a view to apply this knowledge to understand the development of how pathological synchrony may manifest specifically in the MEC. Moreover, this data may shed light on the potential of KARs as targets for new therapeutic interventions for diseases of aberrant neuronal synchrony.
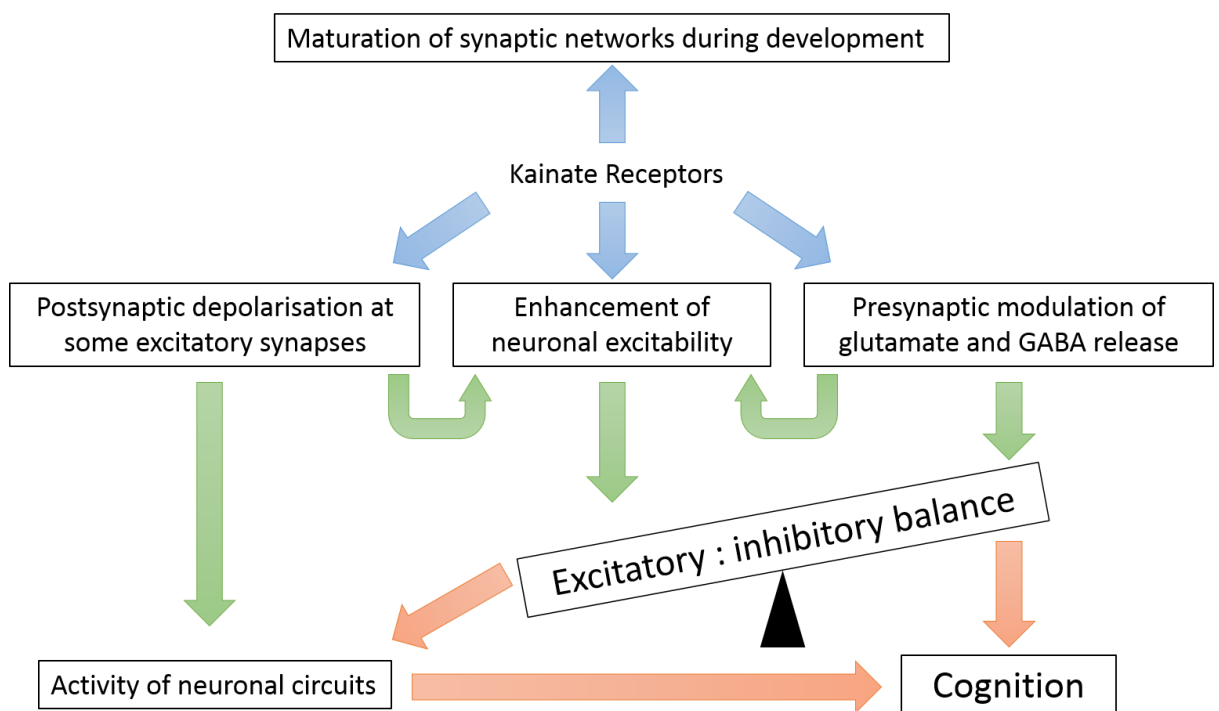
Figure 8.3: The roles of KARs in influencing cognition by modification neuronal and circuit activity. *Dysregulation of these activities could lead to disequilibrium leading to disease states. Adapted from Lerma et al. (2013).*

Data from this thesis has identified KARs located presynaptically at terminals of both excitatory and inhibitory synapses, where they act to facilitate glutamate or GABA release onto principals. Selectively targeting these receptors may provide a means of increasing or decreasing the general inhibitory or excitatory tone of the MEC, respectively, helping to restore the imbalance in excitation underscoring disorders such as TLE, without directly

preventing action potential propagation. On the other hand, targeting postsynaptic KARs may encourage network synchrony in disorders where neuronal communication is lacking. However, the long awaited development of more specific and novel antagonists are essential for understanding the precise functions of KARs in the MEC, and their therapeutic potential.

My results have demonstrated several roles for KARs in LII and LV of the MEC in mediating synchronised neuronal activity at the level of the synapse and the network as a whole. Moreover, that the activity of KARs in the MEC undergoes profound changes during development, which may have implications for the maturation of synaptic networks and the development of cognition associated with the MEC, such as spatial navigation and memory processes. These findings could be relevant for the development of novel therapeutic targets for neurodevelopmental disorders involving pathological synchrony and the MEC.

8.6 Overview and wider implications

The time period of post-natal development studied here in the rat is approximately correlated to a young adolescent human. At this time, many key neurodevelopmental processes are undergoing maturational changes across the whole brain which bare consequences related to sensorimotor, psychosocial and cognitive functioning. These processes include neuronal proliferation and myelination, development of the immune system (microglia) and the blood brain barrier, and synaptogenesis/pruning (Semple et al., 2013). The intensity of development over a relatively short period of time is likely why adolescence is a period of vulnerability for neuropsychiatric disease. The results from this thesis show that both excitatory and inhibitory neurotransmission, specifically within the MEC, undergo dramatic maturation during early adolescent brain development. In particular, there is an increase in synaptic noise which is thought to enable neuronal multiplexing of activity within a network, for example, gamma oscillations and grid cell activity. In addition, increased synaptic noise has been theorised to decrease the likelihood of seizures generation in the network. The results from this thesis also clearly defined the dramatic increase in synchronised neuronal network activity during early post-natal

development, which is pivotal in the development of cognitive processing associated with the MEC and the parahippocampal region in general. Neurotransmitter changes during early postnatal development coupled with decreased synaptic noise may render the immature brain inherently more prone to seizure activity, or other disorders of synchrony, compared to an older brain, and it is likely that such activity may have further consequences by interfering during critical periods of synaptic formation and pruning (Semple et al., 2013).
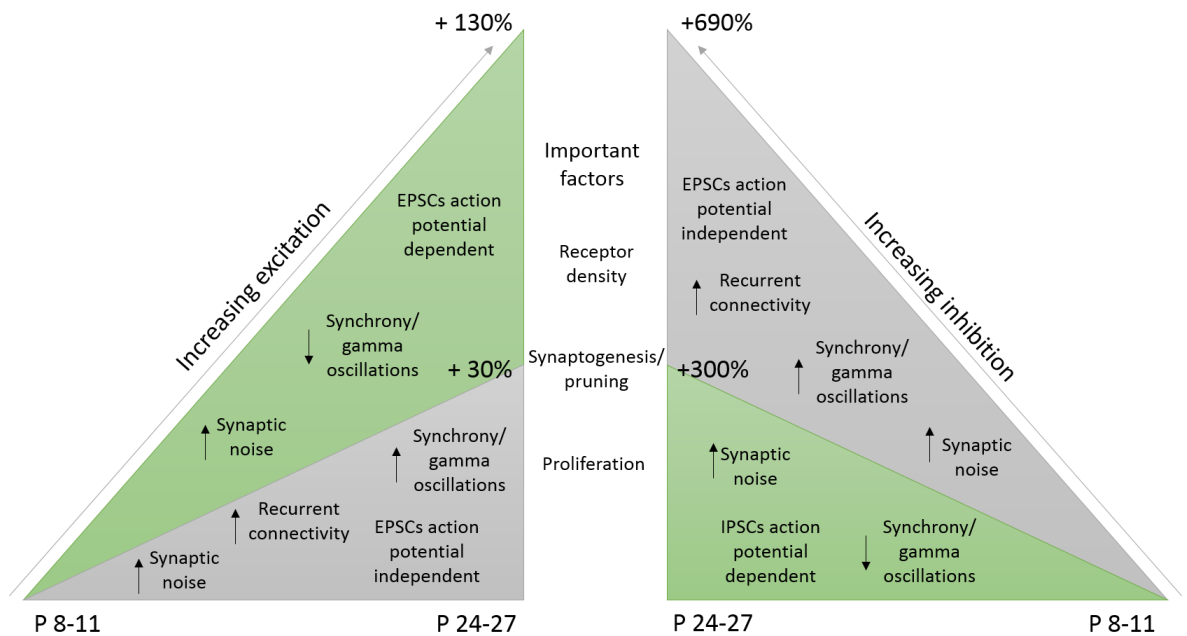
Figure 8.4: A summary of the developmental changes in excitation and inhibition in the MEC. *Grey: LII, Green: LV.*

Chapter 9

Appendix

9.1 Build-up and stability of KA-O

To determine the effects of various pharmacological agents on KA-O, we first had to determine if the KA-O were stable. LII MEC KA-O appear to build-up and stabilise after 1 hour KA, however, the stability of KA-O in LV was more variable. On the other hand, the frequency of KA-O stabilised after 1 hour application of KA in both LII and LV MEC of all age groups tested. The build-up of KA-O after application of 400 nM KA, in all ages and layers, is summarised in figure 9.1.
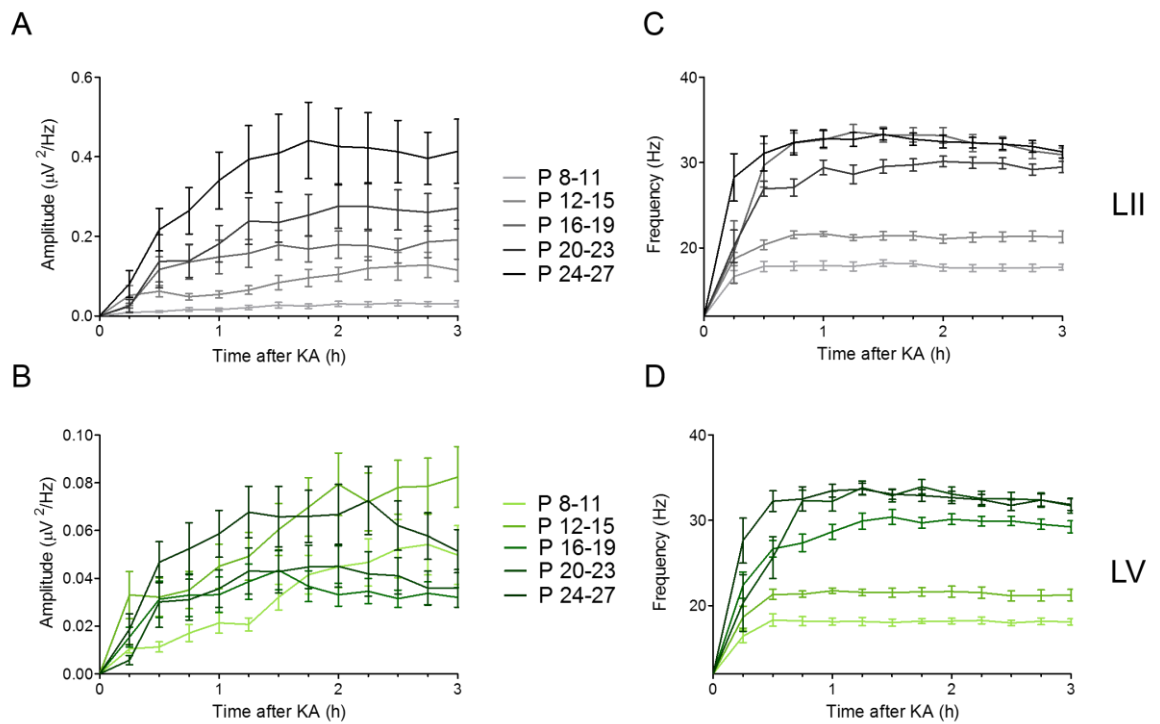
Figure 9.1: A summary of the developmental changes in excitation and inhibition in the MEC. *Graphs show mean and SEM of the amplitude LII (A), amplitude LV (B), frequency LII (C) and frequency LV (D) of KA-O induced after bath application of KA. Amplitude of LII, but not LV, appears to stabilise after 1 hour KA. The frequency of KA-O remains stable in both later after 1 hour KA.*

9.2 Gender differences in KA-O

Throughout this thesis male and female rats were used. No attempts were made to differentiate between male and female in the first 4 results chapters, however, male and female analysis was conducted on KA-O. Most of the comparisons showed similar patterns of activity in males versus females in terms of amplitude and frequency throughout development, summarised in figures 9.2 and 9.3, respectively.
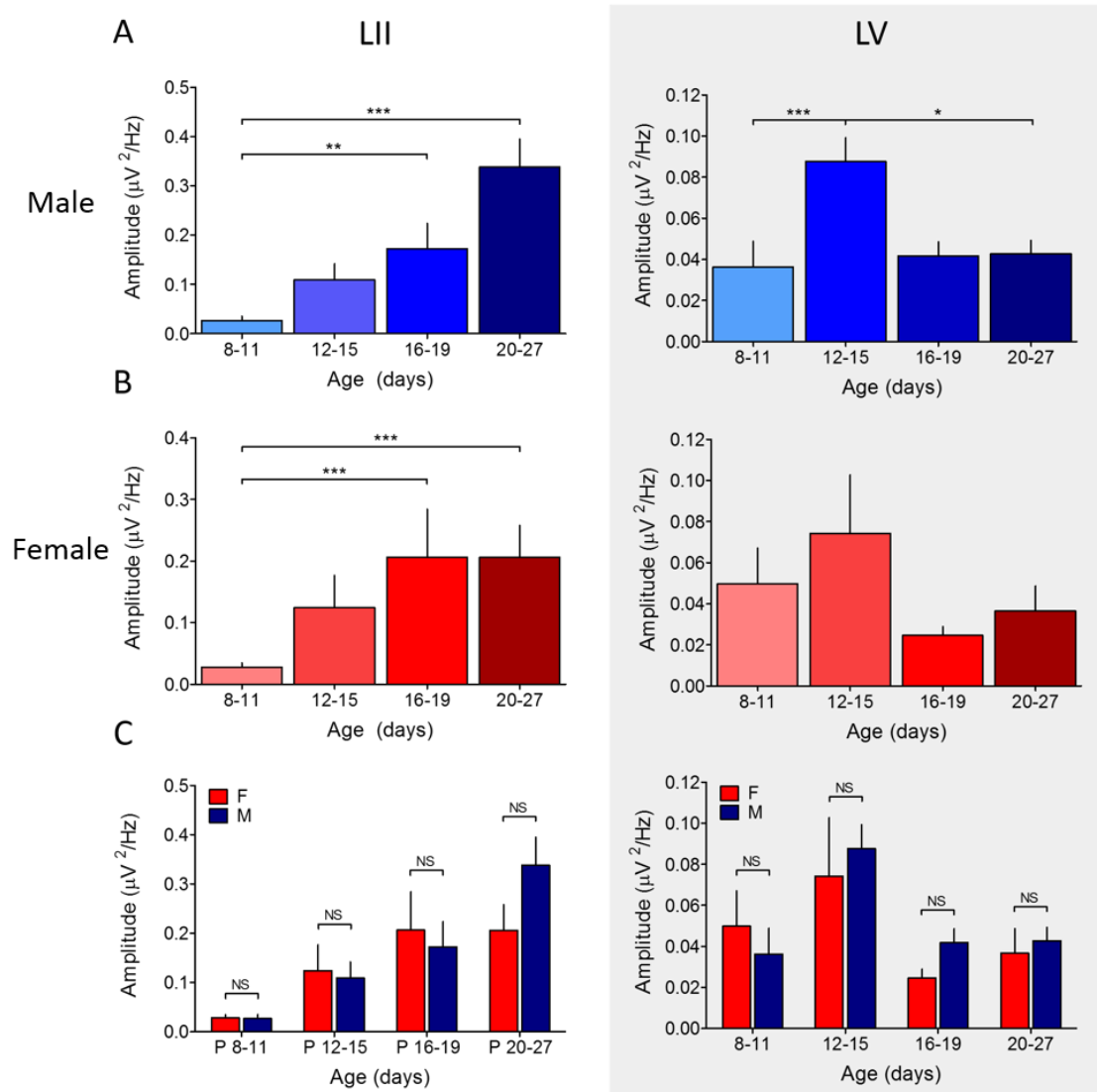
Figure 9.2: Gender differences in the amplitude of KA-O. *Changes to KA-O amplitude follow a similar pattern in LII of both male (blue) and female (red) KA-O, though female KA-O reach a maximum amplitude sooner. In LV, the increase in amplitude in the P12-15 age group is more exaggerated in males compared to female KA-O.*
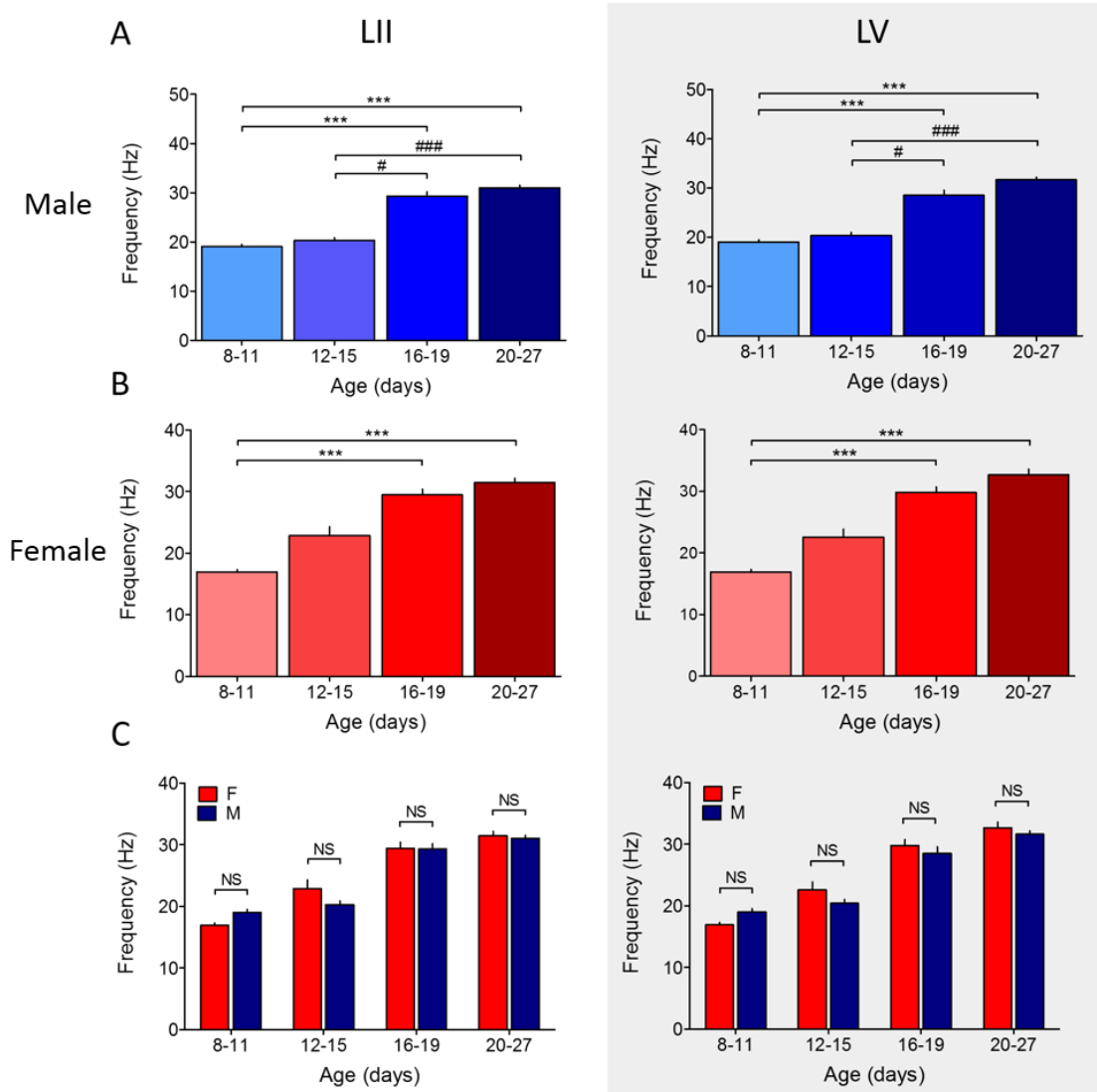
Figure 9.3: Gender differences in the frequency of KA-O. *Changes to KA-O frequency follow a similar pattern in LII of both male (blue) and female (red) KA-O, though female KA-O have a more gradual developmental increase in KA-O, compared to a more step-wise increase in frequency from a beta to a gamma band in the male group of both layers. This is due to a decreased frequency in female KA-O in the youngest age group (see figure 9.4)*

On closer analysis, an interesting observation was found in the youngest age group (P8-11), such that there was a small, but very significant, difference in the frequency of KA-O in males versus females. Specifically, the mean frequency of KA-O in the youngest (P8-11) was sigificantly faster in males (19.0 ± 0.5 Hz; n = 15) compared to females (16.9 ± 0.4 Hz, n = 23) in both layers (same values, P < 0.05). There were no further statistically significant differences in the frequency of KA-O in the older age groups. A comparison of the differences in the frequency of KA-O in the youngest and oldest age group can be seen in figure 9.4.
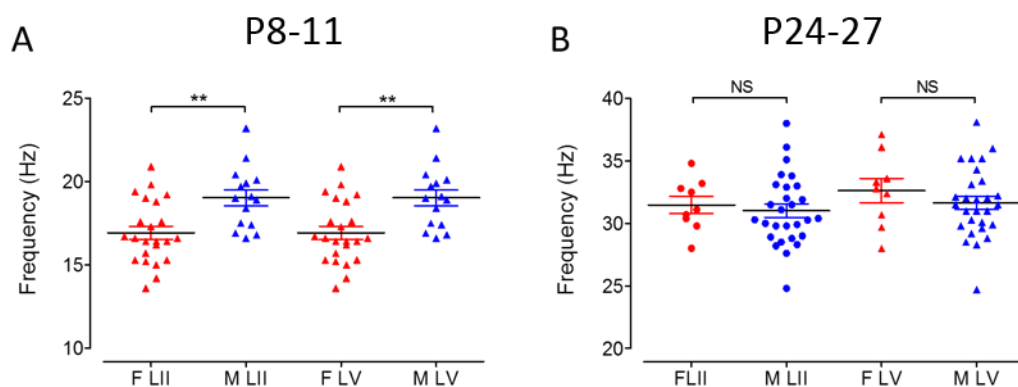
Figure 9.4 Gender differences in the frequency of KA-O at P8-11 and P24-27. *The mean frequency of KA-O was significantly slower in female versus male slices, in both layers (P < 0.01; Mann Whitney test). There were no gender differences in the oldest age groups.*

Male and female comparisons were also made when looking at the build-up and stability of KA-O. It appeared that, whilst KA-O built-up and stabilised after about 1 hour application of KA in MEC slices from male rats, slices from female rats did not appear to stabilise.

The developmental gender differences in KA-O may reflect altered maturation of GABAergic neurotransmission. Many studies have addressed this issue (in the hippocampus), and some show distinct sex differences in chloride co-transporter

expression at P7, an effect which is eliminated by P14 (Nunez and McCarthy, 2007). It is possible that similar sex differences may also be present in the MEC. Indeed, brain oscillations in humans also show gender influences (Nanova et al., 2011, Guntekin and Basar, 2007, Gron et al., 2000).

Gender differences in the MEC may have consequences for the development of cognition associated with this brain region, particularly spatial processing. Spatial reasoning and navigation experiments have previously determined gender bias in the organisation of spatial cognition in rats (Sneider et al., 2015). Female rats rely more on the frontal cortex for spatial navigation, whereas male rats depend more on the MEC (Gron et al., 2000), a trait which has been confirmed in human functional MRI studies. Despite this, current studies have not addressed these gender differences. Future experiments to address determining physiological gender differences in the development of cognition in the MEC would be useful to understand the differences in symptoms or morbidity of neurological disorders associated with this brain region.
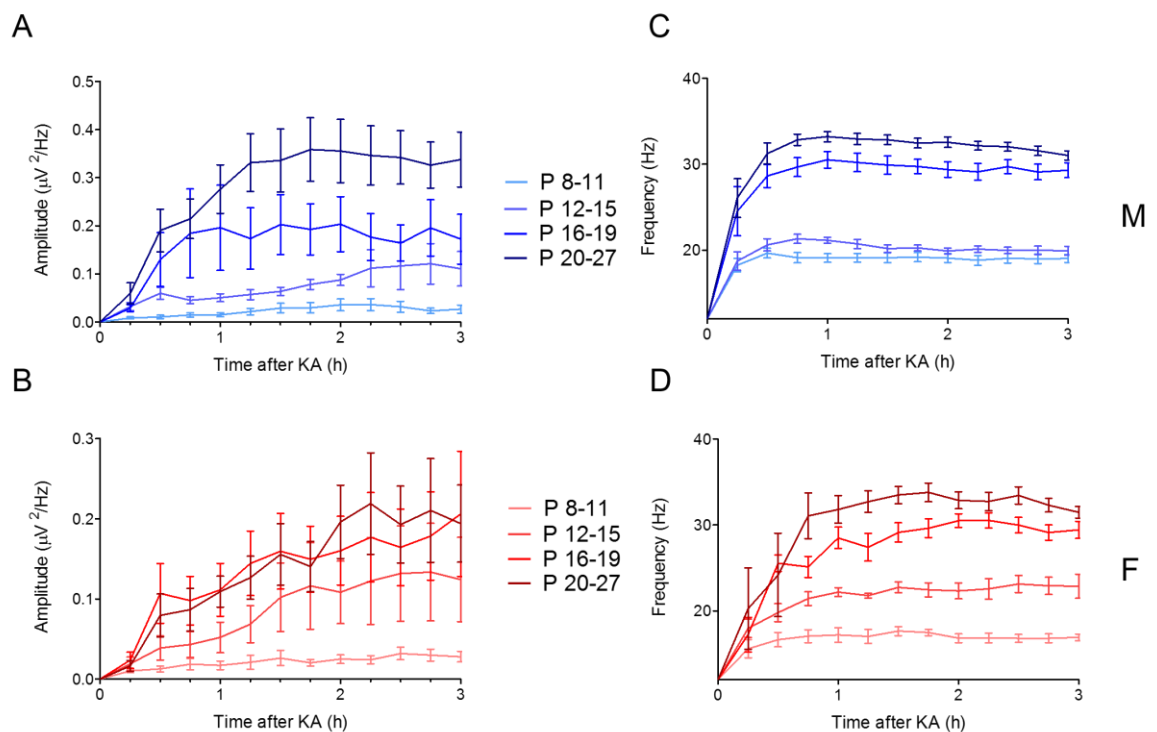
Figure 9.5: The build-up of KA-O in male and female LII *Graphs show mean and SEM of the amplitude of KA-O in male (A) and female (B) slices, frequency of KA-O in male (C) and female (D) slices after bath application of KA. Amplitude of males, but not females, appears*

to stabilise after 1 hour KA. The frequency of KA-O remains stable in both later after 1 hour KA.
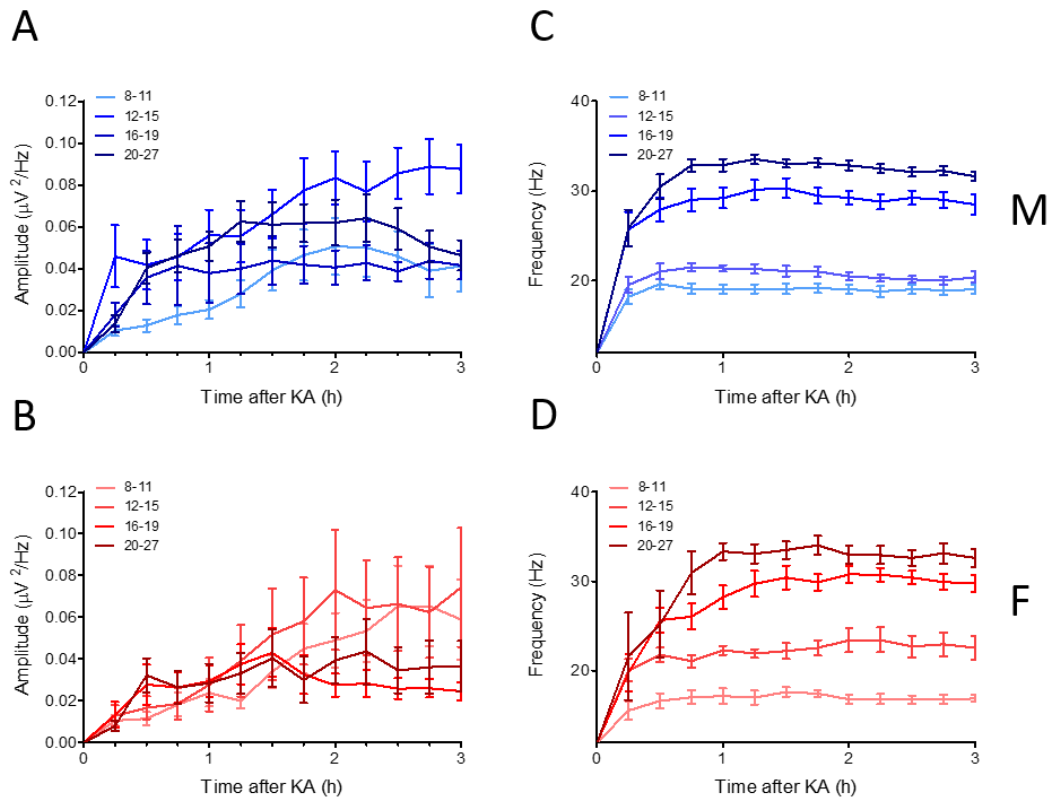
Figure 9.6: The build-up of KA-O in male and female LV. *Graphs show mean and SEM of the amplitude of KA-O in male (A) and female (B) slices, frequency of KA-O in male (C) and female (D) slices after bath application of KA. Amplitude of KA-O does not stabilise in LV. The frequency of KA-O remains stable in male and female slices after 1 hour KA.*

9.3 Spontaneous bursts in neonate LII MEC

Whilst recording extracellular activity in LII of the MEC, it became apparent that bursting activity would present spontaneously, in the absence of any pharmacological manipulation. The prevalence of the bursts appeared to decrease with age (data not shown), and were dependent on both NMDA and GluK-1 containing KARs (Fig. 9.7C&D). Such activity has been reported previously in the MEC, and may reflect endogenous synchronised network activity with roles in circuitry development.
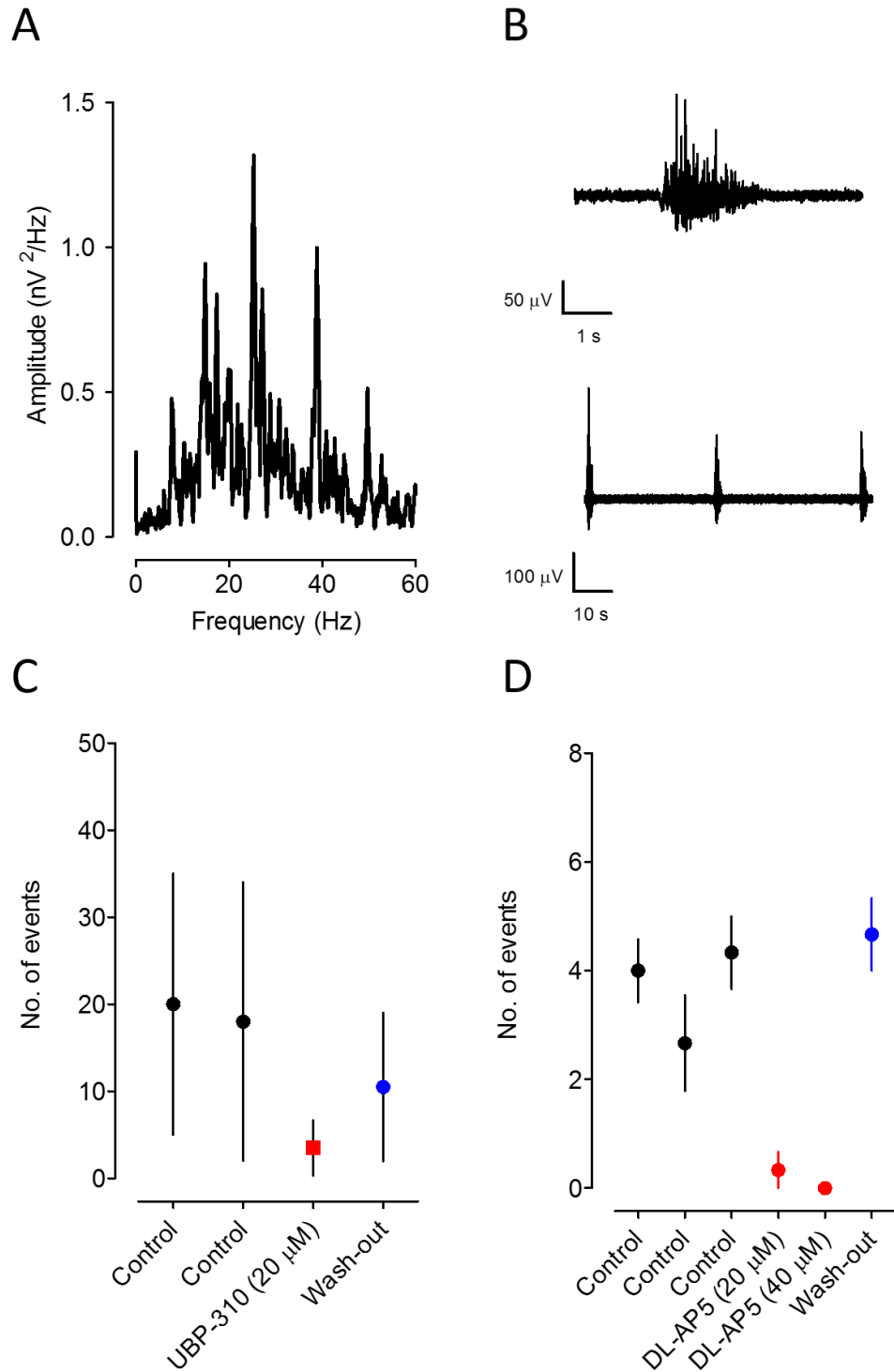
Figure 9.7: Spontaneous bursting activity in LII. (A) *Powerspectra analysis of a single burst.* *(B) Raw traces of LFP recordings of a single and **(C)** multiple spontaneous bursts in LII MEC.* *(D) Graph showing the mean number of bursts before and after the application of UBP-310* *(20 μM), and **(D)** DL-AP5 (20 & 40 μM) with a wash-out in both plots. Bursts were dependent* *on the GluK1-containing KAR and NMDARs.*

References

ALLISON, S. L., FAGAN, A. M., MORRIS, J. C. & HEAD, D. 2016. Spatial Navigation in Preclinical Alzheimer's Disease. *Journal of Alzheimer's disease* 52**,** 77-90.

ANDERSEN, P., MORRIS, R., AMARAL, D., BLISS , T. & O'KEEFE 2006. *The Hippocampus Book,* New York, Oxford University Press.

AOKI, T. & BARABAN, S. C. 2000. Properties of a Calcium-Activated K+Current on Interneurons in the Developing Rat Hippocampus. *Journal of Neurophysiology,* 83**,** 3453-3461.

ARANCIO, O., KORN, H., GULYAS, A., FREUND, T. & MILES, R. 1994. Excitatory synaptic connections onto rat hippocampal inhibitory cells may involve a single transmitter release site. *Journal of Physiology,* 481 (Pt 2)**,** 395-405.

ARMSTRONG, C., WANG, J., YEUN LEE, S., BRODERICK, J., BEZAIRE, M. J., LEE, S.-H. & SOLTESZ, I. 2016. Target-selectivity of parvalbumin-positive interneurons in layer II of medial entorhinal cortex in normal and epileptic animals. *Hippocampus,* 26**,** 779-793.

ARONIADOU-ANDERJASKA, V., QASHU, F. & BRAGA, M. F. 2007. Mechanisms regulating GABAergic inhibitory transmission in the basolateral amygdala: implications for epilepsy and anxiety disorders. *Amino Acids,* 32**,** 305-15.

ATLASON, P. T., SCHOLEFIELD, C. L., EAVES, R. J., MAYO-MARTIN, M. B., JANE, D. E. & MOLNÁR, E. 2010. Mapping the Ligand Binding Sites of Kainate Receptors: Molecular Determinants of Subunit-Selective Binding of the Antagonist UBP310. *Molecular Pharmacology,* 78**,** 1036-1045.

AVOLI, M., BARBAROSIE, M., LUCKE, A., NAGAO, T., LOPANTSEV, V. & KOHLING, R. 1996. Synchronous GABA-mediated potentials and epileptiform discharges in the rat limbic system in vitro. *Journal of Neuroscience,* 16**,** 3912-24.

AVOLI, M., D'ANTUONO, M., LOUVEL, J., KÖHLING, R., BIAGINI, G., PUMAIN, R., D'ARCANGELO, G. & TANCREDI, V. 2002. Network and pharmacological mechanisms leading to epileptiform synchronization in the limbic system in vitro. *Progress in Neurobiology,* 68**,** 167-207.

BACKUS, A. R., SCHOFFELEN, J.-M., SZEBÉNYI, S., HANSLMAYR, S. & DOELLER, C. F. 2016. Hippocampal-Prefrontal Theta Oscillations Support Memory Integration. *Current Biology,* 26**,** 450-457.

BAHN, S., VOLK, B. & WISDEN, W. 1994. Kainate receptor gene expression in the developing rat brain. *Journal of Neuroscience,* 14**,** 5525-47.

BAHN, S. & WISDEN, W. 1997. A Map of Non-NMDA Receptor Subunit Expression in the Vertebrate Brain Derived from In Situ Hybridization Histochemistry. *In:* MONAGHAN, D. T. & WENTHOLD, R. J. (eds.) *The Ionotropic Glutamate Receptors.* Totowa, NJ: Humana Press.

BAHR, S. & WOLFF, J. R. 1985. Postnatal development of axosomatic synapses in the rat visual cortex: morphogenesis and quantitative evaluation. *Journal of Computational Neurology,* 233**,** 405-20.

BAIANO, M., PERLINI, C., RAMBALDELLI, G., CERINI, R., DUSI, N., BELLANI, M., SPEZZAPRIA, G., VERSACE, A., BALESTRIERI, M., MUCELLI, R. P., TANSELLA, M. & BRAMBILLA, P. 2008. Decreased entorhinal cortex volumes in schizophrenia. *Schizophrenia Research,* 102**,** 171-80.

BAKS-TE BULTE, L., WOUTERLOOD, F. G., VINKENOOG, M. & WITTER, M. P. 2005. Entorhinal projections terminate onto principal neurons and interneurons in the subiculum: A quantitative electron microscopical analysis in the rat. *Journal of Neuroscience,* 136**,** 729-739.

BANERJEE, P. N., FILIPPI, D. & HAUSER, W. A. 2009. The descriptive epidemiology of epilepsy-a review. *Epilepsy research,* 85**,** 31-45.

BARD, P. 1933. Studies on the cerebral cortex: I. localized control of placing and hopping reactions in the cat and their normal management by small cortical remnants. *Archives of Neurology & Psychiatry,* 30**,** 40-74.

BARTOLOMEI, F., KHALIL, M., WENDLING, F., SONTHEIMER, A., REGIS, J., RANJEVA, J. P., GUYE, M. & CHAUVEL, P. 2005. Entorhinal cortex involvement in human mesial temporal lobe epilepsy: an electrophysiologic and volumetric study. *Epilepsia,* 46**,** 677-87.

BECKER, J. B., PRENDERGAST, B. J. & LIANG, J. W. 2016. Female rats are not more variable than male rats: a meta-analysis of neuroscience studies. *Biology of Sex Differences,* 7**,** 34.

BEED, P., GUNDLFINGER, A., SCHNEIDERBAUER, S., SONG, J., BÖHM, C., BURGALOSSI, A., BRECHT, M., VIDA, I. & SCHMITZ, D. 2013. Inhibitory Gradient along the Dorsoventral Axis in the Medial Entorhinal Cortex. *Neuron,* 79**,** 1197-1207.

BEERY, A. K. & ZUCKER, I. 2011. Sex Bias in Neuroscience and Biomedical Research. *Neuroscience and biobehavioral reviews,* 35**,** 565-572.

BELLGOWAN, P. S. F., BUFFALO, E. A., BODURKA, J. & MARTIN, A. 2009. Lateralized spatial and object memory encoding in entorhinal and perirhinal cortices. *Learning & Memory,* 16**,** 433-438.

BEN-ARI, Y. 1985. Limbic seizure and brain damage produced by kainic acid: mechanisms and relevance to human temporal lobe epilepsy. *Neuroscience,* 14**,** 375-403.

BEN-ARI, Y. 2010. Kainate and temporal lobe epilepsies: Three decades of progress. *Epilepsia,* 51**,** 40-40.

BEN-ARI, Y., CHERUBINI, E., CORRADETTI, R. & GAIARSA, J. L. 1989. Giant synaptic potentials in immature rat CA3 hippocampal neurones. *Journal of Physiology,* 416**,** 303-325.

BEN-ARI, Y. & COSSART, R. 2000. Kainate, a double agent that generates seizures: two decades of progress. *Trends Neuroscience* 23**,** 580-7.

BEN-ARI, Y., TREMBLAY, E., RICHE, D., GHILINI, G. & NAQUET, R. 1981. Electrographic, clinical and pathological alterations following systemic administration of kainic acid, bicuculline or pentetrazole: Metabolic mapping using the deoxyglucose method with special reference to the pathology of epilepsy. *Neuroscience,* 6**,** 1361-1391.

BENEYTO, M., KRISTIANSEN, L. V., ONI-ORISAN, A., MCCULLUMSMITH, R. E. & MEADOR-WOODRUFF, J. H. 2007. Abnormal glutamate receptor expression in the medial temporal lobe in schizophrenia and mood disorders. *Neuropsychopharmacology,* 32**,** 1888-902.

BERKE, J. D., OKATAN, M., SKURSKI, J. & EICHENBAUM, H. B. 2004. Oscillatory entrainment of striatal neurons in freely moving rats. *Neuron,* 43**,** 883-96.

BERNARD, A., FERHAT, L., DESSI, F., CHARTON, G., REPRESA, A., BEN-ARI, Y. & KHRESTCHATISKY, M. 1999. Q/R editing of the rat GluR5 and GluR6 kainate receptors in vivo and in vitro: evidence for independent developmental, pathological and cellular regulation. *European Journal Neuroscience,* 11**,** 604-16.

BERNARD, C. 2010. Alterations in synaptic function in epilepsy. *Epilepsia,* 51**,** 42-42.

BERNASCONI, N., BERNASCONI, A., ANDERMANN, F., DUBEAU, F., FEINDEL, W. & REUTENS, D. C. 1999. Entorhinal cortex in temporal lobe epilepsy: a quantitative MRI study. *Neurology,* 52**,** 1870-6.

BERNASCONI, N., BERNASCONI, A., CARAMANOS, Z., DUBEAU, F., RICHARDSON, J., ANDERMANN, F. & ARNOLD, D. L. 2001. Entorhinal cortex atrophy in epilepsy patients exhibiting normal hippocampal volumes. *Neurology,* 56**,** 1335-1339.

BERRETTA, N. & JONES, R. S. 1996. A comparison of spontaneous EPSCs in layer II and layer IV-V neurons of the rat entorhinal cortex in vitro. *Journal of Neurophysiology,* 76**,** 1089-1100.

BETTLER, B., BOULTER, J., HERMANS-BORGMEYER, I., O'SHEA-GREENFIELD, A., DENERIS, E. S., MOLL, C., BORGMEYER, U., HOLLMANN, M. & HEINEMANN, S. 1990. Cloning of a novel glutamate receptor subunit, GluR5: Expression in the nervous system during development. *Neuron,* 5**,** 583-595.

BETTLER, B., EGEBJERG, J., SHARMA, G., PECHT, G., HERMANS-BORGMEYER, I., MOLL, C., STEVENS, C. F. & HEINEMANN, S. 1992. Cloning of a putative glutamate receptor: A low affinity kainate-binding subunit. *Neuron,* 8**,** 257-265.

BINNS, K. E., TURNER, J. P. & SALT, T. E. 2003. Kainate receptor (GluR5)-mediated disinhibition of responses in rat ventrobasal thalamus allows a novel sensory processing mechanism. *Journal of Physiology,* 551**,** 525-537.

BONILHA, L., YASUDA, C. L., RORDEN, C., LI, L. M., TEDESCHI, H., DE OLIVEIRA, E. & CENDES, F. 2007. Does Resection of the Medial Temporal Lobe Improve the Outcome of Temporal Lobe Epilepsy Surgery? *Epilepsia,* 48**,** 571-578.

BORTOLOTTO, Z. A., CLARKE, V. R. J., DELANY, C. M., PARRY, M. C., SMOLDERS, I., VIGNES, M., HO, K. H., MIU, P., BRINTON, B. T., FANTASKE, R., OGDEN, A., GATES, M., ORNSTEIN, P. L., LODGE, D., BLEAKMAN, D. & COLLINGRIDGE, G. L. 1999. Kainate receptors are involved in synaptic plasticity. *Nature,* 402**,** 297-301.

BOSMAN, L. W., ROSAHL, T. W. & BRUSSAARD, A. B. 2002. Neonatal development of the rat visual cortex: synaptic function of GABAA receptor alpha subunits. *Journal Physiology* 545**,** 169-81.

BRAGIN, A., JANDO, G., NADASDY, Z., HETKE, J., WISE, K. & BUZSAKI, G. 1995. Gamma (40-100 Hz) oscillation in the hippocampus of the behaving rat. *Journal of Neuroscience,* 15**,** 47-60.

BRAGIN, D. E., SANDERSON, J. L., PETERSON, S., CONNOR, J. A. & MÜLLER, W. S. 2009. Development of epileptiform excitability in the deep entorhinal cortex after status epilepticus. *European journal of neuroscience,* 30**,** 611-624.

BROOKS-KAYAL, A. R., SHUMATE, M. D., JIN, H., RIKHTER, T. Y. & COULTER, D. A. 1998. Selective changes in single cell GABA(A) receptor subunit expression and function in temporal lobe epilepsy. *Nature Medicine,* 4**,** 1166-72.

BROWN, J. T., TERIAKIDIS, A. & RANDALL, A. D. 2006. A pharmacological investigation of the role of GLUK5-containing receptors in kainate-driven hippocampal gamma band oscillations. *Neuropharmacology,* 50**,** 47-56.

BRUN, V. H., SOLSTAD, T., KJELSTRUP, K. B., FYHN, M., WITTER, M. P., MOSER, E. I. & MOSER, M.-B. 2008. Progressive increase in grid scale from dorsal to ventral medial entorhinal cortex. *Hippocampus,* 18**,** 1200-1212.

BUETFERING, C., ALLEN, K. & MONYER, H. 2014. Parvalbumin interneurons provide grid cell-driven recurrent inhibition in the medial entorhinal cortex. *Nature Neuroscience,* 17**,** 710-718.

BUHL, E. H., TAMÁS, G. & FISAHN, A. 1998. Cholinergic activation and tonic excitation induce persistent gamma oscillations in mouse somatosensory cortex in vitro. *Journal of Physiology,* 513**,** 117-126.

BURAK, Y. & FIETE, I. R. 2009. Accurate Path Integration in Continuous Attractor Network Models of Grid Cells. *PLOS Computational Biology,* 5**,** e1000291.

BUREAU, I., DIEUDONNÉ, S., COUSSEN, F. & MULLE, C. 2000. Kainate receptor-mediated synaptic currents in cerebellar Golgi cells are not shaped by diffusion of glutamate. *Proceedings of the National Academy of Sciences,* 97**,** 6838-6843.

BURGALOSSI, A. & BRECHT, M. 2014. Cellular, columnar and modular organization of spatial representations in medial entorhinal cortex. *Current Opinion in Neurobiology,* 24**,** 47-54.

BURGALOSSI, A., HERFST, L., VON HEIMENDAHL, M., FÖRSTE, H., HASKIC, K., SCHMIDT, M. & BRECHT, M. 2011. Microcircuits of Functionally Identified Neurons in the Rat Medial Entorhinal Cortex. *Neuron,* 70**,** 773-786.

BURWELL, R. D. & AMARAL, D. G. 1998a. Cortical afferents of the perirhinal, postrhinal, and entorhinal cortices of the rat. *The Journal of Comparative Neurology,* 398**,** 179-205.

BURWELL, R. D. & AMARAL, D. G. 1998b. Perirhinal and postrhinal cortices of the rat: Interconnectivity and connections with the entorhinal cortex. *The Journal of Comparative Neurology,* 391**,** 293-321.

BUZSAKI, G., LEUNG, L. W. & VANDERWOLF, C. H. 1983. Cellular bases of hippocampal EEG in the behaving rat. *Brain Research,* 287**,** 139-71.

BUZSAKI, G. & MOSER, E. I. 2013. Memory, navigation and theta rhythm in the hippocampal-entorhinal system. *Nature Neuroscience,* 16**,** 130-138.

BUZSÁKI, G. & WANG, X.-J. 2012. Mechanisms of Gamma Oscillations. *Annual review of Neuroscience,* 35**,** 203-225.

CABALLERO-BLEDA, M. & WITTER, M. P. 1993. Regional and laminar organization of projections from the presubiculum and parasubiculum to the entorhinal cortex: An anterograde tracing study in the rat. *Journal of Comparative Neurology,* 328**,** 115-129.

CAJAL, S. R. 1893. Estructura del asta de Ammon y fascia dentata. *Ann Soc Esp Hist Nat.,* 22.

CANTO, C. B. & WITTER, M. P. 2012. Cellular properties of principal neurons in the rat entorhinal cortex. II. The medial entorhinal cortex. *Hippocampus,* 22**,** 1277-1299.

CANTO, C. B., WOUTERLOOD, F. G. & WITTER, M. P. 2008. What Does the Anatomical Organization of the Entorhinal Cortex Tell Us? *Neural Plasticity,* 2008**,** 18.

CASTILLO, P. E., MALENKA, R. C. & NICOLL, R. A. 1997. Kainate receptors mediate a slow postsynaptic current in hippocampal CA3 neurons. *Nature,* 388**,** 182-186.

CASTRO-ALAMANCOS, M. A. & FAVERO, M. 2015. NMDA receptors are the basis for persistent network activity in neocortex slices. *Journal of Neurophysiology,* 113**,** 3816-3826.

CATON, R. 1875. The electric currents of the brain. *British Medical Journal* 2: 278.

CHAMBERLAIN, S. E. L. 2009. The functional role of kainate receptors in the rat entorhinal cortex. *Thesis*.

CHAMBERLAIN, S. E. L., JANE, D. E. & JONES, R. S. G. 2012. Pre- and post-synaptic functions of kainate receptors at glutamate and GABA synapses in the rat entorhinal cortex. *Hippocampus,* 22**,** 555-576.

CHATTOPADHYAYA, B., DI CRISTO, G., HIGASHIYAMA, H., KNOTT, G. W., KUHLMAN, S. J., WELKER, E. & HUANG, Z. J. 2004. Experience and Activity-Dependent Maturation of Perisomatic GABAergic Innervation in Primary Visual Cortex during a Postnatal Critical Period. *Journal of Neuroscience,* 24**,** 9598-9611.

CHERUBINI, E., GAIARSA, J. L. & BEN-ARI, Y. 1991. GABA: an excitatory transmitter in early postnatal life. *Trends in Neurosciences,* 14**,** 515-519.

CHROBAK, J. J. & BUZSAKI, G. 1998. Gamma oscillations in the entorhinal cortex of the freely behaving rat. *Journal of Neuroscience,* 18**,** 388-98.

CHRONWALL, B. & WOLFF, J. R. 1980. Prenatal and postnatal development of GABA-accumulating cells in the occipital neocortex of rat. *The Journal of Comparative Neurology,* 190**,** 187-208.

CLARK, B. J. 2017. Spatial Navigation: Retrosplenial Cortex Encodes the Spatial Structure of Complex Routes. *Current Biology,* 27**,** R649-R651.

CLARKE, V. R. J., BALLYK, B. A., HOO, K. H., MANDELZYS, A., PELLIZZARI, A., BATH, C. P., THOMAS, J., SHARPE, E. F., DAVIES, C. H., ORNSTEIN, P. L., SCHOEPP, D. D., KAMBOJ, R. K., COLLINGRIDGE, G. L., LODGE, D. & BLEAKMAN, D. 1997. A hippocampal GluR5 kainate receptor regulating inhibitory synaptic transmission. *Nature,* 389**,** 599.

CLARKE, V. R. J., MOLCHANOVA, S. M., HIRVONEN, T., TAIRA, T. & LAURI, S. E. 2014. Activity-Dependent Upregulation of Presynaptic Kainate Receptors at Immature CA3–CA1 Synapses. *Journal of Neuroscience,* 34**,** 16902-16916.

CLEMENTS, J. D. 1996. Transmitter timecourse in the synaptic cleft: its role in central synaptic function. *Trends in Neurosciences,* 19**,** 163-171.

COHEN, A. S., LIN, D. D. & COULTER, D. A. 2000. Protracted postnatal development of inhibitory synaptic transmission in rat hippocampal area CA1 neurons. *Journal of Neurophysiology,* 84**,** 2465-76.

CONTI, F. & WEINBERG, R. J. 1999. Shaping excitation at glutamatergic synapses. *Trends in Neurosciences,* 22**,** 451-458.

CONTRACTOR, A., SWANSON, G. & HEINEMANN, S. F. 2001. Kainate Receptors Are Involved in Short- and Long-Term Plasticity at Mossy Fiber Synapses in the Hippocampus. *Neuron,* 29**,** 209-216.

COPITS, B. A., ROBBINS, J. S., FRAUSTO, S. & SWANSON, G. T. 2011. Synaptic targeting and functional modulation of GluK1 kainate receptors by the auxiliary NETO proteins. *Journal of neuroscience* 31**,** 7334-7340.

COSSART, R., EPSZTEIN, J., TYZIO, R., BECQ, H., HIRSCH, J., BEN-ARI, Y. & CRÉPEL, V. 2002. Quantal Release of Glutamate Generates Pure Kainate and Mixed AMPA/Kainate EPSCs in Hippocampal Neurons. *Neuron,* 35**,** 147-159.

COSSART, R., ESCLAPEZ, M., HIRSCH, J. C., BERNARD, C. & BEN-ARI, Y. 1998. GluR5 kainate receptor activation in interneurons increases tonic inhibition of pyramidal cells. *Nature Neuroscience,* 1**,** 470-478.

COSSART, R., TYZIO, R., DINOCOURT, C., ESCLAPEZ, M., HIRSCH, J. C., BEN-ARI, Y. & BERNARD, C. 2001. Presynaptic Kainate Receptors that Enhance the Release of GABA on CA1 Hippocampal Interneurons. *Neuron,* 29**,** 497-508.

COUEY, J. J., WITOELAR, A., ZHANG, S.-J., ZHENG, K., YE, J., DUNN, B., CZAJKOWSKI, R., MOSER, M.-B., MOSER, E. I., ROUDI, Y. & WITTER, M. P. 2013. Recurrent inhibitory circuitry as a mechanism for grid formation. *Nature Neuroscience,* 16**,** 318-324.

COUTUREAU, E. & DI SCALA, G. 2009. Entorhinal cortex and cognition. *Progress in Neuro-Psychopharmacology and Biological Psychiatry,* 33**,** 753-761.

COYLE, J. T. 1996. The glutamatergic dysfunction hypothesis for schizophrenia. *Harvard Review of Psychiatry,* 3**,** 241-53.

CSICSVARI, J., JAMIESON, B., WISE, K. D. & BUZSÁKI, G. 2003. Mechanisms of Gamma Oscillations in the Hippocampus of the Behaving Rat. *Neuron,* 37**,** 311-322.

CUNNINGHAM, M. O., DAVIES, C. H., BUHL, E. H., KOPELL, N. & WHITTINGTON, M. A. 2003. Gamma Oscillations Induced by Kainate Receptor Activation in the Entorhinal Cortex *In Vitro. Journal of Neuroscience,* 23**,** 9761-9769.

CUNNINGHAM, M. O., HALLIDAY, D. M., DAVIES, C. H., TRAUB, R. D., BUHL, E. H. & WHITTINGTON, M. A. 2004a. Coexistence of gamma and high-frequency oscillations in rat medial entorhinal cortex in vitro. *Journal of Physiology,* 559**,** 347-353.

CUNNINGHAM, M. O., HUNT, J., MIDDLETON, S., LEBEAU, F. E. N., GILLIES, M. G., DAVIES, C. H., MAYCOX, P. R., WHITTINGTON, M. A. & RACCA, C. 2006a. Region-Specific Reduction in Entorhinal Gamma Oscillations and Parvalbumin-Immunoreactive Neurons in Animal Models of Psychiatric Illness. *Journal of Neuroscience,* 26**,** 2767-2776.

CUNNINGHAM, M. O., PERVOUCHINE, D. D., RACCA, C., KOPELL, N. J., DAVIES, C. H., JONES, R. S. G., TRAUB, R. D. & WHITTINGTON, M. A. 2006b. Neuronal metabolism governs cortical network response state. *Proceedings of the National Academy of Sciences,* 103**,** 5597-5601.

CUNNINGHAM, M. O., WHITTINGTON, M. A., BIBBIG, A., ROOPUN, A., LEBEAU, F. E. N., VOGT, A., MONYER, H., BUHL, E. H. & TRAUB, R. D. 2004b. A role for fast rhythmic bursting neurons in cortical gamma oscillations in vitro. *Proceedings of the National Academy of Sciences of the United States of America,* 101**,** 7152-7157.

DAILEY, M. E. & SMITH, S. J. 1996. The Dynamics of Dendritic Structure in Developing Hippocampal Slices. *Journal of Neuroscience,* 16**,** 2983-2994.

DAW, M. I., PELKEY, K. A., CHITTAJALLU, R. & MCBAIN, C. J. 2010. Presynaptic Kainate Receptor Activation Preserves Asynchronous GABA Release Despite the Reduction in Synchronous Release from Hippocampal CCK Interneurons. *Journal of neuroscience,* 30**,** 11202-11209.

DEL CASTILLO, J. & KATZ, B. 1954. Quantal components of the end-plate potential. *Journal of Physiology,* 124**,** 560-73.

DELANEY, A. J. & JAHR, C. E. 2002. Kainate Receptors Differentially Regulate Release at Two Parallel Fiber Synapses. *Neuron,* 36**,** 475-482.

DEVLIN, J. T. & PRICE, C. J. 2007. Perirhinal Contributions to Human Visual Perception. *Current Biology,* 17**,** 1484-1488.

DHILLON, A. & JONES, R. S. 2000. Laminar differences in recurrent excitatory transmission in the rat entorhinal cortex in vitro. *Neuroscience,* 99**,** 413-22.

DICKERSON, B. C. & EICHENBAUM, H. 2010. The episodic memory system: neurocircuitry and disorders. *Neuropsychopharmacology,* 35**,** 86-104.

DOELLER, C. F., BARRY, C. & BURGESS, N. 2010. Evidence for grid cells in a human memory network. *Nature,* 463**,** 657-661.

DOISCHER, D., HOSP, J. A., YANAGAWA, Y., OBATA, K., JONAS, P., VIDA, I. & BARTOS, M. 2008. Postnatal differentiation of basket cells from slow to fast signaling devices. *Journal of Neuroscience,* 28**,** 12956-68.

DONATO, F., JACOBSEN, R. I., MOSER, M.-B. & MOSER, E. I. 2017. Stellate cells drive maturation of the entorhinal-hippocampal circuit. *Science,* 355.

DRAGUHN, A., TRAUB, R. D., SCHMITZ, D. & JEFFERYS, J. G. 1998. Electrical coupling underlies high-frequency oscillations in the hippocampus in vitro. *Nature,* 394**,** 189-92.

DRICKS, S. 2016. Effects of neonatal stress on gamma oscillations in hippocampus. *Nature,* 6**,** 29007.

DU, F., WHETSELL, W. O., ABOU-KHALIL, B., BLUMENKOPF, B., LOTHMAN, E. W. & SCHWARCZ, R. 1993. Preferential neuronal loss in layer III of the entorhinal cortex in patients with temporal lobe epilepsy. *Epilepsy Research,* 16**,** 223-233.

DU, J., ZHANG, L., WEISER, M., RUDY, B. & MCBAIN, C. J. 1996. Developmental expression and functional characterization of the potassium-channel subunit Kv3.1b in parvalbumin-containing interneurons of the rat hippocampus. *Journal of Neuroscience,* 16**,** 506-18.

DUNNING, D. D., HOOVER, C. L., SOLTESZ, I., SMITH, M. A. & O'DOWD, D. K. 1999. GABA(A) receptor-mediated miniature postsynaptic currents and alpha-subunit expression in developing cortical neurons. *Journal of Neurophysiology,* 82**,** 3286-97.

DUPONT, E., HANGANU, I. L., KILB, W., HIRSCH, S. & LUHMANN, H. J. 2006. Rapid developmental switch in the mechanisms driving early cortical columnar networks. *Nature,* 439**,** 79-83.

ECCLES, J. C. 1945. An electrical hypothesis of synaptic and neuromuscular transmission. *Nature,* 156**,** 680-3.

EDWARDS, F. A., KONNERTH, A. & SAKMANN, B. 1990. Quantal analysis of inhibitory synaptic transmission in the dentate gyrus of rat hippocampal slices: a patch-clamp study. *Journal of Physiology,* 430**,** 213-249.

EGEBJERG, J., BETTLER, B., HERMANS-BORGMEYER, I. & HEINEMANN, S. 1991. Cloning of a cDNA for a glutamate receptor subunit activated by kainate but not AMPA. *Nature,* 351**,** 745-748.

EGEBJERG, J. & HEINEMANN, S. F. 1993. Ca2+Permeability of Unedited and Edited Versions of the Kainate Selective Glutamate Receptor GluR6. *Proceedings of the National Academy of Sciences of the United States of America,* 90**,** 755-759.

EICHENBAUM, H. & COHEN, NEAL J. 2014. Can We Reconcile the Declarative Memory and Spatial Navigation Views on Hippocampal Function? *Neuron,* 83**,** 764-770.

EKSTROM, A. D., CAPLAN, J. B., HO, E., SHATTUCK, K., FRIED, I. & KAHANA, M. J. 2005. Human hippocampal theta activity during virtual navigation. *Hippocampus,* 15**,** 881-889.

EPSTEIN, R. A. 2008. Parahippocampal and retrosplenial contributions to human spatial navigation. *Trends Cognitive Science,* 12**,** 388-96.

EPSZTEIN, J., REPRESA, A., JORQUERA, I., BEN-ARI, Y. & CRÉPEL, V. 2005. Recurrent Mossy Fibers Establish Aberrant Kainate Receptor-Operated Synapses on Granule Cells from Epileptic Rats. *Journal of Neuroscience,* 25**,** 8229-8239.

ERMENTROUT, G. B., GALÁN, R. F. & URBAN, N. N. 2008. Reliability, synchrony and noise. *Trends in neurosciences,* 31**,** 428-434.

ERMENTROUT, G. B. & KOPELL, N. 1998. Fine structure of neural spiking and synchronization in the presence of conduction delays. *PNAS,* 95**,** 1259-64.

ESPINOSA, J. S. & STRYKER, MICHAEL P. 2012. Development and Plasticity of the Primary Visual Cortex. *Neuron,* 75**,** 230-249.

FATT, P. & KATZ, B. 1952. Spontaneous subthreshold activity at motor nerve endings. *Journal of Physiology,* 117**,** 109-128.

FERNÁNDEZ-RUIZ, A., OLIVA, A., NAGY, G. A., MAURER, A. P., BERÉNYI, A. & BUZSÁKI, G. 2017. Entorhinal-CA3 Dual-Input Control of Spike Timing in the Hippocampus by Theta-Gamma Coupling. *Neuron,* 93**,** 1213-1226.e5.

FINCH, D. M., TAN, A. M. & ISOKAWA-AKESSON, M. 1988. Feedforward inhibition of the rat entorhinal cortex and subicular complex. *J Neurosci,* 8**,** 2213-26.

FISAHN, A. 2005. Kainate receptors and rhythmic activity in neuronal networks: hippocampal gamma oscillations as a tool. *The Journal of Physiology,* 562**,** 65-72.

FISAHN, A., CONTRACTOR, A., TRAUB, R. D., BUHL, E. H., HEINEMANN, S. F. & MCBAIN, C. J. 2004. Distinct roles for the kainate receptor subunits GluR5 and GluR6 in kainate-induced hippocampal gamma oscillations. *Journal of Neuroscience,* 24**,** 9658-68.

FISAHN, A., PIKE, F. G., BUHL, E. H. & PAULSEN, O. 1998. Cholinergic induction of network oscillations at 40 Hz in the hippocampus in vitro. *Nature,* 394**,** 186-9.

FISHER, J. L. 2015. The auxiliary subunits Neto1 and Neto2 have distinct, subunit-dependent effects at recombinant GluK1- and GluK2-containing kainate receptors. *Neuropharmacology,* 99**,** 471-480.

FISHER, J. L. & MOTT, D. D. 2011. Distinct Functional Roles of Subunits within the Heteromeric Kainate Receptor. *Journal of neuroscience* 31**,** 17113-17122.

FISHER, J. L. & MOTT, D. D. 2013. Modulation of homomeric and heteromeric kainate receptors by the auxiliary subunit Neto1. *Journal of Physiology,* 591**,** 4711-4724.

FISHER, M. T. & FISHER, J. L. 2014. Contributions of different kainate receptor subunits to the properties of recombinant homomeric and heteromeric receptors. *Neuroscience,* 278**,** 70-80.

FRANSÉN, E. 2010. Entorhinal Cortex Cells. . *Springer Series in Computational Neuroscience,* vol 5.

FRERKING, M., PETERSEN, C. C. & NICOLL, R. A. 1999. Mechanisms underlying kainate receptor-mediated disinhibition in the hippocampus. *Proc Natl Acad Sci U S A,* 96**,** 12917-22.

FRIES, P. 2005. A mechanism for cognitive dynamics: neuronal communication through neuronal coherence. *Trends Cognitive Science,* 9**,** 474-80.

FRIES, P. 2009. Neuronal Gamma-Band Synchronization as a Fundamental Process in Cortical Computation. *Annual Review of Neuroscience,* 32**,** 209-224.

FRORIEP, U. P., KUMAR, A., COSANDIER-RIMÉLÉ, D., HÄUSSLER, U., KILIAS, A., HAAS, C. A. & EGERT, U. 2012. Altered theta coupling between medial entorhinal cortex and dentate gyrus in temporal lobe epilepsy. *Epilepsia,* 53**,** 1937-1947.

FU, H., RODRIGUEZ, G. A., HERMAN, M., EMRANI, S., NAHMANI, E., BARRETT, G., FIGUEROA, H. Y., GOLDBERG, E., HUSSAINI, S. A. & DUFF, K. E. 2017. Tau Pathology

Induces Excitatory Neuron Loss, Grid Cell Dysfunction, and Spatial Memory Deficits Reminiscent of Early Alzheimer's Disease. *Neuron,* 93**,** 533-541.e5.

FUCHS, ELKE C., NEITZ, A., PINNA, R., MELZER, S., CAPUTI, A. & MONYER, H. 2016. Local and Distant Input Controlling Excitation in Layer II of the Medial Entorhinal Cortex. *Neuron,* 89**,** 194-208.

FUHRER, T. E., PALPAGAMA, T. H., WALDVOGEL, H. J., SYNEK, B. J. L., TURNER, C., FAULL, R. L. & KWAKOWSKY, A. 2017. Impaired expression of GABA transporters in the human Alzheimer's disease hippocampus, subiculum, entorhinal cortex and superior temporal gyrus. *Neuroscience,* 351**,** 108-118.

FUNG, S. J., FILLMAN, S. G., WEBSTER, M. J. & SHANNON WEICKERT, C. 2014. Schizophrenia and bipolar disorder show both common and distinct changes in cortical interneuron markers. *Schizophrenia Research,* 155**,** 26-30.

FURTAK, S. C., WEI, S.-M., AGSTER, K. L. & BURWELL, R. D. 2007. Functional neuroanatomy of the parahippocampal region in the rat: The perirhinal and postrhinal cortices. *Hippocampus,* 17**,** 709-722.

FYHN, M., HAFTING, T., TREVES, A., MOSER, M.-B. & MOSER, E. I. 2007. Hippocampal remapping and grid realignment in entorhinal cortex. *Nature,* 446**,** 190-194.

GARASCHUK, O., LINN, J., EILERS, J. & KONNERTH, A. 2000. Large-scale oscillatory calcium waves in the immature cortex. *Nature Neuroscience,* 3**,** 452-459.

GIBBS, J. W., 3RD, SHUMATE, M. D. & COULTER, D. A. 1997. Differential epilepsy-associated alterations in postsynaptic GABA(A) receptor function in dentate granule and CA1 neurons. *Journal of Neurophysiology,* 77**,** 1924-38.

GILLIES, M. J., TRAUB, R. D., LEBEAU, F. E., DAVIES, C. H., GLOVELI, T., BUHL, E. H. & WHITTINGTON, M. A. 2002. A model of atropine-resistant theta oscillations in rat hippocampal area CA1. *Journal of Physiology,* 543**,** 779-93.

GIOCOMO, LISA M., STENSOLA, T., BONNEVIE, T., VAN CAUTER, T., MOSER, M.-B. & MOSER, EDVARD I. 2014. Topography of Head Direction Cells in Medial Entorhinal Cortex. *Current Biology,* 24**,** 252-262.

GLOVELI, T., DUGLADZE, T., SAHA, S., MONYER, H., HEINEMANN, U., TRAUB, R. D., WHITTINGTON, M. A. & BUHL, E. H. 2005. Differential involvement of oriens/pyramidale interneurones in hippocampal network oscillations in vitro. *Journal of Physiology,* 562**,** 131-47.

GOLDIN, M., EPSZTEIN, J., JORQUERA, I., REPRESA, A., BEN-ARI, Y., CRÉPEL, V. & COSSART, R. 2007. Synaptic Kainate Receptors Tune Oriens-Lacunosum Moleculare Interneurons to Operate at Theta Frequency. *Journal of Neuroscience,* 27**,** 9560-9572.

GOODMAN, C. S. & SHATZ, C. J. 1993. Developmental mechanisms that generate precise patterns of neuronal connectivity. *Cell,* 72 Suppl**,** 77-98.

GRAY, C. M., KONIG, P., ENGEL, A. K. & SINGER, W. 1989. Oscillatory responses in cat visual cortex exhibit inter-columnar synchronization which reflects global stimulus properties. *Nature,* 338**,** 334-7.

GREENE, J. 1996. Cortex Cerebri. Performance, structural and functional organization of the cortex. *Journal of Neurology, Neurosurgery, and Psychiatry,* 60**,** 467-467.

GREENHILL, S. D., CHAMBERLAIN, S. E. L., LENCH, A., MASSEY, P. V., YUILL, K. H., WOODHALL, G. L. & JONES, R. S. G. 2014. Background Synaptic Activity in Rat Entorhinal Cortex Shows a Progressively Greater Dominance of Inhibition over Excitation from Deep to Superficial Layers. *PLOS ONE,* 9**,** e85125.

GREENHILL, S. D. & JONES, R. S. 2010. Diverse antiepileptic drugs increase the ratio of background synaptic inhibition to excitation and decrease neuronal excitability in neurones of the rat entorhinal cortex in vitro. *Neuroscience,* 167**,** 456-74.

GRON, G., WUNDERLICH, A. P., SPITZER, M., TOMCZAK, R. & RIEPE, M. W. 2000. Brain activation during human navigation: gender-different neural networks as substrate of performance. *Nature Neuroscience,* 3**,** 404-408.

GUNN, B., BROWN, A., LAMBERT, J. & BELELLI, D. 2011. Neurosteroids and GABAA Receptor Interactions: A Focus on Stress. *Frontiers in Neuroscience,* 5.

GUNTEKIN, B. & BASAR, E. 2007. Brain oscillations are highly influenced by gender differences. *International Journal Psychophysiology,* 65**,** 294-9.

HAFTING, T., FYHN, M., MOLDEN, S., MOSER, M.-B. & MOSER, E. I. 2005. Microstructure of a spatial map in the entorhinal cortex. *Nature,* 436**,** 801-806.

HANSLMAYR, S., STARESINA, B. P. & BOWMAN, H. 2016. Oscillations and Episodic Memory: Addressing the Synchronization/Desynchronization Conundrum. *Trends in Neurosciences,* 39**,** 16-25.

HARGREAVES, E. L., MATTFELD, A. T., STARK, C. E. & SUZUKI, W. A. 2012. Conserved fMRI and LFP signals during new associative learning in the human and macaque monkey medial temporal lobe. *Neuron,* 74**,** 743-752.

HASHIMOTO, T., VOLK, D. W., EGGAN, S. M., MIRNICS, K., PIERRI, J. N., SUN, Z., SAMPSON, A. R. & LEWIS, D. A. 2003. Gene expression deficits in a subclass of GABA neurons in the prefrontal cortex of subjects with schizophrenia. *Journal of Neuroscience,* 23**,** 6315-26.

HASSELMO, M. E. 2005. What is the function of hippocampal theta rhythm?—Linking behavioral data to phasic properties of field potential and unit recording data. *Hippocampus,* 15**,** 936-949.

HEBB, D. O. 1950. Organization of behavior. *Journal of Clinical Psychology,* 6**,** 307-307.

HERB, A., BURNASHEV, N., WERNER, P., SAKMANN, B., WISDEN, W. & SEEBURG, P. H. 1992. The KA-2 subunit of excitatory amino acid receptors shows widespread expression in brain and forms ion channels with distantly related subunits. *Neuron,* 8**,** 775-785.

HEUSER, J. E. & REESE, T. S. 1973. Evidence for recycling of synaptic vesicle membrane during transmitter release at the frog neuromuscular junction. *Journal of Cell Biology,* 57**,** 315-344.

HEUSER, J. E., REESE, T. S., DENNIS, M. J., JAN, Y., JAN, L. & EVANS, L. 1979. Synaptic vesicle exocytosis captured by quick freezing and correlated with quantal transmitter release. *Journal of Cell Biology,* 81**,** 275-300.

HJORTH-SIMONSEN, A. & JEUNE, B. 1972. Origin and termination of the hippocampal perforant path in the rat studied by silver impregnation. *Journal of Comparative Neurology,* 144**,** 215-231.

HODGKIN, A. L. & HUXLEY, A. F. 1952. A quantitative description of membrane current and its application to conduction and excitation in nerve. *The Journal of Physiology,* 117**,** 500-544.

HOLLMANN, M. & HEINEMANN, S. 1994. Cloned Glutamate Receptors. *Annual Review of Neuroscience,* 17**,** 31-108.

HOLLMANN, M., MARON, C. & HEINEMANN, S. 1994. N-glycosylation site tagging suggests a three transmembrane domain topology for the glutamate receptor GluR1. *Neuron,* 13**,** 1331-1343.

HORMUZDI, S. G., PAIS, I., LEBEAU, F. E., TOWERS, S. K., ROZOV, A., BUHL, E. H., WHITTINGTON, M. A. & MONYER, H. 2001. Impaired electrical signaling disrupts gamma frequency oscillations in connexin 36-deficient mice. *Neuron,* 31**,** 487-95.

HOWARD, M. W., RIZZUTO, D. S., CAPLAN, J. B., MADSEN, J. R., LISMAN, J., ASCHENBRENNER-SCHEIBE, R., SCHULZE-BONHAGE, A. & KAHANA, M. J. 2003. Gamma Oscillations Correlate with Working Memory Load in Humans. *Cerebral Cortex,* 13**,** 1369-1374.

HUBEL, D. H. & WIESEL, T. N. 1963. Receptive fields of cells in striate cortex of very young, visually inexperienced kittens. *Journal of Neurophysiology,* 26**,** 994-1002.

HUNT, M. J., KOPELL, N. J., TRAUB, R. D. & WHITTINGTON, M. A. 2017. Aberrant Network Activity in Schizophrenia. *Trends in Neurosciences,* 40**,** 371-382.

HUTCHEON, B., MORLEY, P. & POULTER, M. O. 2000. Developmental change in GABA(A) receptor desensitization kinetics and its role in synapse function in rat cortical neurons. *Journal of Physiology,* 522**,** 3-17.

HUXTER, J. R., ZINYUK, L. E., ROLOFF, E. V. L., CLARKE, V. R. J., DOLMAN, N. P., MORE, J. C. A., JANE, D. E., COLLINGRIDGE, G. L. & MULLER, R. U. 2007. Inhibition of Kainate Receptors Reduces the Frequency of Hippocampal Theta Oscillations. *Journal of Neuroscience,* 27**,** 2212-2223.

INSAUSTI, R., AMARAL, D. G. & COWAN, W. M. 1987. The entorhinal cortex of the monkey: III. Subcortical afferents. *Journal of Comparative Neurology,* 264**,** 396-408.

ISAAC, J. T. R., NICOLL, R. A. & MALENKA, R. C. 1995. Evidence for silent synapses: Implications for the expression of LTP. *Neuron,* 15**,** 427-434.

J C WATKINS, A. & EVANS, R. H. 1981. Excitatory Amino Acid Transmitters. *Annual Review of Pharmacology and Toxicology,* 21**,** 165-204.

JACOBS, J. 2014. Hippocampal theta oscillations are slower in humans than in rodents: implications for models of spatial navigation and memory. *Philosophical Transactions of the Royal Society B: Biological Sciences,* 369**,** 20130304.

JAMAIN, S., BETANCUR, C., QUACH, H., PHILIPPE, A., FELLOUS, M., GIROS, B., GILLBERG, C., LEBOYER, M. & BOURGERON, T. 2002. Linkage and association of the glutamate receptor 6 gene with autism. *Molecular Psychiatry,* 7**,** 302-10.

JASKOLSKI, F., COUSSEN, F., NAGARAJAN, N., NORMAND, E., ROSENMUND, C. & MULLE, C. 2004. Subunit Composition and Alternative Splicing Regulate Membrane Delivery of Kainate Receptors. *Journal of Neuroscience,* 24**,** 2506-2515.

JETT, D. A. 2012. Chemical toxins that cause seizures. *NeuroToxicology,* 33**,** 1473-1475.

JIANG, L., XU, J., NEDERGAARD, M. & KANG, J. 2001. A Kainate Receptor Increases the Efficacy of GABAergic Synapses. *Neuron,* 30**,** 503-513.

JIN, X.-T. & SMITH, Y. 2007. Activation of presynaptic kainate receptors suppresses GABAergic synaptic transmission in the rat globus pallidus. *Neuroscience,* 149**,** 338-349.

JONES, M. V., SAHARA, Y., DZUBAY, J. A. & WESTBROOK, G. L. 1998. Defining Affinity with the GABAA Receptor. *Journal of Neuroscience,* 18**,** 8590-8604.

JONES, M. V. & WESTBROOK, G. L. 1996. The impact of receptor desensitization on fast synaptic transmission. *Trends in Neurosciences,* 19**,** 96-101.

JONES, R. S. 1993. Entorhinal-hippocampal connections: a speculative view of their function. *Trends Neuroscience,* 16**,** 58-64.

JONES, R. S. 1994. Synaptic and intrinsic properties of neurons of origin of the perforant path in layer II of the rat entorhinal cortex in vitro. *Hippocampus,* 4**,** 335-53.

JONES, R. S. & BUHL, E. H. 1993. Basket-like interneurones in layer II of the entorhinal cortex exhibit a powerful NMDA-mediated synaptic excitation. *Neuroscience Letters,* 149**,** 35-9.

JONES, R. S. & HEINEMANN, U. 1988. Synaptic and intrinsic responses of medical entorhinal cortical cells in normal and magnesium-free medium in vitro. *Journal Neurophysiology,* 59**,** 1476-96.

JONES, R. S. & LAMBERT, J. D. 1990. The role of excitatory amino acid receptors in the propagation of epileptiform discharges from the entorhinal cortex to the dentate gyrus in vitro. *Experimental Brain Research,* 80**,** 310-22.

JONES, R. S. G. & BÜHL, E. H. 1993. Basket-like interneurones in layer II of the entorhinal cortex exhibit a powerful NMDA-mediated synaptic excitation. *Neuroscience Letters,* 149**,** 35-39.

JONES, R. S. G. & HEINEMANN, U. 1989. Spontaneous activity mediated by NMDA receptors in immature rat entorhinal cortex in vitro. *Neuroscience Letters,* 104**,** 93-98.

JONES, R. S. G. & WOODHALL, G. L. 2005. Background synaptic activity in rat entorhinal cortical neurones: differential control of transmitter release by presynaptic receptors. *Journal of Physiology,* 562**,** 107-120.

JUNG, M., WIENER, S. & MCNAUGHTON, B. 1994. Comparison of spatial firing characteristics of units in dorsal and ventral hippocampus of the rat. *Journal of Neuroscience,* 14**,** 7347-7356.

KAJIWARA, R., WOUTERLOOD, F. G., SAH, A., BOEKEL, A. J., BAKS-TE BULTE, L. T. G. & WITTER, M. P. 2008. Convergence of entorhinal and CA3 inputs onto pyramidal neurons and interneurons in hippocampal area CA1—An anatomical study in the rat. *Hippocampus,* 18**,** 266-280.

KAMIYA, H. 2002. Kainate receptor-dependent presynaptic modulation and plasticity. *Neuroscience Research,* 42**,** 1-6.

KARAKAS, E. & FURUKAWA, H. 2014. Crystal structure of a heterotetrameric NMDA receptor ion channel. *Science,* 344**,** 992-7.

KATZ, L. C. 1993. Coordinate activity in retinal and cortical development. *Current Opinion Neurobiology,* 3**,** 93-99.

KAVALALI, E. T. 2014. The mechanisms and functions of spontaneous neurotransmitter release. *Nature Reviews Neuroscience,* 16**,** 5.

KAWAGUCHI, Y. & KUBOTA, Y. 1997. GABAergic cell subtypes and their synaptic connections in rat frontal cortex. *Cerebral Cortex,* 7**,** 476-86.

KERR, K. M., AGSTER, K. L., FURTAK, S. C. & BURWELL, R. D. 2007. Functional neuroanatomy of the parahippocampal region: The lateral and medial entorhinal areas. *Hippocampus,* 17**,** 697-708.

KHALILOV, I., HIRSCH, J., COSSART, R. & BEN-ARI, Y. 2002. Paradoxical Anti-Epileptic Effects of a GluR5 Agonist of Kainate Receptors. *Journal of Neurophysiology,* 88**,** 523-527.

KIDD, F. L., COUMIS, U., COLLINGRIDGE, G. L., CRABTREE, J. W. & ISAAC, J. T. 2002. A presynaptic kainate receptor is involved in regulating the dynamic properties of thalamocortical synapses during development. *Neuron,* 34**,** 635-46.

KIDD, F. L. & ISAAC, J. T. 1999. Developmental and activity-dependent regulation of kainate receptors at thalamocortical synapses. *Nature,* 400**,** 569-73.

KIRWAN, C. B. & STARK, C. E. L. 2004. Medial temporal lobe activation during encoding and retrieval of novel face-name pairs. *Hippocampus,* 14**,** 919-930.

KLEIN, A. S., DONOSO, J. R., KEMPTER, R., SCHMITZ, D. & BEED, P. 2016. Early Cortical Changes in Gamma Oscillations in Alzheimer's Disease. *Frontiers in Systems Neuroscience,* 10**,** 83.

KLINK, R. & ALONSO, A. 1997. Morphological characteristics of layer II projection neurons in the rat medial entorhinal cortex. *Hippocampus,* 7**,** 571-583.

KOBAYASHI, M., WEN, X. & BUCKMASTER, P. S. 2003. Reduced Inhibition and Increased Output of Layer II Neurons in the Medial Entorhinal Cortex in a Model of Temporal Lobe Epilepsy. *Journal of Neuroscience,* 23**,** 8471-8479.

KOGANEZAWA, N., GISETSTAD, R., HUSBY, E., DOAN, T. P. & WITTER, M. P. 2015. Excitatory Postrhinal Projections to Principal Cells in the Medial Entorhinal Cortex. *Journal of Neuroscience,* 35**,** 15860-15874.

KÖHLER, C. 1985. A projection from the deep layers of the entorhinal area to the hippocampal formation in the rat brain. *Neuroscience Letters,* 56**,** 13-19.

KÖHLER, M., BURNASHEV, N., SAKMANN, B. & SEEBURG, P. H. 1993. Determinants of ca2+ permeability in both TM1 and TM2 of high affinity kainate receptor channels: Diversity by RNA editing. *Neuron,* 10**,** 491-500.

KONDO, H. & WITTER, M. P. 2014. Topographic organization of orbitofrontal projections to the parahippocampal region in rats. *Journal of Comparative Neurology,* 522**,** 772-93.

KOVARI, E., GOLD, G., HERRMANN, F. R., CANUTO, A., HOF, P. R., BOURAS, C. & GIANNAKOPOULOS, P. 2003. Lewy body densities in the entorhinal and anterior cingulate cortex predict cognitive deficits in Parkinson's disease. *Acta neuropathologica,* 106**,** 83-8.

KRYSTAL, J. H., KARPER, L. P., SEIBYL, J. P., FREEMAN, G. K., DELANEY, R., BREMNER, J. D., HENINGER, G. R., BOWERS, M. B., JR. & CHARNEY, D. S. 1994. Subanesthetic effects of the noncompetitive NMDA antagonist, ketamine, in humans. Psychotomimetic, perceptual, cognitive, and neuroendocrine responses. *Archives of General Psychiatry,* 51**,** 199-214.

KUUSINEN, A., ARVOLA, M. & KEINÄNEN, K. 1995. Molecular dissection of the agonist binding site of an AMPA receptor. *The EMBO Journal,* 14**,** 6327-6332.

LAURI, S. & TAIRA, T. 2012. Kainate receptors in developing presynaptic terminals. *Wiley Interdisciplinary Reviews: Membrane Transport and Signaling,* 1**,** 45-55.

LAURI, S. E., LAMSA, K., PAVLOV, I., RIEKKI, R., JOHNSON, B. E., MOLNAR, E., RAUVALA, H. & TAIRA, T. 2003. Activity blockade increases the number of functional synapses in the hippocampus of newborn rats. *Molecular and Cellular Neuroscience,* 22**,** 107-17.

LAURI, S. E., SEGERSTRALE, M., VESIKANSA, A., MAINGRET, F., MULLE, C., COLLINGRIDGE, G. L., ISAAC, J. T. & TAIRA, T. 2005. Endogenous activation of kainate receptors regulates glutamate release and network activity in the developing hippocampus. *Journal of Neuroscience,* 25**,** 4473-84.

LAURI, S. E., VESIKANSA, A., SEGERSTRÅLE, M., COLLINGRIDGE, G. L., ISAAC, J. T. R. & TAIRA, T. 2006. Functional Maturation of CA1 Synapses Involves Activity-Dependent Loss of Tonic Kainate Receptor-Mediated Inhibition of Glutamate Release. *Neuron,* 50**,** 415-429.

LAURIE, D. J., WISDEN, W. & SEEBURG, P. H. 1992. The distribution of thirteen GABA(A) receptor subunit mRNAs in the rat brain. III. Embryonic and postnatal development. *Journal of Neuroscience,* 12**,** 4151-4172.

LAXER, K. D., TRINKA, E., HIRSCH, L. J., CENDES, F., LANGFITT, J., DELANTY, N., RESNICK, T. & BENBADIS, S. R. 2014. The consequences of refractory epilepsy and its treatment. *Epilepsy & Behavior,* 37**,** 59-70.

LE MAGUERESSE, C. & MONYER, H. 2013. GABAergic interneurons shape the functional maturation of the cortex. *Neuron,* 77**,** 388-405.

LEGA, B. C., JACOBS, J. & KAHANA, M. 2012. Human hippocampal theta oscillations and the formation of episodic memories. *Hippocampus,* 22**,** 748-761.

LEUNG, L. S. 1982. Nonlinear feedback model of neuronal populations in hippocampal CAl region. *Journal of Neurophysiology,* 47**,** 845-68.

LI, H. & ROGAWSKI, M. A. 1998. GluR5 kainate receptor mediated synaptic transmission in rat basolateral amygdala in vitro. *Neuropharmacology,* 37**,** 1279-86.

LI, J. M., ZENG, Y. J., PENG, F., LI, L., YANG, T. H., HONG, Z., LEI, D., CHEN, Z. & ZHOU, D. 2010. Aberrant glutamate receptor 5 expression in temporal lobe epilepsy lesions. *Brain Research,* 1311**,** 166-74.

LI, Y., YU, C., ZHOU, Z. C., STITT, I., SELLERS, K. K., GILMORE, J. H. & FROHLICH, F. 2017. Early Development of Network Oscillations in the Ferret Visual Cortex. *Scientific Reports,* 7**,** 17766.

LIMON, A., REYES-RUIZ, J. M. & MILEDI, R. 2012. Loss of functional GABA(A) receptors in the Alzheimer diseased brain. *PNAS,* 109**,** 10071-6.

LISMAN, J. 2005. The theta/gamma discrete phase code occuring during the hippocampal phase precession may be a more general brain coding scheme. *Hippocampus,* 15**,** 913-922.

LITWIN, D. B., MACLEAN, D. M. & JAYARAMAN, V. 2017. Reduced Structural Dynamics in Kainate Receptors through Auxiliary Protein Modulation. *Biophysical Journal,* 112**,** 419a.

LOPANTSEV, V. & AVOLI, M. 1998. Laminar organization of epileptiform discharges in the rat entorhinal cortex in vitro. *Journal of Physiology,* 509**,** 785-796.

LORENTE DE NO, R. 1933. Studies on the struture of the cerebral cortex I: The area entorhinalis. *Journal Psychology Neurology,* 45**,** 381-438.

LÖSCHER, W. 2017. Animal Models of Seizures and Epilepsy: Past, Present, and Future Role for the Discovery of Antiseizure Drugs. *Neurochemical Research,* 42**,** 1873-1888.

LOTHMAN, E. W., BERTRAM, E. H., KAPUR, J. & STRINGER, J. L. 1990. Recurrent spontaneous hippocampal seizures in the rat as a chronic sequela to limbic status epilepticus. *Epilepsy Research,* 6**,** 110-8.

LOWEL, S. & SINGER, W. 1992. Selection of intrinsic horizontal connections in the visual cortex by correlated neuronal activity. *Science,* 255**,** 209-12.

LOWET, E., ROBERTS, M., HADJIPAPAS, A., PETER, A., VAN DER EERDEN, J. & DE WEERD, P. 2015. Input-Dependent Frequency Modulation of Cortical Gamma Oscillations Shapes Spatial Synchronization and Enables Phase Coding. *PLOS Computational Biology,* 11**,** e1004072.

LUCARINI, N., VERROTTI, A., NAPOLIONI, V., BOSCO, G. & CURATOLO, P. 2007. Genetic polymorphisms and idiopathic generalized epilepsies. *Pediatric Neurology,* 37**,** 157-64.

LUHMANN, H. J. & PRINCE, D. A. 1991. Postnatal maturation of the GABAergic system in rat neocortex. *Journal of Neurophysiology,* 65**,** 247-63.

MAASS, A., SCHÜTZE, H., SPECK, O., YONELINAS, A., TEMPELMANN, C., HEINZE, H.-J., BERRON, D., CARDENAS-BLANCO, A., BRODERSEN, K. H., ENNO STEPHAN, K. & DÜZEL, E. 2014. Laminar activity in the hippocampus and entorhinal cortex related to novelty and episodic encoding. *Nature,* 5**,** 5547.

MACDONALD, R. & BARKER, J. L. 1978. Benzodiazepines specifically modulate GABA-mediated postsynaptic inhibition in cultured mammalian neurones. *Nature,* 271**,** 563.

MAINGRET, F., LAURI, S. E., TAIRA, T. & ISAAC, J. T. R. 2005. Profound regulation of neonatal CA1 rat hippocampal GABAergic transmission by functionally distinct kainate receptor populations. *Journal of Physiology,* 567**,** 131-142.

MALDONADO, P. E. & GERSTEIN, G. L. 1996. Neuronal assembly dynamics in the rat auditory cortex during reorganization induced by intracortical microstimulation. *Experimental Brain Research,* 112**,** 431-41.

MANN, E. O., SUCKLING, J. M., HAJOS, N., GREENFIELD, S. A. & PAULSEN, O. 2005. Perisomatic feedback inhibition underlies cholinergically induced fast network oscillations in the rat hippocampus in vitro. *Neuron,* 45**,** 105-17.

MAO, D., KANDLER, S., MCNAUGHTON, B. L. & BONIN, V. 2017. Sparse orthogonal population representation of spatial context in the retrosplenial cortex. *Nature Communications,* 8**,** 243.

MAYER, M. L. 2005. Crystal Structures of the GluR5 and GluR6 Ligand Binding Cores: Molecular Mechanisms Underlying Kainate Receptor Selectivity. *Neuron,* 45**,** 539-552.

MCALLISTER, A. K. 2000. Cellular and Molecular Mechanisms of Dendrite Growth. *Cerebral Cortex,* 10**,** 963-973.

MCDONALD, A. J. 1998. Cortical pathways to the mammalian amygdala. *Progress in Neurobiology,* 55**,** 257-332.

MCDONALD, J. K., SPECIALE, S. G. & PARNAVELAS, J. G. 1987. The laminar distribution of glutamate decarboxylase and choline acetyltransferase in the adult and developing visual cortex of the rat. *Neuroscience,* 21**,** 825-832.

MELOM, J. E., AKBERGENOVA, Y., GAVORNIK, J. P. & LITTLETON, J. T. 2013. Spontaneous and Evoked Release Are Independently Regulated at Individual Active Zones. *Journal of Neuroscience,* 33**,** 17253-17263.

MEYERSON, J. R., CHITTORI, S., MERK, A., RAO, P., HAN, T. H., SERPE, M., MAYER, M. L. & SUBRAMANIAM, S. 2016. Structural basis of kainate subtype glutamate receptor desensitization. *Nature,* 537**,** 567-571.

MEYERSON, J. R., KUMAR, J., CHITTORI, S., RAO, P., PIERSON, J., BARTESAGHI, A., MAYER, M. L. & SUBRAMANIAM, S. 2014. Structural mechanism of glutamate receptor activation and desensitization. *Nature,* 514**,** 328.

MIDDLETON, S., JALICS, J., KISPERSKY, T., LEBEAU, F. E., ROOPUN, A. K., KOPELL, N. J., WHITTINGTON, M. A. & CUNNINGHAM, M. O. 2008a. NMDA receptor-dependent switching between different gamma rhythm-generating microcircuits in entorhinal cortex. *PNAS,* 105**,** 18572-7.

MIDDLETON, S. J., RACCA, C., CUNNINGHAM, M. O., TRAUB, R. D., MONYER, H., KNOPFEL, T., SCHOFIELD, I. S., JENKINS, A. & WHITTINGTON, M. A. 2008b. High-frequency network oscillations in cerebellar cortex. *Neuron,* 58**,** 763-74.

MILLER, M. W. 1986. The migration and neurochemical differentiation of gamma-aminobutyric acid (GABA)-immunoreactive neurons in rat visual cortex as demonstrated by a combined immunocytochemical-autoradiographic technique. *Brain Research,* 393**,** 41-6.

MIN, M. Y., MELYAN, Z. & KULLMANN, D. M. 1999. Synaptically released glutamate reduces gamma-aminobutyric acid (GABA)ergic inhibition in the hippocampus via kainate receptors. *PNAS,* 96**,** 9932-7.

MOLLERUD, S., FRYDENVANG, K., PICKERING, D. S. & KASTRUP, J. S. 2017. Lessons from crystal structures of kainate receptors. *Neuropharmacology,* 112**,** 16-28.

MØLLERUD, S., FRYDENVANG, K., PICKERING, D. S. & KASTRUP, J. S. 2017. Lessons from crystal structures of kainate receptors. *Neuropharmacology,* 112**,** 16-28.

MONAGHAN, D. T. & COTMAN, C. W. 1982. The distribution of [3H]kainic acid binding sites in rat CNS as determined by autoradiography. *Brain Research,* 252**,** 91-100.

MORRIS, R. G. M. 1999. D.O. Hebb: The Organization of Behavior, Wiley: New York; 1949. *Brain Research Bulletin,* 50**,** 437.

MOSER, E. I., KROPFF, E. & MOSER, M.-B. 2008. Place Cells, Grid Cells, and the Brain's Spatial Representation System. *Annual Review of Neuroscience,* 31**,** 69-89.

MOTT, D. D., ROJAS, A., FISHER, J. L., DINGLEDINE, R. J. & BENVENISTE, M. 2010. Subunit-specific desensitization of heteromeric kainate receptors. *Journal of Physiology,* 588**,** 683-700.

MULLE, C., SAILER, A., PEREZ-OTANO, I., DICKINSON-ANSON, H., CASTILLO, P. E., BUREAU, I., MARON, C., GAGE, F. H., MANN, J. R., BETTLER, B. & HEINEMANN, S. F. 1998. Altered synaptic physiology and reduced susceptibility to kainate-induced seizures in GluR6-deficient mice. *Nature,* 392**,** 601-605.

MULLE, C., SAILER, A., SWANSON, G. T., BRANA, C., O'GORMAN, S., BETTLER, B. & HEINEMANN, S. F. 2000. Subunit Composition of Kainate Receptors in Hippocampal Interneurons. *Neuron,* 28**,** 475-484.

MURRAY, E. A. & RICHMOND, B. J. 2001. Role of perirhinal cortex in object perception, memory, and associations. *Current Opinion Neurobiology,* 11**,** 188-93.

NANOVA, P., KOLEV, V. & YORDANOVA, J. 2011. Developmental gender differences in the synchronization of auditory event-related oscillations. *Clinical Neurophysiology,* 122**,** 907-15.

NEHER, E. & SAKMANN, B. 1976. Single-channel currents recorded from membrane of denervated frog muscle fibres. *Nature,* 260**,** 799.

NESKE, G. T. 2015. The Slow Oscillation in Cortical and Thalamic Networks: Mechanisms and Functions. *Frontiers in Neural Circuits,* 9**,** 88.

NUNEZ, J. L. & MCCARTHY, M. M. 2007. Evidence for an extended duration of GABA-mediated excitation in the developing male versus female hippocampus. *Developmental Neurobiology,* 67**,** 1879-90.

O'DONOVAN, M. J. 1999. The origin of spontaneous activity in developing networks of the vertebrate nervous system. *Current Opinion Neurobiology,* 9**,** 94-104.

O'KEEFE, J. 1976. Place units in the hippocampus of the freely moving rat. *Experimental Neurology,* 51**,** 78-109.

O'KEEFE, J. & DOSTROVSKY, J. 1971. The hippocampus as a spatial map. Preliminary evidence from unit activity in the freely-moving rat. *Brain Research,* 34**,** 171-175.

OESS, T., KRICHMAR, J. L. & ROHRBEIN, F. 2017. A Computational Model for Spatial Navigation Based on Reference Frames in the Hippocampus, Retrosplenial Cortex, and Posterior Parietal Cortex. *Frontiers in Neurorobotics,* 11**,** 4.

OLSEN, G. M., OHARA, S., IIJIMA, T. & WITTER, M. P. 2017. Parahippocampal and retrosplenial connections of rat posterior parietal cortex. *Hippocampus,* 27**,** 335-358.

OTIS, T. S. & MODY, I. 1992. Modulation of decay kinetics and frequency of GABAA receptor-mediated spontaneous inhibitory postsynaptic currents in hippocampal neurons. *Neuroscience,* 49**,** 13-32.

PALOP, J. J. & MUCKE, L. 2016. Network abnormalities and interneuron dysfunction in Alzheimer disease. *Nature Reviews Neuroscience,* 17**,** 777.

PALVA, J. M., LAMSA, K., LAURI, S. E., RAUVALA, H., KAILA, K. & TAIRA, T. 2000. Fast Network Oscillations in the Newborn Rat Hippocampus *In Vitro*. *Journal of Neuroscience,* 20**,** 1170-1178.

PANTAZOPOULOS, H., LANGE, N., BALDESSARINI, R. J. & BERRETTA, S. 2007. Parvalbumin Neurons in the Entorhinal Cortex of Subjects Diagnosed With Bipolar Disorder or Schizophrenia. *Biological psychiatry,* 61**,** 640-652.

PAPEZ, J. W. 1937. A proposed mechanism of emotion. *Archives of Neurology & Psychiatry,* 38**,** 725-743.

PASTOLL, H., RAMSDEN, H. & NOLAN, M. 2012. Intrinsic electrophysiological properties of entorhinal cortex stellate cells and their contribution to grid cell firing fields. *Frontiers in Neural Circuits,* 6.

PASTOLL, H., SOLANKA, L., VAN ROSSUM, M. C. & NOLAN, M. F. 2013a. Feedback inhibition enables theta-nested gamma oscillations and grid firing fields. *Neuron,* 77**,** 141-54.

PASTOLL, H., SOLANKA, L., VAN ROSSUM, MARK C. W. & NOLAN, MATTHEW F. 2013b. Feedback Inhibition Enables Theta-Nested Gamma Oscillations and Grid Firing Fields. *Neuron,* 77**,** 141-154.

PATERNAIN, A. V., MORALES, M. & LERMA, J. 1995. Selective antagonism of AMPA receptors unmasks kainate receptor-mediated responses in hippocampal neurons. *Neuron,* 14**,** 185-189.

PENFIELD, W. & BOLDREY, E. 1937. Somatic motor and sensory representation in the cerebral cortex of man as studied by electrical stimulation. *Brain,* 60**,** 389-443.

PENFIELD, W. & MILNER, B. 1958. Memory deficit produced by bilateral lesions in the hippocampal zone. *A.M.A. Archives of Neurology & Psychiatry,* 79**,** 475-497.

PEREIRA, I. T., AGSTER, K. L. & BURWELL, R. D. 2016. Subcortical connections of the perirhinal, postrhinal, and entorhinal cortices of the rat I afferents. *Hippocampus,* 26**,** 1189-1212.

PERRAIS, D., PINHEIRO, P. S., JANE, D. E. & MULLE, C. 2009. Antagonism of recombinant and native GluK3-containing kainate receptors. *Neuropharmacology,* 56**,** 131-40.

PERRAIS, D., VERAN, J. & MULLE, C. 2010. Gating and permeation of kainate receptors: differences unveiled. *Trends Pharmacol Sci,* 31**,** 516-22.

PETROVIC, M. M., VIANA DA SILVA, S., CLEMENT, J. P., VYKLICKY, L., MULLE, C., GONZALEZ-GONZALEZ, I. M. & HENLEY, J. M. 2017. Metabotropic action of postsynaptic kainate receptors triggers hippocampal long-term potentiation. *Nat Neurosci,* 20**,** 529-539.

PHILLIPS, C. G. 1972. Reflex activity of the spinal cord. *Journal of the Neurological Sciences,* 22**,** 270.

PILLI, J., ABBASI, S., RICHARDSON, M. & KUMAR, S. S. 2012. Diversity and excitability of deep-layer entorhinal cortical neurons in a model of temporal lobe epilepsy. *Journal of Neurophysiology,* 108**,** 1724-38.

PINHEIRO, P. & MULLE, C. 2006. Kainate receptors. *Cell and Tissue Research,* 326**,** 457-482.

PINHEIRO, P. S., PERRAIS, D., COUSSEN, F., BARHANIN, J., BETTLER, B., MANN, J. R., MALVA, J. O., HEINEMANN, S. F. & MULLE, C. 2007. GluR7 is an essential subunit of presynaptic kainate autoreceptors at hippocampal mossy fiber synapses. *Proceedings of the National Academy of Sciences of the United States of America,* 104**,** 12181-12186.

PORTER, R. H. P., EASTWOOD, S. L. & HARRISON, P. J. 1997. Distribution of kainate receptor subunit mRNAs in human hippocampus, neocortex and cerebellum, and bilateral reduction of hippocampal GluR6 and KA2 transcripts in schizophrenia. *Brain Research,* 751**,** 217-231.

QUILICHINI, P., SIROTA, A. & BUZSÁKI, G. 2010. Intrinsic circuit organization and theta-gamma oscillation dynamics in the entorhinal cortex of the rat. *Journal of neuroscience* 30**,** 11128-11142.

RANDALL, F. E., WHITTINGTON, M. A. & CUNNINGHAM, M. O. 2011. Fast oscillatory activity induced by kainate receptor activation in the rat basolateral amygdala in vitro. *European Journal of Neuroscience,* 33**,** 914-22.

RAY, S. & BRECHT, M. 2016. Structural development and dorsoventral maturation of the medial entorhinal cortex. *eLife,* 5**,** e13343.

RAY, S., NAUMANN, R., BURGALOSSI, A., TANG, Q., SCHMIDT, H. & BRECHT, M. 2014. Grid-Layout and Theta-Modulation of Layer 2 Pyramidal Neurons in Medial Entorhinal Cortex. *Science,* 343**,** 891-896.

REPRESA, A., ROBAIN, O., TREMBLAY, E. & BEN-ARI, Y. 1989. Hippocampal plasticity in childhood epilepsy. *Neuroscience Letters,* 99**,** 351-355.

REPRESA, A., TREMBLAY, E. & BEN-ARI, Y. 1987. Kainate binding sites in the hippocampal mossy fibers: Localization and plasticity. *Neuroscience,* 20**,** 739-748.

REPRESA, A., TREMBLAY, E. & BEN-ARI, Y. 1990. Sprouting of mossy fibers in the hippocampus of epileptic human and rat. *Advances in Experimental Medicine and Biology,* 268**,** 419-24.

RIVERA, C., VOIPIO, J., PAYNE, J. A., RUUSUVUORI, E., LAHTINEN, H., LAMSA, K., PIRVOLA, U., SAARMA, M. & KAILA, K. 1999. The K+/Cl- co-transporter KCC2 renders GABA hyperpolarizing during neuronal maturation. *Nature,* 397**,** 251-5.

RIVEST, R. W. 1991. Sexual maturation in female rats: Hereditary, developmental and environmental aspects. *Experientia,* 47**,** 1026-1038.

RODRIGUES, R. J. & LERMA, J. 2012. Metabotropic signaling by kainate receptors. *Wiley Interdisciplinary Reviews: Membrane Transport and Signaling,* 1**,** 399-410.

RODRÍGUEZ-MORENO, A. & SIHRA, T. S. 2007. Metabotropic actions of kainate receptors in the CNS. *Journal of Neurochemistry,* 103**,** 2121-2135.

ROGAWSKI, M. A., KURZMAN, P. S., YAMAGUCHI, S. I. & LI, H. 2001. Role of AMPA and GluR5 kainate receptors in the development and expression of amygdala kindling in the mouse. *Neuropharmacology,* 40**,** 28-35.

ROOPUN, A. K., MIDDLETON, S. J., CUNNINGHAM, M. O., LEBEAU, F. E. N., BIBBIG, A., WHITTINGTON, M. A. & TRAUB, R. D. 2006. A beta2-frequency (20–30 Hz) oscillation in nonsynaptic networks of somatosensory cortex. *Proceedings of the National Academy of Sciences of the United States of America,* 103**,** 15646-15650.

ROXO, M. R., FRANCESCHINI, P. R., ZUBARAN, C., KLEBER, F. D. & SANDER, J. W. 2011. The Limbic System Conception and Its Historical Evolution. *Scientific World Journal,* 11**,** 2428-41.

RUDY, B., FISHELL, G., LEE, S. & HJERLING-LEFFLER, J. 2011. Three Groups of Interneurons Account for Nearly 100% of Neocortical GABAergic Neurons. *Developmental neurobiology,* 71**,** 45-61.

SALEEM, A. B., LIEN, A. D., KRUMIN, M., HAIDER, B., ROSÓN, M. R., AYAZ, A., REINHOLD, K., BUSSE, L., CARANDINI, M. & HARRIS, K. D. 2017. Subcortical Source and Modulation of the Narrowband Gamma Oscillation in Mouse Visual Cortex. *Neuron,* 93**,** 315-322.

SALLERT, M., MALKKI, H., SEGERSTRALE, M., TAIRA, T. & LAURI, S. E. 2007. Effects of the kainate receptor agonist ATPA on glutamatergic synaptic transmission and plasticity during early postnatal development. *Neuropharmacology,* 52**,** 1354-65.

SALMENPERÄ, T., KÄLVIÄINEN, R., PARTANEN, K. & PITKÄNEN, A. 2000. Quantitative MRI volumetry of the entorhinal cortex in temporal lobe epilepsy. *Seizure: European Journal of Epilepsy,* 9**,** 208-215.

SALMOND, C. H., ASHBURNER, J., CONNELLY, A., FRISTON, K. J., GADIAN, D. G. & VARGHA-KHADEM, F. 2005. The role of the medial temporal lobe in autistic spectrum disorders. *European Journal Neuroscience,* 22**,** 764-72.

SARGOLINI, F., FYHN, M., HAFTING, T., MCNAUGHTON, B. L., WITTER, M. P., MOSER, M.-B. & MOSER, E. I. 2006. Conjunctive Representation of Position, Direction, and Velocity in Entorhinal Cortex. *Science,* 312**,** 758-762.

SASAKI, T., LEUTGEB, S. & LEUTGEB, J. K. 2015. Spatial and memory circuits in the medial entorhinal cortex. *Current Opinion in Neurobiology,* 32**,** 16-23.

SAVE, E. & SARGOLINI, F. 2017. Disentangling the Role of the MEC and LEC in the Processing of Spatial and Non-Spatial Information: Contribution of Lesion Studies. *Frontiers in Systems Neuroscience,* 11.

SCHARFMAN, H. E. 2007. The Neurobiology of Epilepsy. *Current neurology and neuroscience reports,* 7**,** 348-354.

SCHIFFER, H. H., SWANSON, G. T. & HEINEMANN, S. F. 1997. Rat GluR7 and a Carboxy-Terminal Splice Variant, GluR7b, Are Functional Kainate Receptor Subunits with a Low Sensitivity to Glutamate. *Neuron,* 19**,** 1141-1146.

SCHIZOPHRENIA WORKING GROUP OF THE PSYCHIATRIC GENOMICS, C. 2014. Biological insights from 108 schizophrenia-associated genetic loci. *Nature,* 511**,** 421-427.

SCHLESIGER, M. I., CANNOVA, C. C., BOUBLIL, B. L., HALES, J. B., MANKIN, E. A., BRANDON, M. P., LEUTGEB, J. K., LEIBOLD, C. & LEUTGEB, S. 2015. The medial entorhinal cortex is necessary for temporal organization of hippocampal neuronal activity. *Nature Neuroscience,* 18**,** 1123-1132.

SCHMITZ, D., FRERKING, M. & NICOLL, R. A. 2000. Synaptic Activation of Presynaptic Kainate Receptors on Hippocampal Mossy Fiber Synapses. *Neuron,* 27**,** 327-338.

SCHMITZ, D., MELLOR, J., FRERKING, M. & NICOLL, R. A. 2001a. Presynaptic kainate receptors at hippocampal mossy fiber synapses. *Proceedings of the National Academy of Sciences of the United States of America,* 98**,** 11003-11008.

SCHMITZ, D., SCHUCHMANN, S., FISAHN, A., DRAGUHN, A., BUHL, E. H., PETRASCH-PARWEZ, E., DERMIETZEL, R., HEINEMANN, U. & TRAUB, R. D. 2001b. Axo-axonal coupling. a novel mechanism for ultrafast neuronal communication. *Neuron,* 31**,** 831-40.

SCHON, K., NEWMARK, R. E., ROSS, R. S. & STERN, C. E. 2016. A Working Memory Buffer in Parahippocampal Regions: Evidence from a Load Effect during the Delay Period. *Cerebral Cortex,* 26**,** 1965-1974.

SCHULTZ, H., SOMMER, T. & PETERS, J. 2015. The Role of the Human Entorhinal Cortex in a Representational Account of Memory. *Frontiers in Human Neuroscience,* 9**,** 628.

SCOVILLE, W. B. & MILNER, B. 1957. LOSS OF RECENT MEMORY AFTER BILATERAL HIPPOCAMPAL LESIONS. *Journal of Neurology, Neurosurgery, and Psychiatry,* 20**,** 11-21.

SEMPLE, B. D., BLOMGREN, K., GIMLIN, K., FERRIERO, D. M. & NOBLE-HAEUSSLEIN, L. J. 2013. Brain development in rodents and humans: Identifying benchmarks of maturation and vulnerability to injury across species. *Progress in neurobiology,* 0**,** 1-16.

SEMYANOV, A. & KULLMANN, D. M. 2001. Kainate receptor-dependent axonal depolarization and action potential initiation in interneurons. *Nature Neuroscience,* 4**,** 718.

SENGUPTA, P. 2013. The Laboratory Rat: Relating Its Age With Human's. *International Journal of Preventive Medicine,* 4**,** 624-630.

SHALTIEL, G., MAENG, S., MALKESMAN, O., PEARSON, B., SCHLOESSER, R. J., TRAGON, T., ROGAWSKI, M., GASIOR, M., LUCKENBAUGH, D., CHEN, G. & MANJI, H. K. 2008. Evidence for the involvement of the kainate receptor subunit GluR6 (GRIK2) in mediating behavioral displays related to behavioral symptoms of mania. *Molecular Psychiatry,* 13**,** 858-72.

SHERRINGTON, C. S. 1906. *The integrative action of the nervous system,* New Haven, CT, US, Yale University Press.

SHIBATA, H., ARAMAKI, T., SAKAI, M., NINOMIYA, H., TASHIRO, N., IWATA, N., OZAKI, N. & FUKUMAKI, Y. 2006. Association study of polymorphisms in the GluR7, KA1 and KA2 kainate receptor genes (GRIK3, GRIK4, GRIK5) with schizophrenia. *Psychiatry Research,* 141**,** 39-51.

SHUANG, M., LIU, J., JIA, M. X., YANG, J. Z., WU, S. P., GONG, X. H., LING, Y. S., RUAN, Y., YANG, X. L. & ZHANG, D. 2004. Family-based association study between autism and glutamate receptor 6 gene in Chinese Han trios. *American Journal of Medical Genetics Part B Neuropsychiatric Genetics,* 131b**,** 48-50.

SIEGEL, A. M., WIESER, H. G., WICHMANN, W. & YASARGIL, G. M. 1990. Relationships between MR-imaged total amount of tissue removed, resection scores of specific mediobasal limbic subcompartments and clinical outcome following selective amygdalohippocampectomy. *Epilepsy Research,* 6**,** 56-65.

SILVER, R. A., CULL-CANDY, S. G. & TAKAHASHI, T. 1996. Non-NMDA glutamate receptor occupancy and open probability at a rat cerebellar synapse with single and multiple release sites. *Journal of Physiology,* 494**,** 231-250.

SINGER, W. 1995. Development and plasticity of cortical processing architectures. *Science,* 270**,** 758-64.

SINGER, W. A. & GRAY, C. M. 1995. Visual Feature Integration and the Temporal Correlation Hypothesis. *Annual Review of Neuroscience,* 18**,** 555-586.

SIROTA, A., MONTGOMERY, S., FUJISAWA, S., ISOMURA, Y., ZUGARO, M. & BUZSAKI, G. 2008. Entrainment of neocortical neurons and gamma oscillations by the hippocampal theta rhythm. *Neuron,* 60**,** 683-97.

SLOVITER, R. S., ZAPPONE, C. A., HARVEY, B. D. & FROTSCHER, M. 2006. Kainic acid-induced recurrent mossy fiber innervation of dentate gyrus GABAergic interneurons: a possible anatomical substrate of granule cell hyperinhibition in chronically epileptic rats. *Journal of comparative neurology,* 494**,** 944-960.

SNEIDER, J. T., HAMILTON, D. A., COHEN-GILBERT, J. E., CROWLEY, D. J., ROSSO, I. M. & SILVERI, M. M. 2015. Sex differences in spatial navigation and perception in human adolescents and emerging adults. *Behavioural processes,* 111**,** 42-50.

SOLANKA, L. 2015. Modelling microcircuits of grid cells and theta-nested gamma oscillations in the medial entorhinal cortex. *Thesis*.

SOLANKA, L., PASTOLL, H., VAN ROSSUM, M. C. W. & NOLAN, M. F. 2012. Multiplexing of theta-nested gamma oscillations and grid firing fields in an attractor network model of layer II of the medial entorhinal cortex. *Frontiers in Computational Neuroscience*.

SOLANKA, L., VAN ROSSUM, M. C. W. & NOLAN, M. F. 2015. Noise promotes independent control of gamma oscillations and grid firing within recurrent attractor networks. *eLife,* 4**,** e06444.

SOLODKIN, A., VELDHUIZEN, S. D. & VAN HOESEN, G. W. 1996. Contingent vulnerability of entorhinal parvalbumin-containing neurons in Alzheimer's disease. *Journal of Neuroscience,* 16**,** 3311-21.

SOMMER, B., BURNASHEV, N., VERDOORN, T. A., KEINÄNEN, K., SAKMANN, B. & SEEBURG, P. H. 1992. A glutamate receptor channel with high affinity for domoate and kainate. *The EMBO Journal,* 11**,** 1651-1656.

SOMMER, B. & SEEBURG, P. H. 1992. Glutamate receptor channels: novel properties and new clones. *Trends in Pharmacological Sciences,* 13**,** 291-296.

SONG, S. & ABBOTT, L. F. 2001. Cortical Development and Remapping through Spike Timing-Dependent Plasticity. *Neuron,* 32**,** 339-350.

SORIANO, E., MARTINEZ, A., FARIÑAS, I. & FROTSCHER, M. 1993. Chandelier cells in the hippocampal formation of the rat: The entorhinal area and subicular complex. *The Journal of Comparative Neurology,* 337**,** 151-167.

SPEAR, L. P. 2004. Adolescent Brain Development and Animal Models. *Annals of the New York Academy of Sciences,* 1021**,** 23-26.

SPENCER, S. S. & SPENCER, D. D. 1994. Entorhinal-hippocampal interactions in medial temporal lobe epilepsy. *Epilepsia,* 35**,** 721-7.

SQUIRE, L. & ZOLA-MORGAN, S. 1991. The medial temporal lobe memory system. *Science,* 253**,** 1380-1386.

STAFSTROM, C. E. 2006. Kainate Receptors "Sprout" on Epileptic Granule Cells. *Epilepsy Currents,* 6**,** 55-56.

STALEY, K. 2015. Molecular mechanisms of epilepsy. *Nature Neuroscience,* 18**,** 367-372.

STANGER, H. L., ALFORD, R., JANE, D. E. & CUNNINGHAM, M. O. 2008. The Role of GLU(K5)-Containing Kainate Receptors in Entorhinal Cortex Gamma Frequency Oscillations. *Neural Plasticity,* 2008**,** 401645.

STEGENGA, S. L. & KALB, R. G. 2001. Developmental regulation of N-methyl-D-aspartate- and kainate-type glutamate receptor expression in the rat spinal cord. *Neuroscience,* 105**,** 499-507.

STELLA, F. & TREVES, A. 2011. Associative Memory Storage and Retrieval: Involvement of Theta Oscillations in Hippocampal Information Processing. *Neural Plasticity,* 2011.

STENSOLA, H., STENSOLA, T., SOLSTAD, T., FRØLAND, K., MOSER, M.-B. & MOSER, E. I. 2012. The entorhinal grid map is discretized. *Nature,* 492**,** 72.

STERN-BACH, Y., BETTLER, B., HARTLEY, M., SHEPPARD, P. O., O'HARA, P. J. & HEINEMANN, S. F. 1994. Agonist selectivity of glutamate receptors is specified by two domains structurally related to bacterial amino acid-binding proteins. *Neuron,* 13**,** 1345-1357.

STEWARD, O. 1976. Topographic organization of the projections from the entorhinal area to the hippocampal formation of the rat. *Journal of Comparative Neurology,* 167**,** 285-314.

STEWARD, O. & SCOVILLE, S. A. 1976. Cells of origin of entorhinal cortical afferents to the hippocampus and fascia dentata of the rat. *Journal of Comparative Neurology,* 169**,** 347-370.

STEWART, M. & FOX, S. E. 1990. Do septal neurons pace the hippocampal theta rhythm? *Trends in Neurosciences,* 13**,** 163-169.

STRANAHAN, A. M. & MATTSON, M. P. 2010. Selective Vulnerability of Neurons in Layer II of the Entorhinal Cortex during Aging and Alzheimer's Disease. *Neural Plasticity,* 2010**,** 8.

SUCHER, N., AKBARIAN, S., CHI, C., LECLERC, C., AWOBULUYI, M., DEITCHER, D., WU, M., YUAN, J., JONES, E. & LIPTON, S. 1995. Developmental and regional expression pattern of a novel NMDA receptor- like subunit (NMDAR-L) in the rodent brain. *Journal of Neuroscience,* 15**,** 6509-6520.

SUN, Y., FARZAN, F., BARR, M. S., KIRIHARA, K., FITZGERALD, P. B., LIGHT, G. A. & DASKALAKIS, Z. J. 2011. Gamma oscillations in schizophrenia: Mechanisms and clinical significance. *Brain Research,* 1413**,** 98-114.

SÜRMELI, G., MARCU, DANIEL C., MCCLURE, C., GARDEN, DEREK L., PASTOLL, H. & NOLAN, MATTHEW F. 2015. Molecularly Defined Circuitry Reveals Input-Output Segregation in Deep Layers of the Medial Entorhinal Cortex. *Neuron,* 88**,** 1040-1053.

SWANSON, G. T., FELDMEYER, D., KANEDA, M. & CULL-CANDY, S. G. 1996. Effect of RNA editing and subunit co-assembly single-channel properties of recombinant kainate receptors. *Journal of Physiology,* 492**,** 129-142.

TAKETO, M. & YOSHIOKA, T. 2000. Developmental change of GABA(A) receptor-mediated current in rat hippocampus. *Neuroscience,* 96**,** 507-14.

TAKEUCHI, S., MIMA, T., MURAI, R., SHIMAZU, H., ISOMURA, Y. & TSUJIMOTO, T. 2015. Gamma Oscillations and Their Cross-frequency Coupling in the Primate Hippocampus during Sleep. *Sleep,* 38**,** 1085-1091.

TALLON-BAUDRY, C., BERTRAND, O., HÉNAFF, M.-A., ISNARD, J. & FISCHER, C. 2005. Attention Modulates Gamma-band Oscillations Differently in the Human Lateral Occipital Cortex and Fusiform Gyrus. *Cerebral Cortex,* 15**,** 654-662.

TANG, Q., BURGALOSSI, A., EBBESEN, CHRISTIAN L., RAY, S., NAUMANN, R., SCHMIDT, H., SPICHER, D. & BRECHT, M. 2014. Pyramidal and Stellate Cell Specificity of Grid and Border Representations in Layer 2 of Medial Entorhinal Cortex. *Neuron,* 84**,** 1191-1197.

TAYLOR, G. W., MCCARLEY, R. W. & SALISBURY, D. F. 2013. Early auditory gamma band response abnormalities in first hospitalized schizophrenia. *Supplements to Clinical Neurophysiology,* 62**,** 131-45.

TOLNER, E. A., FRAHM, C., METZGER, R., GORTER, J. A., WITTE, O. W., LOPES DA SILVA, F. H. & HEINEMANN, U. 2007. Synaptic responses in superficial layers of medial entorhinal cortex from rats with kainate-induced epilepsy. *Neurobiology of Disease,* 26**,** 419-438.

TOLNER, E. A., KLOOSTERMAN, F., KALITZIN, S. N., DA SILVA, F. H. L. & GORTER, J. A. 2005. Physiological Changes in Chronic Epileptic Rats Are Prominent in Superficial Layers of the Medial Entorhinal Area. *Epilepsia,* 46**,** 72-81.

TRAUB, R. D. & BIBBIG, A. 2000. A model of high-frequency ripples in the hippocampus based on synaptic coupling plus axon-axon gap junctions between pyramidal neurons. *Journal of Neuroscience,* 20**,** 2086-93.

TRAUB, R. D., BIBBIG, A., FISAHN, A., LEBEAU, F. E., WHITTINGTON, M. A. & BUHL, E. H. 2000. A model of gamma-frequency network oscillations induced in the rat CA3 region by carbachol in vitro. *European Journal Neuroscience,* 12**,** 4093-106.

TRAUB, R. D., BIBBIG, A., LEBEAU, F. E., CUNNINGHAM, M. O. & WHITTINGTON, M. A. 2005. Persistent gamma oscillations in superficial layers of rat auditory neocortex: experiment and model. *Journal of Physiology,* 562**,** 3-8.

TRAUB, R. D., BIBBIG, A., LEBEAU, F. E. N., BUHL, E. H. & WHITTINGTON, M. A. 2004. Cellular mechanisms of neuronal population oscillations in the hippocampus in vitro. *Annual Review of Neuroscience,* 27**,** 247-278.

TRAUB, R. D., KOPELL, N., BIBBIG, A., BUHL, E. H., LEBEAU, F. E. & WHITTINGTON, M. A. 2001. Gap junctions between interneuron dendrites can enhance synchrony of gamma oscillations in distributed networks. *Journal of Neuroscience,* 21**,** 9478-86.

TRAUB, R. D., MIDDLETON, S. J., KNOPFEL, T. & WHITTINGTON, M. A. 2008. Model of very fast (> 75 Hz) network oscillations generated by electrical coupling between the proximal axons of cerebellar Purkinje cells. *European Journal of Neuroscience,* 28**,** 1603-16.

TRAUB, R. D., SCHMITZ, D., JEFFERYS, J. G. R. & DRAGUHN, A. 1999. High-frequency population oscillations are predicted to occur in hippocampal pyramidal neuronal networks interconnected by axoaxonal gap junctions. *Neuroscience,* 92**,** 407-426.

TRAUB, R. D., WHITTINGTON, M. A., COLLING, S. B., BUZSAKI, G. & JEFFERYS, J. G. 1996a. Analysis of gamma rhythms in the rat hippocampus in vitro and in vivo. *Journal of Physiology,* 493 (Pt 2)**,** 471-84.

TRAUB, R. D., WHITTINGTON, M. A., STANFORD, I. M. & JEFFERYS, J. G. R. 1996b. A mechanism for generation of long-range synchronous fast oscillations in the cortex. *Nature,* 383**,** 621-624.

TRAYNELIS, S. F., WOLLMUTH, L. P., MCBAIN, C. J., MENNITI, F. S., VANCE, K. M., OGDEN, K. K., HANSEN, K. B., YUAN, H., MYERS, S. J. & DINGLEDINE, R. 2010. Glutamate Receptor Ion Channels: Structure, Regulation, and Function. *Pharmacological Reviews,* 62**,** 405-496.

TREIMAN, D. M. 2001. GABAergic mechanisms in epilepsy. *Epilepsia,* 42 Suppl 3**,** 8-12.

TSINTSADZE, V., MINLEBAEV, M., SUCHKOV, D., CUNNINGHAM, M. O. & KHAZIPOV, R. 2015. Ontogeny of kainate-induced gamma oscillations in the rat CA3 hippocampus in vitro. *Frontiers in Cellular Neuroscience,* 9**,** 195.

TUCHOLSKI, J., SIMMONS, M. S., PINNER, A. L., MCMILLAN, L. D., HAROUTUNIAN, V. & MEADOR-WOODRUFF, J. H. 2013. N-linked glycosylation of cortical NMDA and kainate receptor subunits in schizophrenia. *Neuroreport,* 24**,** 688-691.

UENO, H., SUEMITSU, S., MURAKAMI, S., KITAMURA, N., WANI, K., OKAMOTO, M., AOKI, S. & ISHIHARA, T. 2017. Postnatal development of GABAergic interneurons and perineuronal nets in mouse temporal cortex subregions. *International Journal of Developmental Neuroscience,* 63**,** 27-37.

UHLHAAS, P. J., ROUX, F., SINGER, W., HAENSCHEL, C., SIRETEANU, R. & RODRIGUEZ, E. 2009. The development of neural synchrony reflects late maturation and restructuring of functional networks in humans. *Proceedings of the National Academy of Sciences,* 106**,** 9866-9871.

UHLHAAS, P. J. & SINGER, W. 2010. Abnormal neural oscillations and synchrony in schizophrenia. *Nature Review Neuroscience,* 11**,** 100-113.

VAN CAUTER, T., CAMON, J., ALVERNHE, A., ELDUAYEN, C., SARGOLINI, F. & SAVE, E. 2013. Distinct Roles of Medial and Lateral Entorhinal Cortex in Spatial Cognition. *Cerebral Cortex,* 23**,** 451-459.

VAN DER LINDEN, S., PANZICA, F. & DE CURTIS, M. 1999. Carbachol induces fast oscillations in the medial but not in the lateral entorhinal cortex of the isolated guinea pig brain. *Journal of Neurophysiology,* 82**,** 2441-50.

VAN DER LOOS, H. 1988. Cajal on the cerebral cortex. An annotated translation of the complete writings. (History of neuroscience, no. 1). *Trends in Neurosciences,* 12**,** 520-521.

VAN HAEFTEN, T., BAKS-TE-BULTE, L., GOEDE, P. H., WOUTERLOOD, F. G. & WITTER, M. P. 2003. Morphological and numerical analysis of synaptic interactions between neurons in deep and superficial layers of the entorhinal cortex of the rat. *Hippocampus,* 13**,** 943-952.

VAN HOESEN, G. W. & PANDYA, D. N. 1975. Some connections of the entorhinal (area 28) and perirhinal (area 35) cortices of the rhesus monkey. III. Efferent connections. *Brain Research,* 95**,** 39-59.

VERGHESE, J., LIPTON, R. & AYERS, E. 2017. Spatial navigation and risk of cognitive impairment: A prospective cohort study. *Alzheimer's & Dementia: The Journal of the Alzheimer's Association,* 13**,** 985-992.

VERTES, R. P. 2004. Differential projections of the infralimbic and prelimbic cortex in the rat. *Synapse,* 51**,** 32-58.

VICTOR NADLER, J. 1981. Kainic acid as a tool for the study of temporal lobe epilepsy. *Life Sciences,* 29**,** 2031-2042.

VINCENT, P. & MULLE, C. 2009. Kainate receptors in epilepsy and excitotoxicity. *Neuroscience,* 158**,** 309-323.

VISMER, M. S., FORCELLI, P. A., SKOPIN, M. D., GALE, K. & KOUBEISSI, M. Z. 2015. The piriform, perirhinal, and entorhinal cortex in seizure generation. *Frontiers in Neural Circuits,* 9**,** 27.

VLČEK, K. 2011. Spatial Navigation Impairment in Healthy Aging and Alzheimer's Disease. *In:* MONTE, S. D. L. (ed.) *The Clinical Spectrum of Alzheimer's Disease -The Charge Toward Comprehensive Diagnostic and Therapeutic Strategies.* Rijeka: InTech.

VLCEK, K. & LACZO, J. 2014. Neural correlates of spatial navigation changes in mild cognitive impairment and Alzheimer's disease. *Front Behav Neurosci,* 8**,** 89.

WALTHER, H., LAMBERT, J. D., JONES, R. S., HEINEMANN, U. & HAMON, B. 1986. Epileptiform activity in combined slices of the hippocampus, subiculum and entorhinal cortex during perfusion with low magnesium medium. *Neuroscience Letters,* 69**,** 156-61.

WANG, X.-J. 2010. Neurophysiological and Computational Principles of Cortical Rhythms in Cognition. *Physiological reviews,* 90**,** 1195-1268.

WANG, X. J. & BUZSAKI, G. 1996. Gamma oscillation by synaptic inhibition in a hippocampal interneuronal network model. *Journal of Neuroscience,* 16**,** 6402-13.

WENTHOLD, R. J., TRUMPY, V. A., ZHU, W. S. & PETRALIA, R. S. 1994. Biochemical and assembly properties of GluR6 and KA2, two members of the kainate receptor family, determined with subunit-specific antibodies. *Journal of Biological Chemistry,* 269**,** 1332-9.

WEST, P. J., DALPÉ-CHARRON, A. & WILCOX, K. S. 2007. Differential Contribution of Kainate Receptors to EPSCs in Superficial Layer Neurons of the Rat Medial Entorhinal Cortex. *Neuroscience,* 146**,** 1000-1012.

WHITTINGTON, M. A., CUNNINGHAM, M. O., LEBEAU, F. E. N., RACCA, C. & TRAUB, R. D. 2011. Multiple origins of the cortical gamma rhythm. *Developmental Neurobiology,* 71**,** 92-106.

WHITTINGTON, M. A., JEFFERYS, J. G. & TRAUB, R. D. 1996. Effects of intravenous anaesthetic agents on fast inhibitory oscillations in the rat hippocampus in vitro. *British Journal of Pharmacology,* 118**,** 1977-86.

WHITTINGTON, M. A., STANFORD, I. M., COLLING, S. B., JEFFERYS, J. G. & TRAUB, R. D. 1997a. Spatiotemporal patterns of gamma frequency oscillations tetanically induced in the rat hippocampal slice. *Journal of Physiology,* 502**,** 591-607.

WHITTINGTON, M. A., TRAUB, R. D., FAULKNER, H. J., STANFORD, I. M. & JEFFERYS, J. G. 1997b. Recurrent excitatory postsynaptic potentials induced by synchronized fast cortical oscillations. *PNAS,* 94**,** 12198-203.

WHITTINGTON, M. A., TRAUB, R. D. & JEFFERYS, J. G. 1995. Synchronized oscillations in interneuron networks driven by metabotropic glutamate receptor activation. *Nature,* 373**,** 612-5.

WHITTINGTON, M. A., TRAUB, R. D., KOPELL, N., ERMENTROUT, B. & BUHL, E. H. 2000. Inhibition-based rhythms: experimental and mathematical observations on network dynamics. *International Journal of Psychophysiology,* 38**,** 315-36.

WIESEL, T. N. & HUBEL, D. H. 1963a. Effects of visual deprivation on morphology and physiology of cells in the cats lateral geniculate body. *Journal of Neurophysiology,* 26**,** 978-93.

WIESEL, T. N. & HUBEL, D. H. 1963b. Single-cell responses in striate cortex of kittens deprived of vision in one eye. *Journal of Neurophysiology,* 26**,** 1003-17.

WILDING, T. J. & HUETTNER, J. E. 1996. Antagonist pharmacology of kainate- and alpha-amino-3-hydroxy-5-methyl-4-isoxazolepropionic acid-preferring receptors. *Molecular Pharmacology,* 49**,** 540-546.

WILLIAMS, S. & BOKSA, P. 2010. Gamma oscillations and schizophrenia. *Journal of Psychiatry & Neuroscience* 35**,** 75-77.

WILLS, T., BARRY, C. & CACUCCI, F. 2012. The abrupt development of adult-like grid cell firing in the medial entorhinal cortex. *Frontiers in Neural Circuits,* 6.

WILSON, H. R. & COWAN, J. D. 1972. Excitatory and Inhibitory Interactions in Localized Populations of Model Neurons. *Biophysical Journal,* 12**,** 1-24.

WINTERER, J., MAIER, N., WOZNY, C., BEED, P., BREUSTEDT, J., EVANGELISTA, R., PENG, Y., D'ALBIS, T., KEMPTER, R. & SCHMITZ, D. 2017. Excitatory Microcircuits within Superficial Layers of the Medial Entorhinal Cortex. *Cell Reports,* 19**,** 1110-1116.

WISDEN, W., LAURIE, D., MONYER, H. & SEEBURG, P. 1992. The distribution of 13 GABAA receptor subunit mRNAs in the rat brain. I. Telencephalon, diencephalon, mesencephalon. *Journal of Neuroscience,* 12**,** 1040-1062.

WITTER, M. P. 2007. The perforant path: projections from the entorhinal cortex to the dentate gyrus. *Progress in Brain Research,* 163**,** 43-61.

WITTER, M. P. & AMARAL, D. G. 2004. CHAPTER 21 - Hippocampal Formation *The Rat Nervous System (THIRD EDITION).* Burlington: Academic Press.

WITTER, M. P., DOAN, T. P., JACOBSEN, B., NILSSEN, E. S. & OHARA, S. 2017. Architecture of the Entorhinal Cortex A Review of Entorhinal Anatomy in Rodents with Some Comparative Notes. *Frontiers in Systems Neuroscience,* 11.

WO, Z. G. & OSWALD, R. E. 1994. Transmembrane topology of two kainate receptor subunits revealed by N-glycosylation. *Proceedings of the National Academy of Sciences of the United States of America,* 91**,** 7154-7158.

WOLFF, J. R., BOTTCHER, H., ZETZSCHE, T., OERTEL, W. H. & CHRONWALL, B. M. 1984. Development of GABAergic neurons in rat visual cortex as identified by glutamate decarboxylase-like immunoreactivity. *Neuroscience Letters,* 47**,** 207-12.

WOODHALL, G. L., BAILEY, S. J., THOMPSON, S. E., EVANS, D. I. P. & JONES, R. S. G. 2005. Fundamental differences in spontaneous synaptic inhibition between deep and superficial layers of the rat entorhinal cortex. *Hippocampus,* 15**,** 232-245.

WOUTERLOOD, F. G. & POTHUIZEN, H. 2000. Sparse colocalization of somatostatin- and GABA-immunoreactivity in the entorhinal cortex of the rat. *Hippocampus,* 10**,** 77-86.

YANG, J., WOODHALL, G. L. & JONES, R. S. G. 2006. Tonic facilitation of glutamate release by presynaptic NR2B-containing NMDA receptors is increased in the entorhinal cortex of chronically epileptic rats. *Journal of neuroscience* 26**,** 406-410.

ZARNADZE, S., BÄUERLE, P., SANTOS-TORRES, J., BÖHM, C., SCHMITZ, D., GEIGER, J. R. P., DUGLADZE, T. & GLOVELI, T. 2016. Cell-specific synaptic plasticity induced by network oscillations. *eLife,* 5**,** e14912.

ZEMUNIK, T., PERUZOVIC, M., CAPKUN, V., ZEKAN, L., TOMIC, S. & MILKOVIC, K. 2003. Reproductive ability of pubertal male and female rats. *Brazilian Journal of Medical and Biological Research,* 36**,** 871-877.

ZHANG, W., ST-GELAIS, F., GRABNER, C. P., TRINIDAD, J. C., SUMIOKA, A., MORIMOTO-TOMITA, M., KIM, K. S., STRAUB, C., BURLINGAME, A. L., HOWE, J. R. & TOMITA, S. 2009. A Transmembrane Accessory Subunit that Modulates Kainate-Type Glutamate Receptors. *Neuron,* 61**,** 385-396.

ZHOU, L.-M., GU, Z.-Q., COSTA, A. M., YAMADA, K. A., MANSSON, P. E., GIORDANO, T., SKOLNICK, P. & JONES, K. A. 1997. (2S,4R)-4-Methylglutamic Acid (SYM 2081): A Selective, High-Affinity Ligand for Kainate Receptors. *Journal of Pharmacology and Experimental Therapeutics,* 280**,** 422-427.

ZHOU, M., ZHANG, F., ZHAO, L., QIAN, J. & DONG, C. 2016. Entorhinal cortex: a good biomarker of mild cognitive impairment and mild Alzheimer's disease. *Reviews in the Neurosciences,* 27**,** 185-95.

ZHU, L., BLETHYN, K. L., COPE, D. W., TSOMAIA, V., CRUNELLI, V. & HUGHES, S. W. 2006. Nucleus- and species-specific properties of the slow (<1 Hz) sleep oscillation in thalamocortical neurons. *Neuroscience,* 141**,** 621-636.